



Technische Universität München

Fakultät für Medizin

Next-generation *in vivo* models for improved pancreatic cancer therapies

Mingsong Wang

Vollständiger Abdruck der von der Fakultät für Medizin der Technischen Universität München zur Erlangung des akademischen Grades eines

Doktors der Naturwissenschaften

genehmigten Dissertation.

Vorsitz: Prof. Dr. Maximilian Reichert

Prüferinnen der Dissertation: 1. apl. Prof. Dr. Dieter Saur
2. Prof. Angelika Schnieke, Ph.D.

Die Dissertation wurde am 12.05.2022 bei der Technischen Universität München eingereicht und durch die Fakultät für Medizin am 09.08.2022 angenommen.



Table of contents

Table of Contents	II
List of Tables	V
List of Figures	VI
List of Abbreviation	VII
1 Introduction	1
1.1 Pancreatic ductal adenocarcinoma (PDAC).....	1
1.1.1 Risk factors	1
1.1.2 Diagnosis	3
1.1.3 Current Treatments and Challenges for Pancreatic Cancer	4
1.2 The genomic landscape of PDAC	9
1.2.1 Mutated KRAS in PDAC	9
1.2.2 Mutated KRAS and Biological Processes in PDAC.....	10
1.2.3 PI3K/Akt/mTOR Signaling pathway	11
1.2.4 RAF/MEK/ERK Signaling cascade	12
1.3 Epithelial–mesenchymal transition	14
1.4 Immune landscape in pancreatic cancer	15
1.5 Aims of the project.....	17
2 Materials	18
2.1 Laboratory equipment	18
2.2 Disposables.....	20
2.3 Chemicals, reagents, solutions and enzymes	22
2.4 Kit for Molecular Biology.....	25
2.5 Reagents for Histological, IF & IHC staining.....	25
2.6 Competent cell strains and Plasmids	26
2.7 PCR Primers	27
2.8 Embryonic stem cell (ESC) lines.....	31
2.9 Softwares.....	31
3 Methods	32
3.1 Molecular Biology	32
3.1.1 Gene-Targeting Vectors Construction	32
3.1.2 DNA extraction and purification	36
3.1.3 Polymerase Chain Reaction	39
3.1.4 Agarose gel electrophoresis.....	41
3.1.5 RNA isolation and purification.....	42
3.1.6 RNA sequencing.....	43
3.2 Cell culture.....	43
3.2.1 Primary Pancreatic tumor cell line isolation.....	43
3.2.2 Cell passage.....	43
3.2.3 Cryopreservation of cell lines.....	44



3.2.4	Cell transfection	44
3.2.5	Lentivirus production and infection	45
3.2.6	Doxycycline-inducible Gene Expression	45
3.2.7	Fluorescence-activated cell sorting (FACS)	46
3.2.8	Immunofluorescence staining for adherent cell	46
3.2.9	MTT assay	46
3.2.10	CellTiter Glo luminescent cell viability assay	46
3.2.11	Clonogenic Assay	47
3.2.12	Caspase-Glo 3/7 Assay	47
3.2.13	Drug treatment	47
3.3	Mouse Embryonic Stem Cell (mESC) culture	48
3.3.1	Generation of Puromycin-resistant feeder cells	48
3.3.2	Mouse ESC Culturing, Passaging and Cryopreservation	48
3.3.3	CRISPR/Cas9 Cleavage Assay	49
3.3.4	ESC Electroporation	50
3.3.5	Puromycin selection	51
3.3.6	Picking of positively transfected ESC	51
3.3.7	Screening PCR for ESC clones	51
3.3.8	Functional testing for positive ESC clones	52
3.4	Mouse experiments	52
3.4.1	Mouse strains	52
3.4.2	Genotyping for Mice	54
3.4.3	Mouse Nomenclature	54
3.4.4	Mouse Dissection	54
3.4.5	Documentation of Tissues Morphology	55
3.4.6	Tamoxifen Treatment for Mice	55
3.4.7	Magnetic Resonance Imaging (MRI) for pancreatic tumor of mouse	55
3.4.8	Orthotopic Implantation	56
3.4.9	FACS for Pancreatic Tumor Tissue	56
3.5	Histological Analysis	58
3.5.1	Tissue Fixation, Embedding and Sectioning	58
3.5.2	Hematoxylin and Eosin (H&E) Staining	58
3.5.3	Immunohistochemistry (IHC) Staining	59
3.5.4	Scanning and Analysis of Staining	60
3.6	Protein Immunoblot	60
3.6.1	Protein Sample Preparation	60
3.6.2	Measurement of Protein Concentration	60
3.6.3	SDS-PAGE Gel Electrophoresis	61
3.6.4	Membrane Transfer	62
3.6.5	Antibody staining	62
3.7	Statistical analysis	63



4 Results	64
4.1 Chapter 1. Generation of novel multicolor tracing mouse models for EMT-TFs ..	64
4.1.1 Comparison of fluorescence intensity between FRT-EGFP variants	64
4.1.2 Fluorescent proteins of multicolor tracing system are distinguishable without fluorescence spillover.....	68
4.1.3 <i>In vitro</i> functional testing for FP-iCre fusion proteins	72
4.1.4 <i>In vitro</i> testing for cleavage efficiency of gRNAs	74
4.1.5 Generation of gene knock-in mouse embryonic stem cells.....	76
4.1.6 Functional testing for positive knock-in ESC clones	79
4.2 Chapter 2. Identifying and validating targets for novel PDAC treatment strategies	82
4.2.1 CRISPR/Cas9 mediated gene LOF screening identified <i>c-Raf</i> as a driver of <i>Pdk1</i> deletion resistance.....	82
4.2.2 Functional validation of <i>c-Raf</i> in <i>Pdk1</i> ^Δ resistant PDAC cells.....	85
4.2.3 Generation of <i>Pdk1</i> , <i>Braf</i> and <i>c-Raf</i> conditional deletion PDAC cell lines.....	88
4.2.4 Inactivation of <i>Pdk1</i> , <i>Braf</i> and <i>c-Raf</i> alters gene expression profile in PDAC cells..	90
4.2.5 <i>Pdk1</i> ^Δ ; <i>Braf</i> ^Δ ; <i>c-Raf</i> ^Δ PDAC cells tend to show a similar gene expression pattern	97
4.2.6 Concomitant inactivation of <i>Pdk1</i> , <i>Braf</i> and <i>c-Raf</i> impairs viability and colony formation of PDAC cells, and induces apoptosis.....	100
4.2.7 <i>Pdk1</i> ^Δ resistant cells are more susceptible to RAF inhibitors.....	103
4.2.8 PI3K, Pdk1 and RAF inhibitors display strong synergistic interactions in the treatment for PDAC	108
4.2.9 Triple knock-out of <i>Pdk1</i> , <i>Braf</i> and <i>c-Raf</i> results in tumor regression of <i>Kras</i> ^{G12D} - driven PDAC <i>in vivo</i>	110
4.2.10 Concomitant inactivation of <i>Pdk1</i> , <i>Braf</i> and <i>c-Raf</i> inhibits proliferation and promotes apoptosis of endogenous PDAC cells <i>in vivo</i>	114
4.2.11 Depletion of <i>Pdk1</i> , <i>Braf</i> and <i>c-Raf</i> increases infiltration of lymphocytes in PDAC	116
4.2.12 Genetic depletion of <i>Pdk1</i> in combination with <i>Braf</i> and <i>c-Raf</i> induces complete regression of orthotopically growing PDAC	119
5. Discussion and outlook	123
6. Summary	133
7. Zusammenfassung	134
Acknowledgements	136
References	137



List of Tables

Table 1. Laboratory equipment.....	18
Table 2. Disposables.....	20
Table 3. Chemicals, reagents, solutions and enzymes	22
Table 4. Kit for Molecular Biology	25
Table 5. Histological, IF & IHC staining reagents.....	25
Table 6. Competent bacterial strains	26
Table 7. Plasmids.....	26
Table 8. Genotyping and Recombination PCR Primers	27
Table 9. Molecular cloning and ESC screen Primers.....	27
Table 10. Validation and Screening Primers.....	29
Table 11. Embryonic stem cell (ESC) lines.....	31
Table 12. Software List.....	31
Table 13. Oligonucleotide annealing conditions.....	34
Table 14. Golden Gate Assembly and Conditions	34
Table 15. Ratio of Binding Buffer and DNA Sample.....	37
Table 16. Reaction Setup and Thermocycling conditions for DNA fragment amplification	39
Table 17. Reaction Setup and Thermocycling conditions for ESC clones validation (Touch-Down PCR)	40
Table 18. Reaction Setup and Thermocycling conditions for genotyping	40
Table 19. Reaction Setup and Thermocycling conditions for mycoplasma contamination testing	40
Table 20. Annealing temperatures and PCR products	41
Table 21. Composition of primary tumor cell culture medium.....	43
Table 22. Composition of primary tumor cell freezing medium.....	44
Table 23. Information of inhibitors	48
Table 24. Composition of ESC culture medium	49
Table 25. Composition of ESC freezing medium	49
Table 26. Target gene and DNA sequence of crRNAs.....	50
Table 27. Cas9 Cleavage Assay Reaction Setup	50
Table 28. Nomenclature of mouse lines	54
Table 29. B cells and T cells antibody staining panel.....	57
Table 30. Innate immune cells antibody staining panel.....	57
Table 31. Laser filter configurations for BD LSRFortessa	58
Table 32. Antibodies and dilution of antibodies for IHC staining	60
Table 33. Recipes with Standalone Reagents	61
Table 34. Recipes of the Stacking Gel and Separating Gel	61
Table 35. Antibodies and dilution of antibodies for Western Blotting.....	62
Table 36. Fluorescence intensity of FRT-EGFP and FRT-EGFP-iCre expression variants from HEK293 cells assessed by FACS.....	68
Table 37. The attributes of fluorescent proteins	69
Table 38. The size of uncleaved and cleaved DNA fragments.....	76
Table 39. Summary of ESC gene targeting	77
Table 40. Enriched Hallmark and KEGG pathways in <i>Pdk1^Δ</i> ; <i>Braf^Δ</i> ; <i>c-Raf^Δ</i> cell lines	95
Table 41. Enriched gene signatures in vehicle treated control PDAC cells	96
Table 42. Information of inhibitors and IC50 values of PDAC cell lines.....	107



List of Figures

Figure 1. Comparison of fluorescence intensity between FRT-EGFP expression plasmids ..	67
Figure 2. Fluorescent proteins can be distinguished without fluorescence spillover	71
Figure 3. Functional testing for FP-iCre fusion proteins	74
Figure 4. In vitro testing for cleavage efficiency of gRNAs	75
Figure 5. Generation of gene knock-in mouse embryonic stem cells	79
Figure 6. Functional test for positive KI ES clones	82
Figure 7. CRISPR/Cas9 mediated gene LOF screening identified <i>c-Raf</i> as a driver for <i>Pdk1</i> deletion resistance	84
Figure 8. Functional validation of <i>c-Raf</i> in <i>Pdk1</i> Δ resistant PDAC cells.....	87
Figure 9. Generation of <i>Pdk1</i> , <i>Braf</i> and <i>c-Raf</i> triple Knock-out cell lines	89
Figure 10. Deletion of <i>Pdk1</i> , <i>Braf</i> and <i>c-Raf</i> alters gene expression profile in PDAC cells....	94
Figure 11. <i>Pdk1</i> Δ ; <i>Braf</i> Δ ; <i>c-Raf</i> Δ PDAC cells tend to show similar gene expression pattern in comparison to their wild-type control counterparts.....	99
Figure 12. <i>Pdk1</i> , <i>Braf</i> and <i>c-Raf</i> triple knock-out impairs cell viability, colony formation and induces apoptosis in PDAC cells	102
Figure 13. <i>Pdk1</i> Δ resistant cells are more susceptible to RAF inhibitors	106
Figure 14. PI3K/Pdk1 and RAF inhibitors show the strong synergistic interactions for PDAC cells.....	109
Figure 15. Inactivation of <i>Pdk1</i> , <i>Braf</i> and <i>c-Raf</i> blocks endogenous <i>Kras</i> ^{G12D} -driven PDAC progression	113
Figure 16 . Concomitant inactivation of <i>Pdk1</i> , <i>Braf</i> and <i>c-Raf</i> inhibits proliferation and promotes apoptosis	115
Figure 17. Depletion of <i>Pdk1</i> , <i>Braf</i> and <i>c-Raf</i> increases infiltration of lymphocytes in <i>Kras</i> ^{G12D} -driven PDAC	118
Figure 18. Orthotopic implantation of mPDAC cell lines in mice	121
Figure 19. The potential compensatory mechanisms of Pdk1 and c-Raf to prevent apoptosis	125



List of Abbreviations

°C	degree Celsius
4-OHT	4-Hydroxytamoxifen
5-FU	fluorouracil
ACT	adoptive T cell transfer
ADM	acinar-to-ductal metaplasia
ADP	adenosine diphosphate
ALL	acute lymphoblastic leukemia
ATP	adenosine triphosphate
ANOVA	analysis of variance
BSA	bovine serum albumin
BRCA1	breast cancer type 1 susceptibility protein
CA	carbohydrate
CAFs	cancer-associated fibroblasts
CAR	chimeric antigen receptor
CAR-T cells	chimeric antigen receptor T cells
bp	base pair
CCL5	C-C Motif Chemokine Ligand 5
CDK	cyclin-dependent kinase
CDKN2A	cyclin-dependent kinase (CDK) inhibitor 2A
cDNA	complementary deoxyribonucleic acid
CT	computed tomography
CTLA-4	cytotoxic T lymphocyte antigen-4
CXCL12	CXC-chemokine ligand 12
Da	Dalton
DC	dendritic cell
DFS	disease-free survival
DLBCL	diffuse large B-cell lymphoma
DMEM	Dulbecco's modified Eagle medium
DMSO	dimethylsulfoxide
DNA	deoxyribonucleic acid
DNA DSB	DNA double-strand break
DNA SSB	DNA single-strand break
dNTP	deoxynucleoside triphosphate
Dox	doxycycline
DRS	dual-recombinase system
ECM	extracellular matrix
EDTA	ethylenediaminetetraacetic acid
EGFR	epidermal growth factor receptor



EMT	epithelial-mesenchymal transition
EpCAM	epithelial cell adhesion molecule
ESC	embryonic stem cell
ERCP	endoscopic retrograde cholangiopancreatography
EtOH	ethanol
EUS	endoscopic ultrasound
FCS	fetal calf serum
FDA	Food and Drug Administration
FDR	false discovery rate
FSF	frt-stop-frt cassette
Fwd	forward
g	gram
GPCRs	G-protein-coupled receptors
GDP	guanosine 5'-diphosphate
GEMMs	genetically engineered mouse models
GO	gene ontology
GSEA	gene set enrichment analysis
GTP	guanosine-5'-triphosphate
GLUTs	glucose transporters
HCC	hepatocellular carcinoma
HDR	Homology directed repair
H&E	hematoxylin and eosin
HLA	human leukocyte antigen
IFN- α	interferon α
IFN- γ	Interferon γ
IGF-1	receptorsinsulin-like growth factor-1
IHC	immunohistochemistry
IL-2	cytokine interleukin-2
IL-6	cytokine interleukin-6
IL-10	cytokine interleukin-10
IPMNs	intraductal papillary mucinous neoplasms
IRE	irreversible electroporation
JAK3	Tyrosine-protein kinase 3
Kb	Kilo base pair
KEGG	Kyoto Encyclopedia of Genes and Genomes
KRAS	V-Ki-ras2 Kirsten rat sarcoma viral oncogene homolog
kU/L	kilounits per liter
MEN1	multiple endocrine neoplasia type 1
L	liter



LB	Lysogeny broth
LSL	loxp-stop-loxp cassette
LOF	loss-of-function
M	molar
MAPK	mitogen-activated protein kinase
MAPKK	mitogen-activated protein kinase kinases
MDSCs	myeloid-derived suppressor cells
MEFs	mouse embryonic fibroblasts
mg	milligram
min	minute
miRNA	MicroRNA
mTOR	mammalian target of rapamycin
MTT	3-(4,5-Dimethylthiazol-2-yl)-2,5-Diphenyltetrazolium Bromide
mL	milliliter
mm	millimeter
mM	millimolar
MMF	midazolam, medetomidine, fentanyl
MMP-9	Matrix metalloproteinase 9
mRNA	messenger ribonucleic acid
MRI	magnetic resonance imaging
MRCP	magnetic resonance cholangiopancreatography
NES	normalized enrichment score
ng	nanogram
NGS	next-generation sequencing
NF- κ B	nuclear factor kappa B
nm	nanomolar
NK	natural killer
NOD	non-obese diabetic
OD	optical density
OS	overall survival
P53/Trp53	Tumor protein P53
PAGE	polyacrylamide gel electrophoresis
PALB2	Partner And Localizer Of BRCA2
PanINs	pancreatic intraepithelial neoplasias
PanNETs	Pancreatic neuroendocrine tumors
PARP	Poly (ADP-ribose) polymerase
PBS	phosphate buffered saline
PCA	principal component analysis
PCR	polymerase chain reaction



PDAC	pancreatic ductal adenocarcinoma
PDK1	3-phosphoinositide-dependent protein kinase 1
PDX1	pancreatic and duodenal homeobox 1
PD-1	programmed cell death protein 1
PD-L1	programmed death ligand 1
PPT	primary pancreatic tumor
PIP2	phosphatidylinositol-4,5-bisphosphate
PIP3	phosphatidylinositol-3,4,5-bisphosphate
PI3K	phosphatidylinositol-3-kinase
RAFTs	rapidly accelerated fibrosarcoma family kinases
RaIGDS	ral guanine nucleotide dissociation stimulator
RFA	radiofrequency ablation
PTEN	phosphatase and tensin homolog
Rev	reverse
RNA	ribonucleic acid
RNA-seq	RNA sequencing
RNAi	RNA interference
RT	room temperature
RTK	receptor tyrosine kinase
ROS	reactive oxygen species
SDS	sodium dodecyl sulphate
SEM	standard error of mean
Shh	Sonic hedgehog
SMAD4	mothers against decapentaplegic homolog 4
STAT3	signal transducer and activator of transcription 3
STK11	serine/threonine kinase 11
T2D	Type 2 diabetes
TAA	tumor- associated antigen
TAE	tris-acetate-EDTA
TAMs	tumor-associated macrophages
TEMED	tetramethylethylenediamine
Th1	type 1 T helper
Th2	type 2 T helper
TSA	tumor-specific antigen
KO	Knock-out
KI	Knock-in
TKO	Triple knock-out
TGF- β	transforming growth factor- β
TILs	tumor-infiltrating lymphocytes



TME	tumor microenvironment
TNF- α	tumor necrosis factor α
UV	ultraviolet
V	volt
VEGF	vascular endothelial growth factor
VEGFR	vascular endothelial growth factor receptor
WT	wild type
μg	microgram
μL	microliter
μm	micrometer
μM	Micromolar

1 Introduction

1.1 Pancreatic ductal adenocarcinoma (PDAC)

Pancreatic cancer is the cancer that begins in the cells of the pancreas, which is an important organ in human body. The pancreas can not only regulate blood glucose levels by releasing the hormones like insulin, glucagon. It also can secrete pancreatic juice and digestive enzymes, which break down carbohydrates, proteins, and fats in food entering the duodenum from the stomach.

So far, several types of pancreatic tumors have been identified, including invasive cancerous and non-invasive benign tumors. Among them, invasive pancreatic ductal adenocarcinoma (PDAC) is the most common type and it accounts for more than 90% of all pancreatic cancer cases [1]. PDAC is a highly lethal malignancy with strong and aggressive invasion ability, only around 8% of patients surviving more than 5 years after diagnosis [2]. Although the medical science and technology has got great development in the past decades, it has not resulted in significantly improved survival yet. In 2019, about 56,000 new cases of pancreatic cancer were diagnosed in the USA, and the number of death was predicted to be 45,000, which ranked third position of cancer-related death just after lung cancer and colorectal cancer [3]. PDAC also has been estimated to become the third leading cause of cancer-related death in European Union countries in the near future [4].

This devastating situation is mainly caused by the absence of effective tools for an early detection, consistent with the fact that most of patients are diagnosed at the advanced stages with only or even less than 20% are surgically resectable [5]. The poor prognosis of PDAC is also due to the potential metastasis of PDAC, which is one of the features of PDAC [5]. In advanced stages, PDAC patients always show high rate of metastases to the liver, lung, peritoneum, and other gastrointestinal organs, even the vascular or nervous system in some cases [6]. Third, PDAC always show resistance to chemotherapy and radiation treatment [7-9]. Furthermore, several recent studies showed that cells of the tumor microenvironment (TME) also limit the efficacy of chemotherapy [10, 11].

1.1.1 Risk factors

Although breakthroughs have been made in the past few years for the treatment of a small population of PDAC patients. Unfortunately, for majority of the PDAC patients, our present knowledge on the genetics and biology of this disease has not been translated to a leap in patient survival yet [12]. This is mainly because we still didn't completely figure out the causes of PDAC, but understanding the risk factors for pancreatic cancer may help people take measures to reduce the likelihood of getting this disease. The risk factors for PDAC that we have known so far including: Age - It is generally accepted that the risk of developing

pancreatic cancer and associated mortality increases substantially with age, especially from the age of 65 and older. Most of patients are diagnosed with PDAC when they are aged, the median age of these patients is 71 years, while cases before age 40 are rare [13]. Gender - The statistics show that men are slightly more common to develop PDAC compare with women [14].

Cigarette smoking and alcohol drinking – many studies have shown that smoking is highly related with higher risk for PDAC, about one-third of all pancreatic cancer patients are cigarette smokers. Besides, these researches also indicated that the risk of developing pancreatic cancer for smokers are 80% higher compared with non-smokers [15-17]. This is due to the carcinogens in tobacco, which may induce the activation of oncogene or/and the inactivation tumor suppressor genes in pancreas. Alcohol consumption has been considered as one of the major risk factors for causing chronic pancreatitis, which may predispose to pancreatic cancer [18]. However, considering the fact that smoking behavior is often associated with alcohol consumption, more rigorous studies should be perform to prove alcohol consumption is a direct risk factor for pancreatic cancer [19, 20].

Obesity is another risk factor related with development of pancreatic cancer. Overweight people who body mass index is equal to or greater than 30 kg/m², are more likely to have pancreatic cancer in their life [21]. What's more, the risk for developing pancreatic cancer is increasing when an adult is gaining weight. For people who have large waist may at the higher risk to have pancreatic cancer even they are not very overweight [22].

People who have been diagnosed with the diabetes are more likely to develop pancreatic cancer, especially in Type 2 diabetes (T2D) adult patients. In addition, with the increasing rate of this type of diabetes in children and adolescents due to obesity, the risk of PDAC also rises in these age groups [23, 24]. However, the relationships between diabetes and PDAC are still not very clear.

In addition, family heredity is another important risk factor for pancreatic cancer, around 10% pancreatic cancer cases were caused by family inherited gene mutation, and the risk increase rapidly when one or more lineal relatives of patient had the PDAC before the age of 50 [25]. What's worse, gene mutations passed from parents who had PDAC can also increase the risk of other cancers or health problems. Such as mutations of STK11 gene could cause Peutz-Jeghers syndrome, an autosomal dominant condition characterized by the development of noncancerous growths in the gastrointestinal tract; Dysplastic Nevus Syndrome (also known as the familial atypical multiple mole–melanoma (FAMMM) syndrome) caused by mutations in CDKN2A gene, which are quite common in PDAC; Hereditary breast and ovarian cancer syndrome caused by mutations in the PALB2 and BRCA2 gene separately; Pancreatic neuroendocrine tumors (PanNETs) have been associated with multiple endocrine neoplasia type 1 (MEN1) and von Hippel Lindau syndromes [25-27].

1.1.2 Diagnosis

Around 60 - 70% of PDAC originate from the head part of the pancreas, which are more likely to result in painless jaundice with patients. While the cases of PDAC tumor originally arise in the body and tail of pancreas are about 15% for each location. The pancreatic body tumor always shows a strong ability to invade the vascular system around itself, such as hepatic, celiac and superior mesenteric vessels, which is considered to be a main cause for back pain. While the tail tumor of pancreas tends to grow unimpededly due to fewer anatomical structure in the tail of pancreas. Due to the symptoms of PDAC patients are variable and associated with the location of the tumor, it makes the early diagnosis for PDAC is quite difficult [13, 27, 28]. Nevertheless, the most common symptom of PDAC like unexplained weight loss, should also be considered during diagnosing. In addition, from the statistic report of clinics, around 35% -47% of people diagnosed with the disease have had nausea, anorexia, vomiting accompany migraine, or a feeling of weakness and fatigability, these symptoms may also raise suspicion [13, 28].

Despite all this, the early screening for high-risk people and suspected cases is recommended. The most frequently used methods for the detection and diagnosis of PDAC are Magnetic Resonance Imaging (MRI), Computed Tomography scan (CT), magnetic resonance cholangiopancreatography (MRCP), as well as endoscopic ultrasound (EUS) [29]. In most cases, the results of MRI and MRCP are in good concordance with EUS findings when they were used as one-time screening modality in order to reduce the risk of ionizing radiation [30]. However, when the solid pancreatic tumor is smaller than 2cm, EUS shows higher sensitivity for tumor detecting compared to MRI and CT [31]. What's more, more lesion features of pancreatic cysts can be identified by EUS, and can be further characterized when combined with fine needle aspiration cytology [30].

While endoscopic retrograde cholangiopancreatography (ERCP) has been widely applied for biliary stent placement, the situation of biliary obstruction which caused by tumor infiltration, and its precision of sensitivity and specificity for the diagnosis of pancreatic cancer is higher than 90% [32]. Another imaging method - Abdominal ultrasound is also be used to identify the liver metastasis and build-up of ascites, although it has been considered less sensitive for small tumors in pancreas [29]. In addition, it can be used to guide the preliminary clinical diagnosis of PDAC quickly and cheaply [33].

Serum biomarker like Carbohydrate 19-9 antigen (CA19-9) has also been used for monitoring pancreatic cancer. It usually expresses and attaches to the O-glycans on the surface of cells. There are only small amounts of CA 19-9 (<37kU/L) in the blood of healthy people [34]. But in cancer patients, serum concentration of CA19-9 is often elevated, which be seen as a sign of pancreatic cancer [35]. However, the elevated level of CA19-9 can be detected not only in pancreatic cancer patients, also in colorectal cancer, hepatocellular carcinoma and

esophageal cancer [36]. Despite its limitations, the dynamic changes of CA19-9 shows important value to monitoring treatment response and effect in advanced or metastatic status or during Neoadjuvant Chemotherapy [37, 38]. In this case, the level of CA19-9 should decrease when the tumor is treated, and CA19-9 may rise again if the disease recurs [39]. Therefore, it has been considered as a surrogate marker for relapse rather than as efficient biomarker for early screening.

1.1.3 Current Treatments and Challenges for Pancreatic Cancer

As mentioned above, the poor prognosis of PDAC is mainly because of its complicated, multifactorial pathological mechanism. In addition, due to lack of simple and effective detection techniques for early stage PDAC diagnosis, and the facts that there is no obvious symptoms at the early stage of PDAC until the cancer has worsened, or metastasized to other organs [40]. Nevertheless, many treatment techniques have been developed to treat PDAC depends on the type and stage of the pancreatic cancer, also other clinical pathological factors.

1.1.3.1 Surgery for pancreatic cancer

Currently, surgery was considered as the most effective therapy method for PDAC. Potentially curative surgery and Palliative surgery are two general types of surgery which are used for treating pancreatic cancer commonly [41]. Specifically, potentially curative surgery is used when the diagnosis results suggest that the tumor is highly possible to be removed by operation. Normally, only about 10% pancreatic cancer patients who are diagnosed at early stage (Stage I/II) of PDAC are able to benefit from Potentially Curative Surgical resection [42, 43]. Unfortunately, most of patients had PDAC without any specific symptoms initially and reached at the advanced stage before they have obvious symptoms [44].

In fact, not all cancers turn out to be completely removed. Sometimes the more details of pancreatic cancer can be observed and discovered, which may indicate that the pancreatic cancer already progressed too fast to be completely removed. In that case, only a minor surgery (known as Palliative surgery) can be conducted to relieve or prevent symptoms of patients, even the cancellation of surgery may happen [45]. However, clinical statistics data indicated that surgery alone is insufficient for curing pancreatic cancer, there are still about 90% of patients suffered cancer relapse and even died after surgery without any additional therapies [41].

1.1.3.2 Ablation and Embolization

Although only few patients with pancreatic cancer can be completely cured by surgery, many improved surgical and interventional techniques still have been developed in the last decade for the locoregional treatment of pancreatic cancer. Which give a hope for patients to prolong the survival time and palliate sufferings of them. The most common locoregional therapies include ablation and embolization, these novel therapies can destroy tumors rather than remove them with surgery. They are used more often to treat pancreatic cancer patients with cancer metastases in other organs, especially the liver [46, 47].

There are many different ablative treatments, including but not limited to Radiofrequency ablation (RFA), Microwave thermotherapy, irreversible electroporation (IRE), cryotherapy or cryoablation. Typically, a probe is put into the tumor tissue in RFA treatment, which can release the heat energy that generated by high-frequency alternating current into the dysfunctional tumor tissue, then the tumor can be ablated by the high temperature. Microwave thermotherapy is similar with RFA, but it uses microwaves instead of electrical energy to heat and destroy the cancer cells in solid tumor tissue [48]. It is generally considered much faster and can cover a greater area than RFA. IRE is a technique using the short, high-voltage electrical pulses to achieve soft tissue ablation. Specifically, high-voltage pulses can puncture the cell membrane and induce cell apoptosis or cell necrosis afterwards [49, 50]. However, because of the complex anatomy of the pancreas and peripheral vascular tissues, the clinical outcomes of these therapy methods in the treatment of unresectable advanced pancreatic cancer have been limited.

Recently, a novel ablation technique — Cryoablation has been applied in the treatment for early stage and malignant pancreatic cancer, especially for those tumors that are unable to be removed by operation [51]. This approach uses a thin metal probe to freeze and destroy the tumor. The probe is guided through the skin and into the tumor by ultrasound, the extreme cold gasses are pass through the probe to freeze the tumor and then destroy the cancer cells. This method can be used to treat larger tumors than the other ablation techniques, but the patients are required to treat with cryoablation under general anesthesia sometimes [52].

Though the outcomes of these treatments are certainly obvious for pancreatic cancer, they are still not likely to cure cancers alone. So far, these therapy methods are mainly used to prevent or relieve symptoms, and they are more likely to be applied for treatment when pancreatic cancer only shows a few areas of spread.

1.1.3.3 Chemotherapy and Radiotherapy

Chemotherapy is a drug treatment using effective anti-tumor drugs to kill cancer cells with malignant growth ability, the drugs are normally injected into the vein or took by mouth, then the anti-tumor drugs are delivered to cancer cells through the bloodstream. Chemotherapy is

the most often used therapy method for pancreatic cancer treatment and it can be used at any stage. For example, chemotherapy is often used to shrink the tumor when the tumor is too big to be removed by surgery, which is also known as neoadjuvant chemotherapy [53]. Chemotherapy also can be applied to prevent cancer recurrences after surgery (adjuvant chemotherapy), especially when the solid tumor is removed and there are still few cancer cells have been left behind but they couldn't be detected. Chemotherapy is also used for treatment of advanced pancreatic cancer, when the pancreatic tumor is considered to be unresectable with surgery, or even when tumor cells have spread to other parts of body [54].

In most cases, two or more chemotherapy drugs are used in combination to treat patients with pancreatic cancer, which has been proved to be more effective for cancer treatment [55, 56]. More recently, a novel adjuvant combination chemotherapy – FOLFIRINOX has been developed for treatment of advanced pancreatic cancer. The FOLFIRINOX is made up of several different chemotherapy drugs, including Folinic Acid - a derivative of vitamin B which can enhance the effect of 5-fluorouracil by inhibiting thymidylate synthase, Fluorouracil (5-FU), Irinotecan and Oxaliplatin [26, 57]. Compared with gemcitabine mono-chemotherapy treatment, FOLFIRINOX regimen has prolonged approximately four months survival time of patients at phase III clinical trial, which then became an established option for advanced pancreatic cancer treatment [58]. In addition, a recent phase III trial of gemcitabine and nab-paclitaxel combination treatment showed about two months of increased median overall survival of patients with metastatic pancreatic cancer (from 6.7 to 8.5 months), compared with the gemcitabine alone, which made it as the standard first-line treatment for PDAC [59]. Although the chemotherapy is an effective method for many different types of cancer treatment, it's toxic to healthy cells and may cause serious side effects.

Radiotherapy is a therapy method for cancer treatment using ionizing radiation to kill malignant cancer cells. It has been widely used as part of cancer treatment for decades, and has also been shown to be helpful in treating some pancreatic cancers. Radiation therapy is synergistic with chemotherapy, it has been often applied to treatment of pancreatic cancer along with chemotherapy, which is known as chemoradiotherapy.

The Radiotherapy might be given along with chemotherapy before surgery to try to shrink the tumor and make it easier to remove completely, which is known as neoadjuvant treatment. Also, radiotherapy and chemotherapy are given together as part of the main treatment in patients with locally advanced pancreatic cancer, which is impossible to be removed by surgery. In some cases, radiation is given along with chemotherapy after surgery in order to lower the chance of the cancer coming back, and prolong the survival time of patients [60, 61].

Similar with chemotherapy, there are also some of the common side effects of radiation therapy are observed, such as nausea, diarrhea, fatigue, skin damage, loss of body weight and appetite *etc.* [62, 63]. Therapeutic radiation can also increase the risk of heart disease, even

caused death of patients in breast cancer radiation therapy regimens. The increase of risk is dose dependent, related to the dose strength of radiation therapy, also the volume and location of tumor [64, 65]. Though the radiotherapy has tremendous potential advantages for pancreatic cancer treatment, the role of radiation therapy for pancreatic cancer treatment is still controversial and should be further investigated. In the future, radiation therapy may be conducted with advanced real-time magnetic resonance guidance or other detection techniques, together they will improve the ability to target pancreatic precisely and reduce the unnecessary injury to bowel, so as to achieve the goal of improving the therapeutic index of radiation therapy [66].

1.1.3.4 Targeted therapy

Targeted therapy also known as molecularly targeted therapy, which is one of the major modalities of medical treatment for cancer [67]. As a new and effective method for cancer treatment, targeted therapy can block the carcinogenesis and tumor growth by interfering with specific targeted molecules which are essential for cancer cell growth. Comparing with the chemotherapy, the normal cells are not be killed or only affected slightly with targeted therapy and they can still survive during/after treatment. Therefore, targeted cancer therapy is expected to be more effective than previous treatment methods and less harmful to normal cells.

Currently, numerous targeted agents have been developed for PDAC treatment, such as EGFR inhibitors – erlotinib, it can target the mutated EGFR protein in cancer cells and block the abnormal proliferation of tumor cells. In some cases, erlotinib also be given along with Gemcitabine to patients with advanced pancreatic cancer, which have been proved as an effective combinatorial drug treatment for some of these patients [68]. BRCA genes are normally involved DNA double-strand breaks (DSBs) repair in cells, while PARP plays an important role in DNA single-strand breaks (SSBs), lack of both DNA repair mechanisms in cells can result cell death. The mutation with BRCA1 or BRCA2 is a common event in some of PDAC cases, hence block PARP can be a potential target for tumor cells with BRCA genes mutation [69, 70]. Olaparib is a type of drug known as a PARP inhibitor, which was approved for advanced ovarian cancer treatment recently [71]. By blocking the PARP pathway, Olaparib makes it difficult for tumor cells with the mutated BRCA genes to repair damaged DNA accurately, which can lead to death of tumor cells.

However, the clinical outcomes of most of these agents were not ideal, the probably reason is the molecular heterogeneity of the PDAC [41]. For the future directions of pancreatic cancer treatment, multiple combination of drugs may be used for treatment according to the molecular subtype of pancreatic cancer, which may be more specific and effective than monotherapy.

1.1.3.5 Immunotherapy

Immunotherapy is a treatment method that use the immune system of patients to recognize and destroy cancer cells. In the last decade, many immunotherapy approaches have been tested worldwide for treatment of various types of cancers, and the results of pre-clinical studies showed some promise which made immunotherapy in the limelight [72, 73].

The most common approaches of immunotherapy are checkpoint inhibitors, vaccination, and adoptive T-cell transfer. In term of checkpoint inhibitors, targeting programmed cell death protein 1 (PD-1), programmed death ligand 1 (PD-L1) and cytotoxic T lymphocyte antigen-4 (CTLA-4) in both pre-clinical and clinical studies have already resulted in significant improvements in disease outcomes for several cancer types [74-76]. However, the immune checkpoint inhibitors only showed a limited effect in PDAC when they were taken as mono- or combination therapy for PDAC treatment [77, 78]. This is probably due to poor immunogenicity of PDAC, with the fact that it's somatic mutations are much more less (at least ten times less) than melanoma and lung cancer, which result in the lack of mutated antigens that can be targeted by the T cells [79]. In addition, the complex components of PDAC tumor microenvironment (TME) may function as a barrier for checkpoint inhibitors delivery [44, 80].

Cancer vaccine is a vaccine that can be given for treatment of existing cancer or preventing the development of cancer, this method also known as therapeutic cancer vaccines [81]. The cancer vaccine works by targeting tumor- associated antigens (TAAs) or tumor-specific antigens (TSAs), which are two major classes of molecular components on the tumor cell surface. The TAAs also known as the shared antigens, they are expressed both in healthy cells and various types of tumors. While the tumor-specific antigens are some abnormal proteins, which are produced by concerned genes with mutations. These mutated genes can translate into protein with abnormal functions in cells, may eventually induce tumorigenesis [82, 83]. Although the TSAs can be variable in different types of cancer, they are still used to active the immune system to against tumor. Furthermore, TSAs can also be used as diagnosis biomarker and guide traditional cancer therapies, all of these make TSAs as one of the promising therapeutic strategies to treat cancer [82]. So far, many studies have shown the good therapeutic effects of cancer vaccines in some different cancers, which have been seen as a promising therapeutic measures for treatment of prostate cancer, cervical cancer and vulvar intraepithelial neoplasia [84-86]. However, the therapeutic methods using cancer vaccine only had modest effects in PDAC treatment, this may due to the immunosuppressive TME of PDAC, which can inactive T cells and prevent immune cells killing tumor cells [87].

Adoptive T cell transfer (ACT) is a novel therapeutic approach to transfer T cells into patients to kill the cancer cells, which involves the identification and enrichment of immune cells based on their capability of specific antigen recognition, or for genetic modification of immune cells receptor function [88, 89]. To achieve these purposes, patient's autologous tumor-infiltrating

lymphocytes (TILs) and dendritic cells (DCs) are collected from peripheral blood at the same time, the DCs then can be co-cultured with TILs to activate the function of TILs and expand TILs *ex vivo*. Afterwards, the expanded TILs are returned to the patients along with the cytokine interleukin-2 (IL-2) to enhance the immunity level and antitumor capacity of TILs [90].

Chimeric antigen receptor T cells (CAR-T cells) are T cells that have been genetically engineered to express artificial T cell receptors- Chimeric antigen receptor (CARs), these chimeric antigen receptors have both antigen recognition and T cell immuno-stimulating functions, which make T cells are more effective to target and destroy tumor cells. Compared with the adoptive T cell transfer therapy described above, CAR-T cells therapy shows great advantages: they are not human leukocyte antigen (HLA) –restricted, which allows CAR-T cells can be engrafted to recipients without or only with very weak immune rejection response. Moreover, CAR-T cells can potentially be engineered to target any tumor-associated antigen which expressed on the surface of tumor cells [91]. At present, many impressive results have been achieved in treatments of hematological malignancy by using CAR T-cell therapy. The CAR T-cell therapies that target the B cell specific antigen CD19 in B cell malignancies such as acute lymphoblastic leukemia (ALL) and diffuse large B-cell lymphoma (DLBCL) were approved by FDA as the new clinical treatments [92-94].

However, CAR-T cells are much less effective for solid tumor treatment [95]. The main reasons are that solid tumors like PDAC, they are lack of a specific antigen on the tumor cell surface, which makes CAR-T cells are difficult to target tumor cells [96]. In addition, CAR-T cells are unable to get the sites of solid tumor efficiently because of the physical barrier of solid tumor, and the immunosuppressive TME of solid tumor [97].

1.2 The genomic landscape of PDAC

1.2.1 Mutated KRAS in PDAC

KRAS (Kirsten rat sarcoma virus) gene is one of the members of RAS superfamily, which encodes a small GTPase that can convert the purine nucleoside triphosphate- Guanosine-5'-triphosphate (GTP) into Guanosine 5'-diphosphate (GDP). Once the extracellular stimuli activate the receptor tyrosine kinases (RTKs) and other receptors on the cell surface, the RAS protein and GTP can bind together and to switch on the activity of downstream effectors proteins like RAF-kinases, PI3-kinases and RaIGDS, these effectors can further regulate the cell growth, proliferation and other biological process [98].

In pancreatic cancer, *KRAS* mutation is the major event (around 90% of all cases). The mutated *KRAS* acts as a molecular switch for various intracellular signaling pathways and transcription factors inducing cell proliferation, migration, transformation and survival [99]. In

the majority (70-95%) of PDAC cases, an activating point mutation of the *KRAS* oncogene on codon 12 of exon 2 can always be detected, even at the early stages of pancreatic cancer, like pancreatic intraepithelial neoplasias (PanINs) and intraductal papillary mucinous neoplasms (IPMNs), thus the *KRAS* mutation has been considered as an initiating event of PDAC [100]. Among all the *KRAS* mutations, the most frequent mutation is GGT to GAT on codon 12 (40% of all mutations), which replaces the Glycine by Aspartic acid on protein level [101]. Interestingly, the mutations of oncogene *KRAS* is frequently associated with genetic inactivation of many tumor suppressor pathways such as *INK4a-ARF*, *TP53* and *SMAD4* in the majority of pancreatic carcinomas [101, 102].

Recently, some studies reported that patients with *KRAS*-mutated PDAC had a worse disease-free survival (DFS) and overall survival (OS) than others with *KRAS* wild-type tumors by analyzing DNA alternations from 356 PDAC patients with different driver genes [103]. In addition, in all *KRAS* mutated cases, patients with *KRAS*^{G12D} mutation tumor shown different outcomes and the worst DFS than other subtype *KRAS* mutations. While in metastatic pancreatic cancer patients, *KRAS*^{G12V} mutation subtype is correlated with poor prognosis [104]. Interestingly, Hamidi *et al.* shown that pancreatic tumor cell lines with *KRAS*^{G12V} mutation and *KRAS* copy number variations shown much high drug resistance than the other subtypes. Which proved that copy number variation may also be a biomarker for PDAC diagnosis [105].

1.2.2 Mutated *KRAS* and Biological Processes in PDAC

KRAS is one of critical molecular switch which involves in activation of various signaling molecules and regulation of many essential cellular processes in normal cells. While in cancer cells with *KRAS* mutation, this mutated gene can cause dysfunction of cell and cellular oncogenesis, such as increased the proliferation, survival, migration and invasion of tumor cells. The metabolic reprogramming of tumor cells is one of most common mechanisms changed by oncogenic mutated *KRAS*. Compared with the healthy cells, cancer cells prefer to use a special metabolism method - aerobic glycolysis, which produces lactate and reactive oxygen species (ROS) instead of carbon dioxide and water by metabolizing glucose, this is also known as the Warburg effect [106, 107]. Specifically, the mutated *KRAS* makes these metabolic changes in tumor cells by up-regulating the expression of glycolytic enzymes, which can enhance the glycolysis of tumor cells and produce more lactate. Meanwhile, the increased expression of solute carriers of the glucose transporters (GLUTs) has been reported in numerous cancer types, these glucose transporters mediate the glucose transmembrane transportation and allow tumor cells take more glucose [108, 109].

In addition, oncogenic *KRAS* stimulates the tumor cells to secrete some *KRAS*-dependent chemokines like Sonic hedgehog (Shh) and interleukin-6 (IL-6), also the colony-stimulating

factor 2 secreted by many kinds of cells (macrophages, T cells, fibroblasts *etc.*) in TME. Together, these cytokines can lead to inflammation and promote tumor growth [106, 110]. Furthermore, oncogenic *KRAS* can activate and enhance the communication between tumor cells and cancer-associated fibroblasts (CAFs) through the transforming growth factor- β (*TGF- β*) and *Shh* signaling pathway. Fundamentally, CAFs can produce TGF- β , vascular endothelial growth factor (VEGF), and CXC-chemokine ligand (CXCL12), thereby remodel the structure of tumor stroma and in turn promote tumor cell growth [111-113].

1.2.3 PI3K/Akt/mTOR Signaling pathway

The PI3K/Akt/mTOR signaling pathway is a key intracellular downstream target of the RAS family, which is primarily related to diverse cellular functions like cell proliferation, growth, motility, metabolism, migration and survival [114, 115]. Moreover, the *PI3K* pathway was reported to promote tumor growth by stimulating cells proliferation and inhibiting apoptosis in cancer cells [116]. According to the statistics, the deregulation of the *PI3K/Akt* signaling pathway can be detected in more than 50% of all cancer cases, and in 60% of all PDAC patients, which also indicated that *PI3K/Akt* pathway plays an important role in tumorigenesis [117, 118].

In tumor cells, PI3K regulates many cellular physiological functions by phosphorylating the phosphoinositides of phosphatidylinositol (PtdIns). Subsequently, the phosphorylated PtdIns can bind and recruit various phosphoinositide binding domain-containing effector proteins to further regulate cell activities and functions [119]. In most pancreatic cancer cell lines, the PI3Ks are classified into three groups (Class I, II, III and Class IV) according to their protein structure and lipid substrate specificity [120]. While the Class I PI3Ks are heterodimeric complexes, which are composed of a regulatory and a catalytic subunit. This class is further divided into two subclasses: subclass IA (p110 α / β / δ), they are activated by receptors with protein tyrosine kinase activity, known as receptor tyrosine kinases (RTKs); while subclass IB (p110 γ), which is activated by G-protein-coupled receptors (GPCRs) [121].

In *KRAS*-driven oncogenesis, the catalytic subunits p110 α , β and δ function as the critical downstream effectors to regulate numerous biological processes. Specifically, they can phosphorylate the phosphatidylinositol-4,5-bisphosphate (PIP2) and produce the second messenger phosphatidylinositol-3,4,5-bisphosphate (PIP3) [122]. After that, PIP3 activates various proteins including phosphoinositide-dependent kinase 1 (PDK1), and the AKT serine/threonine kinases. The phosphorylation of AKT can eventually result in promotion of cell growth and cell survival [122]. Meanwhile, the tumor suppressor PTEN can negatively regulate the *PI3K/Akt* pathway by dephosphorylating PIP3 to PIP2 and reduce the activity of PI3K catalytic subunit- p110 α [123].

The kinase mechanistic target of rapamycin (mTOR) is another important downstream effector of PI3K signaling pathway. The activity of mTOR is regulated by both positive and negative upstream regulators. When *PI3K/Akt* pathway is active, the molecular signals are transmitted to mTORC1 (which is a protein complex and composed of mTOR, Gbl, and Raptor) through many growth factors and their corresponding receptors including receptors insulin-like growth factor-1 (IGF-1) and its cognate receptor IFGR-1, vascular endothelial growth factor receptors (VEGFRs) and their ligands [124]. While in complex mTORC2 (Which is composed to mTOR, Gbl, and Rictor and involved in phosphorylation of Akt Ser473), the activity of mTOR is negatively regulated by PTEN, which can reduce the activity of PI3K as described above [125]. Moreover, the mTORC1 inhibitors such as Sirolimus, Temsirolimus or Everolimus are used for treating different kinds of cancers, because mTORC1 is highly sensitive to these macrolide compounds, which are known as the first-generation of mTOR inhibitors. While this kind of mTOR inhibitor is ineffective for inhibiting the activity of mTORC2 complex, the most likely reason is mTORC2 complex is not insensitive to rapamycin. However, some recent studies reported that genetic ablation of mTORC2 subunit Rictor can delayed tumorigenesis significantly in different types of cancer cells [126-128].

1.2.4 RAF/MEK/ERK Signaling cascade

The mitogen-activated protein kinase (MAPK) cascades consist of kinases in cell that transmit the extracellular molecules (such as cytokines, hormones, cell growth factors etc.) into intracellular signals. Eventually, cells respond to these molecular signals and regulate cell proliferation, differentiation, survival and apoptosis [129]. There are three RAF serine-threonine kinases (ARAF, BRAF, and C-RAF/RAF1) in this kinase cascade, they all act as the significant downstream effectors in *KRAS*-driven PDAC. RAFs have a RAS-binding domain (RBD) which allows them to interact with the activated RAS proteins, then RAF proteins are phosphorylated by RAS. The phosphorylation of RAFs leads to conformational changes of RAF proteins, formation of RAFs homodimers/heterodimers and activation of RAF kinases [130, 131]. Subsequently, RAF kinases activate the Mitogen-activated protein kinase kinases (known as MAP2Ks or MEKs) by phosphorylation, then followed by extracellular signal-regulated kinases (ERKs). The phosphorylated ERKs can activate and regulate more than 200 distinct substrates, many of them are identified as transcription factors, such as ELK1, c-Jun, c-Fos, MYC etc. [132-135]. Other important substrates of ERKs also including phospholipases A2 (PLA2s), which involves in inflammatory responses [136]. Besides, ERKs are related to organization of microtubule cytoskeletons, stimulation of various membrane receptors' intercellular domains [137, 138].

In many cancers, the dysfunctions of *RAF/MEK/ERK* pathway have been proved that are highly related to tumorigenesis. Since then, many compounds have been developed for inhibiting *RAF/MRK/ERK* pathway, and for eventual cancers treatment [139, 140]. Among them, RAF inhibitors- vemurafenib and dabrafenib are firstly applied to cancer treatment. In addition, vemurafenib and dabrafenib are BRAF-selective inhibitors, they showed satisfactory effects in treatment of many *BRAF*-mutant cancers. However, Corcoran *et al.* reported that vemurafenib and dabrafenib are ineffective for treating *BRAF*-mutant colorectal carcinoma, which because of the up-regulation of *EGFR* signaling in this type of cancer [141].

In PDAC, the occurrence of *BRAF* mutations is about 3%, while the point mutation of *BRAF* which results in the valine replaces glutamic acid at amino acid position 600 (known as BRAF V600E mutation) is predominant (about 70%-90%) of all *BRAF* mutations, the rest of *BRAF* mutations are deletion, amplifications and fusions [142]. Interestingly, although the *BRAF*^{V600E} mutations are rare in PDAC, they are mutually exclusive with *KRAS* mutations. Furthermore, PDAC cells with *BRAF*^{V600E} mutation were responsive to vemurafenib *in vitro* [143]. While cells with *BRAF* deletion mutation showed no responsive to vemurafenib [144]. On the other hand, the *BRAF*^{V600E} specific inhibitors like vemurafenib and dabrafenib cause paradoxical activation of *MEK/ERK* signaling in cancers harboring mutant *RAS*, the primary reason is the activation of *C-RAF* [145-147]. Specifically, inhibition of *BRAF* in *BRAF*-*C-RAF* heterodimers can lead to allosteric activation of *C-RAF* protein, and the activated *C-RAF* can further reactivate *MEK/ERK* by phosphorylation. This will eventually cause relapse or resistance of cancer in patients [148, 149]. Because of this, the new generation of *RAF* inhibitors have been developed. Among them, the Pan-*RAF* inhibitor LY3009120 showed impressive effect to overcome *ERK* paradoxical activation by blocking all *RAFs* (*ARAF*, *BRAF* and *C-RAF*), in addition to *BRAF*^{V600E} mutant [144, 150]. Besides, another novel *RAF* inhibitor-PLX8394, also has been proved that can disrupt *BRAF* dimers and block the *RAS*-independent *BRAF*-mutant-driven signaling effectively [151]. Furthermore, inhibitors which target *RAF* and *MEK* have been emerged as the combinatorial drug therapy to *RAS*-mutant, *BRAF*-inhibitor resistant cancer cells [152].

While the *MEKs* inhibitors didn't show potent activity in *RAS*-mutant cancers treatments, these disappointing results are most likely, or partially caused by compensation mechanisms of *RAF/MEK/ERK* pathway which can reactivate *ERK* [153, 154]. Moreover, it has been reported that *MEK* inhibitor-Trametinib treatment in *RAS*-mutant cancer cells led to kinome reprogramming of parallel pathways, which resulted in resistance of *RAS*-mutant tumor cells for *MEK* inhibitors [153]. Since both *RAF* and *MEK* inhibitors treatment can cause reactivation of *ERK* due to compensation mechanisms, the inhibitors which directly target *ERK* emerged as an alternative approach for treatment of *RAS*-mutant cancers. Indeed, some studies indicated that approximately 50% of PDAC cell lines displayed sensitive response for the

selective inhibitors of ERK1/2 - SCH772984 and Ulixertinib. Treatments with these ERK inhibitors in both PDAC cell lines and PDX tumor mouse models have shown impressive inhibition effects on tumor cells growth [153, 155]. Interestingly, Hayes *et al.* reported that long-term ERK inhibition treatment in KRAS-mutant PDAC cells induced MYC degradation and senescence-like growth suppression, while these changes did not happen in ERK inhibitor resistant cells, which indicated that the activity of MYC may be one of the resistance mechanisms for ERK inhibitor insensitive cells [156].

1.3 Epithelial–mesenchymal transition

The epithelial-mesenchymal transition (EMT) is a biological process that was first described in early stages of embryonic development [157]. During this process, the epithelial cells lose the cell polarity and adhesion between cells, change the cell morphology to become the mesenchymal cells with migratory and invasive properties in the end. Normally, the EMT process is defined by some molecular markers, such as E-cadherin which is highly expressed in epithelial cells, and N-cadherin, Vimentin in mesenchymal cells. The program of EMT has been shown to be crucial for early embryonic development, like formation of mesoderm and neural tube. In addition, EMT also plays an essential role in process of wound healing, stem cell biology, Fibrosis and even in the cancer progression [158].

In 2004, Ying *et al.* have reported that high expression of Twist1 can lead to loss of cell-cell adhesion in cancer cells and activate the expression of mesenchymal markers, increase of cell motility, it eventually promote the EMT process and contribute to metastasis [159]. Since then, many studies have proposed the EMT process is crucial to tumor cell metastasis due to the results of these studies which indicated that epithelial cells in tumor acquired the malignant phenotypes through EMT process [160, 161]. Some inhibitors that targeting EMT triggers even have been developed to block EMT in cancer cells, which were considered to be a good strategy to reduce the cancer recurrence and metastasis [162]. However, many recent researches have indicated that the EMT process may be not related to cancer progression, while the results of these studies suggested that EMT is more likely to make contribution to chemotherapy resistance in cancers [163, 164].

EMT is a complicate process which is regulated by transcription factors, cytokines, epigenetic modifications and MicroRNAs (miRNAs) at different levels, involved in many different signaling pathways. E-cadherin plays a vital role in regulation of EMT process, and loss of E-cadherin is considered to be a fundamental event in EMT, and associated with increased invasiveness and metastasis of tumor cells [165]. The transcription factors including families of SNAI, TWIST and ZEB, that can bind to the promoter of CDH1 gene and repress the expression of E-cadherin, were identified as the key inducing factors of EMT process, which are well known as

the EMT-inducing transcription factors (EMT-TFs) [158]. The functions of EMT-TFs may be essential for many stages of cancer progression, such as initiation of tumor formation, invasion and metastasis, as well as chemoresistance of cancer cells [163, 164, 166].

In general, the EMT induced by EMT-TFs leads to a complete morphological and functional transition of epithelial cells to mesenchymal cells during the embryonic development. While the cancer cells most often undergo an incomplete transition, or the partial EMT program. In this case, both molecular markers of epithelial and mesenchymal cells can be detected in the same cell [167, 168]. Furthermore, many studies indicated that cancer cells with partial EMT program exhibited an improved migration ability, and these cells were more likely associated with metastasis and chemoresistance [169-171].

Recent years, several studies on functions of EMT-TFs in cancer have shown that cancer metastasis and chemoresistance are indeed related to EMT-TFs, but not totally determined by EMT-TFs. This complicated fact is mainly due to the pleiotropic functions of EMT-TFs and their tissue-specific characteristic. For instance, it was demonstrated that transit overexpression of Snai1 triggered breast cancer metastasis, and depletion of Snai1 in the PyMT breast cancer mouse models reduced metastasis formation, whereas Snai1 showed no effect on metastasis in the pancreatic cancer model [163]. In another study, it was reported that deletion of Twist1 suppressed metastasis in breast cancer but not in pancreatic cancer [172]. In 2015, Zhang *et al.* even demonstrated that depletion of Zeb1 in the pancreatic cancer mouse model strongly reduced metastasis formation [163]. In order to figure out the mechanisms of tumor metastasis and develop more effective therapy methods, the focus of future studies should also include the pleiotropic functions of EMT-TFs and not only classical EMT-associated features.

1.4 Immune landscape in pancreatic cancer

The tumor microenvironment (TME) is the ecosystem around the tumor, it consists of tumor cells, stromal fibroblasts, immune cells, the surrounding blood vessels and the non-cellular components of extracellular matrix (ECM) [173]. Together, they create a microenvironment that promotes tumourigenesis and metastasis in vivo [174].

Recent studies have shown that the communications between tumor cells and non-tumor cells, interactions with tumor cells and ECM in microenvironment are essential to tumor growth and metastasis, all these mechanisms can be potential targets for cancer therapy [175, 176]. Furthermore, these researches have demonstrated that the interactions between tumor cells and non-neoplastic cells reshaped the TME, which also caused the stromal cells, immune cells to lose their original functions and even gain the additional physiologic functions that promote tumor development. In addition, dynamic interactions of tumor cells with ECM affects many

aspects of tumorigenesis such as clonal evolution, cancer heterogeneity, EMT process, apoptosis, immune evasion and chemotherapy resistance of cancer [177-180].

The immune cells in the TME also play a key role in the pancreatic cancer development and progression. Significantly, the immune cells in TME often have anti-cancer, as well as cancer-promoting functions. These functions of immune cells are involved in regulation of cytokines and chemical factors from ECM, also the interaction with tumor cells through specific receptors and related ligands [181]. In pancreatic cancer, especially KrasG12D mutation-driven PDAC, the upregulation of GM-CSF induced the number increase of myeloid-derived suppressor cells (MDSCs), the MDSCs then blocked the activity of anti-tumour T cell in TME, and eventually resulted in promoting tumor progression of PDAC [113]. Besides, the regulatory T (Treg) cells are associated with poor prognosis of PDAC patients due to the fact that Treg cells are observed in early stage of PDAC (PanIN), and are increased with progression to PDAC [182]. Both of MDSCs and Treg cells are participated in suppression of tumor immunity by affecting the present of effector lymphocytes and activation of anti-tumor lymphocytes.

The tumor-associated macrophages (TAMs) have been shown to accelerate the progression of pancreatic acinar-to-ductal metaplasia by secreting the Tumor necrosis factor (TNF) , C-C Motif Chemokine Ligand 5 (CCL5) and inducing secretion of Matrix metalloproteinase 9 (MMP-9) [183]. In the TME, TAMs are generally divided into different two groups, the pro-inflammatory M1 TAMs with tumor suppressive function, while the M2 TAMs are anti-inflammatory with tumor supportive function [184]. Normally, M2 type TAMs fulfill their tumor-promoting functions by induce angiogenesis through releasing cytokines like Vascular endothelial growth factor (VEGF), Interleukin 1 (IL-1), TNF etc. to stimulate angiogenesis [185]. In addition, M2 TAMs can communicate and interact with tumor cells, MDSCs, T cells and nature killer (NK) cells in the TME, then TAMs express HLA-G, PD-1 ligands PD-L1 and PD-L2, also the cytotoxic T lymphocyte antigen 4 (CTLA-4), this can result in tumor immune-evade and tumor growth [185]. The CD8+ T cells also known as the cytotoxic T lymphocytes (CTLs), which can kill the virus-infected cells, cancer cells and other dysfunctional somatic cells. Generally, the naïve CD8+ T cells are activated by interacting with antigen-presenting cells (APCs), these APCs can present the specific fragments of antigen from pathogen or tumor cells to CTLs, which makes CTLs recognize and target infected cells and tumor cells [186]. In this process, the APCs like dendritic cells can also interact with CD4+ T helper cells, this results in a more efficient activation of naïve CD8+ T cells [187]. Specifically, in order to target and kill tumor cells, the T cell receptor of CLTs recognize the major histocompatibility complex (MHC) class I molecules on the surface of tumor cells, then induce apoptosis in the tumor cells [184]. However, tumor cells evolved various methods to avoid the immunologic recognition and response of CLTs. For instance, tumor cells can decrease or even lose the expression of MHC class I, it leads to a reduced tumor cell recognition ability of CLTs [188]. Moreover, the upregulation of anti-

apoptotic proteins and downregulation of death receptors in tumor cells can prevent them from being eliminated by CLTs. The tumor cells can enhance the expression of checkpoint receptors in CTLs, such as PD-1, CTLA-4, TIM3 and BTLA *et al.*, that makes CLTs susceptible of immune exhaustion by specific binding of immune checkpoint ligands and checkpoint receptors [189].

Another important type of infiltrating lymphocytes is CD4+ T cells, also known as T helper cells (Th cells). During tumor development, the T helper cells can release kinds of cytokines and proteins to increase the immune activity of CD8 + T cells, they also mediated anti-tumor immunity by secreting interferon- γ (IFN γ) and tumour necrosis factor- α (TNF α) to eliminate tumour cells [190]. Therefore, CD4+ Th cells are usually seen as essential for the immune system. Indeed, several studies have also shown that PDAC patients with higher levels of CD4 + and/or CD8 + T cells have significantly prolonged survival [191-193]. Nevertheless, PDAC is a complicated cancer that may develop an immunosuppressive TME to repress the anti-tumor functions of infiltrating T lymphocytes and the dual role of Th cells in PDAC were also reported by some researches – these cells not only can inhibit tumor growth, but also can promote tumorigenesis [194].

1.5 Aims of the project

As described above, the Gemcitabine and Nab-Paclitaxel combination treatment and the FOLFIRINOX regimen prolonged survival of advanced pancreatic cancer. However, these treatment methods are also toxic for healthy cells and may cause serious side effects. In addition, the treatment effect of these methods just prolongs survival of approximately 4-6 months, but do not cure the disease. Targeted therapies that block specific cancer relevant pathways offer an option to treat PDAC more precisely with reduced side effects. In our previous work, we have shown that deletion of Pdk1, an important downstream effector molecule of the KRAS-PI3K pathway, could block PanINs formation and PDAC development significantly both *in vitro* and *in vivo*. However, there were still some PDAC cells that could survive and grow even when Pdk1 was deficient, which was thought to be one of the main reasons to cause resistance and recurrence after Kras^{G12D}-driven PDAC treatment. To further investigate the potential of PI3K/Pdk1 as a specific and efficient target in PDAC, we identified synergistic and synthetic lethal interaction partners of Pdk1 inactivation in pancreatic tumor cells by CRISPR/Cas9-based large-scale gene loss-of-function (LOF) screens. In my thesis, I validated candidates for combination therapy with Pdk1 inactivation both *in vitro* and *in vivo*. In addition, I generated novel mouse models and tools to study the functions of EMT-TFs *in vivo*. These models will allow us to monitor the activity of EMT-TFs at different EMT states and trace pancreatic cancer cells from the primary tumor to the metastatic sites.

2 Materials

2.1 Laboratory equipment

Table 1. Laboratory equipment

Device	Supplier
AxioCam HRc	Carl Zeiss AG, Oberkochen, Germany
Analytical balance A 120 S	Sartorius AG, Göttingen, Germany
Analytical balance BP 610	Sartorius AG, Göttingen, Germany
Aperio VERSA Digital Pathology Scanner	Leica Biosystems GmbH, Wetzlar, Germany
Autoclave 2540 EL	Tuttnauer Europe B.V., Breda, The Netherlands
Autoclave Systec VX-75	NeoLab Migge GmbH, Heidelberg, Germany
Automated Vacuum Tissue Processor- Leica ASP300S	Leica Biosystems GmbH, Wetzlar, Germany
Biometra Agarose Gel Electrophoresis Compact S and XL	Analytik Jena GmbH, Jena, Germany
CytoFLEX LX Flow Cytometer	Beckman Coulter, Brea, CA, USA
Confocal microscope Leica TCS SP5 DMI 6000 CS	Leica Microsystems GmbH, Wetzlar
CoolLED pE-300 white illuminator	CoolLED Limited, Andover, UK
CLARIO star Plus Microplate Reader	BMG Labtech GmbH, Ortenberg, Germany
CryoPod™ Carrier	Avantor, Radnor Township, PA, US
Cryostat Microm HM 560	Thermo Fisher Scientific, Inc., Waltham, MA, USA
Dewar carrying flask, type B	KGW-Isotherm, Karlsruhe, Germany
Electrophoresis PowerPac 1000 Power supply	Bio-Rad Laboratories GmbH, Munich, Germany
Electrophoresis PowerPac Universal Power Supply	Bio-Rad Laboratories GmbH, Munich, Germany
FACSAria™ III Cell Sorter	BD Medical Device company, Franklin Lakes, NJ, USA
Flu-O-Blu blue light table	Biozym Scientific GmbH, Hessisch Oldenburg, Germany
Fluorescence microscope HG 100 APO HC	Leica Microsystems GmbH, Wetzlar, Germany
Gel Doc™ XR+ system	Bio-Rad Laboratories GmbH, Munich, Germany
Gene Pulser® II Electroporation Systems	Bio-Rad Laboratories GmbH, Munich, Germany
GentleMACS™ Dissociator	Miltenyi Biotec B.V. & Co. KG, Bergisch Gladbach, Germany

Heidolph Rotamax 120 Orbital Shaker	Heidolph Instruments GmbH & Co. KG, Schwabach, Germany
HERAsafe® biological safety cabinet	Thermo Fisher Scientific, Inc., Waltham, MA, USA
Heracell VIOS 250i CO2 incubator	Thermo Fisher Scientific, Inc., Waltham, MA, USA
HERAfreeze™ HFU T Series -86°C Upright Ultra-Low Temperature Freezers	Thermo Fisher Scientific, Inc., Waltham, MA, USA
HiSeq 2500 Sequencing System	Illumina, Inc., San Diego, CA, USA
Infors Ecotron Incubator shaker	Infors GmbH, Sulzemoos, Germany
IKA Genius 3 - Vortex mixers	IKA Werke GmbH & Co. KG, Staufen, Germany
Leica Microscope DM E	Leica Microsystems GmbH, Wetzlar, Germany
Zeiss Axiovert 25 Inverted Microscope	Carl Zeiss AG, Oberkochen, Germany
Zeiss Axio Imager A1	Carl Zeiss AG, Oberkochen, Germany
Leica HistoCore Arcadia modular tissue embedding system	Leica Biosystems GmbH, Wetzlar, Germany
Li-Cor Odyssey® Fc Imaging System	LI-COR Biosciences, Lincoln, NE, USA
LSRFortessa™ cell analyzer/ Flow Cytometer	BD Medical Device company, Franklin Lakes, NJ, USA
Multipette® stream	Eppendorf AG, Hamburg, Germany
Magnetic Stirrer IKA® RET basic IKAMAG® safety control	IKA-Werke GmbH & Co. KG, Staufen, Germany
Microwave	Siemens, Munich, Germany
Microtome Microm HM355S Cool-Cut	Thermo Fisher Scientific, Inc., Waltham, MA, USA
Microcentrifuge 5427 R	Eppendorf AG, Hamburg, Germany
Microcentrifuge 5425	Eppendorf AG, Hamburg, Germany
MCO-5AC 17AI CO2 incubator	SANYO Sales & Marketing Europe GmbH, Munich, Germany
Mini centrifuge MCF-2360	LMS Consult GmbH & Co. KG, Brigachtal, Germany
NALGENE® Cryo 1°C Freezing Container	Thermo Fisher Scientific, Inc., Waltham, MA, USA
Neubauer chamber (Hemocytometer)	Lo-Labortechnik GmbH, Friedrichsdorf
NanoPhotometer® NP80	Implen GmbH, Munich, Germany
NanoScan® PET/ MRI system	Mediso Company, Budapest, Hungary
pH meter 521 WTW	Wissenschaftlich-Technische Werkstätten GmbH, Weilheim
Photometer Gene quant Pro RNA/DNA Calculator	Pharmacia Biotech Inc., Piscataway, NJ, USA

Pipettes Eppendorf Research Plus	Eppendorf AG, Hamburg
Pipetus Hirschmann	Hirschmann Laborgeräte GmbH & Co. KG, Eberstadt
ROTINA 380 R Centrifuge	Andreas Hettich GmbH & Co. KG, Tuttlingen
Stereomicroscope Stemi SV 11	Carl Zeiss AG, Oberkochen
Surgical instruments	Thermo Fisher Scientific, Inc., Waltham, MA, USA
Schott Duran Glass ware	Schott AG, Mainz, Germany
Stripettor™ Plus pipetting controller	Corning Inc., Corning, NY, USA
Stripettor™ Ultra pipetting controller	Corning Inc., Corning, NY, USA
ThermoMixer 5437 (2ml)	Eppendorf AG, Hamburg, Germany
ThermoMixer Comfort 5355 (1.5ml)	Eppendorf AG, Hamburg, Germany
Thermoshake incubator shaker	Gerhardt GmbH & Co. KG, Königswinter
Thermocycler Biometra TOne	Biometra GmbH, Göttingen, Germany
Thermocycler Biometra TAdvanced	Biometra GmbH, Göttingen, Germany
Thermocycler TGradient	Biometra GmbH, Göttingen, Germany
Thermocycler TProfessional Basic	Biometra GmbH, Göttingen, Germany
UVP PCR UV ³ HEPA cabinet	Analytik Jena GmbH, Jena, Germany
UVP UVsolo touch Gel documentation system	Analytik Jena GmbH, Jena, Germany
Water bath WTB50	Memmert GmbH & Co.KG, Büchenbach, Germany
Western Blotting Electrophoresis Chambers	Bio-Rad Laboratories GmbH, Munich, Germany
Western Blotting Criterion Blotter Chambers	Bio-Rad Laboratories GmbH, Munich, Germany

2.2 Disposables

Table 2. Disposables

Disposables	Supplier
BioPur® Safe-lock reaction tubes	Eppendorf AG, Hamburg, Germany
CELLSTAR® Cell culture multiwell plate (6, 12, 24, 48, 96 well)	Greiner Bio-One GmbH, Kremsmünster, Austria
Costar® Multiple Well Cell Culture Plates (6, 12, 24, 48, 96 well)	Corning Inc., Corning, NY, USA
Corning® Centrifuge Tubes (15ml, 50ml)	Corning Inc., Corning, NY, USA
Conical Tubes (15 ml, 50 ml)	Greiner Bio-One GmbH, Kremsmünster, Austria
Cryo Tubes (1.5ml, 3.5ml)	Sarstedt AG & Co., Nümbrecht, Germany
Cuvette	Greiner Bio-One GmbH, Kremsmünster, Austria

Disposable Gloves	Abena A/S, Aabenraa, Denmark
Falcon® 96-well Polypropylene Storage Plates	Corning Inc., Corning, NY, USA
Feather® disposable scalpels	Socorex Isba SA, Écublens, Switzerland
Gene Pulser Electroporation Cuvette (0.4mm gap)	Bio-Rad Laboratories GmbH, Munich, Germany
Glass slides Superfrost® Plus	Glasbearbeitungswerk GmbH & Co. KG. Brunswick, Germany
Menzel™ Microscope Coverslips	Glasbearbeitungswerk GmbH & Co. KG. Brunswick, Germany
Multichannel Reagent Reservoirs	INTEGRA Biosciences AG, Zizers, Switzerland
Microtome Blades DB80	Leica Biosystems GmbH, Wetzlar, Germany
Microvette® 500 Z-Gel tube	Sarstedt AG & Co., Nümbrecht, Germany
Nitrocellulose Membrane 0.45 µm	Bio-Rad Laboratories GmbH, Munich, Germany
Nunc™ EasYFlask™ Cell Culture Flasks (T25, T75, T175)	Thermo Fisher Scientific, Inc., Waltham, MA, USA
PCR reaction tubes 8-strip	Brand GmbH & Co. KG, Wertheim and Eppendorf AG, Hamburg, Germany
PCR Plates	Eppendorf AG, Hamburg, Germany
Parafilm M	Brand GmbH & Co. KG, Wertheim, Germany
Pasteur pipettes	Hirschmann Laborgeräte GmbH & Co. KG, Eberstadt, Germany
Petri dishes	Sarstedt AG & Co., Nümbrecht, Germany
Pipette tips with filter (10µl, 100µl, 200 µl, 1000 µl)	nerbe plus GmbH & Co. KG, Winsen, Germany
Pipette tips without filter (10µl, 100µl, 200 µl, 1000 µl)	Sarstedt AG & Co., Nümbrecht, Germany
Reaction tubes, 0.5 ml, 1.5 ml and 2 ml	Eppendorf AG, Hamburg, Germany
Serological Pipettes (2ml, 5ml, 10ml, 25ml, 50ml)	Greiner Bio-One GmbH, Kremsmünster, Austria
Syringe filtration unit Filtropur S 0.2	Sarstedt AG & Co., Nümbrecht, Germany
Syringe filtration unit Filtropur S 0.45	Sarstedt AG & Co., Nümbrecht, Germany
Sterile Inoculation loop	Sarstedt AG & Co., Nümbrecht, Germany
Sterile Inoculation spreader	Sarstedt AG & Co., Nümbrecht, Germany
Single use needles Sterican® 27 gauge	B. Braun Melsungen AG, Melsungen, Germany
Single use syringes Omnifix®	B. Braun Melsungen AG, Melsungen, Germany
Tissue embedding cassettes	MEDITE Medical GmbH, Burgdorf, Germany
Tissue Culture Dish (6cm, 10cm, 15cm)	TPP AG, Trasadingen, Switzerland
Western Blotting Filter Paper	Bio-Rad Laboratories GmbH, Munich, Germany

2.3 Chemicals, reagents, solutions and enzymes

Table 3. Chemicals, reagents, solutions and enzymes

Reagent	Supplier
2-Mercaptoethanol	Sigma-Aldrich Chemie GmbH, Taufkirchen, Germany
2-Propanol	Carl Roth GmbH & Co. KG, Karlsruhe, Germany
2x Taq PCR Master Mix	Thermo Fisher Scientific, Inc., Waltham, MA, USA
4-hydroxytamoxifen (4-OHT)	Sigma-Aldrich Chemie GmbH, Taufkirchen, Germany
Agarose Standard for DNA/RNA electrophoresis	Carl Roth GmbH & Co. KG, Karlsruhe, Germany
Ammonium sulfate ((NH ₄) ₂ SO ₄)	Sigma-Aldrich Chemie GmbH, Taufkirchen, Germany
Ampicillin sodium salt	Carl Roth GmbH & Co. KG, Karlsruhe, Germany
Bovine serum albumin (BSA)	Serva Electrophoresis GmbH, Heidelberg
Blunt/TA Ligase Master Mix	New England Biolabs GmbH, Frankfurt am Main, Germany
Cresol Red	AppliChem GmbH, Darmstadt
Calcium chloride (CaCl ₂)	Sigma-Aldrich Chemie GmbH, Taufkirchen, Germany
Collagenase Type II	Gibco, Life Technologies GmbH, Darmstadt, Germany
Dimethyl sulfoxide (DMSO)	Carl Roth GmbH & Co. KG, Karlsruhe, Germany
Dulbecco's phosphate buffered saline (1x DPBS) solution	Thermo Fisher Scientific, Inc., Waltham, MA, USA
dNTP Mix, 10 µM each	Sigma-Aldrich Chemie GmbH, Taufkirchen, Germany
Dulbecco's Modified Eagle Medium (DMEM) - High Glucose	Sigma-Aldrich Chemie GmbH, Taufkirchen, Germany
KnockOut™ DMEM	Thermo Fisher Scientific, Inc., Waltham, MA, USA
Effectene® Transfection Reagent	QIAGEN GmbH, Hilden, Germany
ES Cell Qualified FBS	Sigma-Aldrich Chemie GmbH, Taufkirchen, Germany
Ethanol absolute for analysis	Merck KGaA, Darmstadt, Germany
ESGRO Leukemia Inhibitory Factor	Merck KGaA, Darmstadt, Germany
Ethanol (70%, 80%, 96%)	Otto Fischer GmbH & Co. KG, Saarbrücken, Germany
Ethylenediaminetetraacetic acid (EDTA)	Life Technologies GmbH, Karlsruhe, Germany
Ethidium Bromide	Sigma-Aldrich Chemie GmbH, Taufkirchen, Germany

Forene® Isoflurane	Abbott GmbH & Co. KG, Ludwigshafen, Germany
Gateway® LR Clonase	Invitrogen GmbH, Karlsruhe
GelStar Nucleic Acid Stain	Lonza Group AG, Basel, Switzerland
Glycerol	Sigma-Aldrich Chemie GmbH, Taufkirchen, Germany
Gelatin	Sigma-Aldrich Chemie GmbH, Taufkirchen, Germany
GeneRuler DNA Ladders - 1 kb	Thermo Fisher Scientific, Inc., Waltham, MA, USA
HotStarTaq DNA Polymerase	QIAGEN GmbH, Hilden, Germany
Hydrochloric acid (HCl)	Merck KGaA, Darmstadt, Germany
Kanamycin	Carl Roth GmbH & Co. KG, Karlsruhe, Germany
Laemmli Sample Buffer	Bio-Rad Laboratories GmbH, Munich, Germany
L-Glutamine solution	Sigma-Aldrich Chemie GmbH, Taufkirchen, Germany
LB Medium (Luria/Miller)	Carl Roth GmbH & Co. KG, Karlsruhe, Germany
LB-Agar (Luria/Miller)	Carl Roth GmbH & Co. KG, Karlsruhe, Germany
LB-Broth (Luria/Miller)	Carl Roth GmbH & Co. KG, Karlsruhe, Germany
Magnesium chloride (MgCl ₂)	Carl Roth GmbH & Co. KG, Karlsruhe, Germany
Magnesium sulfate (MgSO ₄)	Merck KGaA, Darmstadt, Germany
Methanol	Carl Roth GmbH & Co. KG, Karlsruhe, Germany
MEM-Non Essential Amino Acids Solution-100x	Sigma-Aldrich Chemie GmbH, Taufkirchen, Germany
Mung Bean Nuclease	New England Biolabs GmbH, Frankfurt am Main, Germany
NEBuilder® HiFi DNA Assembly Master Mix	New England Biolabs GmbH, Frankfurt am Main, Germany
N,N-Dimethylformamide	Sigma-Aldrich Chemie GmbH, Taufkirchen, Germany
Orange G	Carl Roth GmbH & Co. KG, Karlsruhe, Germany
Phusion® Hot Start Flex DNA Polymerase	New England Biolabs GmbH, Frankfurt am Main, Germany
Pierce™ IP Lysis Buffer	Thermo Fisher Scientific, Inc., Waltham, MA, USA
Puromycin Dihydrochloride	Merck KGaA, Darmstadt, Germany
Phosphate Buffered Saline (PBS), Powder	Merck KGaA, Darmstadt, Germany
Polyethylene glycol 4000	Merck KGaA, Darmstadt, Germany
Proteinase K, recombinant, PCR grade	Roche Deutschland Holding GmbH, Grenzach-Wyhlen, Germany
Penicillin (10000 units/ml)- Streptomycin (10000 µg/ml) solution	Gibco, Life Technologies GmbH, Darmstadt, Germany
Q5® High-Fidelity DNA Polymerase	New England Biolabs GmbH, Frankfurt am Main, Germany

Quick-Load® 2-Log DNA Ladder	New England Biolabs GmbH, Frankfurt am Main, Germany
Quick Blunting Kit	New England Biolabs GmbH, Frankfurt am Main, Germany
Quick Start™ Bradford Protein Solution	Bio-Rad Laboratories GmbH, Munich, Germany
Restriction endonucleases	New England Biolabs GmbH, Frankfurt am Main, Germany
Ranger Mix DNA Ladder	Meridian Bioscience, Cincinnati, OH ,USA
rAPid alkaline phosphatase	Roche Deutschland Holding GmbH, Grenzach-Wyhlen, Germany
REDTaq® ReadyMix PCR reaction mix	Sigma-Aldrich Chemie GmbH, Taufkirchen, Germany
Saponin	AppliChem GmbH, Darmstadt, Germany
Sodium acetate buffer solution	Sigma-Aldrich Chemie GmbH, Taufkirchen, Germany
Sodium chloride (NaCl)	Merck KGaA, Darmstadt, Germany
Sodium dodecyl sulfate (SDS)	Serva Electrophoresis GmbH, Heidelberg, Germany
Sucrose	Merck KGaA, Darmstadt, Germany
Sodium pyruvate solution	Sigma-Aldrich Chemie GmbH, Taufkirchen, Germany
Tamoxifen Chow	Envigo Corporation, Indianapolis, IN, USA
T4 DNA Ligase	New England Biolabs GmbH, Frankfurt am Main, Germany
Taq DNA Polymerase	PEQLAB Biotechnologie GmbH, Erlangen, Germany
Tissue-Tek® O.C.T. compound	Sakura Finetek Europe B.V, Alphen aan den Rijn, The Netherlands
TransIT®-LT1 Transfection Reagent	Mirus Bio Corporation, Madison, WI, USA
Tris Hydrochloride	J.T. Baker Inc., Phillipsburg, NJ, USA
Tris Pufferan	Carl Roth GmbH & Co. KG, Karlsruhe, Germany
Triton® X-100	Merck KGaA, Darmstadt, Germany
Tween® 20	Carl Roth GmbH & Co. KG, Karlsruhe, Germany
Trypsin-EDTA (0.5%)	Gibco, Life Technologies GmbH, Darmstadt, Germany

2.4 Kit for Molecular Biology

Table 4. Kit for Molecular Biology

Kit	Supplier
GenElute™ Mammalian Genomic DNA Miniprep Kit	Sigma-Aldrich Chemie GmbH, Taufkirchen, Germany
Monarch® DNA Clean-up Kit	New England Biolabs GmbH, Frankfurt am Main, Germany
Monarch® DNA Gel Extraction Kit	New England Biolabs GmbH, Frankfurt am Main, Germany
Monarch® HMW DNA Extraction Kit for Tissue Kit	New England Biolabs GmbH, Frankfurt am Main, Germany
Mouse Tumor Tissue Dissociation Kit	Miltenyi Biotec B.V. & Co. KG, Bergisch Gladbach, Germany
NucleoSpin Plasmid EasyPure DNA purification Mini kit	MACHEREY-NAGEL GmbH & Co. KG, Düren , Germany
NucleoBond Xtra Midi kit for transfection-grade plasmid DNA kit	MACHEREY-NAGEL GmbH & Co. KG, Düren , Germany
NucleoBond Xtra Maxi kit for transfection-grade plasmid DNA kit	MACHEREY-NAGEL GmbH & Co. KG, Düren , Germany
QIAprep® Spin Miniprep Kit	QIAGEN GmbH, Hilden, Germany
RNeasy Protect Mini Kit (250)	QIAGEN GmbH, Hilden, Germany
TruSeq® Stranded mRNA Sample Preparation Kit	Illumina Biotechnology company, San Diego, CA, USA

2.5 Reagents for Histological, IF & IHC staining

Table 5. Histological, IF & IHC staining reagents

Reagent	Supplier
Antigen unmasking solution, citric acid based	Vector Laboratories, Inc., Burlingame, CA, USA
Avidin/biotin blocking kit	Vector Laboratories, Inc., Burlingame, CA, USA
Dako Target Retrieval Solution (pH6)	Dako Deutschland GmbH, Hamburg
DAB substrate kit, Peroxidase (HRP)	Vector Laboratories, Inc., Burlingame, CA, USA
Donkey serum D9663	Sigma-Aldrich Chemie GmbH, Taufkirchen, Germany
Eosin Solution	Merck KGaA, Darmstadt, Germany
Glacial acetic acid	Merck KGaA, Darmstadt, Germany
Goat serum G9023	Sigma-Aldrich Chemie GmbH, Taufkirchen, Germany
Hematoxylin Solution	Merck KGaA, Darmstadt, Germany

Hydrogen peroxide 30%	Merck KGaA, Darmstadt, Germany
Pertex® histology mounting medium	Histolab Products AB, Västra Frölunda, Sweden
Mounting Medium With DAPI	Abcam, Cambridge, UK
Permanent AP Red Kit	Zytomed Systems GmbH, Berlin-Zehlendorf, Germany
ROTI®Histol (Xylene)	Carl Roth GmbH & Co. KG, Karlsruhe, Germany
Roti® Histofix (4% Paraformaldehyde)	Carl Roth GmbH & Co. KG, Karlsruhe, Germany
Super PAP pen	Thermo Fisher Scientific, Inc., Waltham, MA, USA
TOPRO®-3 iodide	Invitrogen GmbH, Karlsruhe, Germany
Vectastain® Elite ABC Kit	Vector Laboratories, Inc., Burlingame, CA, USA
Vectashield® Mounting Medium	Vector Laboratories, Inc., Burlingame, CA, USA

2.6 Competent cell strains and Plasmids

Table 6. Competent bacterial strains

Competent Bacteria	Source
One shot® Stbl3™ chemically competent E. coli	Invitrogen GmbH, Karlsruhe, Germany
One shot® TOP10™ chemically competent E. coli	Invitrogen GmbH, Karlsruhe, Germany

Table 7. Plasmids

Plasmid	Catalog	Source
paavCAG-iCre	#51904	Addgene, Watertown, MA, USA
pAAV-HDR-mEGFP-Actin	#121843	Addgene, Watertown, MA, USA
pcDNA 6.2/GW/D-TOPO	K246020	Thermo Fisher Scientific, Inc., Waltham, MA, USA
pCR™II-TOPO™	K461020	Thermo Fisher Scientific, Inc., Waltham, MA, USA
pCS2+ H2B-mTagBFP2	#99267	Addgene, Watertown, MA, USA
pGEMT-PT2A-iRFP670-Tdtomato-GFP	#111817	Addgene, Watertown, MA, USA
pSpCas9(BB)-2A-Puro (PX459) V2.0	#62988	Addgene, Watertown, MA, USA
pThy1-Brainbow3.1	#45178	Addgene, Watertown, MA, USA
LeGO-mOrange2	#85212	Addgene, Watertown, MA, USA
MSCV-N SV40 ST	#37858	Addgene, Watertown, MA, USA
TLCV2	#87360	Addgene, Watertown, MA, USA
psPAX2	#12260	Addgene, Watertown, MA, USA
pMD2	#12259	Addgene, Watertown, MA, USA
TOPO mKate2	#68441	Addgene, Watertown, MA, USA

2.7 PCR Primers

Primer oligonucleotides were synthesized by Eurofins Genomics (Ebersberg, Bavaria, Germany)

Table 8. Genotyping and Recombination PCR Primers

PCR	Primer ID	Sequence
Rosa26-FSF-CAG	R26-td-E-Mut- Reverse	TCAATGGGCGGGGGTTCGTT
	R26-Tva-GT-Forward	AAAGTCGCTCTGAGTTGTTAT
	R26-Tva-GT-WT- Reverse	GGAGCGGGAGAAATGGATATG
Frt-Stop-Frt	pGL3-pA-pause-4645-Forward	TGAATAGTTAATTGGAGCGGCCGCAATA
	Cre-Neu-Reverse	CCTGGAAAATGCTTCTGTCCG
Cre-ERT2	CreERT2-sc-Forward3	GAATGTGCCTGGCTAGAGATC
	CreERT2-sc-Reverse1	GCAGATTCATCATGCGGA
Pdk1	Pdk1-Forward	ATCCCAAGTTACTGAGTTGTGTTGGAAG
	Pdk1- Reverse	TGTGGACAAACAGCAATGAACATACACGC
FSF-Kras	Kras-WT_ Forward1	CACCAGCTTCGGCTTCCTATT
	Kras-URP_ Reverse1	AGCTAATGGCTCTCAAAGGAATGTA
	R26-Tva-GT-SA-mut_Reverse	GCGAAGAGTTTGTCTCAACC
Pdx-Flp	Gabra1_Reverse	AACACACACTGGAGGACTGGCTAGG
	Gabra1_Forward	CAATGGTAGGCTCACTCTGGGAGATGATA
	Flpopt-sc Reverse	CGTTGTAAGGGATGATGGTGAAC
	Pdx5utr-sc Forward	AGAGAGAAAATTGAAACAAGTGCAGGT
Braf	Braf_Reverse	GCATAGCGCATATGCTCACA
	Braf_Forward1	CCATGCTCTAACTAGTGCTG
	Braf_Forward2	GTTGACCTTGAACCTTCTCC
c-Raf	Raf1-lox-Reverse	AACATGAAGTGGTGTCTCCGGGCGCC
	Raf1-lox-Forward	TGGCTGTGCCCTTGGAACTCAGCACC
	Raf1-Forward-Deleted	ATGCACTGAAATGAAAACGTGAAGACGACG
Trp53 ^{frt}	p53_Frt-Forward	CAAGAGAAGTGTGCCTAAGAG
	p53_Frt-Reverse	CTTTCTAACAGCAAAGGCAAGC
Pdk1 deletion	Pdk1-del-Forward	CTATGCTGTGTTACTTCTTGGAGCACAG
	Pdk1-Reverse	TGTGGACAAACAGCAATGAACATACACGC

Table 9. Molecular cloning and ESC screen Primers

PCR	Primer ID	Sequence
EGFP-PKP_linker amplification	ATG-EGFP-SC- Forward	CTCGCCCTTGCTCACCAT
	PKP-ATG-EGFP-SC- Reverse	GCTCACCATGGGCTTAGG
iCre fragment amplification	iCre- AleI-Forward	TGGTGCCCAAGAAGAAGAGGAA
	iCre- HindIII-Reverse	ATTATCGATAAGCTTTCAGTCCCCATC
PhiYFP-PolyA fragment amplification	PhiYFP-PA- Forward	TTAGCGGCCGCACCTGAGCACCATGGA
		AGTTCCTATTCCGAAGTTCCTATTCTCTA
		GAAAGTATAGGAATTCATGGCTCCTAA
	PhiYFP-PA- Reverse	GAAGAAGAAGAAGGTGAT
		TACCTCGAGGTTAATTAAGCCTTAAGAT
	ACATTGATGAGTTTGGACAAAC	

Materials

Col6a1-LeftArm fragment Amplification	AsiSI-Col6a1-LeftArm-Forward	TATTAGCGATCGCCGGCGATTTAAATGG CCTGCCTATCTGCTTGTGTAGAG
	Col6a1Avitag-LeftArm-Reverse	ACTCGAGGCGGCCGCTACTCGTGCCAC TCGATTTTCTGGGCCTCAAAGATATCGT TCAGGCCAGAGCCACCGGTGCCAGTG CCACCTTCCTGGA
Col6a1-RightArm fragment Amplification	Ascl-Col6a1-RightArm-Forward	GCACGGCGCGCCAGGGCCACACACGT GGCTGGACACTCATTCCATGGAG
	Col6a1-RightArm-Sall-Reverse	GTACGTGACGGGTGCTGTGTTCTCA GTGCTA
mTagBFP2- fragment Amplification	Xbal-mTagBFP2-linker-Forward	TATTCTCTAGAAAGTATAGGAAGTTCCC TAAGCCCATGGTTTTCGAAGGGAGAGGA
	EcoRI -mTagBFP2-PK-Reverse	GATCCGAATTCGCCAGAACCAGCAGCG GAGCCAGCGGATCCGTTGAGCTTATGA CCCAACTTACTAG
Zeb1-LeftArm fragment Amplification	AsiSI-Zeb1-LeftArm-Forward	ATTAGCGATCGCCGGCGATTTACTTACC AGCCACTTACCTA
	Agel-Zeb1- LeftArm-Reverse	ATCGTTCAGGCCAGAGCCACCGGTAGC TTCATTTGTCTTCTCTTCAGACAG
Zeb1-RightArm fragment Amplification	Ascl-Zeb1-RightArm-Forward	GCACGGCGCGCCGAGTTCTTCTAAAAG GAAATTCTTCTTTCTAATG
	Sall-Zeb1-RightArm-Reverse	GTACGTGACGTGACTGAATTCTCATAA CTTCTTGAC
AviTag-P2A-T2A HiFi Assembly	AviTag-HiFi-Forward	AGGTGGCACTGGGCACCGGTGGCTCTG GCCTGAACGATATCTTTGAGG
	P2A-HiFi-Rev	AAGTTCCTATACTTTCTAGAGAATAGGA ACTTCGGAATAGGAATTCCATGGAAGG CCCGGGTTTTCTTCAACA
iRFP670 fragment Amplification	Xbal-iRFP670-Forward	TATTCTCTAGAAAGTATAGGAAGTTCCC TAAGCCCATGGCGCGTAAGGTCGATCT
	EcoRI-iRFP670-Reverse	ATCCGAATTCGCCAGAACCAGCAGCGG AGCCAGCGGATCCAGTGCGTTGGTGGT GGGCGG
Snai1-LeftArm fragment Amplification	AsiSI-Snai1-LeftArm-Forward	TTGTGCGATCGCACAGATTGCCAAGGT CCAC
	Agel-Snai1-LeftArm-Reverse	ATACACCGGTGCGAGGGCCTCCGGAGC AG
Snai1-RightArm fragment Amplification	Ascl-Snai1-RightArm-Forward	TAGGCGCGCCCCCTGCTACCTCCCAT GATCGGTGGCATCTTCCCGGAGCT
	Sall- Snai1-RightArm-Reverse	AATGTCGACCGCCTGCGGGTCACCATT TCCTGTTTAG
Twist1-LeftArm fragment Amplification	AsiSI-Twist1-LeftArm-Forward	GCCGCGATCGCCGTTAGATGGACTCG GTTGT
	Sall-Twist1- LeftArm -Reverse	TCACCGGTGTGGGACGCGGACATGGAC CAG
Twist1-RightArm fragment Amplification	Ascl-Twist1-RightArm-Forward	TTGGCGCGCCAGCGGAGCTCCCCAGC GACTGTGCAGGCCGAGACCTAGGT
	Sall-Twist1-RightArm-Reverse	GCCGTCGACAGTTCGGTAAGAAGTAGG TGTTAGCAAAT
Fsp1-LeftArm fragment Amplification	AsiSI-Fsp1-LeftArm-Forward	AGTGCATCGCCTGGCTTCCCCACCCT CTCCTCT
	Sall- Fsp1- LeftArm -Reverse	ACACCGGTCTTCTTCCGGGGCTCCTTAT CTG

Fsp1-RightArm fragment Amplification	Ascl-Fsp1-RightArm-Forward	TAGGCGCGCCAGACTAGTCACATGAAG TGTTGGGGTGTAGTTTGCCAGT
	Sall-Fsp1-RightArm-Reverse	TACGTCGACTTCACCCCAGAAGCACTG CCCTT
mOrange2 fragment amplification	Xbal-mOrange2-Forward	TATTCTCTAGAAAGTATAGGAACTTCCC TAAGCCCATGGTGAGCAAGGGCGAGGA
	EcoR1-mOrange2-Reverse	ATCCGAATTCGCCAGAACCAGCAGCGG AGCCAGCGGATCCCTTGTACAGCTCGT CCATGCCG
mKate2 fragment amplification	Xbal-mKate2-Forward	TATTCTCTAGAAAGTATAGGAACTTCCC TAAGCCCATGGTGAGCGAGCTGATTAA GGAGAAC
	EcoR1-mKate2-Reverse	GATCCGAATTCGCCAGAACCAGCAGCG GAGCCAGCGGATCCTCTGTGCCCCAGT TTGCTAGGGAG
Px459-Col6a1 sgRNA expression plasmid cloning	Col6a1-sgRNA-oligo-Forward	CACCGCACACGTGGCTGGACACACA
	Col6a1-sgRNA- oligo-Reverse	AAACTGTGTGTCCAGCCACGTGTGC
Px459-Zeb1 sgRNA expression plasmid cloning	Zeb1-sgRNA-oligo-Forward	CACCGTTCTAAAAGGAAATTCTACT
	Zeb1-sgRNA- oligo-Reverse	AAACAGTAGAATTTCTTTTAGAAC
Px459-Snai1 sgRNA expression plasmid cloning	Snai1-sgRNA-oligo-Forward	CACCGGCTCCGGGAAGATGCCAGCG
	Snai1-sgRNA- oligo-Reverse	AAACCGCTGGCATCTTCCCGGAGCC
Px459-Twist1 sgRNA expression plasmid cloning	Twist1-sgRNA-oligo-Forward	CACCGTAGGTCTCCGGCCTGCAGAG
	Twist1-sgRNA- oligo-Reverse	AAACCTCTGCAGGCCGGAGACCTAC
Px459-Fsp1 sgRNA expression plasmid cloning	Fsp1-sgRNA-oligo-Forward	CACCGACACCCCAACTTCATCTG
	Fsp1-sgRNA- oligo-Reverse	AAACCAGATGAAGTGTTGGGGTGTC
TLCV2-Raf1 sgRNA-1 plasmid cloning	Raf1-sgRNA1-oligo-Forward	CACCGACCTGGCGATTGTGACTCAG
	Raf1-sgRNA1-oligo-Reverse	AAACCTGAGTCACAATCGCCAGGTC
TLCV2-Raf1 sgRNA-2 plasmid cloning	Raf1-sgRNA2-oligo-Forward	CACCGCCGAATAAGCAAAGGACTG
	Raf1-sgRNA2-oligo-Reverse	AAACCAGTCCTTTGCTTATTCGGC

Table 10. Validation and Screening Primers

PCR	Primer ID	Sequence
Col6a1-KI-Left side Screening PCR	Col6a1-KI-Left-Screen-Forward	AAGAAGTGTCCGGATTATACCTGTCC
	PhiYFP-KI-Left-Screen-Reverse	GGATCTTGCCGTGGAACAGC
Col6a1-KI-Right side Screening PCR	iCre-KI-Right-sc-Forward	GGCTGGACCAATGTGAACATTG
	Col6a1-KI- Right-Screen-Reverse	CCTTATGGACTTTTGGGGGAGTGATC

Materials

Twist1-KI-Left side Screening PCR	Twist1-KI-Left-Screen-Forward PhiYFP-KI-Left-Screen- Reverse	AGAGGTTTCCGACTAGAGGTTTCCT GGATCTTGCCGTGGAACAGC
Twist1-KI-Right side Screening PCR	iCre-KI-Right-sc- Forward Twist1-KI-Right-Screen-1650- Reverse Twist1-KI-Right-Screen-2100- Reverse	GGCTGGACCAATGTGAACATTG GGTATCACATTGCTTATTTTCAGTGC CCAGCACCATCTGTCCTTGTT
Zeb1-KI-Left side Screening PCR	Zeb1-KI-Left-Screen-Forward PhiYFP-KI-Left-Screen- Reverse	GCCCTTACCAGCCACTTACCT GGATCTTGCCGTGGAACAGC
Zeb1-KI-Right side Screening PCR	iCre-KI-Right-sc-Forward PhiYFP-KI-Left-Screen- Reverse	GGCTGGACCAATGTGAACATTG CATCACCTGGGTCCGTAATAACTAACA
Snai1-KI-Left side Screening PCR	Snai1-KI-Left-Screen-Forward PhiYFP-KI-Left-Screen- Reverse	CACAGATTGCCAAGGTCCACCA GGATCTTGCCGTGGAACAGC
Snai1-KI-Right side Screening PCR	iCre-KI-Right-sc-Forward Snai1-KI- Right-Screen- Reverse	GGCTGGACCAATGTGAACATTG GCCTGCGGGTCACCATTTC
Fsp1-KI-Left side Screening PCR	Fsp1-KI-Left-Screen-Forward PhiYFP-KI-Left-Screen- Reverse	TCCAAGTCTCTGCCGTGCC GGATCTTGCCGTGGAACAGC
Fsp1-KI-Right side Screening PCR	iCre-KI-Right-sc-Forward Fsp1-KI- Right-Screen- Reverse	GGCTGGACCAATGTGAACATTG CCCAAAGGGGAGGCAACGTTA
Col6a1 sgRNA Cleavage Activity	Col6a1 sgRNA_CA-Forward Col6a1 sgRNA_CA -Reverse	TTGAGAAGGCTGTGCAGGAG TGGAACTCCTCCTGTGTTCA
Zeb1sgRNA Cleavage Activity	Zeb1 sgRNA_CA -Forward Zeb1 sgRNA_CA -Reverse	GCAGGCAGCTTAGAGCAGAA ACGTCAGAGGTCCTATCTCCT
Snai1 sgRNA Cleavage Activity	Snai1 sgRNA_CA -Forward Snai1 sgRNA_CA -Reverse	CAACCGTGCTTTTGCTGACC TGGTCCCTTCTGAGACAGTT
Fsp1 sgRNA Cleavage Activity	Fsp1 sgRNA_CA -Forward Fsp1 sgRNA_CA -Reverse	TGCCTGCAGATTATCCTCTCAA TCCCGGAGTTTGCTCTGTTG
Twist1 sgRNA Cleavage Activity	Twist1 sgRNA_CA -Forward Twist1 sgRNA_CA -Reverse	AGCGGGTCATGGCTAACG AGGAGGGGGTGGAATTTGGA
Raf1 sgRNA-1 KO efficiency	Raf1 sgRNA-1_KO-Forward Raf1 sgRNA-1_KO-Reverse	GGAAGCCAGAAGAGCCCTTTT CTTACAACCTGATTCCAGCCCA
Raf1 sgRNA-3 KO efficiency	Raf1 sgRNA-3_KO-Forward Raf1 sgRNA-3_KO-Reverse	TCTGACATAAGGCTCAAAGGGA ATTTGACCTCGTGACCTCTGGA
Mycoplasma contamination testing PCR	Mycoplasma-test-Fwd (Mix)	CGCCTGAGTAGTACGTTTCGC CGCCTGAGTAGTACGTACGC TGCCTGGGTAGTACATTTCGC TGCCTGAGTAGTACATTTCGC CGCCTGAGTAGTATGCTCGC CACCTGAGTAGTATGCTCGC
Mycoplasma contamination testing PCR	Mycoplasma-test-Rev (Mix)	CGCCTGGGTAGTACATTTCGC GCGGTGTGTACAAGACCCGA GCGGTGTGTACAAAACCCGA GCGGTGTGTACAAAACCCGA

Homology directed repair (HDR) vector sequencing	HDR Vector Seq -0	CAGGAAACAGCTATGAC
	HDR Vector Seq -1	CCGCTGCTCATCACCTTCCT
	HDR Vector Seq -2	GAAAGTATAGGAACTTCATGGCT
	HDR Vector Seq -3	GCACCTCGAGGTTAATTAAGC
	HDR Vector Seq -4	TTGTGGTTTGTCCAAACTCATC
	HDR Vector Seq -5	GATCCGAATTCGCCAGAAC
	HDR Vector Seq -6	TTCTGGCGAATTCGGAT
	HDR Vector Seq -7	CTCCATGGAATGAGTGTCCA
	HDR Vector Seq -8	GCTGGTGTGTCCATCCCTGA
TLCV2 plasmid sequencing	HDR Vector Seq -9	GAAATTAATACGACTCACTATAGG
	Human_U6-Forward	GAGGGCCTATTTCCCATGATT

2.8 Embryonic stem cell (ESC) lines

Table 11. Embryonic stem cell (ESC) lines

ESC line	Source
W4/129S6 embryonic stem (ES) cells	Taconic Farms, Inc., Hudson, NY, USA
JM8/ C57BL/6N embryonic stem (ES) cells	The Jackson Laboratory, Bar Harbor, ME, USA

2.9 Softwares

Softwares have been used for data analyzing in this work were listed in table 12.

Table 12. Software List

Software	Source
AxioVision (Version 4.8)	Carl Zeiss AG, Oberkochen, Germany
FACSDiva	BD Biosciences, Franklin Lakes, NJ, USA
FlowJo™ v10.0	, Ashland, OR, USA
Graphpad Prism (Version 8.0)	Graphpad Company, San Diego, CA, USA
ImageJ	University of Wisconsin, Madison, WI, USA
ImageScope v12.3	Leica Biosystems, Wetzlar, Germany
Leica Application Suite X (LAS X)	Leica Biosystems, Wetzlar, Germany
Li-cor Image Studio™ Lite	LI-COR Biosciences, Lincoln, NE, USA
OsiriX MD Viewer v7.0	Pixmeo SARL, Geneva, Switzerland
R v4.0.3	R Core Team
Snapgene (Version 4.3.0)	GSL Biotech LLC, Chicago, IL, USA

3 Methods

3.1 Molecular Biology

3.1.1 Gene-Targeting Vectors Construction

3.1.1.1 Amplification of Homology Arms

For amplification of homology arms (HAs) of gene-targeting vectors, the genome sequence of all EMT-TF genes were downloaded from the Ensembl Genome Database, at least 2 pairs of PCR amplification primers were then designed by Primer-Blast program from NCBI (National Center for Biotechnology Information, Bethesda, Maryland, United States). Meanwhile, restriction recognition sites of *Asi*I and *Age*I, *Asc*I and *Sal*I were added with primers for left arm, right arm amplification individually, which made amplified HAs can be cloned to vector backbone (pCR™II-TOPO™). At the same time, *Avi*Tag sequence was introduced at the 3'-end of the Left Arm PCR product with the Left-Arm reverse primer.

Considering the spCRISPR/Cas9 may also cut the gene-targeting vectors which contain the sgRNA recognition sequence. Two synonymous mutations have been brought into Right Homology Arm forward primer at the core positions (from 5' to 3') of the protospacer adjacent motif (PAM) and crRNA binding region, which can prevent spCRISPR/Cas9 from cutting the targeting vector.

The homology arms for EMT-TF genes were amplified by Phusion® Hot Start Flex DNA Polymerase (Reaction setup and condition see Table 15-1), the PCR products with accurate size were purified with Monarch® PCR & DNA Cleanup Kit. After that, the purified DNA fragments and pCRII vector were further digested by restriction. The PCR products were ligated into vector backbone by T4 ligase, these cloned vectors were amplified in *Stb*I3 chemically competent *E. coli* bacteria. For each cloning reaction, 24 bacteria clones were picked and lysed at 95°C for 10 min, then 2µl of bacterial lysate was used as the DNA template for screening PCR. The plasmid was extracted from positive bacteria clones via MACHEREY-NAGEL NucleoSpin Plasmid EasyPure kit and sequenced with M13-Rev and T7-Pro-Fwd primers for further validation. Meanwhile, the bacteria were stored with glycerol at -80°C freezer.

3.1.1.2 Cloning and Testing for Fluorescent Protein expression Cassettes

In order to simulate the situation of Flp/Frt-mediated DNA recombination, the DNA sequence of enhanced green fluorescent protein (EGFP) with FRT site (FRT-EGFP) has been cloned into pcDNA 6.2 expression vector. In the meantime, the FRT-EGFP plasmid with DNA linker sequences PKP (Pro-Lys-Pro) and GGS (Gly-Gly-Ser) have been cloned for further testing. After that, FRT-PKP-EGFP, FRT-GGS-EGFP plasmids were expanded in *Stb*I3 competent *E. coli* bacteria and extracted with MACHEREY-NAGEL NucleoBond Xtra Midi kit to generate transfection-grade plasmid DNA. Plasmids were transfected into HEK293T and mouse Primary

Pancreatic Tumor Cells (mPPT Cells) individually using QIAGEN Effectene Transfection Reagent. After 48 hours, the transfected cells were sorted by flow cytometer to assess the fluorescence intensity of different EGFP-expressing constructs.

Afterward, the iCre (improved Cre) fragment was inserted behind the EGFP sequence to obtain EGFP-iCre fusion expression cassettes. A similar experiment was performed to select the best EGFP-iCre expression plasmid. The most efficient EGFP-iCre expression vector then was further used for other fluorescent proteins (FPs)-iCre plasmids cloning by XbaI and EcoRI-HF enzyme digestion and T4 ligation (New England Biolabs).

3.1.1.3 Construction of FRT-PhiYFP-PolyA cassette

The FRT-PhiYFP-PolyA fragment was cloned by PCR amplification using Q5® High-Fidelity 2X Master Mix (New England Biolabs). Firstly, restriction enzyme sites of NotI and PacI were introduced at the 5' and 3'- end of FRT-PhiYFP-PolyA PCR fragment simultaneously. Next, the FRT-PhiYFP-PolyA DNA fragment was digested with NotI-HF and PacI enzymes, and then it was inserted into pCRII-HAs vector with the same DNA sticky ends. The plasmids were screened by NotI-HF, PacI digestion and DNA sequencing with primer HDR Vector Seq - 1 (Table 10).

3.1.1.4 Golden Gate Assembly

For the P2A-T2A self-cleaving peptide fragment cloning, a double-strains DNA fragment containing the P2A-T2A sequence was chemically synthesized by Eurofins Genomics Company. The P2A-T2A fragment with AgeI (at the 5' end) and NotI (at the 3' end) restriction enzyme sites was obtained by PCR amplification. Then the digested, purified backbone vector and P2A-T2A DNA fragment were mixed with NEBuilder® HiFi DNA Assembly Master Mix reagent (New England Biolabs) to get the 5'-homology arm- P2A-T2A- homology arm-3' plasmid. The mixed sample was incubated in the thermocycler at 50°C for 15 minutes to assemble the DNA fragment and backbone vector.

3.1.1.5 Construction of the complete targeting vector

In the last step of molecular cloning, the FRT-PKP-FP-iCre fragments were inserted behind the plasmid with FRT-PhiYFP-PolyA cassette and homology arms by enzyme digestion and ligation. Specifically, the backbone vectors and FRT-PKP-FP-iCre fragment were digested with PacI and AscI enzymes at the same time, then the purified vector and fragment were ligated with T4 ligase.

The plasmid was expanded in Stbl3 chemically competent E. coli bacteria, 24 bacteria clones were picked and screen by PCR. The plasmids were extracted from positive bacteria with MACHEREY-NAGEL NucleoBond Xtra Midi kit to get transfection-grade plasmid DNA.

In the end, these plasmids were sequenced with primers of HDR Vector Seq -0 to HDR Vector Seq -9 successively (see Table 10).

3.1.1.6 Cloning of TLCV2-sgLacZ and TLCV2-sgRaf1 plasmids

In the LentiCRISPR v2 (TLCV2) plasmid, the expression of Cas9-P2A-GFP is induced by doxycycline, while the sgRNA and puromycin expression are driven by human U6 and EF-1 α promoter respectively. To disrupt the c-Raf gene in PDAC cells, sgRNAs that target LacZ and Raf1 genes were designed and selected with Online CRISPick (Broad Institute of MIT and Harvard, Cambridge, MA, USA). The DNA oligonucleotides for each single guide RNA (sgRNA) expression were synthesized by Eurofins Genomics. The Forward oligonucleotide (5'-3') and Reverse oligonucleotide (5'-3') at a concentration of 100 μ M were mixed with T4 DNA Ligase Buffer (New England Biolabs), then incubated with each other at 95°C for 5 minutes and cooled down at 25°C for 45 minutes to obtain Double-stranded DNA (Table 13).

Afterwards, 990 μ l of sterile H₂O was mixed with 10 μ l annealed oligonucleotides (1: 100 Dilution). Golden Gate Assembly was performed for TLCV2-sgLacZ and TLCV2-sgRaf1 plasmids cloning according to reaction and condition depicted in Table 14. Then the plasmids were transformed to competent bacteria, single bacteria colonies were picked up from LB agar plates and cultured in LB medium with antibiotic of ampicillin.

Plasmids were extracted from bacteria with MACHEREY-NAGEL NucleoSpin Plasmid EasyPure DNA Purification Mini kit (see 3.1.2.1). These plasmids were validated by DNA sequencing with Human_U6 primer (see Table 10), the plasmids with accurate DNA sequence were used for lentivirus producing.

Table 13. Oligonucleotide annealing conditions

Reaction mix	Conditions
1 μ l Forward oligo (100 μ M)	95°C 5 min
1 μ l Reverse oligo (100 μ M)	25°C 45 min
1 μ l T4 DNA Ligase Buffer	
7 μ l Distilled H ₂ O	

Table 14. Golden Gate Assembly and Conditions

Reaction mix	Conditions
1 μ l TLCV2 (90ng/ μ L)	37°C 5 min
1 μ l annealed & diluted oligo	16°C 10 min
2 μ l T4 DNA Ligase Buffer	55°C 5 min
1 μ l T4 DNA Ligase	80°C 5 min
1 μ l BsmBI (NEB; 10 Unites)	16°C Hold
14 μ l Distilled H ₂ O	

3.1.1.7 Generation of Competent Bacteria

In order to amplify the plasmid for gene targeting, one shot Stbl3 chemically competent *E. coli* bacteria were used for plasmid amplification. The Stbl3 Bacteria for expanding culture was firstly streaked on an Agar-plate without antibiotics, the single bacteria clone was picked up and grew in 5ml LB medium at 25°C for 12 hours.

After that, 4ml of this saturated *E. coli* culture was transferred to 250ml of fresh LB medium and grew at 20°C for around 6 hours until the OD600 value reached 0.3-0.6. Bacteria cells were centrifuged at 1,000g for 10 min at 4°C, the pellet was resuspended with 25ml cold TSB solution and incubated on ice for another 10 min.

In the end, 100µl aliquot bacteria was pipetted into the sterile 1.5ml tube and froze in the liquid nitrogen immediately. All the tubes were transferred and stored at -80°C for long-term storage.

3.1.1.8 Bacterial transformation

First, thawed frozen competent bacteria on ice slowly. Plasmid or ligation reactions were mixed with 5x KCM buffer (5x KCM- 20µl; Plasmid-5µl; Sterile H₂O-75 µl) when competent bacteria was thawing. Afterward, 100µl of DNA solution was mixed with 100µl bacteria gently, incubated at 4°C for 20 min and at room temperature for 10 min sequentially. Then 750 µl LB medium was added into competent bacteria, and the bacteria-containing medium was shaken horizontally at 37°C for 60 min to permit expression of the resistance gene.

In the end, competent bacteria were spread on the Agar plate containing appropriate antibiotics and incubated at 30°C for 16-24 hours until the bacteria clones were plump.

3.1.1.9 Removal of Single-Stranded Extension

The homology arms of targeting vectors for knock-in at EMT-TFs loci were shortened by Restriction enzymes and Mung Bean Nuclease (New England Biolabs). 1.5µg of targeting plasmids were first digested with specific Restriction enzyme at the end of homologous arms, then 1 unit of Mung Bean Nuclease was mixed with 1.0µg of digested plasmid and incubated at 30°C for 30 minutes.

Subsequently, the Mung Bean Nuclease was inactivated by phenol/chloroform extraction, and the plasmid DNA was recovered by method of ethanol precipitation. 200 ng of purified plasmid DNA was taken and mixed with 5 µl 2x T4 Blunt/TA Ligase Master Mix by 5 times of gentle pipetting up and down. The mixture was incubated at room temperature for 15 minutes, then 5 µl of the ligation reaction mixture was used for transformation. Last, the positive plasmids were confirmed by Sanger sequencing.

3.1.2 DNA extraction and purification

3.1.2.1 Plasmid DNA MiniPrep

2~10 mL of a saturated *E. coli* was used for plasmid isolation and purification, bacteria cells were centrifuged in a standard benchtop microcentrifuge for 1 min at 12,000 x rpm, the supernatant was discarded while the pellet of bacteria was kept.

The bacteria pellet was resuspended completely with 250 µl of Resuspension Buffer A1 by vortexing or pipetting up and down. 250 µl Lysis Buffer A2 (with LyseControl Blue) was added after Buffer A1 until there were no cell clumps remaining, the solution was then mixed gently by inverting the tube 5 times and incubated at room temperature for 2 min until lysate appeared clear. Added 300 µl Neutralization Buffer A3 and mixed thoroughly by inverting the tube until LyseControl turned colorless. The bacteria were centrifuged for 10 min at 12,000 rpm at room temperature.

The supernatant from the last step was decanted onto the NucleoSpin® Plasmid TG Column (MACHEREY-NAGEL GmbH & Co. KG), and the column was centrifuged for 30 sec at 12,000 rpm to absorb the plasmid DNA onto the silica membrane of spin column. Subsequently, the of the TG Column membrane was washed with 700 µl Detoxification Buffer and 650 µl Wash Buffer AQ to further clean the DNA on silica membrane. After twice centrifugation at 12,000 rpm, the flow-through was discarded completely, and the column was placed in a clean 1.5ml microcentrifuge tube. In the final step, 50 µl Buffer AE was added to the silica membrane of column. The column was centrifuged for 2min at 12,000 rpm after 1 min incubation at room temperature. Eluted plasmid DNA has been kept at 4°C for short-term storage or at 20 °C for long-term storage.

3.1.2.2 Plasmid DNA Xtra MidiPrep

Inoculated a 3–5 ml starter culture of LB medium with a single colony picked from a freshly streaked agar plate. LB medium was shaken at 300 rpm for 8 h at 37 °C. 200 µl starter culture was diluted into the 200 ml of LB medium (1: 1,000 dilution) containing the appropriate selective antibiotic. The culture then grew overnight at 37 °C and at 300 rpm for 12–16 h.

The bacteria cells were pelleted by centrifugation at 6,000 x g for 10 min at 4 °C and the supernatant was discarded completely. The cell pellet was resuspended completely with 8 ml Resuspension Buffer RES + RNase A by pipetting up and down the cells. 8ml Lysis Buffer LYS was added to the suspension and mixed by inverting the tube 5 times. Afterward, the mixture was incubated at room temperature for 5 min. Meanwhile, 12 ml Equilibration Buffer EQU was applied onto the rim of the NucleoBond® Xtra Column filter (MACHEREY-NAGEL GmbH & Co. KG), the column was emptied by gravity flow. 8 ml Neutralization Buffer NEU was added to the suspension and the lysate was mixed gently by inverting the tube until the blue sample turned

colorless completely. The lysate was simultaneously cleared and loaded onto the column, and the column was emptied by gravity flow.

Column filter and column were washed with 5 ml Equilibration Buffer EQU. After discarded the filter, the column was washed with 8 ml Wash Buffer WASH alone. Next, plasmid DNA was eluted with 5 ml Elution Buffer ELU and collected in a clean 50 ml centrifuge tube. In order to precipitate the eluted plasmid DNA, 3.5 ml room-temperature isopropanol was added to the eluate, it was then centrifuged at 15,000 x g for 30 min at 4 °C. The plasmid DNA pellet was washed with 3 ml 70 % ethanol and eventually dissolved in 250 µl of buffer TE or sterile H₂O.

3.1.2.3 PCR DNA Product Clean-up

The DNA from PCR and other enzymatic reactions were detected by DNA agarose gel electrophoresis firstly. Once the positive band was observed, the DNA sample was diluted with DNA Cleanup Binding Buffer according to the table below (Table 15). The DNA sample and Binding buffer were mixed well by pipetting up and down or flicking the tube. The mixed sample was loaded onto Monarch DNA Cleanup Column (New England Biolabs), spun at 13,000 x g for 1 min. The flow-through was discarded after centrifugation.

The DNA Cleanup Column was washed twice with 200 µl DNA Wash Buffer for each time. In order to remove the Wash Buffer completely, the column containing DNA was centrifuged again for 2 min at 13,000 x g. In the end, 15 µl prewarmed DNA Elution Buffer or sterile H₂O was added to the center of the column membrane, spun at 13,000 x g for 2 min to elute the purified DNA.

Table 15. Ratio of Binding Buffer and DNA Sample

Sample Type	Ratio of Binding Buffer: Sample	Example
dsDNA > 2 kb (plasmids, gDNA)	2 : 1	200 µl :100 µl
dsDNA < 2 kb (some amplicons, fragments)	5 : 1	500 µl :100 µl
ssDNA (cDNA, M13)	7 : 1	700 µl :100 µl

3.1.2.4 DNA Gel Extraction

The DNA fragment needs to be purified was excised from the Agarose Gel using a clean scalpel. After trimming the excess Agarose, it was transferred to a 1.5 ml microcentrifuge tube and the gel slice was weighed. 4 volumes of Monarch Gel Dissolving Buffer was added to the tube with the gel slice (e.g., 400 µl buffer per 100 mg agarose). The tube containing agarose gel slice was incubated with the Thermomixer at 50°C for 5- 10 minutes, the sample was inverted periodically until the gel slice is completely dissolved.

During this time, a Monarch® DNA Gel Extraction column (New England Biolabs) was inserted into a 2 ml collection tube, the sample was then loaded onto the column. The tube was spun at 13,000 x g for 1 minute, then the flow-through was discarded. After that, 200 µl DNA Wash Buffer was added into the column, the tube was spun at 13,000 x g for 1 minute. The column was centrifuged again for 2 min at 13,000 x g to remove Wash Buffer completely. In the end, 15 µl pre-warmed DNA Elution Buffer or sterile H₂O was added to the center of the column membrane, spun at 13,000 xg for 2 min to elute the purified DNA.

3.1.2.5 Genomic DNA isolation

Cells were released with trypsin and centrifuged in a 1.5 ml clean tube at 300 x g to get the pellet, cell culture medium was completely by the aspirator. The pellet was resuspended with 200 µl of Resuspension Solution, then 20 µl of RNaseA Solution was added into the pellet to remove the cell RNA, and the tube was incubated for 2 minutes at room temperature. Next, 20 µl of the Proteinase K solution was added to the sample, followed by 200 µL of Lysis Solution C. The sample was mixed thoroughly with vortex for about 15 seconds and incubated at 70 °C for 10 minutes.

For mammalian tissue DNA extraction, a piece of fresh or frozen tissue was quickly minced and weighed (the frozen tissue was thawed slightly on ice before slicing, the ice can protect against DNA degradation). The tissue was cut into small pieces to enable more efficient lysis and transferred to a DNase-free 1.5 ml microcentrifuge tube. In order to digest tissue, 180 µl of Lysis Solution T was added to the sample, followed by 20 µl of the Proteinase K solution to the tissue. The tissue was incubated at 55 °C for around 12 hours with a thermomixer until it was completely digested and no particles remain. After digestion, 200 µl of Lysis Solution C was added to the sample and it was mixed thoroughly with vortex for about 15 seconds, and incubated at 70 °C for 10 minutes.

Before loaded the samples to the GenElute™ Miniprep Binding Column, the column was activated with 500 µl of the Column Preparation Solution and centrifuge at 12,000 x g for 1 minute, the flowthrough liquid was discarded. 200 µL of ethanol (95–100%) was added to the lysate; mixed thoroughly by vortexing for 10 seconds to get the homogeneous solution. The entire content of the tube was transferred into the treated binding column from the last step. The column was centrifuged at 13,000 x g for 1 minute. The collection tube containing the flowthrough liquid was discarded and the binding column was placed in a new 2 ml collection tube.

The column was washed with 500 µl of Wash Solution and centrifuge for 1 minute at 13,000 x g. The flowthrough liquid was discarded and the binding column was placed in a new 2 ml collection tube. Column was washed with 500 µl of Wash Solution again and centrifuged for 3 minutes at maximum speed (16,000 x g) to dry the binding column.

200 µL of the prewarmed Elution Solution was added directly into the center of the binding column, then the column was incubated for 5 minutes at room temperature after adding the Elution Solution. In the end, column was centrifuged for 2 minutes at 13,000 x g to elute the DNA. The concentration of genomic DNA was then measured by NanoPhotometer® NP80 for PCR reaction or DNA sequencing.

3.1.3 Polymerase Chain Reaction

Polymerase chain reaction (PCR) was used for obtaining DNA fragments with Phusion Hot Start Flex DNA Polymerase (NEB). Validation of ESC clones was performed with HotStarTaq DNA Polymerase (QIAGEN). While Taq DNA Polymerase 2x-PreMix (Thermo Fisher Scientific) was used for Bacterial colony screening, Recombination PCR, mouse genotyping and mycoplasma contamination testing.

All the annealing temperatures and PCR products size of ESC clones PCR validation, Recombination PCR and mouse genotyping were listed in table 20.

Table 16. Reaction Setup and Thermocycling conditions for DNA fragment amplification

Component	Volume	Conditions		
Template DNA	2 µl (120ng)			
5X Phusion HF Buffer	10 µl	98°C	30 Seconds	x 30 cycles
10 µM Forward Primer	2.5 µl	98°C	10 Seconds	
10 µM Reverse Primer	2.5 µl	54- 68°C	30 Seconds	
10 mM dNTPs	1 µl	72°C	30 Seconds/kb	
Phusion Hot Start Polymerase	0.5 µl	72°C	10 Minutes	
Nuclease-free water	31.5 µl	16°C	Hold	

Table 17. Reaction Setup and Thermocycling conditions for ESC clones validation (Touch-Down PCR)

Component	Volume	Conditions		
Template DNA	2 μ l (120ng)	95°C	15 Minutes	
10x Taq PCR Buffer	5 μ l	70°C	135 Seconds	
10 μ M Forward Primer	2.5 μ l	94°C	30 Seconds	
10 μ M Reverse Primer	2.5 μ l	68°C	135 Seconds	
10 mM dNTPs	1 μ l	94°C	30 Seconds	ΔT -0.5°C x 18 cycles
HotStarTaq DNA Polymerase	0.5 μ l	68°C	45 Seconds	
Distilled Water	36.5 μ l	68°C	135 Seconds	Δt +2s
		94°C	30 Seconds	
		58°C	40 Seconds	x 39 cycles
		68°C	3 Minutes	
		68°C	5 Minutes	
		22°C	Hold	

Table 18. Reaction Setup and Thermocycling conditions for genotyping

Component	Volume	Conditions		
Template DNA	1 μ l (100ng)	95°C	3 Minutes	
2x PCR Master Mix	12.5 μ l	95°C	30 Seconds	x 40 cycles
10 μ M Forward Primer	1 μ l	T _m - 5°C	30 Seconds	
10 μ M Reverse Primer	1 μ l	72°C	60 Seconds/kb	
Distilled Water	9.5 μ l	72°C	15 Minutes	
		16°C	Hold	

Table 19. Reaction Setup and Thermocycling conditions for mycoplasma contamination testing

Component	Volume	Conditions		
Template DNA	2 μ l	95°C	15 Minutes	
2x PCR Master Mix	15 μ l	94°C	30 Seconds	x 40 cycles
Mixed Forward Primer (10 μ M each)	2 μ l	60°C	60 Seconds	
Mixed Reverse Primer (10 μ M each)	2 μ l	74°C	60 Seconds	
Distilled Water	9 μ l	72°C	10 Minutes	
		16°C	Hold	

Table 20. Annealing temperatures and PCR products

(Mut=Mutant Allele; WT=Wild Type Allele; Rec=Recombined Allele; KI= Knock-In Allele)

PCR Reaction	Annealing Temperature	Size of PCR Product (bp)
R26-FSF-CAG	62°C	450bp (Mut) /650bp (WT)
FSF-Stop	60°C	800bp (Mut)
CreERT2	55°C	190bp (Mut)
Pdx-Flp	56°C	620bp (Mut) /300bp (Internal Control)
FSF-Kras	55°C	350bp (Mut) /270bp (WT)
Trp53-Frt	57°C	292bp (Mut) /258bp (WT)
Pdk1 ^{flox}	63°C	280bp (Mut) /200bp (WT)
Braf ^{flox}	63°C	413bp (Mut) /357bp (WT)
C-Raf ^{flox}	58°C	250bp (Mut) /180bp (WT)
FSF-Kras Del	58°C	196bp (Rec)
Pdk1 Del	63°C	250bp (Rec) /380bp (Mut) /310bp (WT)
Braf Del	63°C	282bp (Rec) /413bp (Mut) /357bp(WT)
c-Raf Del	58°C	350bp(Rec) /250bp (Mut) /132bp (WT)
Twist1-KI-Left	Touch-Down	1617bp (KI)
Twist1-KI-Right	Touch-Down	2102bp (KI)
Snai1-KI-Left	Touch-Down	1775bp (KI)
Snai1-KI-Right	Touch-Down	1359bp (KI)
Fsp1-KI-Left	Touch-Down	1862bp (KI)
Fsp1-KI-Right	Touch-Down	1607bp (KI)
Zeb1-KI-Left	Touch-Down	1748bp (KI)
Zeb1-KI-Right	Touch-Down	1049bp (KI)
Col6a1-KI-Left	Touch-Down	1447bp (KI)
Col6a 1-KI-Right	Touch-Down	3933bp (KI)

3.1.4 Agarose gel electrophoresis

All the PCR products and restriction digestion reactions were validated by DNA agarose gel electrophoresis firstly. Generally, 1% - 2% DNA garose gel (4g - 8g agarose powder in 400 ml 1xTAE buffer) was use for agarose gel electrophoresis depend on the size of PCR or restriction digestion products. In order to observe the progress of the electrophoresis, gel loading buffer contains colored dyes (Orange G solution/Gel Loading Purple) was mixed with the DNA sample, then DNA samples were loaded into the wells of DNA Gel. 5µl DNA ladder was also loaded in the well and ran together with samples for estimation of the molecular weight of the

DNA bands. Here GeneRuler™ 100 bp DNA Ladder (size range up to 1,000 bp) and Ranger Mix DNA Ladder (size range from 100bp to 10 kb) were used for estimation. The agarose gel was then ran at the 120V for 1-2 hours until the expected bands were completely distinguished or separated.

Normally, the DNA agarose gel was stained with ethidium bromide (0.06mg/L) for visualization, images were taken by UVP UVsolo touch gel documentation system (Analytik Jena). While for DNA Gel purification, GelStar Nucleic Acid Stain (Lonza) was used for visualization. In this case, the agarose gel solution was prepared and cooled to 55°C - 60°C, then 10 µl of stain stock added to each 100 ml of gel solution. DNA bands were visualized with Flu-O-Blu blue light table, the bands with correct size were cut with clean scalpel.

3.1.5 RNA isolation and purification

Cells for RNA isolation were cultured in the 10cm dishes until their confluency was 50-80%. When cells were confluent enough, we aspirated the cell culture medium, and washed cells with 5ml 1x DPBS (Thermo Fisher Scientific). After 1x DPBS has been removed, cells were trypsinized with 1ml 0.5% Trypsin-EDTA (Gibco) at 37°C for 3 min. When cells were detaching from the dish, 4ml cell culture medium (contains 10% serum, 1% Penicillin-Streptomycin) was added to inactivate the trypsin. All the cells were transferred to an RNase-free polypropylene centrifuge tube and centrifuged at 1,000 rpm for 5min at 4°C, the supernatant was completely aspirated afterwards.

In order to disrupt the cells, 350 µl Buffer RLT (contains 1% β-mercaptoethanol) was added to the cell pellet, RLT buffer and cell pellet were mixed by vortex. Then cell lysate was transferred into a spin column (QIAGEN QIAshredder) and centrifuged for 2 min at the max speed to remove cell debris. After that, 1 volume of 70% ethanol was added to the homogenized cell lysate, and they were mixed by pipetting. The mixed sample was transferred to each RNeasy spin column (QIAGEN) completely by centrifuging at 13,000 rpm for 2min.

700 µl Buffer RW1 was added to the RNeasy spin column after discarded the flow-through, the RNeasy spin column was centrifuged for 1 min 13,000 rpm to wash the spin column membrane. Another 500 µl Buffer RPE was added to the RNeasy spin column and centrifuged for 1 min 13,000 rpm for spin column membrane further washing. In order to remove ethanol from column membrane completely, RNeasy spin column has been centrifuged again at 13,000 rpm for 2min.

In the last step, RNeasy spin column was placed in a new 1.5ml RNase-free collection tube, 50 µl RNase-free water was added directly to the center of the spin column membrane and the tube was centrifuged at 13,000 rpm for 2min to elute the RNA.

3.1.6 RNA sequencing

In order to deeply understand the changes of gene expression in PDAC cells after Pdk1, Braf and c-Raf genes have been deleted which may support for developing new treatment methods of pancreatic cancer, the Next Generation Sequencing (NGS) technology was used for whole RNA sequencing in this work.

First, the RNA of cells was isolated as described in section 3.1.5. Then the whole RNA was converted into a cDNA library with TruSeq® Stranded mRNA Sample Preparation Kit. After that, adapters were added to each end of the cDNA fragments, these adapters containing functional elements which could be sequenced with the HiSeq2500 sequencing system. Once the transcript data has been produced, the RNAseq data was aligned to the mouse genome with TopHat (Trapnell *et al.*, 2009), and the data was analyzed with software of RSEM and BitSeq.

3.2 Cell culture

3.2.1 Primary Pancreatic tumor cell line isolation

All the pancreatic tumor cell lines were isolated from tumor mice. These tumor mice were housed in our Specific-pathogen-free (SPF) animal facility until they had solid tumor in pancreas. After the tumor mouse was dissected, one or more pieces of tumor tissue were taken with clean scissors and forceps. The tumor tissues were minced by sterile scalpels under the working biological safety cabinet (Thermo Fisher Scientific), the minced tumor tissues then were transferred into clean 15ml centrifuge tubes with 5ml fresh cell culture medium (Table 16-1) containing 1,000 Units Collagenase Type II (Gibco).

After that, the tumor tissues were pipetted and incubated in 37 °C water bath for 12 hours. On the second day, the digested tissues were centrifuged at 1,200 rpm for 5min and resuspended again with 10ml prewarmed medium. All the medium containing tumor tissues were transferred into cell culture flasks for tumor cells expanding.

Table 21. Composition of primary tumor cell culture medium

Reagent	Quantity
Dulbecco's Modified Eagle Medium (DMEM) - High Glucose	445 ml
Fetal Calf Serum	50 ml
Penicillin-Streptomycin (10,000 U/mL)	5 ml

3.2.2 Cell passage

All the cell lines were passaged when they were at 80-90% cell confluence. The cell culture medium was removed by aspirator firstly, then the cells were washed with 5ml sterile 1x DPBS.

1ml prewarmed 0.5% Trypsin-EDTA (Gibco) was added to each dish/flask after DPBS was removed, the dishes/flasks were incubated at 37°C for 5 min to trypsinize cells completely. When cells were detached, 5ml cell culture medium was added to each dish for Trypsin inactivation. The cells were transferred to a 15ml centrifuge tube and centrifuged at 1,200 rpm for 5min.

The supernatant was discarded after centrifugation, cell pellet was resuspended with 5ml prewarmed cell culture medium, 0.5 ml - 1ml homogeneous single cell suspension was transferred to a new dish/flask containing fresh cell culture medium for passaging.

3.2.3 Cryopreservation of cell lines

Cell lines were freeze when they were at 80-90% cell confluence. The cell culture medium was removed by aspirator firstly, then the cells were washed with 5ml sterile 1x DPBS. 1ml prewarmed 0.5% Trypsin-EDTA was added to each dish/flask after DPBS was removed, the dishes/flasks were incubated at 37°C for 5 min to trypsinize cells completely. When cells were detached, 5ml cell culture medium was added to each dish for Trypsin inactivation. The cells were transferred to a 15ml centrifuge tube and centrifuged at 1,200 rpm for 5min.

Cell pellet was resuspended with 3ml freezing medium (Table 22) by pipetting up and down three times. 1ml homogeneous single cell suspension was transferred to a cryovial, the cryovials were put into prefroze Cryo Freezing Container (Thermo Fisher Scientific) and stored at -80°C freezer. On the next day, the frozen cells were transferred to Liquid Nitrogen Container for long term reservation.

Table 22. Composition of primary tumor cell freezing medium

Reagent	Quantity
DMEM - High Glucose	6 ml
Fetal Calf Serum	2 ml
DMSO	2 ml

3.2.4 Cell transfection

Cell transfections were performed with Effectene Transfection Reagent (QIAGEN) and TransIT®-LT1 Transfection Reagent (Mirus Bio) separately for different experiments.

For general cell transfection, 2.5×10^6 cells were seeded in each well of 6-well plate containing 2ml complete growth medium approximately 24 hours before transfection. 600 µg plasmid DNA was mixed with DNA-condensation Buffer EC to a total volume of 100 µl, and 4.8 µl Enhancer was added to DNA-Buffer EC. The mixed solution was then incubated at Room Temperature (15–25°C) for 5 minutes. After that, 10 µl Effectene Reagent was added to the DNA–Enhancer

solution and mixed by vortexing for 10 seconds. The samples was incubated for another 10 minutes at room temperature to allow transfection-complex formation. 600 μ l prewarmed cell culture medium was added to the transfection complexes and mixed by pipetting up and down twice, then these transfection complexes were added drop-wise in each well of 6-well plate. For lentivirus produce, 1.0×10^6 HEK293FT cells were seeded in the 10 cm dish with 10 ml fresh cell growth medium 16-24 hours before transfection. On the next day, TransIT-LT1 Reagent: DNA transfection complex was prepared at the room temperature according to ratio in the table 15. The mixture was incubated for 15 minutes at room temperature to allow transfection-complex formation. In the end, the TransIT-LT1 Reagent: DNA complexes was added drop-wise to different areas of the 10 cm dish, the dish was swirled gently afterwards to ensure uniform distribution of the complexes.

3.2.5 Lentivirus production and infection

For Lentivirus producing, transfer plasmid TLCV2, packaging plasmid psPAX2 and envelope plasmids pMD2 were delivered into HEK293FT cells by TransIT-LT1 Transfection Reagent as we described in 3.2.4. Cell growth medium was exchanged with 10 ml fresh medium at 24th-hour post-transfection. After 48 hours, the viral supernatant was collected and filtered with a 0.45 μ m filter. The viral supernatant was then divided into small aliquots and frozen at -80 °C. At the same time, 2.0×10^5 targets were seeded in a 6-well plate with 2ml fresh medium in each well. The cell culture medium was replaced with 1ml of fresh media containing 8 μ g Polybrene when cells were 50% confluent. 100 μ l viral supernatant was added to each well of 6-well plate, then cells were centrifuged at 800 rpm for 30min at 33 °C for increasing the lentivirus infection efficiency. 24 hours after infection, the medium containing lentivirus was removed completely, and 2ml fresh medium was added to each well. On the next day, the medium was replaced with 2ml fresh medium with Puromycin (3 μ g/ml) every day, until the uninfected control cells were all dead.

3.2.6 Doxycycline-inducible Gene Expression

Doxycycline with the concentration of 3 μ g/ml was used for inducing Cas9 and EGFP expression after lentivirus infection. 1.0×10^6 cells selected by Puromycin were seeded in 10 cm dish. After 24 hours, cell culture medium was changed with fresh medium with Doxycycline, cells were incubated at cell culture incubator for another 48 hours. GFP positive cells were sorted by flow cytometer, these GFP positive cells were seeded into a new 10 cm dish and treated with Doxycycline for another 48 hours afterward. Cell RNA, DNA and protein were isolated from these GFP+ cells at the endpoint for further detection.

3.2.7 Fluorescence-activated cell sorting (FACS)

Cells were sorted by BD FACSAria III Cell Sorter 48 hours after transfection. Cells were trypsinized and centrifuged firstly, cells pellets were resuspended with 400 μ l FACS medium (2% FCS in PBS). Cells were transferred to a clean 1.5 ml centrifuge tube and stained with Zombie Aqua in the dark environment for 10 min on the ice. After that, cells were filtered by the 70 μ m cell strainer and collected with the Flow Cytometry tube. Afterward, the fluorescence positive cells were collected in the sterile Flow Cytometry tube with 2ml fresh cell growth medium and seeded in 10 cm dish.

3.2.8 Immunofluorescence staining for adherent cell

The sterile coverslip was coated with 500 μ l 0.2% gelatin at 37°C for 1 hour, 2.0×10^5 cells were then grown on the glass coverslip in the well of 6-well plate. 48 hours after transfection, cell growth medium was removed, cells were washed with 1 ml ice-cold PBS three times.

The cells were fixed with 4% paraformaldehyde (PFA) in PBS pH 7.4 for 10 min at room temperature and washed with 1ml ice-cold PBS twice. Cells were incubated with 1% BSA in PBST (PBS+ 0.1% Tween 20) for 30 min to block unspecific binding of the antibodies. After the step of blocking, cells were incubated with TO-PRO®-3 or DAPI for 3 min, rinsed with PBS. The coverslip was mounted with a drop of mounting medium, sealed with nail polish to prevent drying and movement under the microscope.

3.2.9 MTT assay

Primary PDAC cells (triplicate) were seeded in each well of 96-well plate with a concentration of 1,000 cells/ well in 100 μ l culture growth medium containing 10% FCS and 1% Penicillin-Streptomycin (10,000 U/mL). Cells were incubated at 37 °C with 5% CO₂ for 24 hours. After the incubation period, 10 μ l of the MTT reagent (0.5 mg/ml) was added to each well. The 96-well microplate was incubated at 37°C atmospheres for 4 hours. The medium and MTT reagent was removed after 4 hours of incubation, and 200 μ l DMSO/Absolute EtOH (1:1) was added to each well, then the plate was shaken at 100 rpm for 15min. The absorbance of the cell samples was measured by CLARIO star Plus Microplate Reader.

3.2.10 CellTiter Glo luminescent cell viability assay

1,000 PDAC cells were seeded in each well of the opaque-walled 96-well plate with 100 μ l cell growth medium. At the same time, three control wells containing medium without cells were prepared to obtain a value for background luminescence.

The test compounds were added to each experimental wells on the next day, and incubated at 37 °C with 5% CO₂ for 72 hours. After incubation, 25 μ l of CellTiter-Glo Reagent was added

to each well of the plate. The contents were mixed for 5 minutes on an orbital shaker to induce cell lysis. The plates were incubated at room temperature for another 10 minutes to stabilize the luminescent signal. In the end, the luminescence intensity of the cell samples was recorded by CLARIO star Plus Microplate Reader.

3.2.11 Clonogenic Assay

For the gene deletion experiment, 1.0×10^6 PDAC cells in 10 cm dish were firstly treated with 0.1% Ethanol (10 μ l of absolute ethanol in 10 ml medium) and Tamoxifen for 8 days separately. After treatment, 2,000 cells from each group were seeded in each well of 6-well plate with 2 ml cell culture medium until the ethanol-treated cells were 80-90% confluent. Cells were washed with PBS and stained with 1% crystal violet at room temperature for 10 minutes. Cells were washed with tap water for 3 minutes after crystal violet has been removed. The plate was inverted on the bench overnight to dry the water completely.

For inhibitor screening experiment, 2,000 untreated cells were seeded in each well of 24-well plate with 500 μ l complete medium. The next day 150 μ l of medium containing inhibitors was added into each well, the cells were then cultured at 37 °C with 5% CO₂. The medium (with the same concentration of inhibitor) was changed every 5 days until the cells in control the group at 80-90% confluence. Cells were stained with crystal violet as described above.

3.2.12 Caspase-Glo 3/7 Assay

1,000 PDAC cells were cultured in each well of the white-walled 96-well plate containing 100 μ l culture medium per well. Cells were divided into two groups: Ethanol and Tamoxifen treatment, each treatment group was in triplicate (3 wells in each 96-well plate). The positive control wells were treated with 500 nM bortezomib to induce apoptosis 36 hours after seeding. After 48 hours of culturing, 100 μ l of Caspase-Glo 3/7 Reagent was added to each well of the 96-well plate. The contents of wells were mixed by a plate shaker at 300 rpm for 3 minutes and incubated at room temperature for 30 minutes. The luminescence of each sample was measured by the plate-reading luminometer.

3.2.13 Drug treatment

1,000 *Pdk1*^{WT} and *Pdk1* ^{Δ} PDAC cells were first seeded in each well of 96-well plate respectively. 16 hours after cell seeding, inhibitors were added to each well and mixed them well by gentle pipetting. After 72 hours of drug treatment, 25 μ l CellTier Glo reagent was added directly to each well to determine cell viability based on quantification of ATP present, and the luminescence value of the cells was measured and recorded using CLARIO star Plus

Microplate Reader (BMG Labtech GmbH, Germany). The detailed information of inhibitors is listed in the table 23.

Table 23. Information of inhibitors

Inhibitor	Supplier	Catalog number
Sorafenib (BAY 43-9006)	Selleck Chemicals LLC, Houston, TX, USA	S1040
AZ628	Selleck Chemicals LLC, Houston, TX, USA	S2746
PLX4720	Selleck Chemicals LLC, Houston, TX, USA	S1152
CEP32496	Selleck Chemicals LLC, Houston, TX, USA	S8015
BAW2881	Selleck Chemicals LLC, Houston, TX, USA	S8189
Ro5126766	Selleck Chemicals LLC, Houston, TX, USA	S7170
Vemurafenib	Selleck Chemicals LLC, Houston, TX, USA	S1267
Dabrafenib	Selleck Chemicals LLC, Houston, TX, USA	S2807

3.3 Mouse Embryonic Stem Cell (mESC) culture

3.3.1 Generation of Puromycin-resistant feeder cells

The primary mouse embryonic fibroblasts (PMEFs) were used as feeder cells to maintain mouse ESC in the undifferentiated state in my experiments. Puromycin-resistant MEF cell line SNLP 76/7-4 was purchased from ATCC Company, and expanded in 40 x 15cm dishes. 5 plates of MEF were frozen as back-up cells, the rest of MEFs were trypsinized with 0.25% Trypsin- 0.53 mM EDTA at 37°C for 5 minutes until cell layer was dispersed. 6 ml of complete growth medium was added to inactive Trypsin-EDTA, the supernatant was removed by aspirator after centrifugation. The cell pellets were resuspended with 40 ml MEF growth medium (Table 21) and transferred to the 50 ml Falcon tube. These cells were immediately irradiated under 34 Gray irradiation dose for 16 minutes. After X-ray irradiation, the irradiated MEFs were centrifuged at 1200 rpm for 5 minutes and resuspended with 42 ml freezing medium, cells were frozen in the cryopreservation tube with a concentration of 2×10^6 cells per 1 ml. Cell culture medium from MEFs culturing was taken for mycoplasma testing before and after irradiation.

3.3.2 Mouse ESC Culturing, Passaging and Cryopreservation

One day before starting of ESC culture, a 10 cm dish or T75 flask was coated with 0.1% Gelatin at 37 °C for at least 1 hour. After the Gelatin has been removed, MEF cells were cultured in the dish or flask with 15 ml fresh MEF culture medium. On the next day, changed the MEF

culture medium to ESC culture medium (Table 24) in the cell culture dish, W4 or JM8 ESC were thawed and cultured on the monolayer of MEF cells.

ESCs were passaged every 2-3 days before the spontaneous differentiation take place. Firstly, the ESC growth medium was removed by the aspirator, ESCs were rinsed with 5ml PBS. 1ml 0.25% Trypsin- EDTA was added to trypsinize the cells. After 3-5 minutes of incubation at 37 °C, the trypsinization was inactivated with 5 ml complete ESC growth medium, cells were resuspended by pipetting several times, 1/8-1/5 volume of whole cells were seeded in a new culture dish with cultured MEF.

For ESC cryopreservation, 5ml fresh ESC freezing medium was prepared before the start of trypsinization. The trypsinized cells were centrifuged at 1200 rpm for 5 minutes at room temperature, and the supernatant was removed by an aspirator. Cell pellets were suspended with 5ml ESC freezing medium (Table 25), and transferred to cryovials. Cells were then frozen slowly in the Cryo 1°C Freezing Container (Thermo Fisher) and stored in the liquid nitrogen for the long-term storage.

Table 24. Composition of ESC culture medium

Reagent	Quantity
KnockOut™ DMEM	405 ml
Fetal Calf Serum	75 ml
L-Glutamin (200 mM)	5 ml
Non-Essential Amino Acids (100X)	5 ml
Sodium Pyruvate (100 mM)	5 ml
Penicillin-Streptomycin (10,000 U/mL)	5 ml
β-Mercaptoethanol (10 ⁻¹ M)	0.5 ml
Leukemia Inhibitory Factor (10 ⁷ Units/ml)	50 μl

Table 25. Composition of ESC freezing medium

Reagent	Quantity
KnockOut™ DMEM	6 ml
Fetal Calf Serum	3 ml
DMSO	1 ml

3.3.3 CRISPR/Cas9 Cleavage Assay

The CRISPR/Cas9 cleavage assay was performed to test the cleavage efficiency of guide RNAs (gRNAs) which are targeting different EMT-TF locus. First, the DNA fragments containing gRNA targeting sequence were amplified from wild-type genomic DNA by PCR. 5

µl of each PCR product was validated by Agarose Gel electrophoresis and the rest of PCR products were purified by Monarch PCR & DNA Cleanup Kit. Meanwhile, crRNAs (target DNA sequence see Table 19), tracrRNA and Cas9 Protein with nuclear localization signal (Cas9-NLS protein) were prepared to form Ribonucleoprotein (RNP) complex in the DNase-free Hood. Next, the purified DNA fragments were mixed with RNP in the Biopur tubes (Eppendorf) respectively as described in Table 19, and the mixtures were incubated at 37°C for 1 hour afterwards.

After 1 hour incubation, 1 µl of RNase A was added into each reaction to hydrolyzes crRNA and tracrRNA, then DNA samples were loaded into the DNA Agarose Gel for electrophoresis. In the end, the images of DNA gel were taken by the UVP UVsolo touch gel documentation system to detect the cleavage efficiency of gRNAs.

Table 26. Target gene and DNA sequence of crRNAs

Target gene	Target DNA sequence	Orientation
Twist1	TAGGTCTCCGGCCTGCAGAG	Antisense
Zeb1	TTCTAAAAGGAAATTCTACT	Sense
Snai1	GCTCCGGGAAGATGCCAGCG	Antisense
Col6a1	CACACGTGGCTGGACACACA	Sense
Fsp1	ACACCCCAACACTTCATCTG	Antisense

Table 27. Cas9 Cleavage Assay Reaction Setup

Reagent	Quantity
Purified PCR product	150 ng
CrRNA (20 µM)	0.5 µl
TracrRNA (44.5 µM)	0.5 µl
10X NEB Buffer 3.1	1.5 µl
Cas9 protein	1.0 µg
Nuclease-Free H ₂ O	to 15 µl

3.3.4 ESC Electroporation

ESCs were digested with trypsin-EDTA for 3-5 minutes at 37 °C, the reaction was stopped with 4ml ESC culture medium, pipetted into a clean 15 ml falcon tube. Meanwhile, cells were counted in a Neubauer hemocytometer, and 1x 10⁷ cells were taken for centrifuging. The cell pellet was resuspended with 700 µl sterile PBS, and mixed with 20 µg of gene targeting donor plasmid, 15 µg of CRISPR/Cas9 protein and guide RNA. The mixed contents were transferred into a sterile 0.4 cm-gap GenePulser electroporation cuvette. After that, electroporation was performed using Bio-Rad Gene Pulser II under the parameter of 250 V, 500 µF. 600 µl

prewarmed ESC medium was added into the cuvette immediately after the electroporation, and cells were incubated at room temperature for 1 minute to ease the burden of electroporation. Afterward, cells were transferred to a new 10 cm dish with a monolayer of MEF cells and 12 ml fresh ESC growth medium.

3.3.5 Puromycin selection

ESC puromycin selection started at 24th hour after electroporation. The ESC growth medium was removed by aspirating and cells were washed with 5ml sterile PBS to remove the dead cells. Afterward, 12 ml fresh ESC culture medium containing puromycin (3 µg/ml) was added to the 10 cm dish. Meanwhile, equal volume of puromycin selection medium was also added to the Mock transfection cell culture dish. The selection medium was changed daily until the ESCs were totally dead in the control dish, puromycin selection medium was replaced with normal ESC culture medium for another 12 hours culture.

3.3.6 Picking of positively transfected ESC

One day before picking ESC clones, two 48-well plates were layered with mitotically inactivated MEFs in D10 medium. Prior to picking of ESC colonies, all the surfaces of equipment such as Microscope, Manual pipette were sterilized with 80% ethanol and UV lights for at least 30 minutes. The MEF culture medium was changed to complete ESC growth medium just before picking ESC clones. Meanwhile, one sterile 96-well plate with 100 µl trypsin-EDTA in each well was prepared.

The ESC culture medium was removed at the beginning of ESC clones picking, and 10 ml KnockOut DMEM basal medium for ESC culture was added in the 10 cm dish, and the petri dish was placed under the inverted microscope at 20 x magnification. Subsequently, ESC clones were loosed and picked by a 10 µl pipette tip, then they were transferred into wells of 96-well plate. After filling 24 wells of a 96-well plate, the plate was put into the cell culture incubator and incubated at 37°C for 5 minutes.

After 5 minutes of incubation, ESC clones were mixed by several times up and down pipetting to break up each ESC colony, then 30 µl of these ESCs were transferred to a well of the 48-well plate, the rest of the cells were used for DNA isolation and genotype identification. The ESC clones in a 48-well plate were cultured at 37°C, 5% CO₂, until the positive ESC clones were identified.

3.3.7 Screening PCR for ESC clones

The genomic DNA of ESC clones was prepared as described in section 3.1.2.5. The screening PCR reaction was performed with one internal primer (located in knock-in cassettes) and one

external primer (upstream or downstream of the targeted chromosomal region), the PCR primer sequence and thermocycling conditions see in Table 9 and Table 15-2 separately.

Both left-side and Right-side positive ESC clones were considered as targeted ESC clones. Afterward, these clones were expanded in 6-cm dishes and froze in cryotubes individually. Meanwhile, few ESCs were culture in one well of 24-well plate for 3-4 days until the ESC medium turned yellow. After that, 1 ml of ESC medium was collected for mycoplasma testing, the settings for PCR reaction see in Table 15-4.

3.3.8 Functional testing for positive ESC clones

The MEF was firstly cultured on the sterile coverslip in the 6-well plate, the positive ESC clones were thawed in the same 6-well plate on the next day. In order to induce the expression of EMT-TFs, ESCs were cultured in the ESC growth medium without Leukemia inhibitory factor (LIF). After 24 hours, ESCs in each well were infected with 200 μ l adenovirus (1×10^{10} GC/ml) which can express Recombinase Flippase (Flp) and EGFP simultaneously. Then ESCs were treated with 10 ng/mL TGF- β 1 for 48 hours.

After that, cells were fixed with 4% paraformaldehyde (4% PFA) when the medium turned yellow, and the Immunofluorescence Staining was performed as described in section 3.2.8. The fluorescence expression of ESCs was detected by Confocal Microscope (Leica Microsystems).

3.4 Mouse experiments

All the mouse experiments were conducted in full compliance with European guidelines for the care and use of laboratory animals and approved by the local authorities (Institutional Animal Care and Use Committees, IACUC) of Technical University of Munich and the Bavarian Government in Germany.

3.4.1 Mouse strains

Conditional *Cre/loxP* (Orban *et al.*, 1992) and *Flp/Frt* (Dymecki and Tomaszewicz, 1998) mouse models were used in this work for tissue-specific targeted mutagenesis. In order to induce PDAC in the mouse models, a *Kras*^{G12D} mutation was introduced in exon 2 of the mouse endogenous *Kras* allele, this allele also contains an *Frt-Stop-Frt* (*FSF*) cassette to block the spontaneous expression of *Kras*^{G12D}. However, the *FSF-Kras*^{G12D} mouse can be intercrossed with the mouse strain which expresses *Flp* recombinase under the control of a tissue-specific promoter to achieve deletion of the *FSF* cassette to activate or inactivate the expression of genes.

Additionally, the inducible inactivation or activation of genes was achieved using the Cre/loxP system by intercrossing with tamoxifen-activatable CreERT2 allele under the control of the Rosa26 promoter (*Rosa26-CreER^{T2}*) and the respective floxed mouse strain to evaluate the functions of genes of interest during the pancreatic tumor cells development process.

The mice which have been used in this study were kept on a mixed C57BL/6J; 129S6/SvEv genetic background unless otherwise stated. Experiments performed with mice backcrossed to C57BL/6J background were indicated.

Pdx1-Flp (Schönhuber *et al.*, 2014). This transgenic mouse strain was firstly generated in the group of Prof. Dieter Saur. The recombinase *Flp* is expressed under the control of the promoter of the *Pdx1* gene, which is expressed in the pancreatic progenitor cells at the beginning of pancreatic development, and eventually, *Pdx1* is expressed in the whole pancreas including exocrine, endocrine, and ductal cell populations.

FSF-Kras^{G12D} (Schönhuber *et al.*, 2014). This Genetically engineered mouse model (GEMM) was generated in the laboratory of Prof. Dieter Saur. In this mouse model, a G12D mutation was introduced in exon 2 of the mouse endogenous *KRAS* allele, and this allele contains a Stop cassette - a yeast gene with multiple polyA signals flanked by loxP sites. The mouse model allows conditional and sequential expression of oncogenic G12D mutant form of *Kras* following *Flp* recombinase-mediated excision of the *FRT*-flanked Stop cassette.

FSF-R26^{CAG-CreERT2} (Schönhuber *et al.*, 2014). This mouse strain was also generated in the laboratory of Prof. Dieter Saur. A latent Tamoxifen-inducible *CreER^{T2}* cassette was introduced in the *Rosa26* locus, it can start to express *CreER^{T2}* protein under the control of CAG promoter after FSF cassette has been excised by recombinase *Flp*. This can eventually manipulate the constitutional gene inactivation or activation in the PDAC mouse model.

Trp53^{frt} (Lee *et al.*, 2012). This mouse strain was kindly provided by Dr. David Kirsch (Medical Center of Duke University, Durham, NC, USA). In these mice, exons 2 to 6 of the transformation-related protein 53 (*Trp53*) gene were flanked by *Frt* sites. Therefore, the *Trp53* gene is allowed for disruption of gene expression by recombinase *Flp*.

Pdk1^{fllox} (Lawlor *et al.*, 2002). The exon 3 and exon 4 of the *Pdk1* locus were flanked by loxP sites in this mouse strain, it permits conditional deletion of *Pdk1* gene when Cre recombinase is activated in the cell nucleus.

Braf^{fllox} (Pritchard *et al.*, 2007). This mouse strain was kindly provided by Dr. Alcino J. Silva (University of California, Los Angeles, CA, USA). The floxed mutant mice possessed loxP sites flanking exon 12 of the *Braf* gene. *Braf* gene can be deleted when *CreER^{T2}* starts to express and tamoxifen is provided at the same time.

c-Raf^{fllox} (Yamaguchi *et al.*, 2004). The *c-Raf^{fllox}* mouse model was kindly provided by Dr. Benjamin Neel (NYU Grossman School of Medicine, New York, NY, USA). In the *c-Raf^{fllox}* allele,

the exons 13 and 16 of *c-Raf* gene were flanked by *loxP* sites. When this mouse line bred with mice expressing germline *Cre*, the *c-Raf* gene will be inactivated *in vivo*.

3.4.2 Genotyping for Mice

Genotyping PCR for mouse was performed when mice were 16-21 days old, all the mice were earmarked with autoclaved ear clipper. A small piece of ear biopsy was taken from the mouse for genotyping and the ear wound was disinfected with 75% ethanol. The genomic DNA was extracted from the biopsy as described in 3.1.2.5. The thermocycling conditions of genotyping PCR were listed in Table 19, and Table 20.

3.4.3 Mouse Nomenclature

For better readability of the text, abbreviations of mouse genotypes are used in the following chapters and listed in Table 20.

Table 28. Nomenclature of mouse lines

Mouse genotype	Abbreviation
<i>Pdx^{Flp/+}; FSF-R26^{CAG-CreERT2/+}; FSF-Kras^{G12D/+}; Pdk1^{lox/lox}; Braff^{lox/lox}; C-Raf^{lox/lox}</i>	PKPBC
<i>Pdx^{Flp/+}; FSF-R26^{CAG-CreERT2/+}; FSF-Kras^{G12D/+}; Pdk1^{lox/lox}; Braff^{lox/lox}; C-Raf^{lox/lox}; Trp53^{frt/+}</i>	PKPBC; Trp53 ^{frt/+}
<i>Pdx^{Flp/+}; FSF-R26^{CAG-CreERT2/+}; FSF-Kras^{G12D/+}; Pdk1^{lox/lox}; Braff^{lox/lox}; C-Raf^{lox/lox}; Trp53^{frt/frt}</i>	PKPBC; Trp53 ^{frt/frt}

3.4.4 Mouse Dissection

The tumor mice were closely monitored by Laboratory Animal Veterinarian and animal responsible person under the regulations of IACUC. The tumor mice have been taken out from the experimental animal room for dissection when their spontaneous pancreatic tumor was palpated.

Before mouse dissection, all the dissection tools and tables were disinfected with 80% Ethanol and UV light for at least 30 minutes. The tumor mouse was firstly anesthetized with clean tissue paper which was soaked with 1 ml isoflurane under the biosafety cabinet, the mouse was sacrificed by cervical dislocation and bleeding. After that, the abdomen of the mouse was disinfected with 70% Ethanol before cutting open it. Small pieces of tissue (around 1-2 mm³) were cut carefully from the pancreatic tumor for DNA, RNA and tissue protein extraction separately. Next, the samples for RNA and protein extraction were mixed and homogenized with 600 µl RLT buffer containing 10µl β- Mercaptoethanol, 500 µl of IP buffer containing 1% phosphatase and 4% protease inhibitors, respectively. All the samples were snap-frozen in the liquid nitrogen immediately and then stored at -80 °C to prevent DNA, RNA and protein

degradation. In addition, 1-3 pieces of tissue samples were taken from different parts of the pancreatic tumor for primary cell line culture depending on the size of solid tumor.

At the same time, a piece of pancreatic tumor sample (around 1/3 large) was taken and fixed in 4% Roti® Histofix for 2 h for Frozen Tissue Sectioning. Another same size pancreatic tumor sample was used for bulk tumor Flow cytometry analysis. The rest of tumor mouse organs including liver, spleen, lung, heart, stomach, intestine and kidneys were all fixed in 4% Roti® Histofix at room temperature for 24-36 hours for paraffin embedding and histological analysis.

3.4.5 Documentation of Tissues Morphology

The size and weight of mouse pancreatic tumor tissue was measured. The observable metastases in liver, lung, spleen and thoracic diaphragm were documented by the microscope. In addition, the morphology of the pancreatic tumor tissue was also photographed by the camera.

3.4.6 Tamoxifen Treatment for Mice

In order to activate the CreER^{T2} and translocate it into the nucleus, tumor mice in this study were fed with tamoxifen-containing diet (400 mg tamoxifen citrate per kg diet) between 15 and 20 weeks of mouse life. Meanwhile, non-tumor mice with *FSF-Rosa26CAG-CreER^{T2}* allele were also fed with tamoxifen-containing diet at the same age to evaluate the potential effects of CreER^{T2} toxicity and side-effect for mice.

For the orthotopic implantation experiments, 4-hydroxytamoxifen was dissolved in the corn oil at the concentration of 20 mg/ml, and the mice were injected by intraperitoneal injection of tamoxifen solution with a dose of 4 mg Tamoxifen/30g body weight twice per week after 1 week of implantation.

3.4.7 Magnetic Resonance Imaging (MRI) for pancreatic tumor of mouse

Magnetic resonance imaging (MRI) technology was used for scan the tumor size of PDAC animals. The mice which have been identified as pancreatic tumor mice after genotyping were divided into two groups of Tamoxifen treatment and vehicle controls. Tamoxifen treatment was started when the tumor of mice could be palpated. On the same day, mice were scanned by nanoScan® PET/ MRI system with the gradient coil of 205/120 HD and the flexible receive array coil following a protocol adapted to the abdomen. After that, tumor mice were scanned every two weeks to monitor the pancreatic tumor development and the changes of tumor size.

3.4.8 Orthotopic Implantation

PDAC cells were trypsinized to single cells, these cells were diluted to a final concentration of 125 cells/ μ l in 1 ml DMEM without FCS. Next, mice were anesthetized by injecting 50 μ l MMF (150 μ g/ kg Medetomidine, 4.0 mg /kg Midazolam and 50 μ g/ kg Fentanyl) via intraperitoneal injection. The eye cream was applied to the mouse eyes when it has no response, and the upper left belly of mouse was shaved with an electric razor. Meanwhile, the heating lamp was turned on to warm the mouse during operation.

After that, an approximately 5 mm straight line skin wound was cut with sterile scissors next to the position of the spleen, the peritoneum around the skin wound was separated with scissors. The peritoneum was cut opened with inner scissors and forceps at the same position under the skin wound, and the tail of pancreas was taken out with blunt forceps. Subsequently, 2500 cells in 20 μ l DMEM was injected into the pancreas by clean glass syringe, then both sides of the peritoneum wound were grabbed with a pair of forceps to make the pancreas falls back into the abdomen slowly and gently.

The peritoneum wound was closed with around 3 stitches by sewing thread. The skin wound was clipped with around 3-4 metal clips. The mouse was injected around 200 μ l of AFN and 150 μ l of Metacam. Next, the mouse was put in the warming chamber and transferred to the cage until it woke up and moved actively. Clean water, oat flakes and food were supplied to the cage.

3.4.9 FACS for Pancreatic Tumor Tissue

The mouse was dissected as described in section 3.5.4, a part of tissue around 1/4 - 1/3 large of the pancreatic tumor was taken and put into cold PBS for Flow cytometry analysis. Tumor tissue was transferred into a 10 cm Petri dish and minced on ice with a clean scalpel. Next, the tumor tissue was digested with enzymes and solution in Mouse Tumor Tissue Dissociation Kit via GentleMACS™ Dissociator.

After digestion, the tissue was centrifuged at 1,500 rpm for 5 min at 4°C, the pellet was resuspended in 5 mL cold PBS+2% FCS and passed through a 70 μ m mesh to remove the large tissue residual. The filtered cells were centrifuged and resuspended again in 200 μ l cold PBS, cell number was counted with the hemocytometer. After counting, cells were diluted 4,000,000 cells in 400 μ l PBS and split into 2 equal groups in clean 1.5 ml Eppendorf tubes (200 μ l in each tube). After that, 0.6 μ l Zombie Aqua (BioLenged) was stained in 100 μ l PBS and added into one of 1.5 ml Eppendorf tubes with 200 μ l cells to achieve a final concentration of 1:500, the cells were stained with Zombie Aqua on ice for 10 minutes. Meanwhile, another group of cells was kept on ice and used as the unstained control. After Zombie Aqua staining, 1 μ L TruStain fcX™ CD16/32 (Biolegend) was added to the tube and incubated on ice for 10 minutes for blocking the Fc Receptor-involved unwanted staining.

After Fc Receptor blocking, 700 μ l cold PBS+2% FCS was added into cells, then cells were divided into two 1.5 mL Eppendorf tubes, 500 μ l for each, for BT panel and innate panel staining, respectively. Cells were centrifuged at 1500 rpm for 5 min to remove the supernatant, cell pellets in different tubes were stained with 100 μ l BT or Innate panel antibody master mixes for 30 min on ice (BT and innate staining panel are listed in Table 29 and 30). At last, cells were resuspended in 200 μ l of cold PBS and passed through 40 μ m mesh into FACS tubes, all groups of cells were analyzed by BD LSRFortessa flow cytometer (The laser filter configurations for BD LSRFortessa are listed in Table 31).

Table 29. B cells and T cells antibody staining panel

Antigen	Fluorochrome	Amount of antibody for each sample (μ l)	Company	Catalogue number	Clone
CD3 ϵ	APC-Fire	5	BD	563565	145-2C11
CD44	APC-Fire	3	Biolegend	103027	IM7
CD25	BV650	2	Biolegend	102037	PC61
TCR γ/δ	BV421	2	Biolegend	118119	GL3
CD4	BUV805	1	BD	564922	GK1.5
CD8a	BV785	1	Biolegend	100749	53-6.7
CD45	PerCP-Cy5.5	1	Biolegend	147705	I3/2.3
CD19	FITC	1	Biolegend	115505	6D5
EpCAM	AF647	0.5	Biolegend	118212	G8.8
CD62L	PE	0.2	Biolegend	104407	MEL-14

Table 30. Innate immune cells antibody staining panel

Antigen	Fluorochrome	Amount of antibody for each sample (μ l)	Company	Catalogue number	Clone
CD68	APC-CY7	5	Biolegend	137023	FA-11
NK1.1	BUV395	4	BD	564144	PK136
CD11c	BUV737	3	BD	564986	HL3
F4/80	BV421	3	Biolegend	123131	BM8
CD45	PerCP-Cy5.5	1	Biolegend	147705	I3/2.3
Siglec-F	BB515	1	BD	564514	E50-2440
CD11b	BV650	1	Biolegend	101239	M1/70
Ly6G	PE	0.5	Biolegend	127607	1A8
EpCAM	AF647	0.5	Biolegend	118212	G8.8
Ly6C	BV785	0.5	Biolegend	128041	HK1.4

Table 31. Laser filter configurations for BD LSRFortessa

Laser (Excitation /nm)	Detector	Longpass Filter	Bandpass Filter	Fluorochrome
355	A	735 LP	775/50	BUV805/ BUV737
	B	450 LP	515/30	
	C	-	379/28	BUV395
405	A	750 LP	780/60	BV787
	B	685 LP	710/50	
	C	630 LP	670/30	BV650
	D	600 LP	610/20	
	E	505 LP	525/50	BV510
	F	-	450/50	BV421
488	A	685 LP	710/50	PerCP-Cy5.5
	B	505 LP	530/30	FITC
	C	-	488/10	SSC
561	A	750 LP	780/60	
	B	685 LP	710/50	
	C	650 LP	610/20	
	D	570 LP	586/15	PE
640	A	750 LP	780/60	APC-Cy7
	B	690 LP	730/45	
	C	-	670/14	APC

3.5 Histological Analysis

3.5.1 Tissue Fixation, Embedding and Sectioning

Mouse tissue fixation was achieved by immersing in the Roti® Histofix immediately following dissection for around 24 hours. After fixation, tissue was washed with PBS and dehydrated in increasing concentrations of ethanol with Leica ASP300S Tissue Processor. The mouse tissue was then embedded in paraffin with HistoCore Arcadia modular tissue embedding system, the embedded paraffin samples were stored at room temperature for sectioning. Finally, the tissue was sectioned by Rotary Microtome Microm HM355S, then the sections of 2.5µm -3.0 µm thick were used for further staining.

For frozen sectioning, mouse tissue was firstly fixed in the Roti® Histofix for 2 hours at 4 °C, then tissue was dehydrated in 15% Sucrose for 6 hours and 30% Sucrose for 8 hours until the tissue was completely dehydrated. Subsequently, the tissue was embedded in the Optimal Cutting Temperature Compound (O.C.T. compound) and stored at -80 °C for further use. The frozen samples were cut into 15µm - 20 µm thick sections by Microm HM 560 Cryostat, and the sections were used for immunofluorescence (IF) staining.

3.5.2 Hematoxylin and Eosin (H&E) Staining

The paraffin sections were dewaxed by immersion in Roti® Histol Xylene solution (2x 5 min), rehydrated in the decreasing concentrations of ethanol (from 2x 100%, 2x 96%, 2x 80%,

incubated for 3 minutes in each glass of ethanol), and paraffin sections were washed in the distilled water for 5 minutes.

After rehydration, the sections were stained with hematoxylin for 20 seconds at room temperature and washed 2-3 times with clean tap water until the tissue became blue. Subsequently, the tissue sections were stained with Eosin for around 20 seconds and washed with distilled water for 3 times. Next, the sections were dehydrated in the ascending concentrations of ethanol (from 2x 80%, 2x 96%, 2x 100%, incubated for 1 minute in each glass of ethanol) and incubated in Xylene solution (2x 5 min) again to make the dehydration completely. In the end, 1-2 drops of Pertex® histology mounting medium were added to the slides, and covered with clean coverslips for preservation.

3.5.3 Immunohistochemistry (IHC) Staining

For Immunohistochemistry Staining, Paraffin-embedded tissue sections of 2.5µm -3.0 µm thick were prepared by Rotary Microtome Microm HM355S, and sections were dewaxed and rehydrated as described in 3.6.2.

At the step of antigen /epitope retrieval, 1x SignalStain® Citrate Unmasking Solution was prepared and used for Paraffin-embedded tissue antigen retrieval. The tissue sections were immersed in unmasking solution, and the solution was heated to boil in the microwave at 360W for 10 min. The tissue slides in unmasking solution were left at the room temperature environment for at least 20 minutes for cooling down. After antigen retrieval the sections were washed with water three times for 5 minutes each, then sections were incubated in 3% hydrogen peroxide for 15 min in the dark environment to inactivate the activity of endogenous peroxidase. After washing in the water and PBST (Phosphate buffer saline and 0.1% Tween 20), each slide was incubated with 200 µl of blocking solution (PBST containing 10% Avidin solution and 5% serum) for 1 hour at room temperature. Next, the blocking solution was removed by pipette tip, and 200 µl of primary antibody diluted in antibody diluent (PBST containing the primary antibody, 10% biotin solution and 5% serum) was added to each slide, tissue sections were incubated overnight at 4°C. On the next day, the slides were washed with PBST 3 times, and slides were incubated with secondary antibody solution (PBS containing biotinylated secondary antibody and 5% serum) at room temperature for 1 hour. Meanwhile, Avidin-Biotin Complex (ABC) solution was prepared by mixing 2 drops of Reagent A (VECTASTAIN® Elite® ABC HRP Kit) and 2 drops of Reagent B in 5 ml PBS and stored at 4°C for 30-60 minutes.

After secondary antibody incubation, the slides were washed with PBST three times for 5 min each to remove the antibody completely, then tissue slides were incubated with pre-cooled ABC solution at room temperature for 1 hour. Subsequently, 3, 3'-diaminobenzidine (DAB) solution from VECTASTAIN® Elite® DAB Peroxidase Substrate Kit was prepared by mixing 2

drops of Buffer 7.5, 4 drops of DAB and 2 drops of Hydrogen Peroxide in 5 ml distilled water. 200 µl of DAB solution was applied on each slide until the color of the tissue turned brown. In the end, the slides were stained with hematoxylin for 10-20 seconds and proceeded with dehydration in ascending concentration of ethanol as described in the section of 3.6.2, then tissue slides were mounted with Pertex® histology mounting medium.

Table 32. Antibodies and dilution of antibodies for IHC staining

Antibody	Source / Company	Catalogue	Dilution
Ki-67	Cell Signaling Technology Inc., Danvers, MA, USA	#9027	1:600
Goat Anti-Rabbit IgG Antibody (H+L), Biotinylated	Vector Laboratories, Inc., Burlingame, CA, USA	BP-9100-50	1:200

3.5.4 Scanning and Analysis of Staining

In order to document the staining results of H&E staining and IHC staining, Leica Aperio VERSA Digital Pathology Scanner was used for tissue slides scanning, the images of staining were all saved in the Aperio eSlide Manager online server.

The pathology slide viewing software- Aperio ImageScope was used to analyze the staining results, the details of image analysis are presented in the results part. Meanwhile, the tumor grading and lesion counting of H&E staining slides were defined by Pathology Institute of Technical University of Munich.

3.6 Protein Immunoblot

3.6.1 Protein Sample Preparation

Cells that reached about 80% confluence were used for protein extraction. Firstly, the cell culture medium was removed by an aspirator, and cells were washed with PBS three times. Afterward, 200 µl of Pierce™ IP Lysis Buffer containing 4% Proteinase inhibitor and 1% phosphatase inhibitor was added to the 10 cm dish, cells were harvested with a cell scraper and the lysate was left on ice for 30 minutes for cell lysis. After that, the lysate of cells was centrifuged with at 13,000 rpm for 30 minutes at 4°C. The supernatant was transferred to another 1.5 ml Eppendorf tube, 1 µl of protein supernatant was taken and mixed with Quick Start™ Bradford Protein Solution for calculation of the concentration of protein.

3.6.2 Measurement of Protein Concentration

Bradford assay was performed to measure the concentration of protein. 300 µl of Bradford solution was used for each well of 96-well plate measurement, and each protein sample was prepared in triplicate. When Bradford solution was ready in 96-well plate, 1 µl of protein sample

was added and mixed well with Bradford solution in each well. Meanwhile, standard protein samples with ascending concentrations were added in wells to make a standard curve. The samples were then incubated at room temperature for 10 minutes, and the absorbance at 600nm was measured by CLARIO star Plus Microplate Reader.

After concentration measurement, protein samples were diluted to a certain concentration with 5x Laemmli Sample Buffer and IP Lysis Buffer. Protein samples were boiled at 95°C for 5 min, aliquoted in 2.0 ml Eppendorf tubes and stored at -20°C for future use.

3.6.3 SDS-PAGE Gel Electrophoresis

The stacking gel and separating gel were prepared depending on the size of the protein of interest (The recipes of the stacking gel and separating gel are shown in Table 33 and 34). When the SDS-PAGE gel was prepared, equal amounts of protein (40-60 µg) were loaded into the wells of the SDS-PAGE gel, along with a molecular weight marker.

The gel with protein samples was running with the 1x running buffer (the recipe is shown in Table 33) at 80 V for about 30 minutes, then the voltage was adjusted to 100 V when protein samples were in separating gel. The gel was running at 100 V until the samples reached the bottom of the SDS-PAGE gel.

Table 33. Recipes with Standalone Reagents

Solution / Chemical	Separating Gel Buffer	Stacking Gel Buffer	10x Running Buffer	10x Transfer Buffer
Tris Base	60.6 g	22.8 g	15.1 g	7.3 g
Deionized H ₂ O	300 ml	300 ml	300 ml	300 ml
Glycine	-	-	72.0 g	36 g
SDS	-	-	5.0 g	-
	Adjust pH to 8.8 with HCL	Adjust pH to 6.8 with HCL	Adjust pH to 8.3 with NaOH	Adjust pH to 8.3 with NaOH

Table 34. Recipes of the Stacking Gel and Separating Gel

Solution	10% Separating Gel (µl)	4% Stacking Gel (µl)
Deionized H ₂ O	2050	1500
Separating Gel Buffer	1300	-
Stacking Gel Buffer	-	650
30% acrylamid	1650	1375
10% SDS	50	25
10% APS	25	12.5
TEMED	7.5	5

3.6.4 Membrane Transfer

Before starting membrane transfer, the 1x transfer buffer (the recipe is shown in Table 33) was prepared and kept at 4°C for 30 minutes. Meanwhile, the PVDF was activated with methanol for 1 min and rinsed with transfer buffer before preparing the stack. Then the sponge, filter paper, separating gel, nitrocellulose (NC) membrane, filter paper and sponge were put together from bottom to up to form a stack. Afterward, the stack was put into the transferring chamber with pre-cooled transfer buffer, and it was running at 100 V for 2 hours at 4 °C. After membrane transfer, the NC membrane was taken out from the stack and put in a light-proof box.

3.6.5 Antibody staining

After the protein has been transferred to the membrane, the membrane was incubated with 5% BSA in PBS for 1 hour at room temperature to achieve blocking of non-specific binding. Next, the membrane was washed three times with PBST, and incubated with appropriate dilutions of primary antibody in 5% BSA overnight at 4°C. After primary antibody incubation, the membrane was washed three times with PBST again, 5 minutes each. Subsequently, the membrane was incubated with the recommended dilution of conjugated secondary antibody in 5% BSA at room temperature for 1 hour in the light-proof box, and washed with PBST to remove unspecific binding antibodies.

Before membrane scanning, the membrane was kept in transparent plastic wrap for 30 minutes to remove the excess reagent. In the end, the membrane was scanned by Li-Cor Odyssey® Fc Imaging System at 700 nm or 800 nm wavelength.

Table 35. Antibodies and dilution of antibodies for Western Blotting

Antibody	Source / Company	Catalogue	Dilution
MEK1/2	Cell Signaling Technology Inc., Danvers, MA, USA	#4694	1:1000
p44/42 MAPK (Erk1/2)	Cell Signaling Technology Inc., Danvers, MA, USA	#4696	1:2000
Akt (pan)	Cell Signaling Technology Inc., Danvers, MA, USA	#4691	1:1000
Phospho-Akt (Ser473)	Cell Signaling Technology Inc., Danvers, MA, USA	#9271	1:1000
Phospho-Akt (Thr308)	Cell Signaling Technology Inc., Danvers, MA, USA	#2965	1:1000
Caspase-3	Cell Signaling Technology Inc., Danvers, MA, USA	#9662	1:1000
Pdk1	Cell Signaling Technology Inc., Danvers, MA, USA	#3062	1:1000
c-Raf	Cell Signaling Technology Inc., Danvers, MA, USA	#9422	1:1000

α -Tubulin	Cell Signaling Technology Inc., Danvers, MA, USA	#2144	1:1000
β -Actin	Cell Signaling Technology Inc., Danvers, MA, USA	#8457	1:1000
GAPDH	Cell Signaling Technology Inc., Danvers, MA, USA	#2118	1:1000
Cre Recombinase	Cell Signaling Technology Inc., Danvers, MA, USA	#15036	1:1000
Hsp90 alpha/beta	Santa Cruz Biotechnology, Inc., Dallas, TX, USA	SC-13119	1:1000
turboYFP	BioCat GmbH, Heidelberg, Germany	AB605-EV	1:1000
Anti-mouse IgG (H+L) (DyLight™ 800 4X PEG Conjugate)	Cell Signaling Technology Inc., Danvers, MA, USA	#5257	1:2000
Anti-rabbit IgG (H+L) (DyLight™ 800 4X PEG Conjugate)	Cell Signaling Technology Inc., Danvers, MA, USA	#5151	1:2000

3.7 Statistical analysis

All the graphic analyses, statistical analyses and data correlation were done using GraphPad Prism version 8.0. Experimental data were presented as Mean \pm Standard error of mean (SEM). For MTT assay, caspase-3/7 assay and cell viability assay, all experiments were conducted in triplicate, and the two-way analysis of variance (ANOVA) test was used for comparisons between experimental and control groups. While the two-tailed Student's t-test was applied to compare the statistical differences between datasets with single variable. In order to analyze the changes of lymphocytes in pancreatic tumors, the two-tailed Student's t-test was used during the analysis. For analysis of the drug screening assay, the Half-maximal inhibitory concentration (IC50) was determined by nonlinear regression analysis.

Kaplan-Meier and Log-rank tests were used for statistical analysis of animal survival curves. Student's t-test was used to calculate the statistical difference of immune cell populations in the bulk tumor. In this thesis, statistical significance was considered in all analyses only when the p-value is less than 0.05. For RNA sequencing analysis, the false discovery rate (FDR) cutoff of 25% (FDR q-value < 0.25) was set to report the enrichment of gene sets.

4 Results

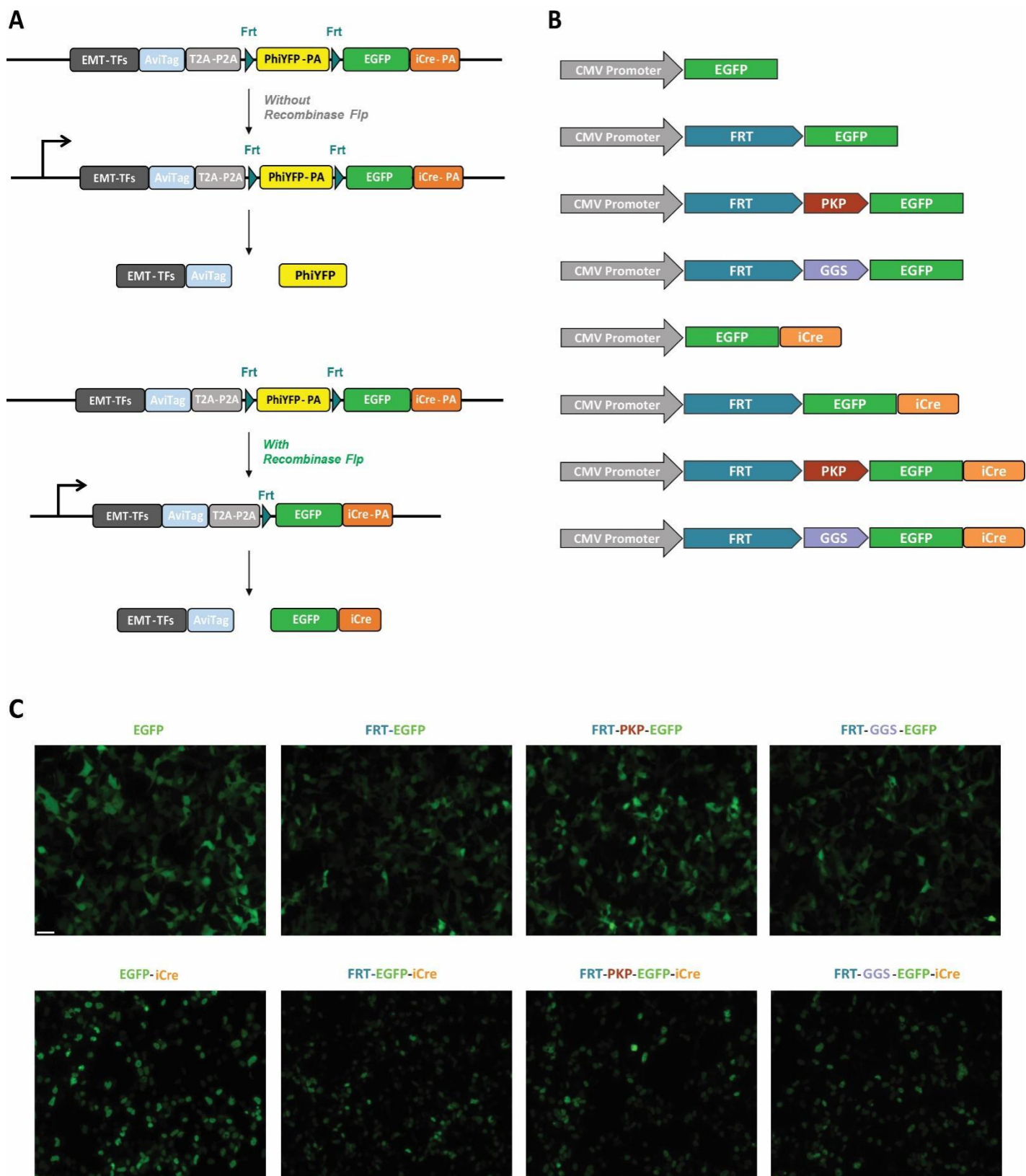
4.1 Chapter 1. Generation of novel multicolor tracing mouse models for EMT-TFs

Due to the controversial findings of previous studies on the functions of EMT-inducing transcription factors (EMT-TFs) in cancer, an improved animal model able to monitor the dynamic changes of EMT-TFs and the EMT process is urgently needed, to develop a better, unbiased understanding of their role in tumorigenesis. The schematic diagram of improved animal models for this study is shown in **Figure 1A**. The Avi-tag can be fused with EMT-TF proteins, the Avi-tag is a 15 amino acid peptide that can be biotinylated by biotin ligase-BirA in a process known as biotinylation. Following this, the protein of interest labeled by the Avi-tag can be isolated using streptavidin, or detected directly using an Avi-tag antibody. 2A peptides are a kind of self-cleaving peptides that can induce ribosome skipping at the peptide C-terminus, resulting in the separation of the end of the 2A sequence and the next peptide downstream. 2A peptides are commonly used to separate a long peptide into two short peptides that share the same open reading frame (ORF) in the cell [195]. The mutated PhiYFP (Y65A) in this novel model can function as the STOP cassette – although it lost the endogenous fluorescence, it could still be detected with antibodies, and could therefore be used for eliminating the inaccurate expression of fluorescent proteins.

4.1.1 Comparison of fluorescence intensity between FRT-EGFP variants

Theoretically, these mouse models can express the EMT-TFs tagged with Avi-tag, and the PhiYFP protein when the flippase (Flp) recombinase is absent. Conversely, while Flp exists, the PhiYFP cassette will be deleted by the Flp/FRT recombination system, and the cells will be able to express EMT-TFs and fluorescence protein-codon-improved Cre recombinase (FP-iCre) fusion proteins simultaneously. As the residual flippase recognition target (FRT) sequence may affect the expression of FP-iCre, we constructed different EGFP plasmid variants (Figure 1B). These plasmids were delivered to human embryonic kidney (HEK) 293 cells using Effectene Transfection Reagent (QIAGEN), and the expression of EGFP was

detected after 48 hours using a fluorescence microscope and flow cytometer under the same settings. Indeed, the expression of EGFP was affected by the residual FRT sequence; however, the variants with protein linker Pro-Lys-Pro (PKP) between FRT and FP-iCre could reduce the impact of FRT on expression of both EGFP and EGFP-iCre. This effect was not observed with protein linker Gly-Gly-Ser (GGS) (Figure 1C). In addition, the fluorescence intensity of plasmid variants was assessed using FlowJo v10.0 (FlowJo LLC, USA), and found that variants with the PKP linker show stronger expression of EGFP (Figure 1D and Table 36). Together, these results proved that the PKP linker can reduce the impact of residual FRT sequences, and improve the expression of fluorescent protein.



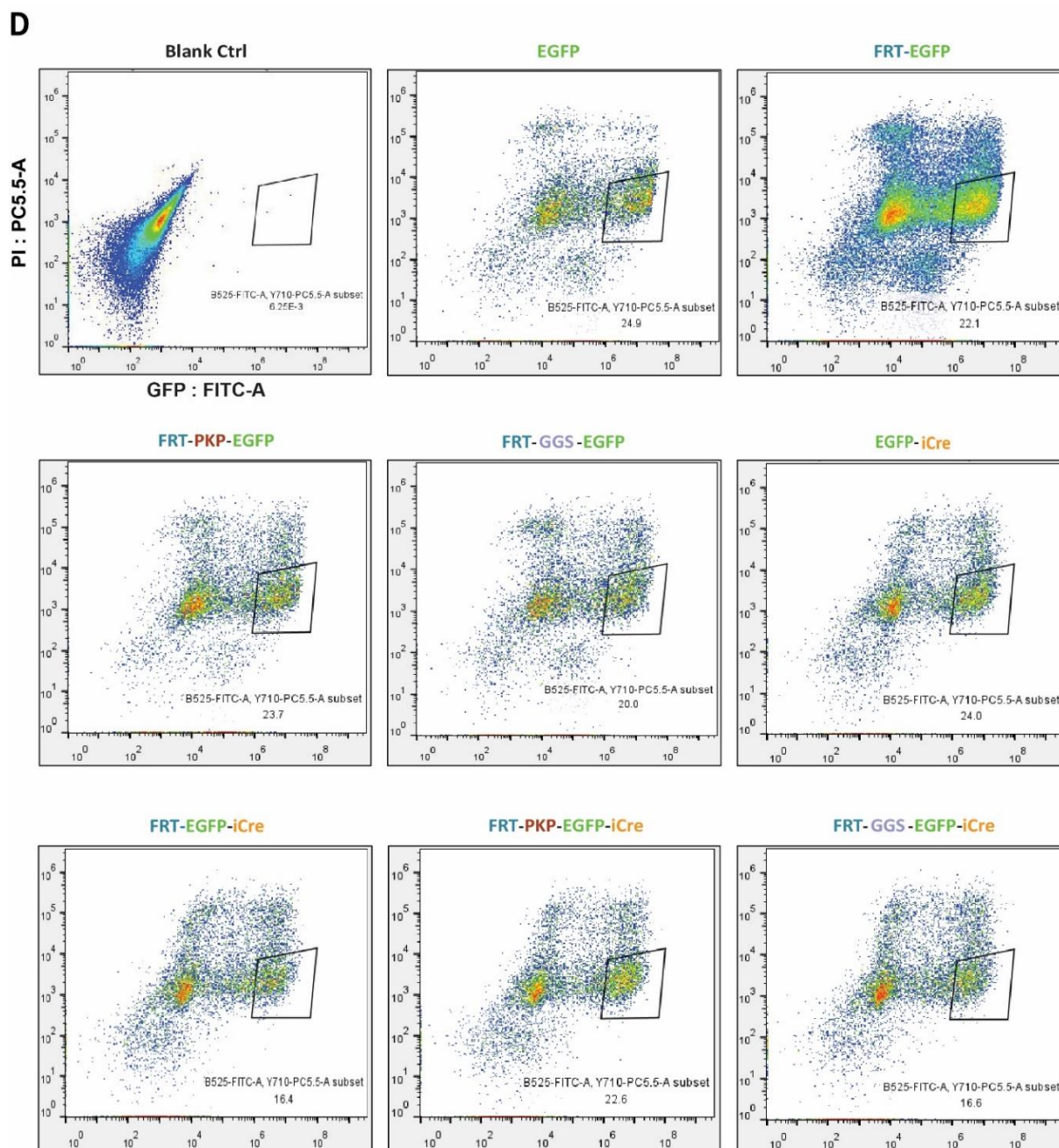


Figure 1. Comparison of fluorescence intensity between FRT-EGFP expression plasmids

(A) The schematic illustration of improved mouse models for EMT-TFs tracing. Proteins of EMT-TFs is fused with AviTag. The self-cleaving peptide T2A-P2A separates the long peptide into EMT-TF-Avitag and PhiYFP proteins when flippase (Flp) is absent, or EMT-TF-Avitag and EGFP-iCre with Flp. PA: Polyadenylation signal, iCre: Codon improved Cre recombinase, FRT: flippase recognition target.

(B) Different types of FRT-EGFP expression cassette. The expression of all cassettes is driven by Cytomegalovirus (CMV) promoter. Protein linker PKP: Pro-Lys-Pro, GGS: Gly-Gly-Ser.

(C) The fluorescent images of different FRT-EGFP (Top) and FRT-EGFP-iCre (Bottom) expression plasmids. HEK293 cells were seeded in each well of 6-well plate, cells were then transiently transfected with FRT-EGFP expression plasmids by DNA transfection method. The expression of EGFP was detected by fluorescence microscope after 48 hours. Scale bars indicate 50 μ m.

(D) The FACS plots represent EGFP-positive cells percent of different FRT-EGFP plasmid variants in HEK293T cells. HEK293 cells were seeded in each well of 6-well plate, cells were then transiently transfected with FRT-EGFP expression plasmids. 48 hours after transfection, the EGFP positive HEK293 cells were assessed by flow cytometer. PI: Propidium Iodide; Fluorochrome: PC5.5 (PerCP-Cyanine5.5), FITC (Fluorescein isothiocyanat).

Table 36. Fluorescence intensity of FRT-EGFP and FRT-EGFP-iCre expression variants from HEK293 cells assessed by FACS

Variants	GFP %	Fluorescence Intensity (Mean)	Fluorescence Intensity (Median)
EGFP	24.9	1.06E7	7.84E6
FRT-EGFP	22.1	7.28E6	5.01E6
FRT-PKP-EGFP	23.7	7.74E6	5.35E6
FRT-GGS-EGFP	20.0	6.68E6	4.63E6
EGFP-iCre	24.0	6.53E6	4.88E6
FRT-EGFP-iCre	16.4	4.85E6	3.57E6
FRT-PKP-EGFP-iCre	22.6	5.66E6	4.20E6
FRT-GGS-EGFP-iCre	16.6	4.63E6	3.19E6

4.1.2 Fluorescent proteins of multicolor tracing system are distinguishable without fluorescence spillover

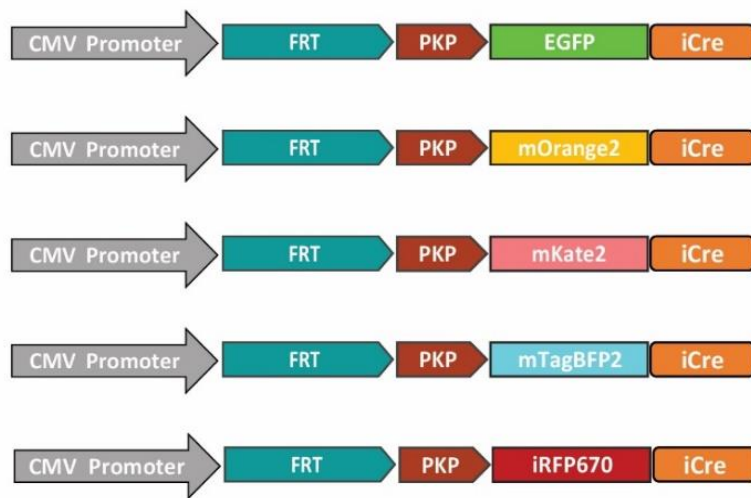
To monitor the dynamic expression changes of EMT-TFs in PDAC cells during tumor progression, we decided to label the genes of EMT-TFs (such as *Snai1*, *Zeb1*, *Twist1*) and genes related to mesenchymal state (*Col6a1*, *Fsp1*) with different fluorescence markers. In this way, the spatial and temporal expression of these genes could be monitored during pancreatic cancer development. To test the application potential of our multicolor tracing system, five fluorescence proteins with distinct excitation and emission spectra were chosen as candidates (Table 37). The DNA of selected fluorescence proteins was then cloned into the backbone vector with a PKP protein linker, as described in section 4.1 (Figure 2A). Subsequently, equal amounts of FP-iCre plasmids were transfected together into HEK293 cells. 48 hours after transfection, cells were fixed with 4% Paraformaldehyde (PFA) for detection of fluorescence with a confocal laser scanning microscope (CLSM). The results

showed that all FP-iCre fusion proteins displayed a strong expression in transfected cells (Figure 2B). In addition, the fluorescence signal of all fusion proteins could be detected and distinguished using the CLSM (Figure 2B). Additionally, the FP-iCre plasmids were also delivered into cells separately, to identify fluorescence spillover between different channels. Theoretically, signals of each FP-iCre protein can only be detected by its corresponding channel; however, if fluorescence spillover between FP-iCre proteins occurs, the fluorescence signal will be observed in different channels. As the result shown, the fluorescence signal of each fusion protein was found to be present in the specific corresponding channel, and no fluorescence spillover was observed from the rest of the channels (Figure 2C). Together, these results demonstrated that different fluorescence could be distinguished in this system without spillover, and proved that the multicolor labeling system is capable of monitoring multiple proteins simultaneously.

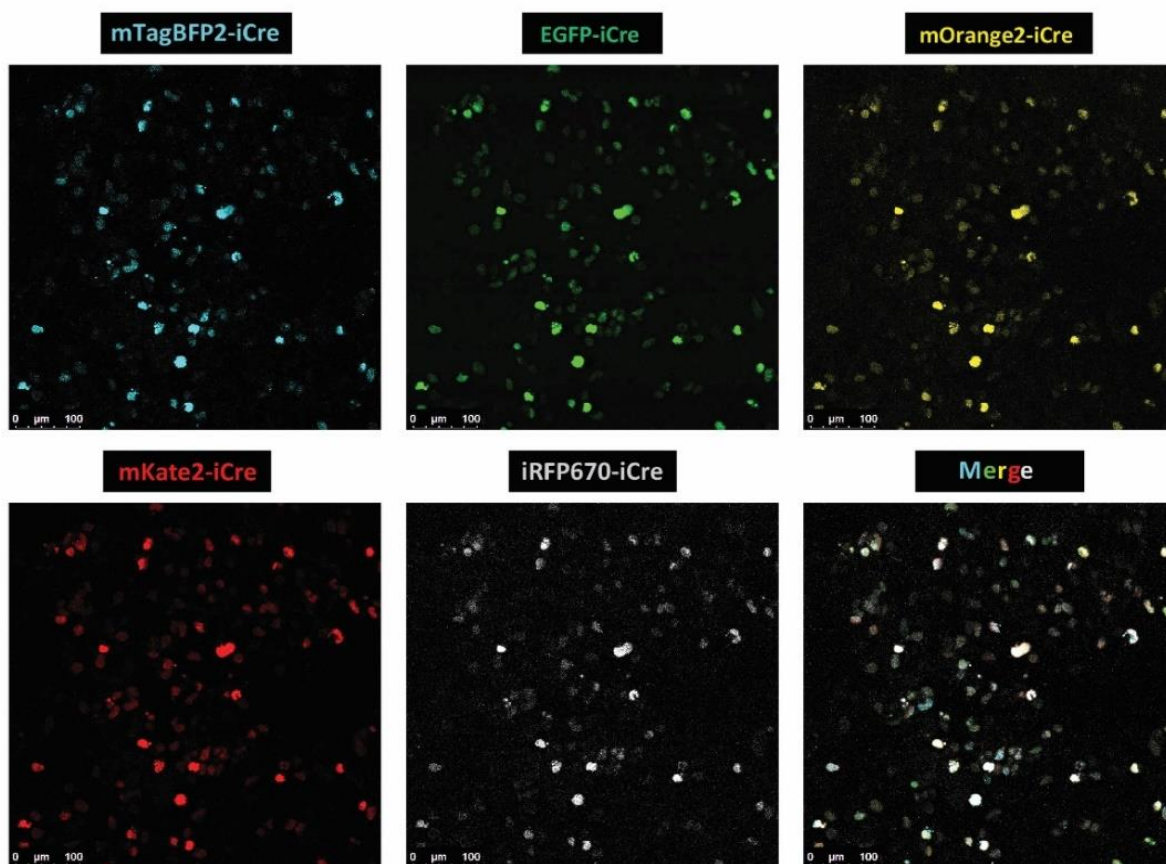
Table 37. The attributes of fluorescent proteins

Color	Ex λ (nm)	Em λ (nm)	Brightness(s)	Oligomerization
EGFP	488	507	33.6	Weak dimer
mOrange2	548	562	49	Monomer
mKate2	588	633	25	Monomer
mTagBFP2	399	454	32.38	Monomer
iRFP670	643	670	12.54	Weak dimer

A



B



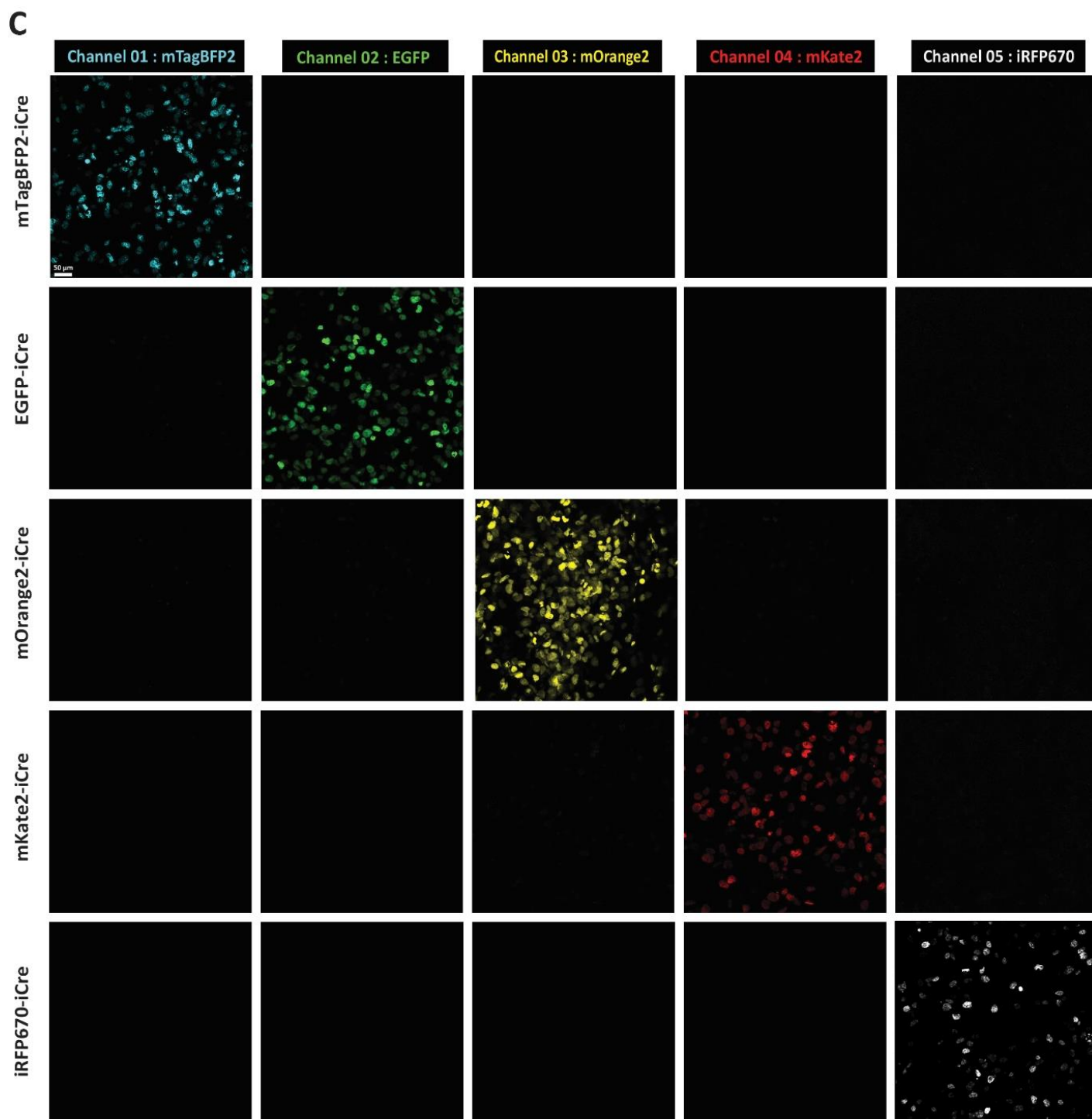


Figure 2. Fluorescent proteins can be distinguished without fluorescence spillover

(A) The plasmids with different FRT-PKP-FP-iCre expression cassette.

(B) Fluorescence images for FP-iCre fusion proteins. HEK293T cells were co-transfected with the FP-iCre expression plasmids and imaged with CLSM. Scale bar, 100 μ m.

(C) Fluorescence spillover identification for FP-iCre plasmids. HEK293T cells were transfected with different FP-iCre expression plasmids separately. Scale bar, 50 μ m.

4.1.3 *In vitro* functional testing for FP-iCre fusion proteins

To further validate the application potential of the multicolor labeling system, functional testing of the FP-iCre fusion proteins was performed using the *Rosa26*^{CAG-mTmG} PDAC cell line, which was isolated from mouse pancreatic tumors. *Rosa26*^{mTmG} cells possess the loxP sites on both sides of the membrane-targeted tdTomato (mT) cassette, and express the fluorescence protein tdTomato ubiquitously. When Cre recombinase is present in these cells, the tdTomato cassette can be deleted by the Cre/loxP recombination system, which causes cells to then begin expressing the membrane-targeted EGFP (mG). The expression change of fluorescence proteins in these cells between tdTomato and EGFP can thus be observed (Figure 3A).

The FP-iCre plasmids were delivered to *Rosa26*-mTmG cells separately, while the plasmid lacking the fluorescence protein and Cre expression cassette was introduced into *Rosa26*-mTmG cells as a negative control. After 48 hours, cells were fixed with 4% PFA for confocal fluorescence imaging. As the result shown, the membrane-located EGFP (mEGFP) was observed in cells expressing FP-iCre fusion proteins, and was absent in negative control cells (Figure 3B). Moreover, as iCre contains a nuclear localization signal (NLS) at its N-terminus, FP-iCre proteins were detected in mEGFP positive cells, and displayed nuclear localization. The cell membrane located tdTomato (mtdTomato) was replaced by mEGFP, indicating that the tdTomato cassette was excised by iCre in the nucleus of these cells, and that the FP-iCre fusion proteins displayed the normal functions of both fluorescence protein and iCre recombinase. Notably, the mEGFP could also be observed in the cytoplasm of some cells, maybe due to the continuous transportation of protein from the cell cytoplasm to the cell membrane. However, spillover between mOrange2 from the multi-color system and tdTomato from *Rosa26*^{mTmG} cells was also detected, due to the close emission spectra of these two fluorescent proteins. Despite this, it was still possible to distinguish them by their distinct protein localization. In summary, the results of functional testing of FP-iCre showed that the fusion proteins of the multi-color labeling system have the same functions with individual fluorescence protein and Cre recombinase, which is capable to be used for cell lineage tracing and Cre mediated DNA recombination.

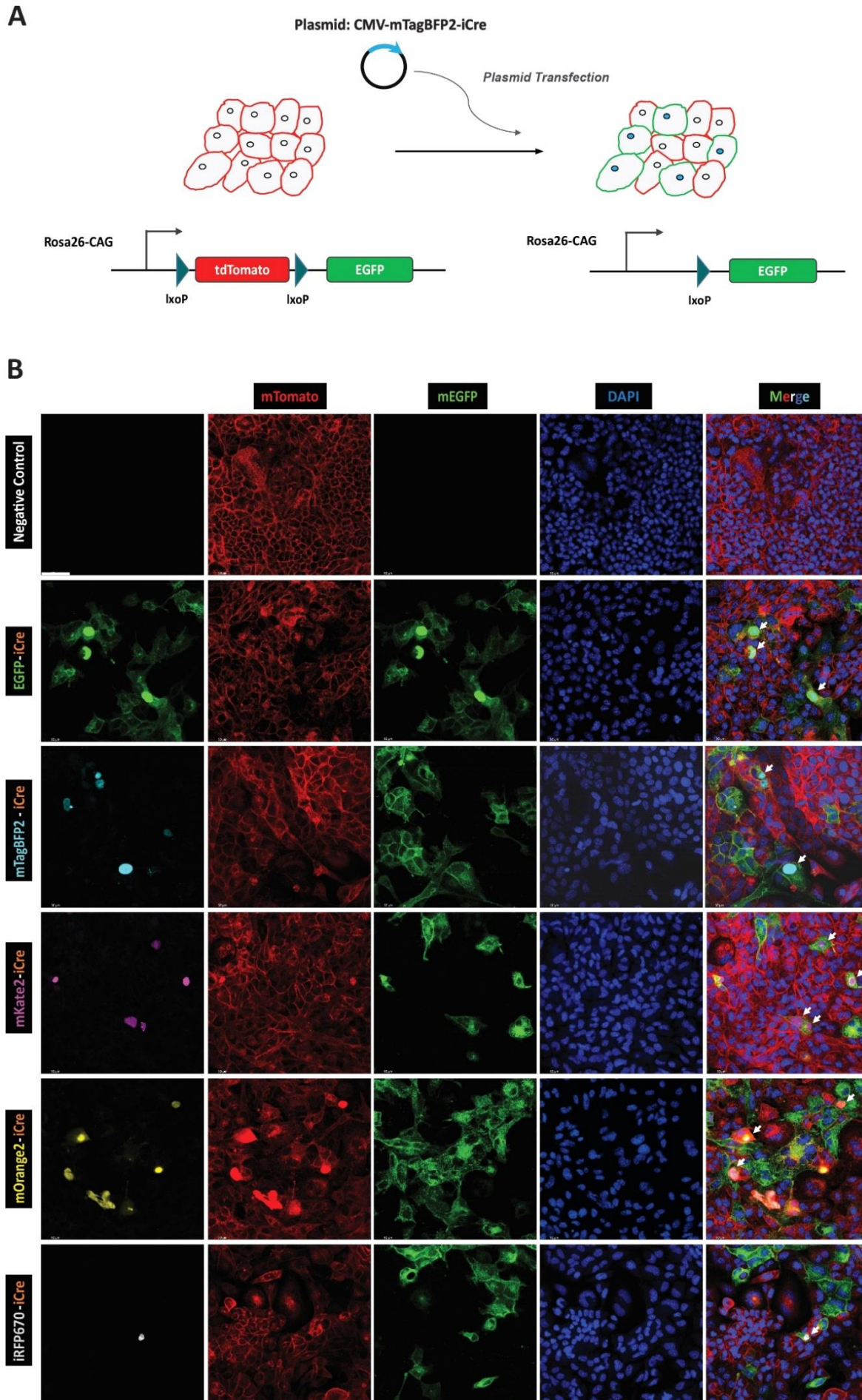


Figure 3. Functional testing for FP-iCre fusion proteins

(A) The schematic diagram of *Rosa26*^{CAG-mT/mG} allele recombination in primary PDAC cells mediated by Cre recombinase. Cells express the membrane-targeted tandem dimer Tomato (mT) prior to DNA recombination, and start to express membrane-targeted GFP after mT cassette has been excised by Cre. Meanwhile, FP-iCre protein can be detect in the nucleus of positive transfected cells.

(B) The representative fluorescent images of FP-iCre plasmids transfected *Rosa26*^{CAG-mT/mG} cells. The expression of mGFP and FP-iCre proteins with nuclear localization can be observed in the same cells (white arrows), and mT is disappearing in these cells. It indicates the mT cassette is excised by FP-iCre successfully, the FP-iCre fusion proteins have both normal function of fluorescent protein and Cre recombinase.

4.1.4 *In vitro* testing for cleavage efficiency of gRNAs

Clustered Regularly Interspaced Short Palindromic Repeats (CRISPR) are DNA sequences found originally in the genomes of prokaryotic organisms, such as bacteria and archaea, and function as a part of the defense systems of these organisms [196]. The endonuclease CRISPR-associated protein 9 (Cas9) can recognize and cleave specific DNA sequences with the help of the CRISPR sequence. Based on these functions, the Cas9 endonuclease and CRISPR sequence form the technology known as CRISPR-Cas9, which is widely used in genome editing [197].

This study aimed to label and monitor EMT-TFs *in vivo*, without disrupting their normal functions. The Class 2 CRISPR/Cas9 from *Streptococcus pyogenes* was applied to improve the efficiency of generation of genetically engineered mouse models (GEMMs). Normally, the active CRISPR/Cas9 complex (also known as Cas9 Ribonucleoprotein, RNP) consists of spCas9 protein, CRISPR RNA (crRNA) and trans-activating CRISPR RNA (tracrRNA) (Figure 4A). The crRNA is a short RNA that can guide endonuclease Cas9 to cleave a specific DNA sequence in the genome, while the tracrRNA sequence is necessary for the maturation of crRNA [198]. Together, they are referred to as guide RNA (gRNA) in the CRISPR/Cas9 genome editing system.

To test the cleavage efficiency of gRNAs that target EMT-TFs, the DNA fragments containing the gRNA target DNA sequence were obtained using PCR amplification. Subsequently, the same amount (800ng) of purified DNA was incubated with Cas9 RNP as described in the methods **section 3.3.3**. Following this, gel electrophoresis of nucleic acids was performed to

check the cleaved fragments from each reaction. As shown in **Figure 4B**, all DNA fragments were cleaved by the Cas9 RNP efficiently *in vitro*, and the separated bands of DNA were observed clearly (the sizes of cleaved and uncleaved DNA fragments are listed in Table 38). Furthermore, the cleavage efficiency of gRNAs was quantified based on the grayscale intensity analysis of DNA bands. The gRNA targets *Fsp1* and *Twist1* showed the highest cleavage activity (98% and 85% respectively), while the gRNAs targeting *Col6a1*, *Zeb1* and *Snai1* were also found to have relatively high levels of cleavage efficiency (Figure 4C). These results demonstrated that the gRNAs designed for EMT-TFs loci targeting have high DNA cleavage activity, and could be used to improve the efficiency of exogenous DNA cassette insertion.

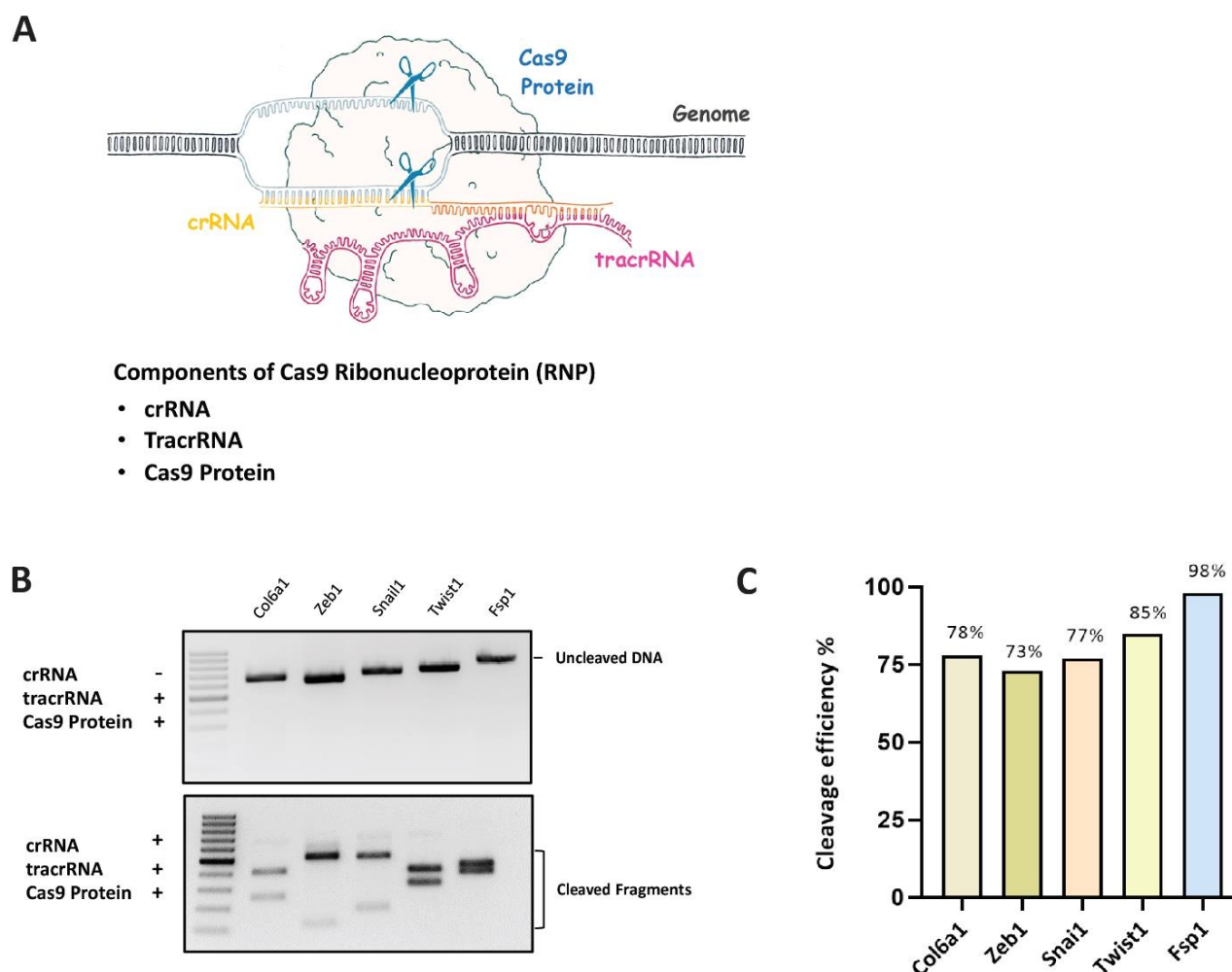


Figure 4. In vitro testing for cleavage efficiency of gRNAs

(A) The schematic diagram of CRISPR/Cas9-mediated genome editing and the components of CRISPR/Cas9 Ribonucleoprotein (RNP). The crRNA is a short sequence with 17-20 nucleotides, which can bind the target DNA specifically by recognizing bases complementary pairing. The tracrRNA is

complementary to the partial sequence of pre-crRNA, and together they form an RNA duplex to guide the Cas nuclease for DNA cleaving. crRNAs: CRISPR RNAs, tracrRNA: trans-activating CRISPR RNA. (B) Images of agarose gel electrophoresis for *in vitro* gRNAs cleavage assay. The DNA fragments containing gRNAs target sequence remain uncleaved when they incubate with Cas9 RNP without crRNA (Top). The separate DNA fragments are produced by Cas9 RNP cleavage (Bottom). (C) Cleavage efficiency of different gRNAs are quantified by gel densitometry.

Table 38. The size of uncleaved and cleaved DNA fragments

Gene	Uncleaved DNA	Cleaved DNA
Col6a1	655bp	405bp + 250bp
Zeb1	625bp	509bp + 116bp
Snai1	681bp	501bp + 180bp
Twist1	700bp	495bp + 305bp
Fsp1	790bp	425bp + 371bp

4.1.5 Generation of gene knock-in mouse embryonic stem cells

Following gRNA cleavage efficiency testing, the DNA sequence of gRNA was cloned into the spCas9 and gRNA expression vector. Meanwhile, the homologous recombination donor vectors (also known as the targeting vectors) for CRISPR knock-in (KI) were generated for mouse embryonic stem cell (mESC) -based gene targeting, with approximately 1.5 kb-long homology arms.

DNA double-strand breaks (DSBs) were generated by the CRISPR/Cas9 system at the gRNA recognition site close to the stop codon. This subsequently allowed the double-stranded DNA (dsDNA) targeting vector with homology arms to insert into the exogenous DNA at the DSB site, via the homology-directed repair (HDR) pathway (Figure 5A). As a result, the exogenous

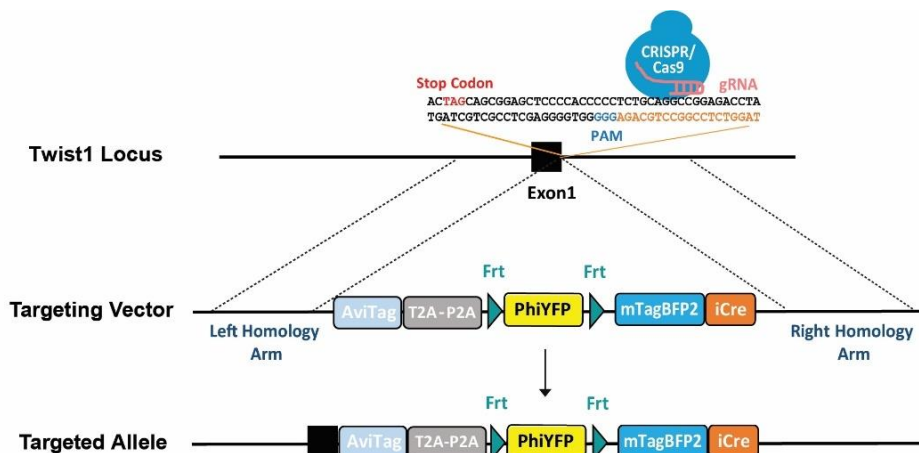
DNA was integrated into the genome of the mESC. The EMT-TFs were then labeled with AviTag, and the integrated allele of the mESC can express the FP-iCre fusion protein when Flp was present.

In order to identify the precise gene-targeted allele of mESCs, two pairs of PCR primers were designed for both left-side and right-side PCR analysis. In each pair of primers, one locates to the region of exogenous DNA, while the other locates to the external region of the homology arm (Figure 5B, C). In the screen PCRs, genomic DNA of ESC clones was examined using KI allele-specific PCR, and 20 were verified as positive clones by both 5' and 3' junction PCR amplification (Figure 5B, C). Meanwhile, the PCR products of positive ESC clones were sequenced for further confirmation of DNA integration. The KI positive ESC clones for other EMT-TFs were obtained in the same way, and the KI efficiency for all genes can be found in **Table 39**. As mycoplasmas can affect the cell growth, metabolism and genome stability of mESC, the positive ESC clones in good condition were cultured further for mycoplasma contamination testing prior to mESC blastocyst microinjection. The result of mycoplasma contamination testing proved that all KI-positive ESC clones were certified as mycoplasma-free (Figure 5D).

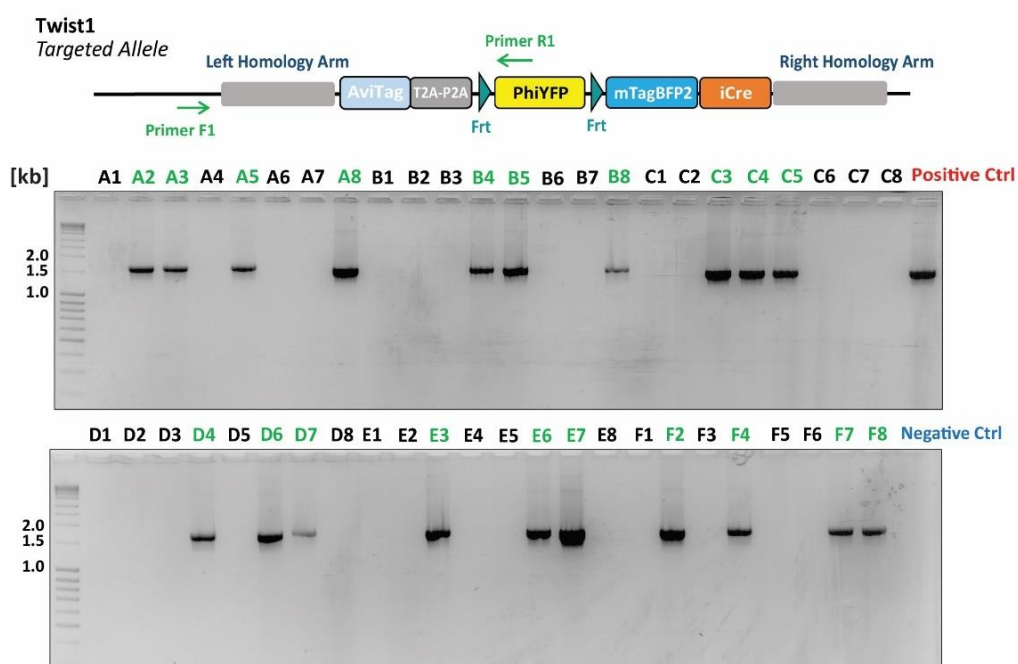
Table 39. Summary of ESC gene targeting

Gene	ES Clone Number	Positive clone	KI efficiency
Twist1	48	20	20/48 = 41.6%
Zeb1	72	0	0/72 = 0%
Snai1	56	6	6/56 = 10.7%
Col6a1	48	3	3/48 = 6.25%
Fsp1	43	4	4/43 = 9.3 %

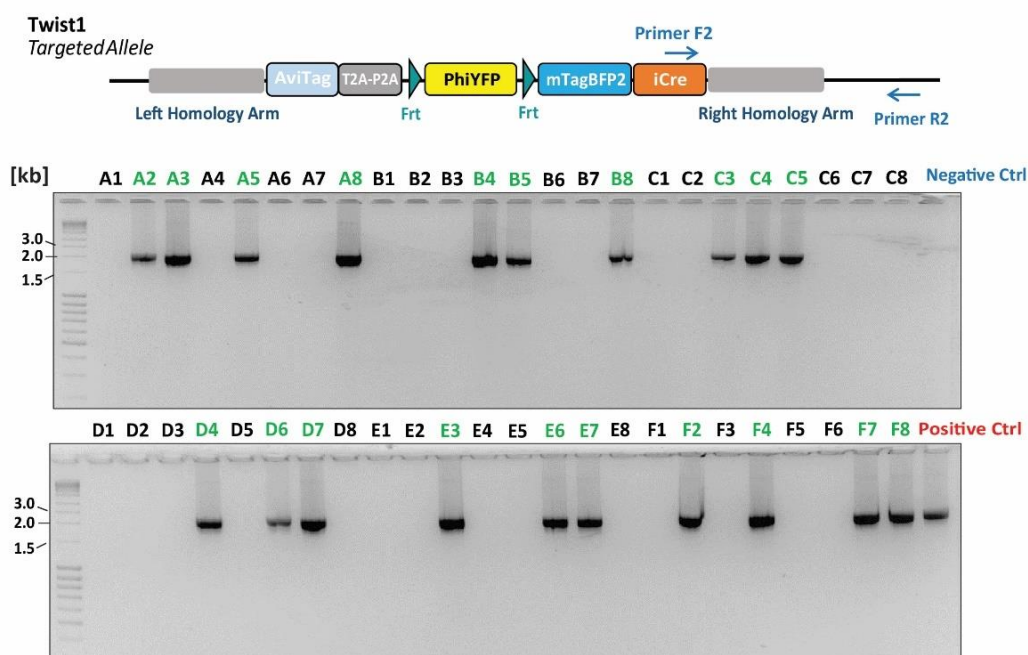
A



B



C



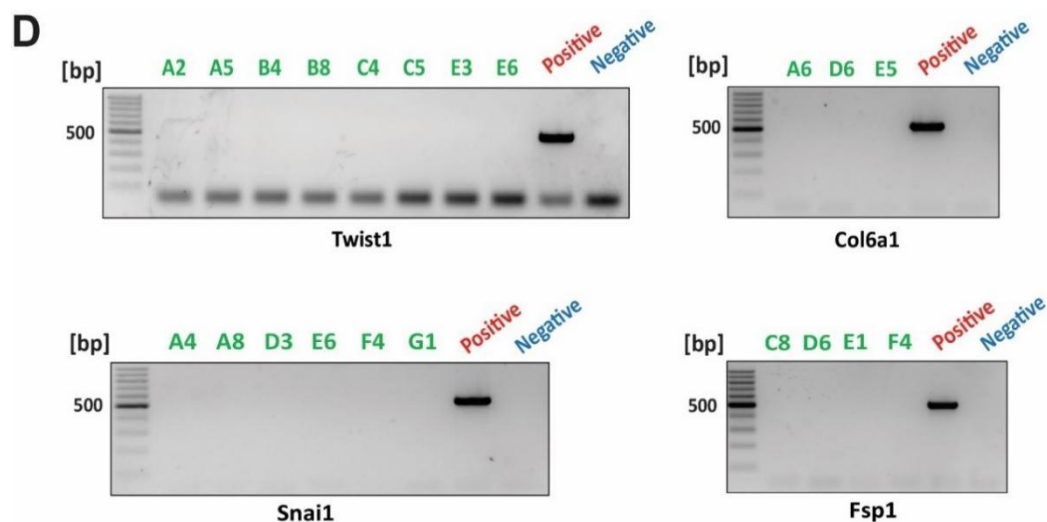


Figure 5. Generation of gene knock-in mouse embryonic stem cells

(A) Schematic representation of CRISPR/Cas9-mediated gene targeting at *Twist1* locus. spCas9 nuclease cuts the genome and produces DSBs near the stop codon, then the targeting vector inserts the knock-in DNA cassettes into the genome precisely via homology-directed repair. The stop codon of *Twist1* is shown in red, the base sequence with orange color represents the recognition sequence of gRNA for CRISPR/Cas9-mediated gene targeting, the protospacer adjacent motifs (PAMs) of gRNA is highlighted in blue.

(B-C) Schematic for left- and right-arm PCR analysis of *Twist* KI ES clones, the size of expected bands for left-side and right-side PCR analysis are 1650bp and 2100 bp, respectively. The genomic DNA from Wild-type ES cells was used as negative control. The positive control samples were DNA plasmids with long homology arms, they contain the binding sequences for both primers. Correctly targeted ES cell clones are labeled in green.

(D) Agarose gel electrophoresis images for mycoplasma contamination PCR detection of KI ES clones.

4.1.6 Functional testing for positive knock-in ESC clones

To determine whether the precise knock-in ESC clones function normally *in vitro*, the KI ESCs were infected with an adenovirus capable of expressing flp recombinase (Adeno-Flp) and EGFP simultaneously. The ESCs were then treated with TGF β -1 to induce expression of *Twist1*, and subsequently fixed with 4% PFA. The fluorescence of the FP-iCre fusion protein was detected using a confocal microscope (Figure 6A).

As shown in the diagrammatic sketch (Figure 6B), the ESCs can express the *Twist1*-AviTag fusion protein and the PhiYFP protein in the absence of flp recombinase. The *Frt*-PhiYFP-*Frt* cassette can be excised by the Flp/Frt recombination system when flp recombinase is present in KI positive ESCs. In this case, the *Twist1*-Avitag and mTagBFP2-iCre fusion proteins were

detected in the ESCs (Figure 6B). The results proved that mTagBFP2-iCre was detected in the nuclei of KI positive ESCs that were infected with adenovirus. No fluorescent signals of mTagBFP could be detected using CLSM in cells not infected with adenovirus, indicating that mTagBFP was not expressed in these cells (Figure 6C).

Meanwhile, immunoblotting was performed to detect the expression of PhiYFP and FP-iCre proteins in KI positive ESCs. The PhiYFP was detected in the control ESCs that without Adeno-Flp infection, while PhiYFP in Adeno-Flp infected ESCs was absent as the Frt-PhiYFP-Frt cassette has been excised by Flp recombinase (Figure 6C). Nonetheless, tiny amount of residual PhiYFP was still observed in Snai1-KI and Fsp1-KI adenovirus-infected ESCs, it may be due to the incomplete recombination of Frt-PhiYFP-Frt cassette (Figure 6D). Furthermore, the FP-iCre proteins were found in KI-allele-positive ESCs with Adeno-Flp infection. On the contrary, there was no FP-iCre protein could be detected in control ESCs (Figure 6D). Together these results proved that the KI positive ESCs work sufficiently well, the novel multi-color labeling system is capable to be applied for EMT-TF-positive cell tracing.

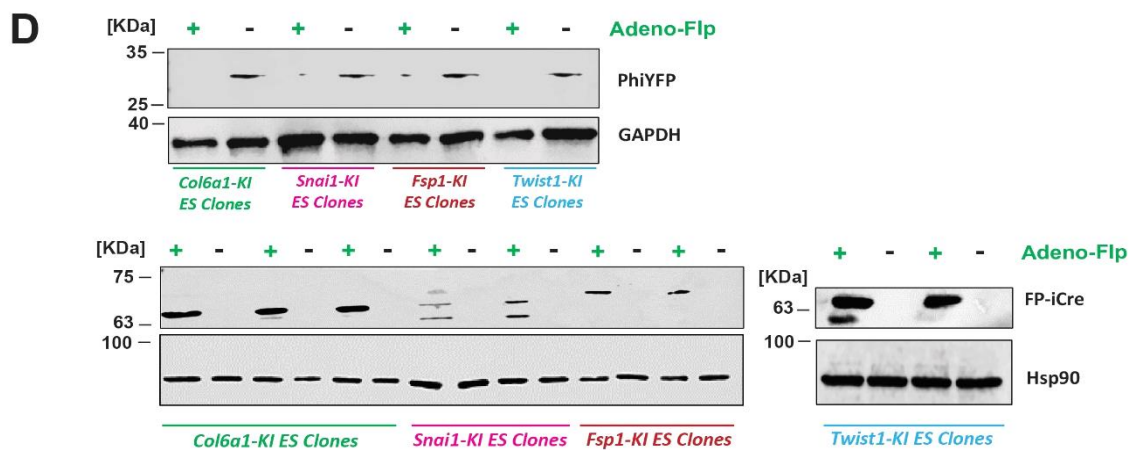
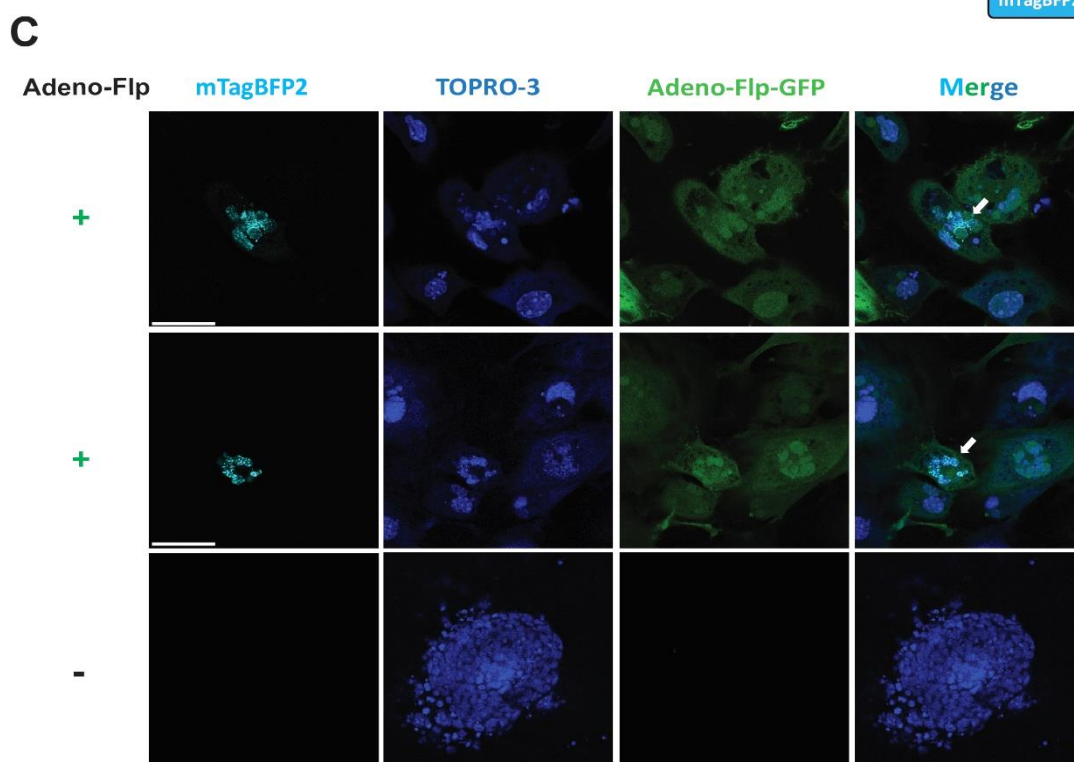
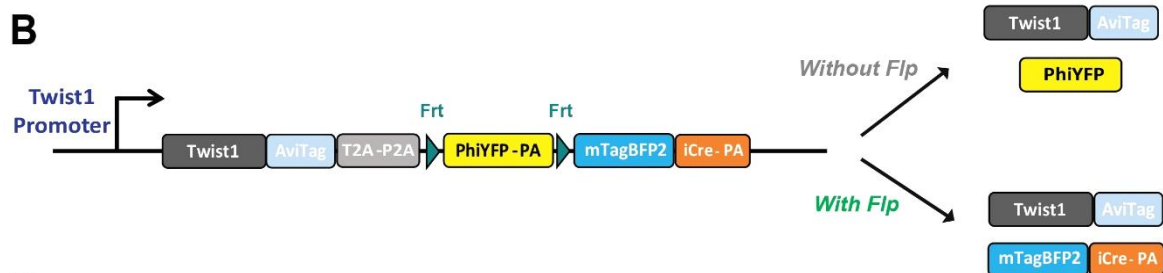
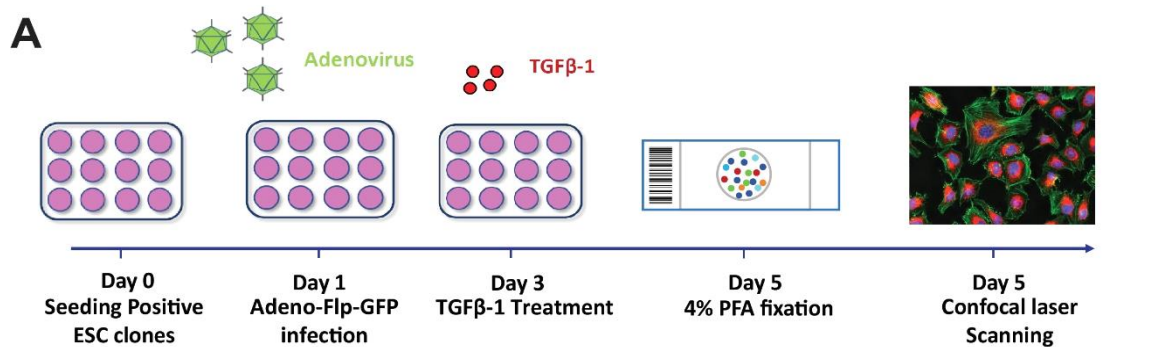


Figure 6. Functional test for positive KI ES clones

(A) Workflow diagram for functional verification experiments of KI ESCs.

(B) The schematic illustrates the different gene expression status of Twist1-KI ESCs.

(C) The representative fluorescent images of mTagBFP2-iCre expressing (white arrow) and non-expressing ES cells. Scale bar, 50 μ m.

(D) Western blot analysis for PhiYFP (Top) and FP-iCre (Bottom) expression of KI-allele-positive ESCs. PhiYFP protein was detected by turboYFP antibody, the expected size of PhiYFP protein is 27 KDa; the FP-iCre fusion proteins were detected by Cre recombinase antibody, the size of EGFP-iCre, mKate2-iCre, iRFP670-iCre and mTagBFP2-iCre fusion proteins are 63.5 KDa, 63.2 KDa, 71.5 KDa and 63.5 KDa, respectively. GAPDH and Hsp90 α/β are used as endogenous reference proteins for detection of PhiYFP and FP-iCre fusion proteins, respectively.

4.2 Chapter 2. Identifying and validating targets for novel PDAC treatment strategies

In a previous study of our group, we demonstrated that *Pdk1* inactivation could block the formation of pancreatic intraepithelial neoplasia (PanIN) and proliferation of pancreatic tumor cells in *Kras*^{G12D}-driven PDAC mouse models. In addition, deletion of *Braf* had only a slight effect on PDAC maintenance, and the effect of *c-Raf* deletion on PDAC progression was negligible.

4.2.1 CRISPR/Cas9 mediated gene LOF screening identified *c-Raf* as a driver of *Pdk1* deletion resistance

To identify synergistic genetic interaction that mediate cell death after *Pdk1*-ablation as well as resistance mechanisms in PDAC cells, our lab performed a CRISPR/Cas9-mediated gene loss-of-function (LOF) screen in *Pdk1*^{lox/lox} PDAC cells using the Genome-scale CRISPR Knock-Out v2.0 pooled library. This contains 62,804 single guide RNAs (sgRNAs) constructs to target 20,611 genes in mice (3 gRNA constructs per gene), and 1000 control sgRNAs were designed to not target any sequence in the genome [199, 200]. A lentivirus (LentiCas9-Blast) that expresses the protein spCas9 was produced to generate Cas9-expressing stable cell lines. A lentiviral sgRNA library (lenti-sgRNA-puro) was also created for infection of PDAC cells (Figure 7A).

Once a *Pdk1*^{lox/lox} PDAC cell line with stable Cas9 expression was generated, cells were divided into 2 groups: In the experimental group, cells were treated with 4-OHT to induce the

genetic deletion of *Pdk1*, while cells in the control group were cultured in the normal cell culture medium with 0.1% ethanol. Following 4-OHT treatment, cells in both groups were infected with lenti-sgRNA-puro. Further selection was then carried out using puromycin to isolate the cells with successful lentiviral integration. Finally, the cell genomic DNA was extracted and purified for next-generation sequencing (NGS) (Figure 7B).

One of the top hits from the gene LOF screen was the *c-Raf (Raf1)* gene, an intriguing result given that our previous study found that *c-Raf* deletion alone in PDAC cells had almost no inhibitory effect on the growth of PDAC cells (Figure 7C). On the contrary, in this study, CRISPR/Cas9-mediated *c-Raf* knock-out in *Pdk1*^Δ resistant PDAC cells inhibited their growth significantly and resulted in increased cell death. This suggests that *c-Raf* is essential for the survival of *Pdk1*^Δ resistant cells, and it could be a potential therapeutic target for PDAC treatment.

(A) The diagram represents the construct of plasmid vectors of Genome-scale CRISPR Knock-Out v2.0 pooled library for lentivirus packaging. (B) Schematic illustrates the workflow of genome-wide CRISPR/Cas9 mediated gene Loss-of-function screening in both *Pdk1^{WT}* and *Pdk1^Δ* cells. (C) Scatterplot depicting the results of sgRNA enrichment analysis in gene-level. The essential hits are displayed in red and the grey dots represent unannotated genes. R^2 values were calculated based on the normalized count values. The CRISPR screens have been performed and analyzed by PhD student of Saur lab - Katia Sleiman. These results are unpublished so far, they are just cited in this thesis.

4.2.2 Functional validation of *c-Raf* in *Pdk1^Δ* resistant PDAC cells

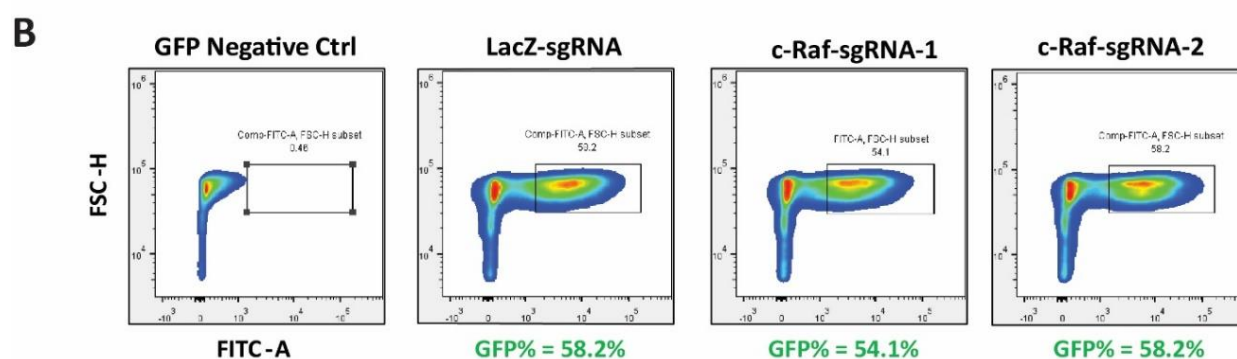
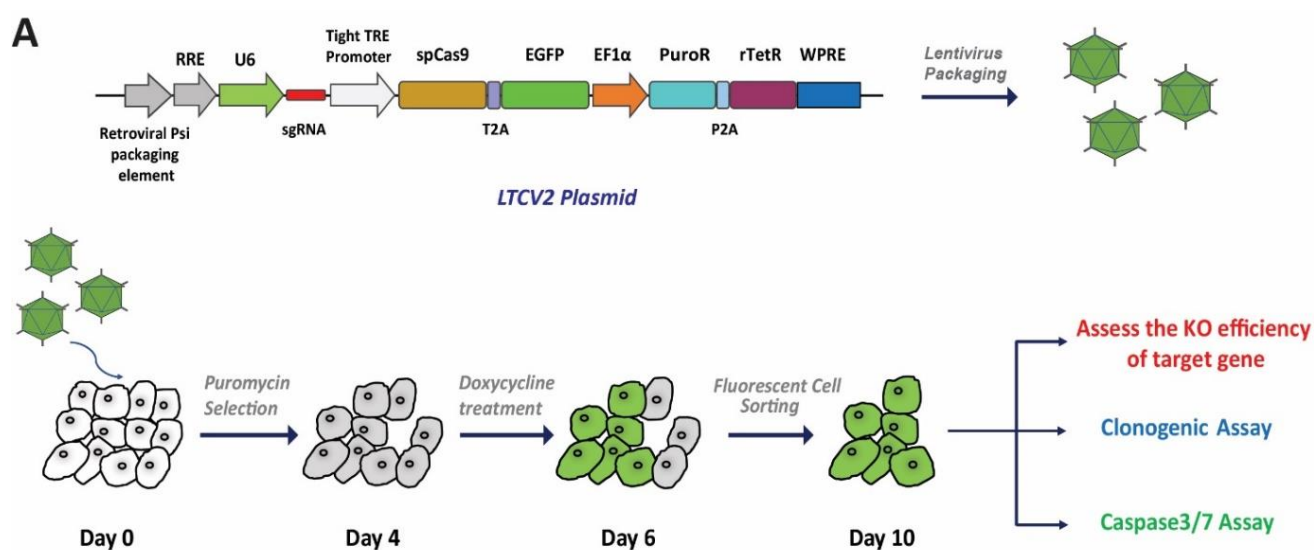
To determine the function of *c-Raf* in *Pdk1* deletion resistant cells, we constructed inducible lentiviral vectors expressing the Cas9 protein and sgRNAs that target *c-Raf*. Firstly, the *Pdk1^Δ* resistant cells were infected with the Cas9/sgRNA lentivirus. The cells were then treated with puromycin for 4 days to generate the stable cell lines expressing sgRNA and Cas9 protein from the integrated lentiviral vector. These cells were subsequently treated with doxycycline and sorted further using fluorescence-activated cell sorting (FACS) for clonogenic and caspase 3 & 7 assay experiments. Genomic DNA was also extracted from these cells for *c-Raf* knock-out efficiency analysis (Figure 8A).

In addition, the sgRNA that targets *LacZ* gene was cloned into the lentiviral vector to serve as a control. The percentage of GFP-positive cells in lacZ-sgRNA, c-Raf-sgRNA1 and c-Raf-sgRNA2 groups following treatment with doxycycline to induce Cas9 expression were 58.2%, 54.1%, and 58.2%, respectively, indicating that the expression of the Cas9 protein was similar across cell groups (Figure 8B), as spCas9 and the EGFP DNA sequence are expressed from the same ORF. Genomic DNA of *Pdk1^Δ* resistant cells was isolated and purified to determine the KO efficiency of the *c-Raf* gene using Sanger sequencing. These results were analyzed further using the CRISPR Tracking of Indels by Decomposition (CRISPR TIDE) analysis tool, which can identify and quantify insertions and deletions (indels), as well as point mutations caused by Cas9-mediated DNA cleavage.

Overall, the cleavage efficiency of c-Raf-sgRNA-1 and c-Raf-sgRNA-2 were 53.7% and 69.3% respectively, with c-Raf-sgRNA-2 displaying higher cleavage activity than c-Raf-sgRNA-1. More point mutations were identified at the cutting site of sgRNA-1 (23%) compared to sgRNA-2 (5.5%), which may increase the number of silent mutations and decrease the

phenotypic effects, as the silent mutations might not change the ORF and the protein with normal function can still be produced. In contrast, sgRNA-2 resulted in a higher percentage of base pair insertions, which cause frameshift mutations that shift the ORF after the site of insertion. This can lead to the production of a nonfunctional protein product (Figure 8C).

To further investigate the role of *c-Raf* in maintaining the survival of PDAC cells following *Pdk1* deletion, 2000 cells were seeded in a 6-well plate for clonogenic assay after *c-Raf* inactivation. Compared to the group of *c-Raf*-sgRNA-1, the *c-Raf* -sgRNA-2 group displayed a stronger inhibition effect on cell colony formation, which is consistent with the results of sgRNAs cleavage efficiency (Figure 8D). Furthermore, downregulation of *c-Raf* induced by sgRNA also increased apoptosis of *Pdk1*^Δ resistant cells slightly. Specifically, *c-Raf*-sgRNA-2 induced a higher level of apoptosis than *c-Raf*-sgRNA-1, as Cas9/*c-Raf*-sgRNA-2 has higher gene editing activity for *c-Raf* (8E). Together, these results revealed that inactivation of *c-Raf* produced a synergistic lethal response in *Pdk1*^Δ resistant PDAC cells, which significantly impaired colony formation and induced apoptosis in *Pdk1*^Δ resistant cells.



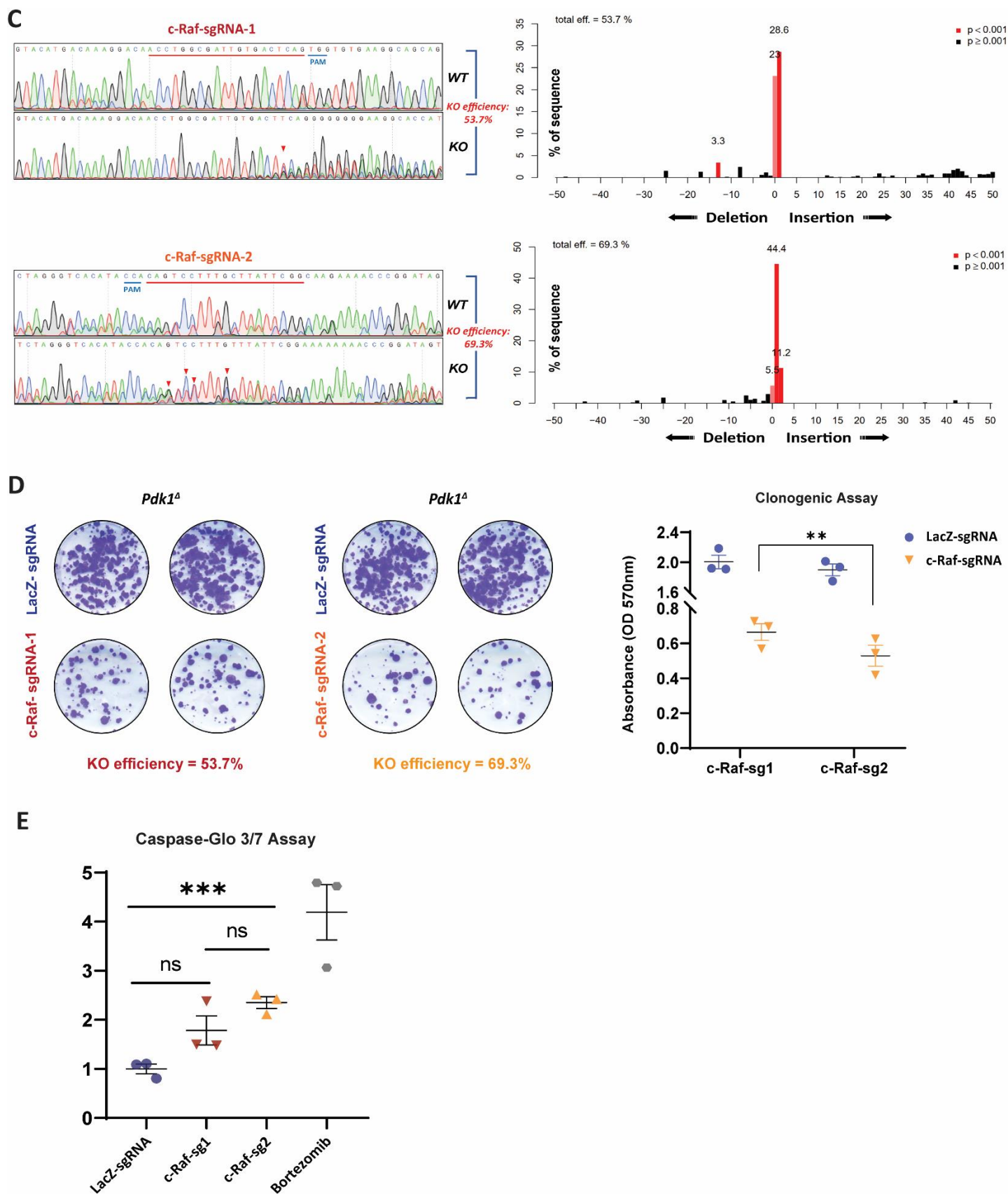


Figure 8. Functional validation of *c-Raf* in *Pdk1^d* resistant PDAC cells

(A) Schematic representation of workflow for *c-Raf* functional validation experiments. gRNAs targeting *c-Raf* are cloned into LTCV2 plasmid for lentivirus producing. The expression of Cas9 protein and EGFP are induced by Doxycycline (Dox), and EGFP positive cells are sorted by FACS.

(B) Fluorescence-activated cell sorting (FACS) of EGFP-expressing cells after 2-days of Dox treatment.

(C) Cleavage efficiency of gRNAs and the insertion-deletions (indels) frequency are assessed by Sanger Sequencing and TIDE online platform.

(D) Left: Clonogenic assay of *Pdk1*^Δ resistant PDAC cells after *c-Raf* inactivation in *c-Raf*-gRNA1 and *c-Raf*-gRNA2 groups; Right: Crystal violet is dissolved using 1% SDS and quantified by measuring the absorbance at 570 nm. Data represent mean ± S.E.M. Triplicates are shown. ***p* value < 0.01; ****p* value < 0.001, two-tailed student's t test.

(E) Result of Caspase 3/7 assay for *c-Raf*-gRNA1 and *c-Raf*-gRNA2 KO cells. Positive control: Cells are treated with 0.5 μM Bortezomib for 12 hours to induce the apoptosis. Data are shown as mean ± SD, n = 3 replicates. ****p* value < 0.001, two-tailed student's t test.

4.2.3 Generation of *Pdk1*, *Braf* and *c-Raf* conditional deletion PDAC cell lines

To investigate the effects of *Pdk1*, *Braf*, and *c-Raf* triple-knockout (TKO) on PDAC development, *Pdk1*, *Braf* and *c-Raf* gene floxed (flanked by loxP sites) GEMMs were generated using ESC gene targeting. These mice were then interbred with the *Pdx-Flp*, *FSF-Kras*^{G12D}, *FSF-Rosa26*^{CAG-CreERT2}, *Trp53*^{frt/+} (one of the *Trp53* alleles was flanked by Frt sites) mouse line to produce the *Pdk1*, *Braf*, *c-Raf* conditional inducible KO PDAC mouse models (Figure 9A). The primary tumor cell lines were isolated from these mice after they developed solid pancreatic tumors. Following this, the mouse PDAC cell lines were treated with 4-Hydroxytamoxifen (4-OHT) for 8 days to induce the conditional gene deletion of *Pdk1*, *Braf* and *c-Raf*. The genomic DNA of these cells was extracted at different time points (Day2, Day4, Day6 and Day8, respectively) for DNA recombination PCR testing. Once the tumor cells were treated with 4-OHT, the CreERT² translocated to the cell nuclei, and the genes flanked by loxP sequences excised by the Cre/loxP recombination system. Meanwhile, different PCR primers were designed to detect the recombination status of target genes (Figure 9B). The results showed that *Pdk1*, *Braf* and *c-Raf* in PDAC cells were completely excised after at least 6-day of 4-OHT treatment (Figure 9C).

In addition, proteins were extracted for immunoblotting from PDAC cells that were treated with 4-OHT for 8 days. The phosphorylation of the AKT protein at the T308 site (pAKT-T308) was markedly reduced in *Pdk1* deletion cells, while phosphorylation at the pAKT-s473 site

remained unchanged, as pAKT-s473 has been shown to be phosphorylated by mTOC2. The decreased phosphorylation of ERK1 and ERK2 observed also indicated that the expression of *Braf* and *c-Raf* in PDAC cells was blocked following 4-OHT treatment (Figure 9D).

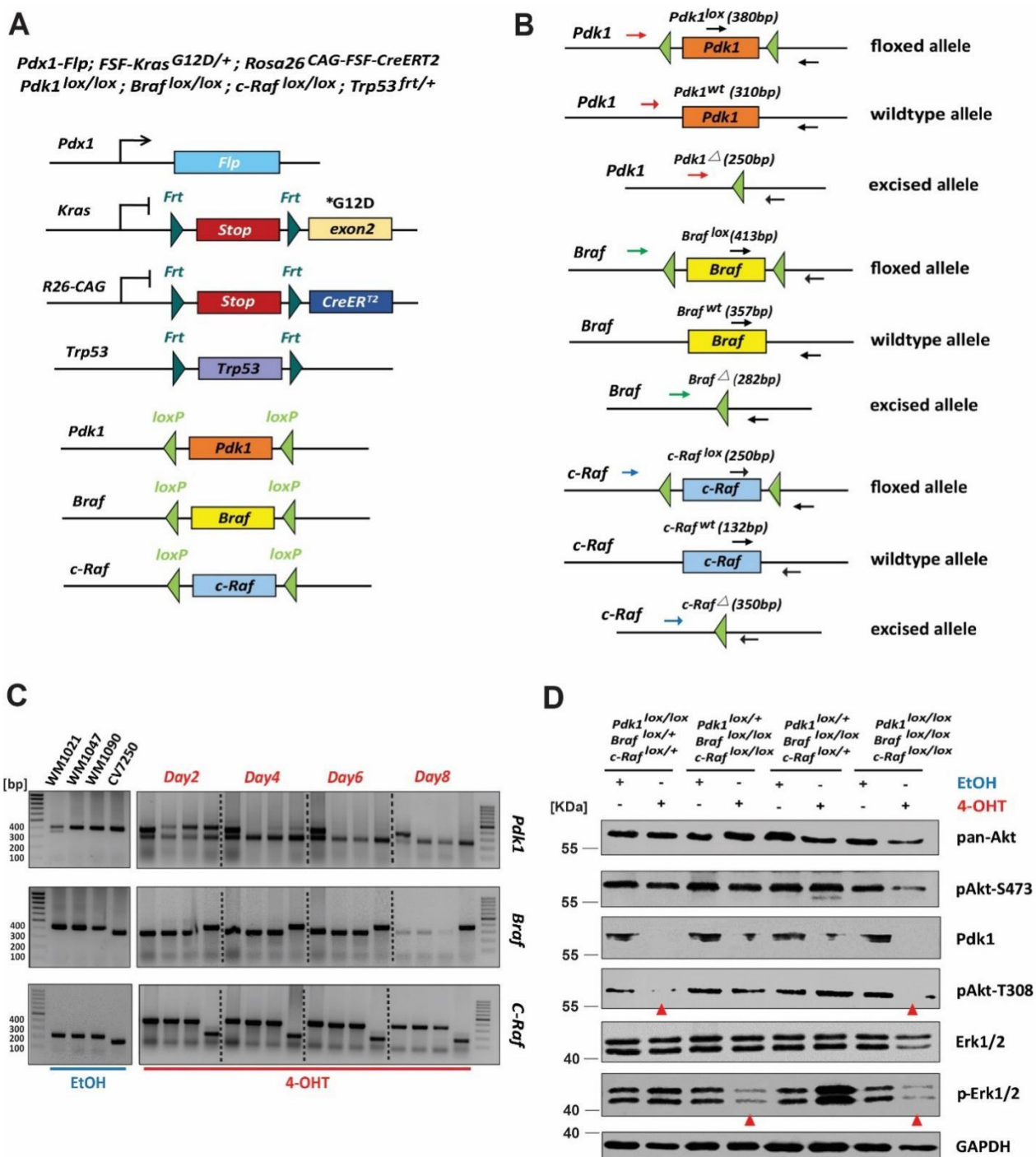


Figure 9. Generation of *Pdk1*, *Braf* and *c-Raf* triple Knock-out cell lines

(A) Schematic of modified alleles of *Pdk1*, *Braf* and *c-Raf* genes. The *Pdx1* promoter-driven Flp excises *Frt-Stop-Frt* cassettes and activates the expression of *Kras^{G12D}* and *CreERT2*. Flippase also removes the *Trp53* modified allele to accelerate the progression of PDAC.

(B) Schematic representation of the PCR-based genotyping strategies to detect Cre/loxP mediated DNA recombination at *Pdk1*, *Braf* and *c-Raf* loci.

(C) Agarose gel electrophoresis results of genotyping PCRs show *Pdk1*, *Braf* and *c-Raf* modified alleles are excised by *CreER^{T2}* after 8-day 4-OHT (0.5 μ M) treatment in PDAC cells.

(D) The protein expression of downstream effectors of *Pdk1*, *Braf* and *c-Raf* is assessed by western blotting analysis. GAPDH is the endogenous reference protein. Size of proteins: Akt- 60 KDa; pAkt(S473)- 60 KDa; Pdk1- 58~68 KDa; pAkt (T308) - 60 KDa; Erk1/2- 44, 42 KDa; pErk1/2- 44,42 KDa; GAPDH -37KDa.

4.2.4 Inactivation of *Pdk1*, *Braf* and *c-Raf* alters gene expression profile in PDAC cells

To have a comprehensive view of alterations to the transcriptome following *Pdk1*, *Braf* and *c-Raf* ablation, the total-RNA from cell lines was extracted using the QIAGEN RNeasy Kit, then sequenced with a HiSeq2500 sequencing system (Illumina, Inc. USA). To improve the accuracy of the RNAseq results, 5 mouse primary PDAC cell lines harboring floxed *Pdk1*, *Braf* and *C-Raf* alleles (*Pdk1*^{lox/lox}; *Braf*^{lox/lox}; *C-Raf*^{lox/lox}; *Trp53*^{Frt/+}) were used for RNA sequencing. These cell lines were treated with EtOH and 4-OHT for 8 days separately, and total-RNA was then extracted and purified using QIAGEN RNeasy Kits.

Prior to further analysis, the raw count values of each gene were first normalized with TPM (transcripts per kilobase million). The gene set enrichment analysis (GSEA) showed that 10 hallmark and 13 Kyoto Encyclopedia of Genes and Genomes (KEGG) gene sets were significantly upregulated in PDAC cells following 4-OHT treatment. Among them, hallmark KRAS signaling was downregulated upon deletion of *Pdk1*, *Braf* and *c-Raf*, suggesting that the growth of PDAC cells was impaired due to the downregulation of KRAS downstream effectors following inactivation of *Pdk1*, *Braf* and *c-Raf* (Figure 10A, 10B). KEGG lysosome and autophagy pathways were upregulated in 4-OHT-treated cells, which may indicate that TKO triggers autophagy in PDAC cells. Furthermore, upregulated interferon-alpha and gamma responses were observed in *Pdk1*, *Braf* and *C-Raf* -deficient PDAC cells, suggesting that these tumor cells might have a more positive response to immune surveillance (Figure 10A, 10B). Interferon-alpha and gamma can stimulate immune cells and prevent tumor immune escape, thereby enabling a more efficient recognition of PDAC cells by the immune system [201, 202]. Of note, the Hallmark and KEGG pathways EMT, IL-6/JAK/STAT3, Wnt

and TGF- β signaling pathways were also significantly enriched in PDAC cells following 4-OHT treatment (Table 40). The underlying mechanisms are unclear and need further investigation.

Conversely, DNA replication pathways and the Hallmark and KEGG pathways of the cell cycle were found to be enriched in control cell lines that received EtOH treatment. This suggests that PDAC cells with functional genes of *Pdk1*, *Braf*, and *c-Raf* display strong proliferation and DNA synthesis ability, which is vital for tumor growth, maintenance and self-renewal, corroborating the effects of the TKO on PDAC cell viability and proliferation shown in Figure 12. In addition, *PI3K/AKT/mTOR*, glycolysis and *c-Myc* signaling pathways are enriched in control cells treated with EtOH. *Pdk1* is a crucial effector of the *PI3K/AKT* pathway, as it can activate AKT by phosphorylating the amino acid Thr308(T308) [203]. *Pdk1* also serves as a gatekeeper for glycolysis, and can promote tumor cells to produce pyruvate, thus maintaining their growth and survival [204]. *Pdk1* can directly regulate the activity of Polo-like kinase 1 (*PLK1*), which in turn phosphorylates c-Myc protein. The activated c-Myc is then able to further regulate the proliferation of pancreatic cancer cells [205, 206]. Taken together, the results of this GSEA provided a general view of perturbations in the transcriptional profile following inactivation of *Pdk1*, *Braf* and *c-Raf* in PDAC cells.

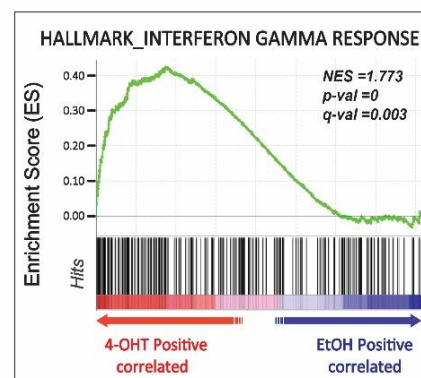
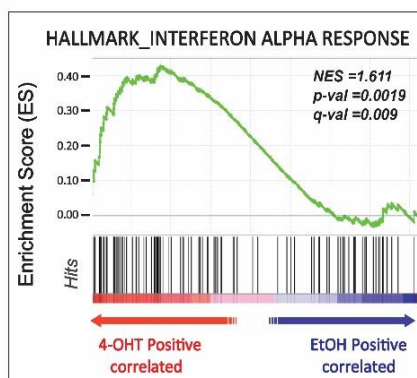
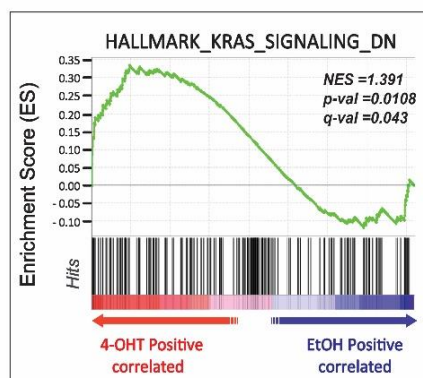
Concurrently with the GSEA discussed above, genes with at least 2.0-fold changes ($\text{Log}_2\text{FC} \geq 1$, $p\text{-value} \leq 0.05$, $\text{FDR} \leq 0.05$) were analyzed using the Protein ANalysis THrough Evolutionary Relationships (PANTHER) Classification System, to gain insight into changes in biological processes in PDAC cells receiving 4-OHT treatment. Notably, genes associated with regulation of programmed cell death (in particular, apoptosis and autophagy) were significantly enriched ($p\text{-value} = 7.86\text{e-}09$, $\text{FDR} = 1.88\text{e-}06$) in PDAC cells following 4-OHT treatment (Figure 10C). This data further supports the conclusion that *Pdk1*, *Braf* and *c-Raf* deletion induces programmed cell death in PDAC cells as shown by Caspase assay in Figure 12.

Genes with at least 2.0-fold changes in mean expression (Log_2 fold change ≥ 1 or ≤ -1 , $p\text{-value} \leq 0.01$) are presented in the volcano plot (Figure 10D). Of the genes with statistically significant changes in mean expression, the tumor suppressor *Atoh8* was reported to regulate

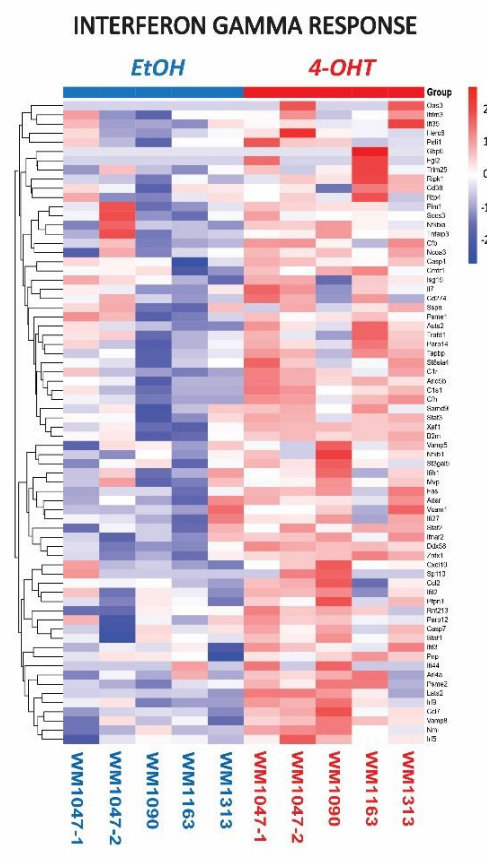
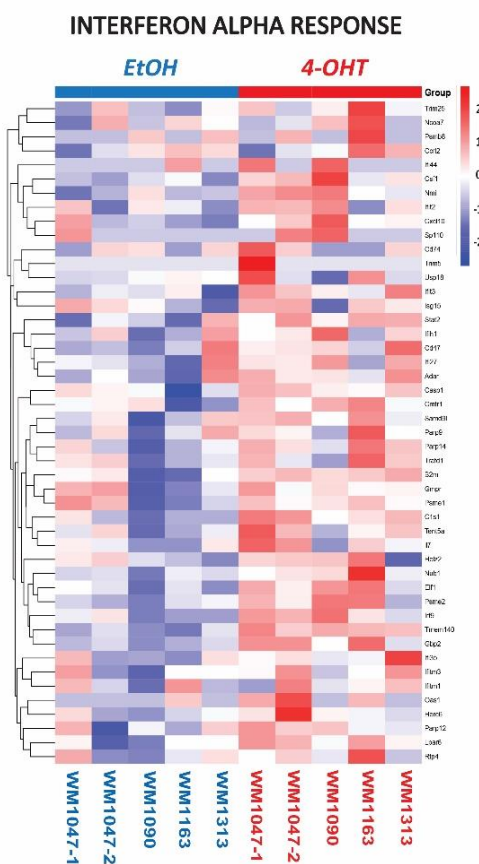
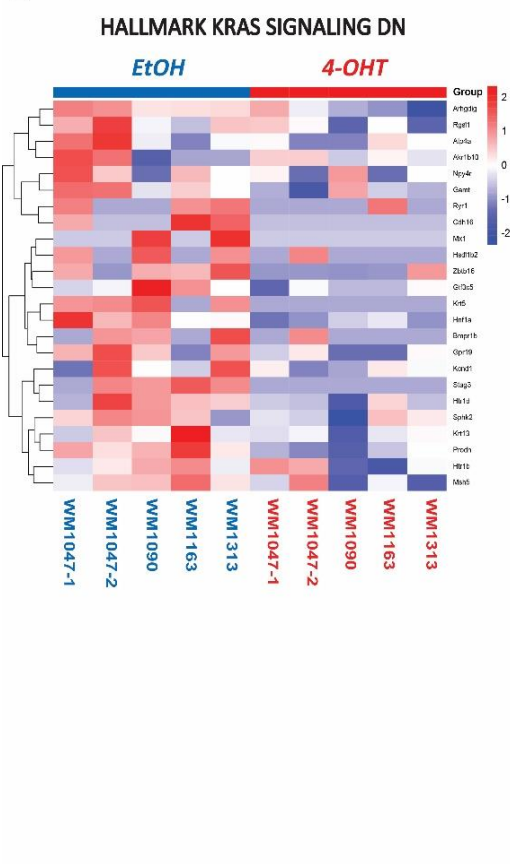
tumor cell differentiation and stemness. Upregulated expression of *Atoh8* can inhibit cell proliferation and reduce chemotherapy resistance in hepatocellular carcinoma (HCC) cells [207]. The *Pbxip1* gene encodes a protein that can block the activity of the oncogenic gene *E2A-PBX1* indirectly [208]. The upregulated *Trim56* gene is also involved in the suppression of tumor development, as previous studies showed that *Trim56* could impede the progression of HCC and multiple myeloma by inactivating *Wnt* signaling and activating *TLR3/TRIF* signaling, respectively [209, 210]. In addition, increased activity of both lysosome-associated membrane protein 2 (*Lamp2*) and the *Syt11* protein are highly associated with regulation of the autophagy-lysosome pathway [211, 212]. These results are consistent with the enrichment of Hallmark or KEGG autophagy-lysosomal pathways observed in our GSEA analysis described above. However, increased expression of the gene *Serpinb9* could lead to tumor cell rescue, as it prevents cell apoptosis and promotes tumorigenesis [213]. Moreover, high expression of the *Tmem140* gene is likely to increase the viability, migration, and invasion of tumor cells [214]. These phenomena were probably caused by the activation of compensatory cell signaling pathways, which are based on stress responses or feedback loops.

Conversely, expression of cell cycle and proliferation-associated genes such as *Top2a*, *Ube2C*, *Cdca3* and *ki-67* was found to be remarkably down-regulated in PDAC cells with TKO, supporting our cell viability and proliferation assays shown in Figure 12. Recently, *Top2a* was even reported to promote proliferation and metastasis of gallbladder cancer [236]. Down-regulation of the genes *Pold2* and *Mcm3* could reduce DNA replication and repair in cells, which is thought to interfere with cell division. The processes of chromosome movement, spindle assembly, and elongation, which are critical for the cell cycle and, thus, for cell survival, were impeded due to decreased expression of *Cenpe*, *Bub1b*, *Mcm3*, and *Nusap1* [215-218].

A



B



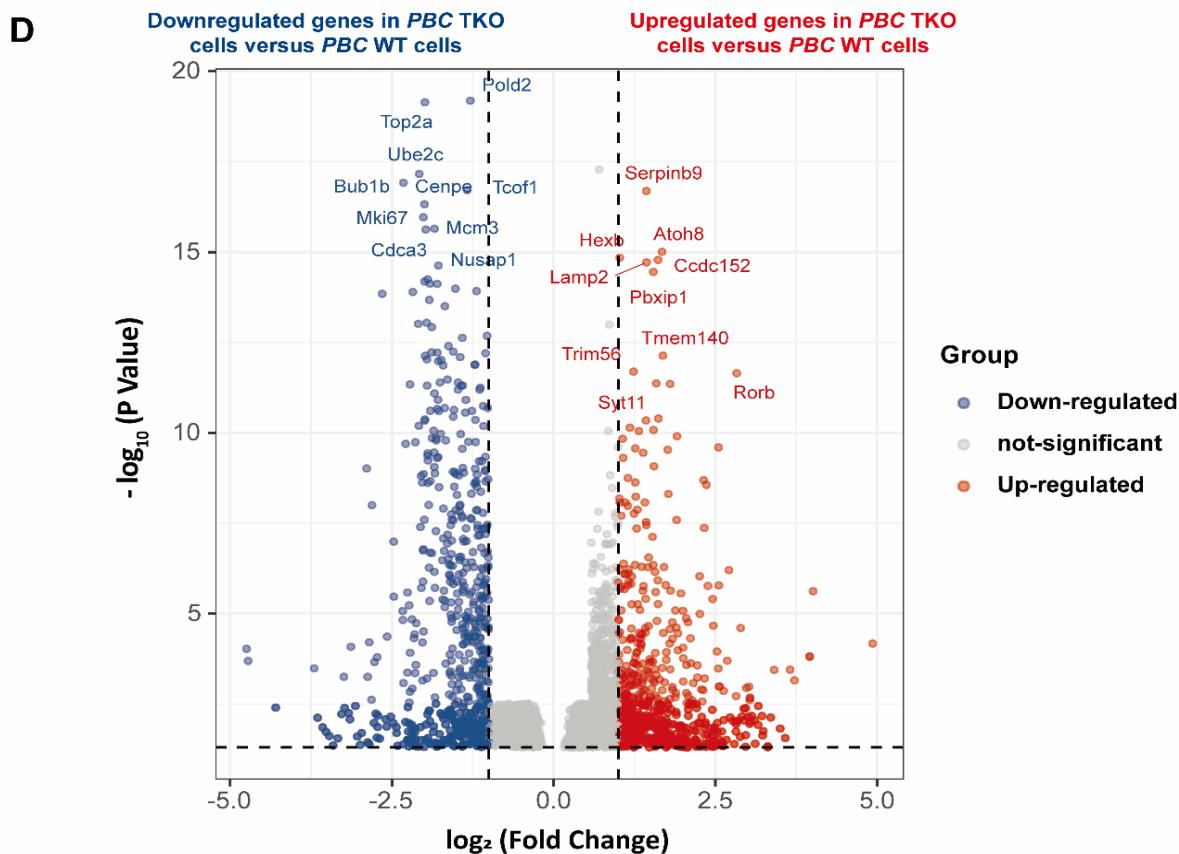
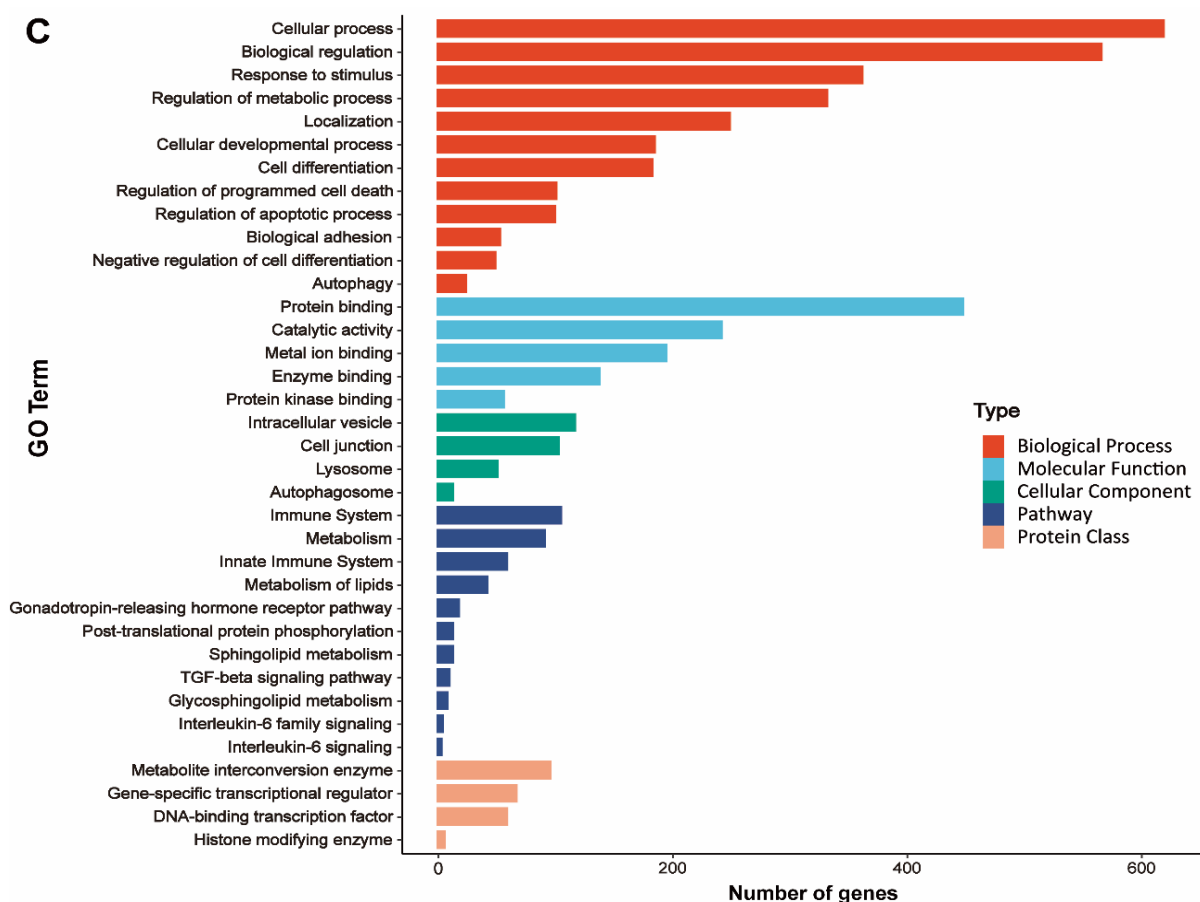


Figure 10. Deletion of *Pdk1*, *Braf* and *c-Raf* alters gene expression profile in PDAC cells

(A) Gene set enrichment analysis (GSEA) reveals that Hallmark Kras signaling downregulation, Interferon alpha and gamma response are significantly enriched in PDAC cells with inactivation of *Pdk1*, *Braf* and *c-Raf* genes (n=5).

(B) Heatmaps show the distinct gene expression profile of indicated Hallmarks and signaling pathways between *Pdk1*^{WT}; *Braf*^{WT}; *c-Raf*^{WT} and *Pdk1*^Δ; *Braf*^Δ; *c-Raf*^Δ cohorts (n=5).

(C) Gene ontology analysis depicts the significantly enriched gene categories including biological process, molecular function, cellular component, signaling pathway and protein class in PDAC cells after inactivation of *Pdk1*, *Braf* and *c-Raf*. Gene count represents the frequency of input genes which are matched with that in database. All the cell lines (WM1047-1, WM1047-2, WM1090, WM1163 and WM1313) are mouse pancreatic cancer cell lines with same genotype. The genotype of cell lines is: *Pdx1-Flp*; *FSF-Kras*^{G12D/+}; *FSF-Rosa26*^{CAG-CreERT2}; *Pdk1*^{lox/lox}; *Braf*^{lox/lox}; *c-Raf*^{lox/lox}; *Trp53*^{flr/+}.

(D) The volcano plot shows the most upregulated and downregulated genes with statistical significance in *Pdk1*^Δ; *Braf*^Δ; *c-Raf*^Δ PDAC cells versus wild-type cells. The red dot represents genes with up-regulated expression in *Pdk1*^Δ; *Braf*^Δ; *c-Raf*^Δ PDAC cells when they compared with *Pdk1*^{WT}; *Braf*^{WT}; *c-Raf*^{WT} PDAC cells, and the blue denotes down-regulated gene expression in *Pdk1*^Δ; *Braf*^Δ; *c-Raf*^Δ PDAC cells, and grey indicates non-significant (log2 fold change ≥1 or ≤ -1, p-value ≤ 0.01), n=5.

Table 40. Enriched Hallmark and KEGG pathways in *Pdk1*^Δ; *Braf*^Δ; *c-Raf*^Δ cell lines

Gene set	Size	NES	p-val	FDR q-val
HALLMARK_COAGULATION	131	1.968326	0	0
HALLMARK_EPITHELIAL_MESENCHYMAL_TRANSITION	196	1.934309	0	0
HALLMARK_INTERFERON_GAMMA_RESPONSE	192	1.773614	0	3.75E-04
HALLMARK_IL6_JAK_STAT3_SIGNALING	85	1.713644	0.001912	0.00344
HALLMARK_INTERFERON_ALPHA_RESPONSE	95	1.611779	0.001905	0.009796
HALLMARK_TGF_BETA_SIGNALING	53	1.569203	0.012821	0.012302
HALLMARK_ANGIOGENESIS	35	1.476409	0.029144	0.023165
HALLMARK_PROTEIN_SECRETION	96	1.419586	0.0217	0.037828
HALLMARK_TNFA_SIGNALING_VIA_NFKB	195	1.416309	0.001739	0.035798
HALLMARK_KRAS_SIGNALING_DN	177	1.391475	0.01083	0.04351
KEGG_LYSOSOME	117	2.004404	0	0.004212
KEGG_AXON_GUIDANCE	125	1.960127	0	0.006747
KEGG_BASAL_CELL_CARCINOMA	53	1.90752	0	0.008053
KEGG_MELANOGENESIS	95	1.728417	0	0.052746

KEGG_HEDGEHOG_SIGNALING_PATHWAY	51	1.66363	0.001923	0.088044
KEGG_ABC_TRANSPORTERS	42	1.610347	0.014028	0.126995
KEGG_RENIN_ANGIOTENSIN_SYSTEM	15	1.5862	0.014056	0.136743
KEGG_WNT_SIGNALING_PATHWAY	141	1.579935	0	0.127683
KEGG_TGF_BETA_SIGNALING_PATHWAY	83	1.570381	0.005226	0.126015
KEGG_REGULATION_OF_AUTOPHAGY	22	1.551429	0.028736	0.13376
KEGG_CHEMOKINE_SIGNALING_PATHWAY	162	1.547845	0	0.126432
KEGG_GLYCOSAMINOGLYCAN_DEGRADATION	19	1.544727	0.037402	0.12026
KEGG_TYPE_II_DIABETES_MELLITUS	46	1.48817	0.020794	0.150721

Table 41. Enriched gene signatures in vehicle treated control PDAC cells

Gene set	Size	NES	p-val	FDR q-val
HALLMARK_E2F_TARGETS	200	-3.31349	0	0
HALLMARK_G2M_CHECKPOINT	196	-3.06083	0	0
HALLMARK_MYC_TARGETS_V1	200	-3.01382	0	0
HALLMARK_MYC_TARGETS_V2	57	-2.70263	0	0
HALLMARK_MTORC1_SIGNALING	198	-2.54141	0	0
HALLMARK_CHOLESTEROL_HOMEOSTASIS	72	-2.09694	0	0
HALLMARK_GLYCOLYSIS	196	-1.9521	0	1.49E-04
HALLMARK_SPERMATOGENESIS	122	-1.817	0	6.35E-04
HALLMARK_DNA_REPAIR	149	-1.78592	0	0.001129
HALLMARK_MITOTIC_SPINDLE	199	-1.70664	0	0.001272
HALLMARK_OXIDATIVE_PHOSPHORYLATION	196	-1.40019	0.009368	0.032887
HALLMARK_ESTROGEN_RESPONSE_EARLY	195	-1.38418	0.004751	0.03647
HALLMARK_KRAS_SIGNALING_UP	198	-1.38299	0.009009	0.034708
HALLMARK_PI3K_AKT_MTOR_SIGNALING	101	-1.33228	0.041958	0.047313
KEGG_DNA_REPLICATION	35	-2.69424	0	0
KEGG_RIBOSOME	83	-2.67733	0	0

KEGG_SPLICEOSOME	122	-2.42866	0	0
KEGG_CELL_CYCLE	122	-2.39186	0	0
KEGG_HOMOLOGOUS_RECOMBINATION	27	-2.28436	0	0
KEGG_MISMATCH_REPAIR	22	-2.25445	0	0
KEGG_STEROID_BIOSYNTHESIS	17	-2.17727	0	0
KEGG_AMINOACYL_TRNA_BIOSYNTHESIS	41	-2.12114	0	0
KEGG_TERPENOID_BACKBONE_BIOSYNTHESIS	15	-2.04747	0	7.92E-05
KEGG_NUCLEOTIDE_EXCISION_REPAIR	42	-1.99462	0	8.66E-04
KEGG_RNA_DEGRADATION	56	-1.96018	0	8.77E-04
KEGG_BASE_EXCISION_REPAIR	33	-1.92021	0	0.001249

4.2.5 *Pdk1*^Δ; *Braf*^Δ; *c-Raf*^Δ PDAC cells tend to show a similar gene expression pattern

PDAC is well recognized as one of the most lethal types of malignancy, with a high degree of tumor heterogeneity observed not only between individual tumors (inter-tumor heterogeneity), but also within the same tumor (intra-tumor heterogeneity) [219]. In this study, cell lines were isolated from different parts of individual pancreatic tumors, and from different endogenous mouse models with the same genotype. To better understand how tumor heterogeneity affects the suppression effect of *Pdk1*, *Braf* and *c-Raf* inhibition in PDAC cells, the Principal Component Analysis (PCA) method was applied to reduce the dimensionality of large RNAseq data sets. This transformed the complexity of high-dimensional variables into a smaller and simpler data, without losing the trends and patterns of the large set of information. The results of the PCA showed that the transcriptional features of control PDAC cell lines treated with EtOH (blue dots) were scattered (Figure 11A). Although the cell lines WM1047-1 and WM1047-2 were isolated from the same pancreatic tumor, they displayed heterogeneity in their transcriptional profiles. In contrast, the pink triangles that represent PDAC cell lines were clustered together following 4-OHT treatment, indicating that the differences in global gene expression between all cell lines became smaller and less diverse

(Figure 11A). The gene expression heatmap also showed that PDAC cells treated with 4-OHT had a more similar gene expression profile than control cell lines treated with EtOH (Figure 11B). These changes could suggest that all PDAC cell lines showed a uniform response to concomitant inactivation of *Pdk1*, *Braf* and *c-Raf*, despite the transcriptional diversity of these cell lines.

In summary, the results of the RNA sequencing analysis revealed that deletion of *Pdk1*, *Braf* and *c-Raf* genes could inhibit the cell cycle, affect cell metabolism, and induce programmed cell death of PDAC cells. Furthermore, PDAC cell lines displayed a similar gene expression pattern following deletion of *Pdk1*, *Braf* and *c-Raf* genes, suggesting that different PDAC cell lines had similar responses to simultaneous inactivation of *Pdk1*, *Braf*, and *c-Raf*, despite their heterogenous gene expression. However, the enrichment of the *IL-6/JAK/STAT3*, *Wnt* and *TGF- β* signaling pathways indicate that these pathways may be involved in the development of resistance mechanisms to tumor therapies targeting *Pdk1*, *Braf* and *c-Raf* in the treatment of PDAC.

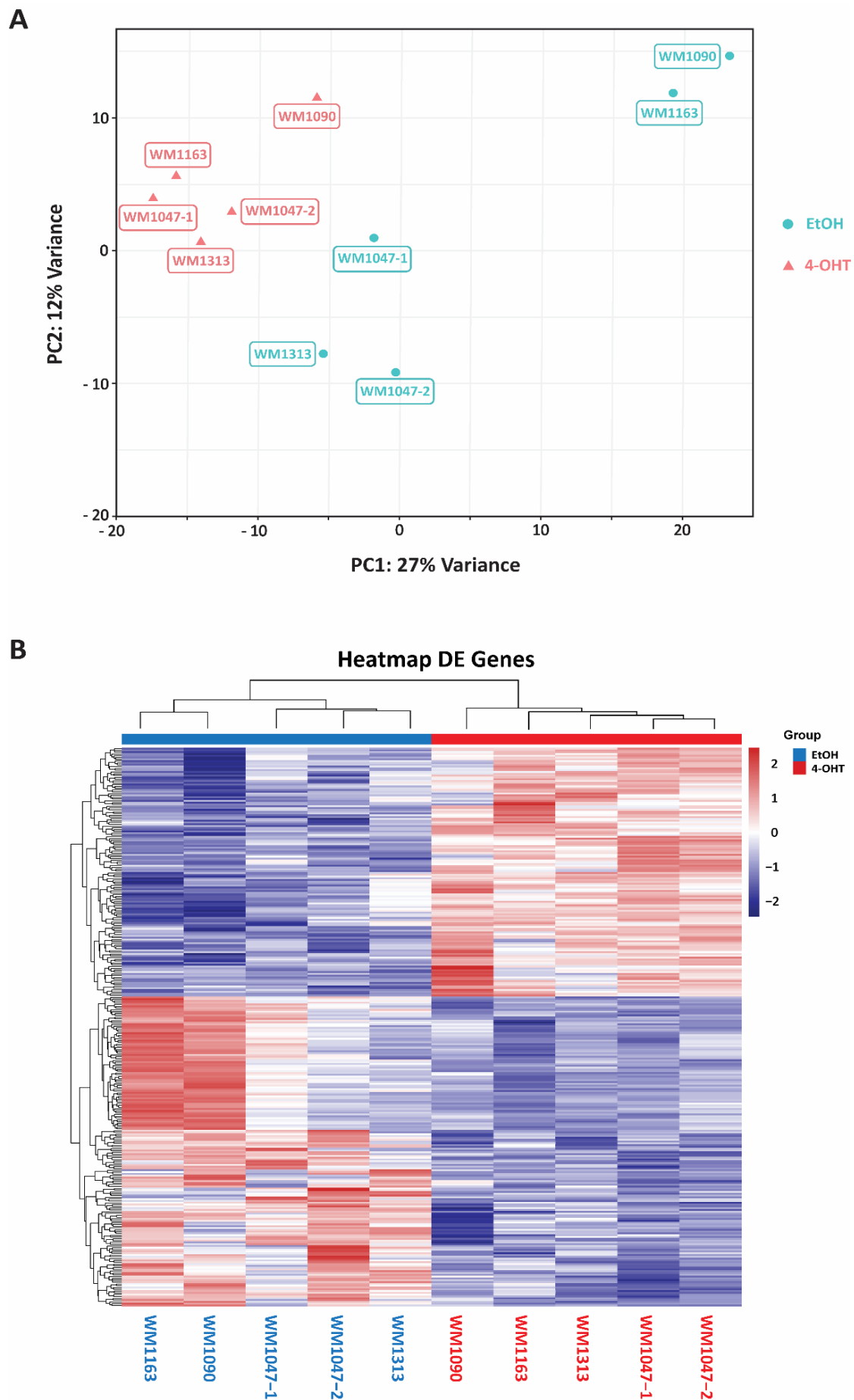


Figure 11. *Pdk1*^Δ; *Braf*^Δ; *c-Raf*^Δ PDAC cells tend to show similar gene expression pattern in comparison to their wild-type control counterparts

(A) Principal component analysis (PCA) plot of the RNA-Seq data characterizes the gene expression trends of in each ethanol treated control *Pdk1*^{WT}; *Braf*^{WT}; *c-Raf*^{WT} (cyan dot, n=5) and 4-OHT treated *Pdk1*^Δ; *Braf*^Δ; *c-Raf*^Δ knock-out cell line (pink triangle, n=5). All the cell lines have the same genotype: *Pdx1-Flp*; *FSF-Kras*^{G12D/+}; *FSF-Rosa26*^{CAG-CreERT2}; *Pdk1*^{lox/lox}; *Braf*^{lox/lox}; *c-Raf*^{lox/lox}; *Trp53*^{fl/+}.

(B) Heatmap of top differentially expressed (DE) genes in ethanol treated control *Pdk1*^{WT}; *Braf*^{WT}; *c-Raf*^{WT} (cyan dot, n=5) and tamoxifen treated *Pdk1*^Δ; *Braf*^Δ; *c-Raf*^Δ knock-out cohorts. The upper blue bar represents cohort of *Pdk1*^{WT}; *Braf*^{WT}; *c-Raf*^{WT}, the red is *Pdk1*^Δ; *Braf*^Δ; *c-Raf*^Δ cohort. Color scale (right side) in blue indicates low expressed genes and red represents genes with high expression.

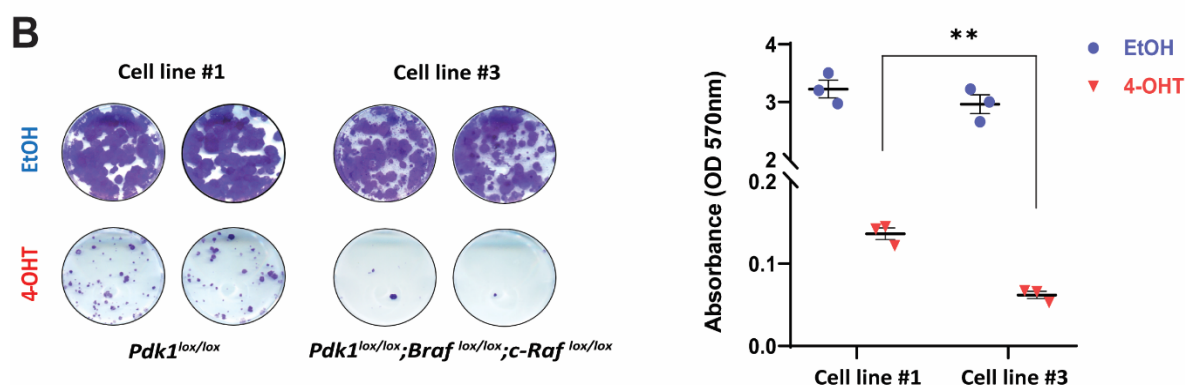
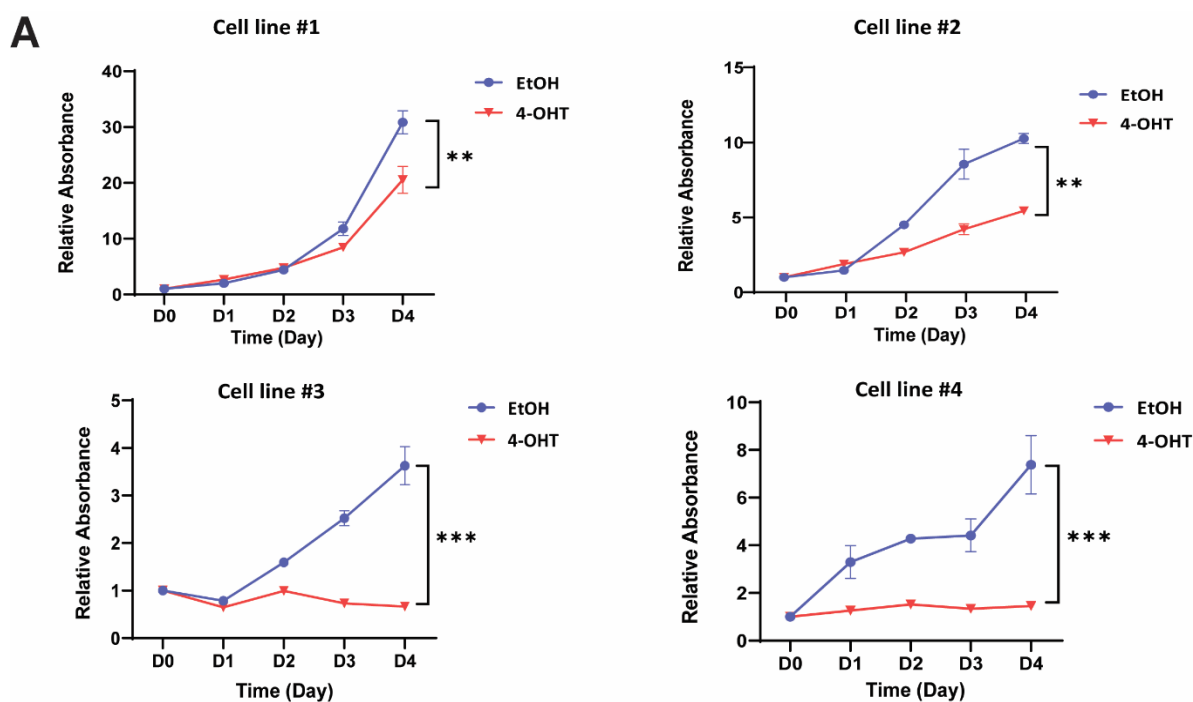
4.2.6 Concomitant inactivation of *Pdk1*, *Braf* and *c-Raf* impairs viability and colony formation of PDAC cells, and induces apoptosis

To determine the functional significance of *Pdk1*, *Braf* and *c-Raf* TKO in PDAC cells, an MTT (3-[4,5-dimethylthiazol-2-yl]-2,5 diphenyl tetrazolium bromide) assay was performed to determine PDAC cell viability following deletion of *Pdk1*, *Braf* and *c-Raf* genes. The results showed that both *Pdk1* deletion and *Braf*, *c-Raf* double KO could inhibit the viability of PDAC cells, but that the inhibitory effects were incomplete, and some cells were still able to grow even after these genes were deleted. The triple KO of *Pdk1*, *Braf* and *c-Raf* was found to significantly reduce cell proliferation in PDAC cells (Figure 12A). Together, the results of the MTT assay indicate that inhibition of *Pdk1*, *Braf* and *c-Raf* could impede PDAC cell viability significantly *in vitro*.

Next, we used clonogenic growth assays to assess the effect of deleting *Pdk1* alone or in combination with *Braf* and *c-Raf*. Despite *Pdk1* deletion producing an inhibitory effect on the cell viability and growth of PDAC cells in the clonogenic assays, many cell colonies were still able to form following 4-OHT treatment. In contrast, PDAC cell colony formation was blocked almost completely following simultaneous excision of *Pdk1*, *Braf* and *c-Raf* by Cre recombinase *in vitro* (Figure 12B). The viable cell colonies following 4-OHT treatment were isolated and cultured in the normal cell culture medium for the DNA recombination test. For the *Pdk1*^{lox/lox} cell line, 18 of 22 clones displayed *Pdk1* complete KO, and 4 clones still harbored a *Pdk1* mutant allele following treatment with 4-OHT (Figure 12C). Cell clones from the *Pdk1*^{lox/lox}; *Braf*^{lox/lox}; *c-Raf*^{lox/lox} cell line treated with 4-OHT showed non-recombined alleles at both *Braf* and *c-Raf* loci, while the DNA deletions at the *Pdk1* locus were complete, suggesting that this is why they were still able to grow following 4-OHT treatment. Of note, most of the *Pdk1* KO clones (17/22) could survive when they were treated with 4-OHT again,

while *Pdk1*, *Braf* and *c-Raf* TKO clones all died when they were further cultured in 4-OHT-containing medium.

RAF proteins play a key role in the mitogen-activated protein kinase (MAPK) cascade, which drives *KRAS*-dependent PDAC growth, cell proliferation and survival. We therefore hypothesized that simultaneous inactivation of *Pdk1*, *Braf* and *c-Raf* could induce significant apoptosis in PDAC cells. As expected, increased level of cleaved caspases 3 & 7 (the markers of apoptosis) were detected after 4-OHT treatment in *Pdk1*^{lox/lox}, *Braf*^{lox/lox}, *c-Raf*^{lox/lox} PDAC cells. *Pdk1* deletion alone had limited effects on apoptosis in PDAC cells, as did *Braf*, *c-Raf* double KO (Figure 12D). Although *Pdk1* KO can inhibit the growth of PDAC cells, it is evident that PDAC cells are able to maintain their survival using compensatory mechanisms following *Pdk1* deletion. In contrast, *Pdk1*, *Braf*, *c-Raf* deletion can prevent the survival of PDAC cells significantly, as no PDAC cells were able to survive long-term following *Pdk1*, *Braf*, *c-Raf* inactivation as assessed by clonogenic assays.



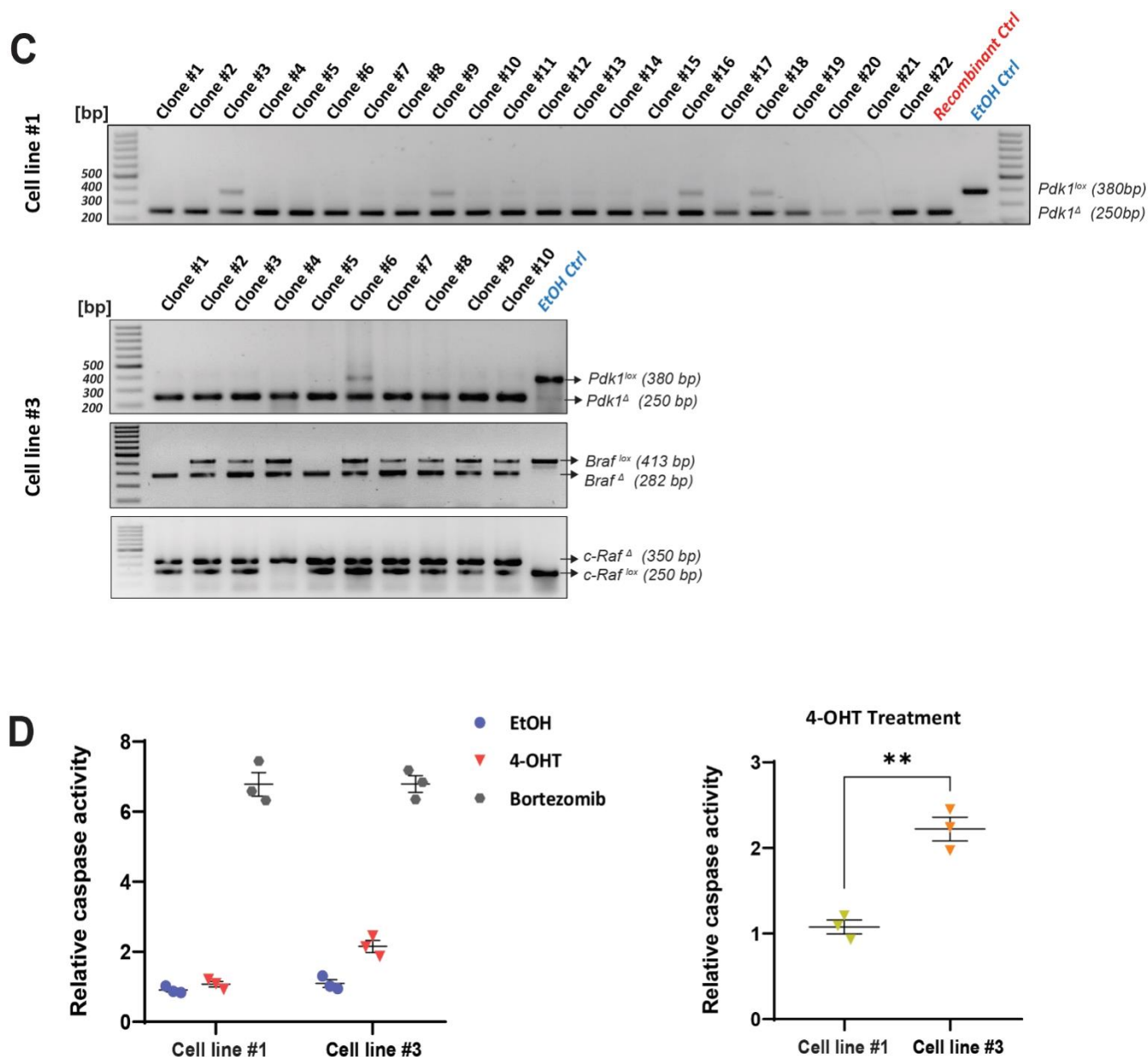


Figure 12. *Pdk1*, *Braf* and *c-Raf* triple knock-out impairs cell viability, colony formation and induces apoptosis in PDAC cells

(A) MTT cell viability assays of primary PDAC cell lines (cell line #1- #4) with 0.1 % EtOH and 0.5 μ M 4-OHT treatments. Cell line #1: *Pdx1-Flp*; *FSF-Kras^{G12D/+}*; *FSF-Rosa26^{CAG-CreERT2}*; *Pdk1^{lox/lox}*; *Trp53^{frt/+}*, Cell line #2: *Pdx1-Flp*; *FSF-Kras^{G12D/+}*; *FSF-Rosa26^{CAG-CreERT2}*; *Pdk1^{lox/+}*; *Braf^{lox/lox}*; *c-Raf^{lox/lox}*; *Trp53^{frt/+}*, Cell line #3: *Pdx1-Flp*; *FSF-Kras^{G12D/+}*; *FSF-Rosa26^{CAG-CreERT2}*; *Pdk1^{lox/lox}*; *Braf^{lox/lox}*; *c-Raf^{lox/lox}*; *Trp53^{frt/+}*, Cell line #4: *Pdx1-Flp*; *FSF-Kras^{G12D/+}*; *FSF-Rosa26^{CAG-CreERT2}*; *Pdk1^{lox/lox}*; *Braf^{lox/lox}*; *c-Raf^{lox/lox}*; *Trp53^{frt/+}*. Data are represented as mean \pm S.E.M. Triplicates are shown. ***p* value < 0.01; ****p* value < 0.001, two-way ANOVA.

(B) Cell colony formation assay of *Pdk1^{lox/lox}* and *Pdk1^{lox/+}*; *Braf^{lox/lox}*; *c-Raf^{lox/lox}* treated with 0.1 % EtOH and 0.5 μ M 4-OHT for 8 days (left graph); The absorbance values of crystal violet staining for cell lines at the wavelength of 570nm was measured (right graph). One representative image of three independent experiments is shown. ***p* value < 0.01, two-tailed student's *t* test.

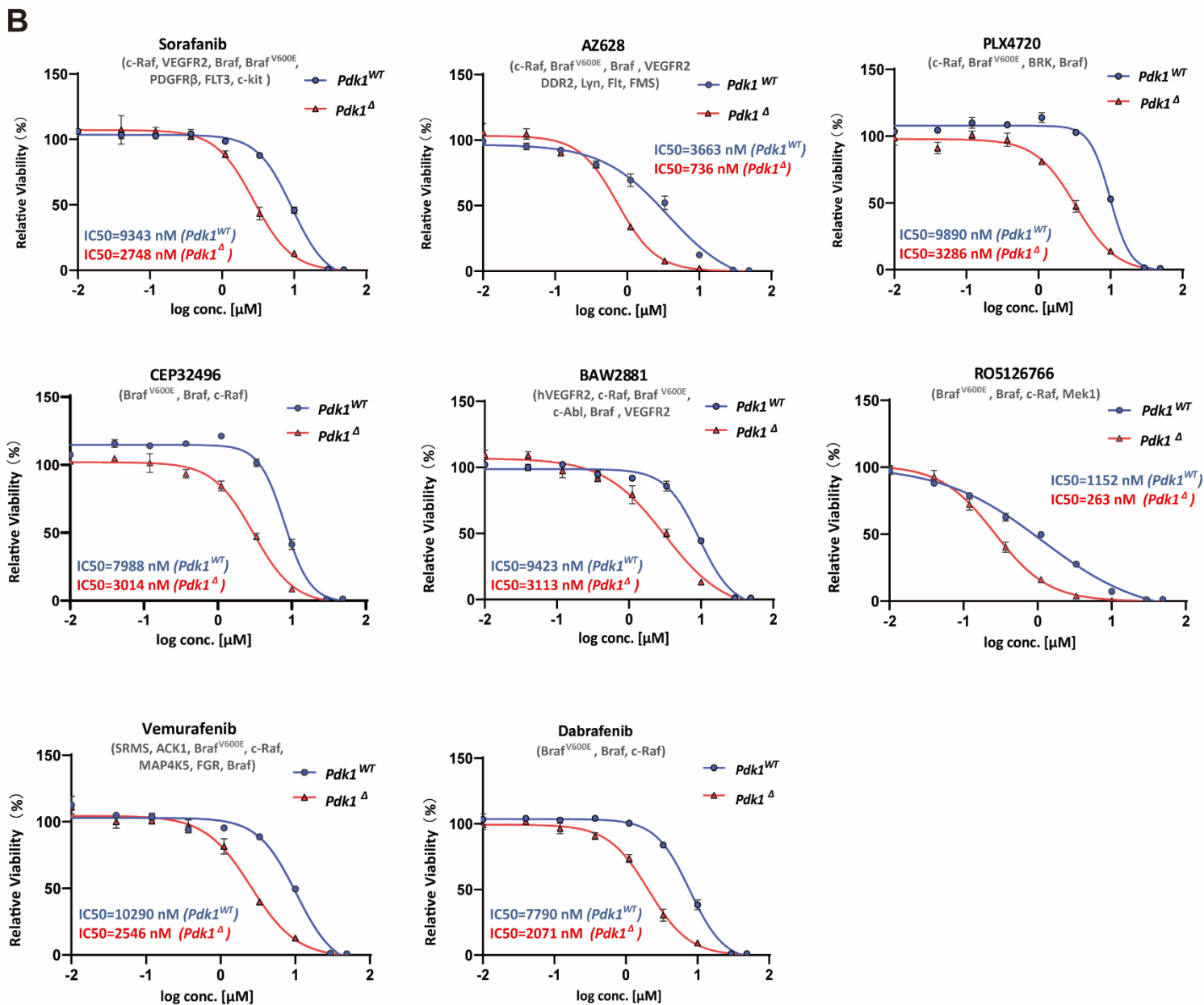
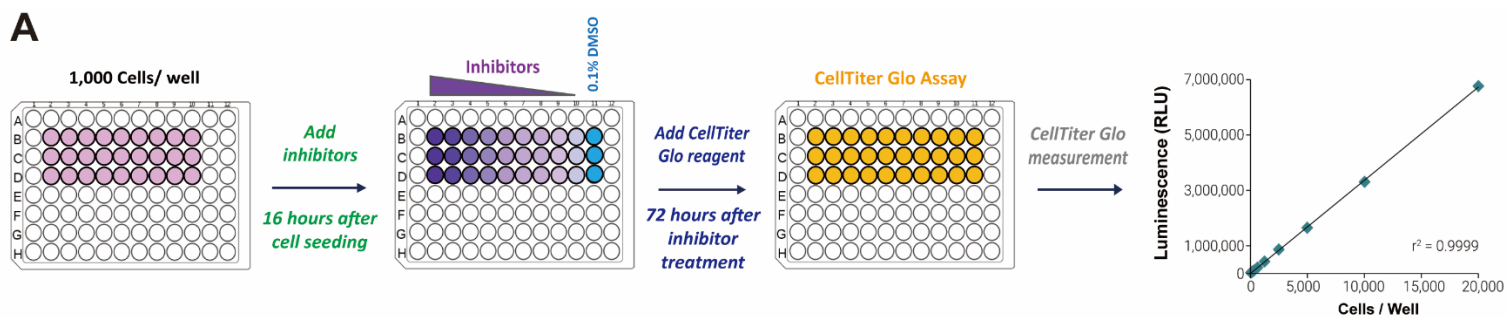
(C) The PCR results show the DNA recombination statuses of *Pdk1^{lox/lox}* (Top) and *Pdk1^{lox/lox}; Brafl^{lox/lox}; c-Raf^{lox/lox}* cell clones (Bottom) which could grow after 14 days 4-OHT (0.5 μ M) treatment.

(D) The comparison of Caspase 3/7 activity between *Pdk1^{lox/lox}* and *Pdk1^{lox/lox}; Brafl^{lox/lox}; c-Raf^{lox/lox}* cell lines after 8-day 4-OHT (0.5 μ M) treatment. Positive control: Cells are treated with 0.5 μ M Bortezomib for 12 hours to induce the apoptosis. Data are shown as mean \pm SD, n = 3 independent experiments. ***p* value < 0.01, two-tailed student's t test.

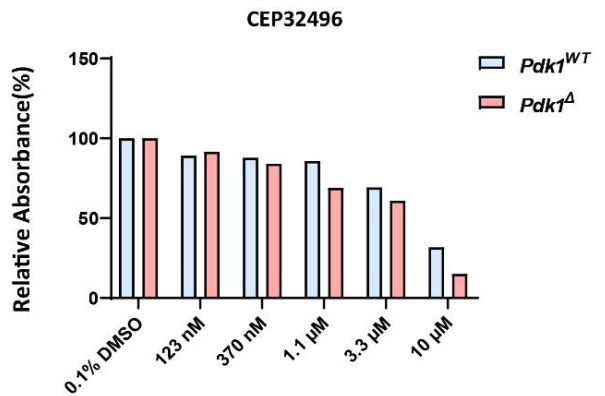
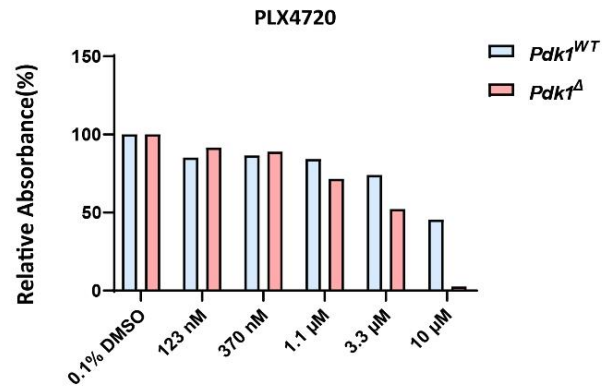
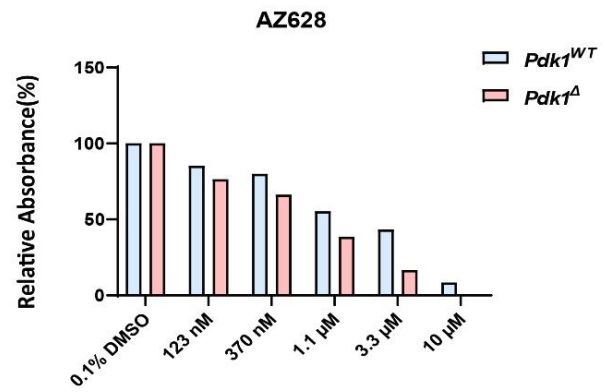
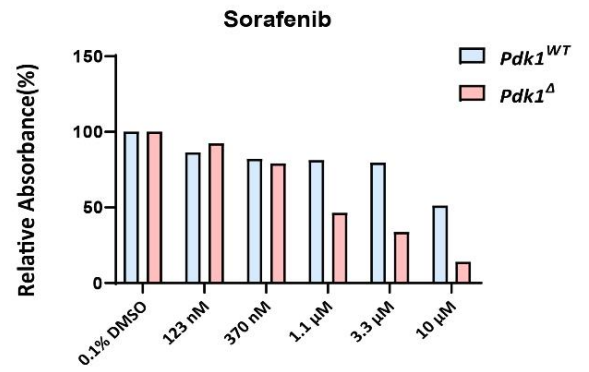
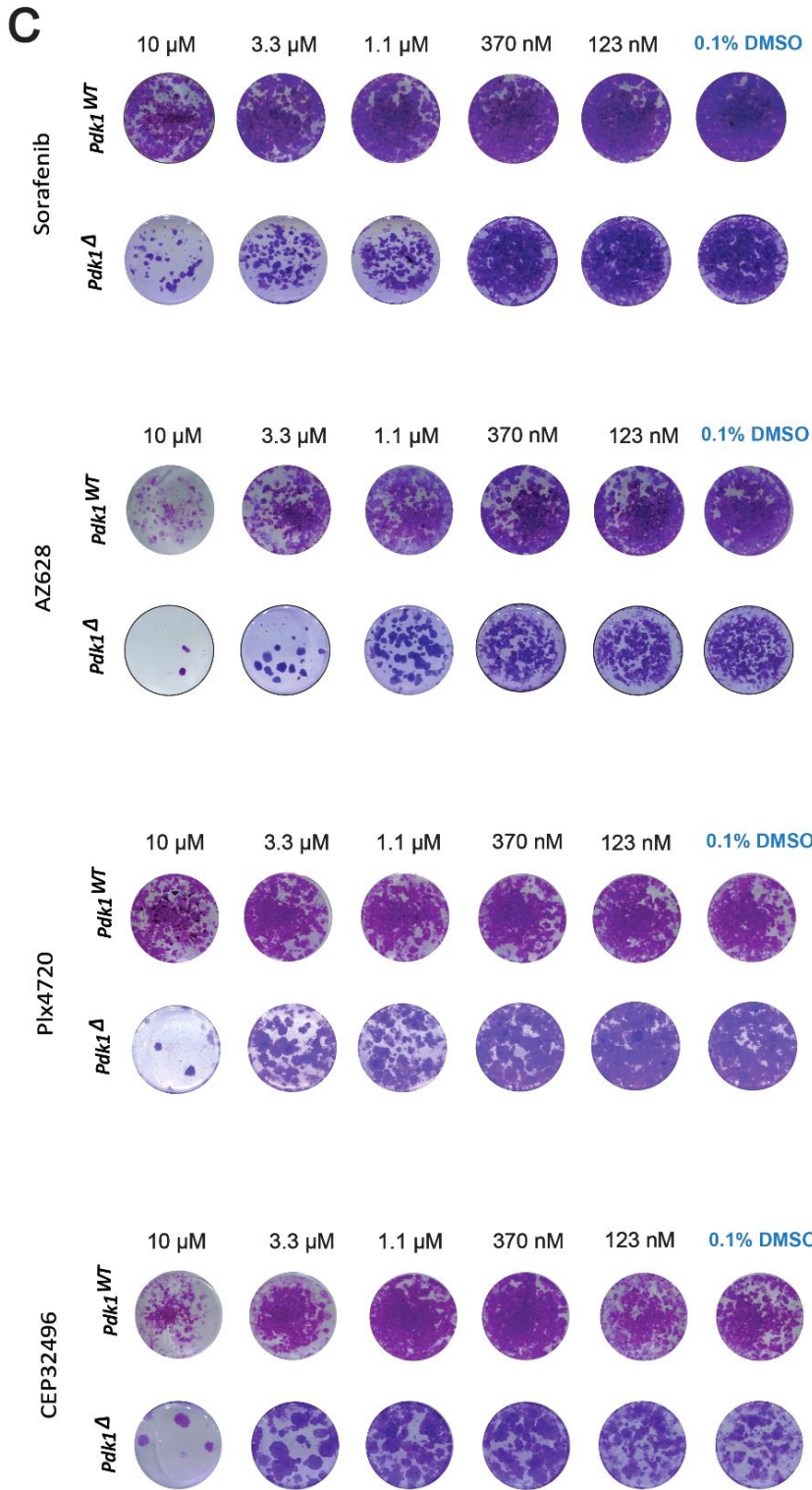
4.2.7 *Pdk1 Δ* resistant cells are more susceptible to RAF inhibitors

The data presented previously in this thesis showed that deletion of members of the Raf family significantly inhibits cell growth and survival in *Pdk1 Δ* resistant cells. Based on this, a single-drug treatment screen was performed to further validate the effect of drugs targeting different KRAS downstream pathways in *Pdk1 Δ* resistant cells. Cells were first seeded in a 96-well plate. The following day, inhibitors were added to each well and mixed with the cells. After 72 hours of treatment, CellTier Glo reagent was added directly to each well to determine cell viability based on quantification of ATP present, and the luminescence value of the cells was measured and recorded using CLARIO star Plus Microplate Reader (BMG Labtech GmbH, Germany) (Figure 13A).

Eight inhibitors targeting *c-Raf* were tested in both *Pdk1^{WT}* and *Pdk1 Δ* PDAC cells (the information of inhibitors and their related targets are listed in table 42). Overall, the resistant PDAC cells showed much greater susceptibility to all inhibitors (Figure 13B). This was also evident for inhibitors, such as Darafenib, which has been already approved for clinical use by both the US Food and Drug Administration (FDA) and the European Medicines Agency (EMA). Among these, the novel pan-Raf inhibitor AZ628 and the dual *RAF/MEK* inhibitor Ro5126766 produced the most significant effects in both *Pdk1^{WT}* and *Pdk1 Δ* PDAC cells, even at low concentrations (Figure 13C, 13D and Table 42). Taken together, the results of the single-drug treatment screen demonstrated that inhibition of Raf proteins and the MAPK pathway could suppress the growth of *Pdk1 Δ* resistant tumor cells.



Results



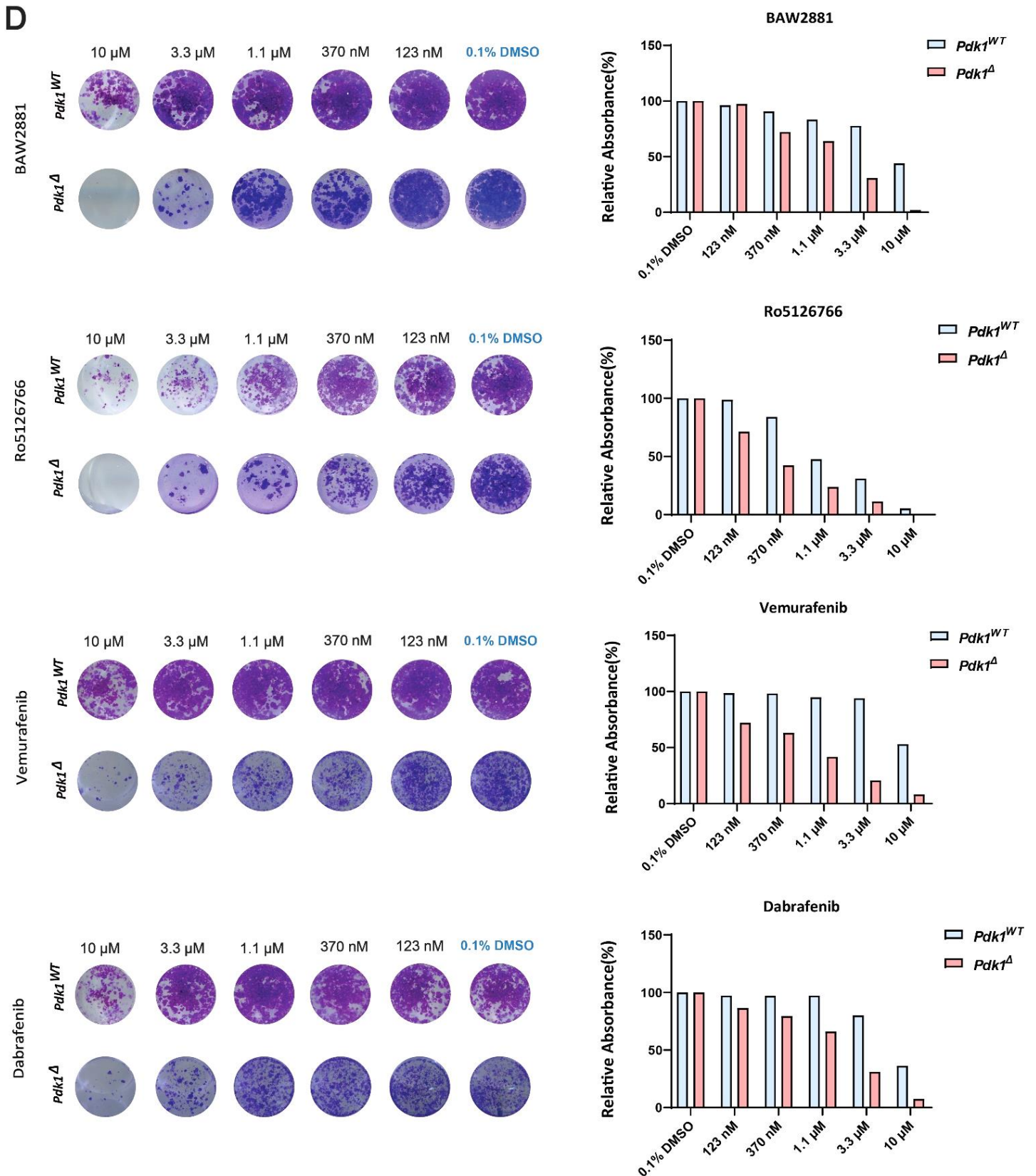


Figure 13. *Pdk1*^Δ resistant cells are more susceptible to RAF inhibitors

(A) The workflow of drug treatments for *Pdk1*^{WT} and *Pdk1*^Δ resistant cells.

(B) The results of CellTiter-Glo luminescent cell viability assay performed as depicted in panel A show the inhibition effect of different inhibitors in *Pdk1^{WT}* and *Pdk1^Δ* cells. Targets of the drugs are showed in brackets. Values were normalized to DMSO. Data presented as mean ± S.E.M, n=3 replicates.

(C-D) The representative images of clonogenic assay of PDAC cells after drug treatment (left) and the relative absorbance values of crystal violet staining for cell lines at the wavelength of 570nm were measured (right).

Table 42. Information of inhibitors and IC50 values of PDAC cell lines

Inhibitor	Targets	IC50 of <i>Pdk1^{WT}</i> PDAC cell [nM]	IC50 of <i>Pdk1^{WT}</i> PDAC cell [nM]
Sorafenib	c-Raf, VEGFR2, Braf , Braf ^{V600E} , PDGFRβ, FLT3 , c-Kit	9343	2748
AZ628	c-Raf , Braf ^{V600E} , Braf , VEGFR2, DDR2, Lyn, Flt1, FMS	3663	736
PLX4720	c-Raf, Braf ^{V600E} , BRK, Braf	9890	3286
CEP32496	Braf ^{V600E} , Braf , c-Raf	7976	3014
BAW2881	hVEGFR2, c-Raf, Braf ^{V600E} , c-Abl, Braf, mVEGF2	9423	3113
Ro5126766	Braf ^{V600E} , BRAF, c-Raf, MEK1	1152	263
Vemurafenib	SRMS, ACK1, Braf ^{V600E} , c-Raf, MAP4K5, FGR, Braf	10290	2546
Dabrafenib	Braf ^{V600E} , Braf, c-Raf	7790	2071

4.2.8 PI3K, Pdk1 and RAF inhibitors display strong synergistic interactions in the treatment for PDAC

In order to test *KRAS*^{G12D}-mutant PDAC cell growth in response to combination therapies that target the PI3K/Pdk1 and the RAF/MEK/ERK pathway, we assessed the synergistic interaction between Pdk1/PI3K and RAF inhibitors (hereinafter referred to as Pdk1i/PI3Ki and RAFi, respectively) in Pdk1 proficient and deficient cells.

Concentrations of each inhibitor that are close to the half-maximal inhibitory concentration (IC50) were chosen for further investigation. *Pdk1*^{WT} and *Pdk1*^Δ resistant PDAC cells were seeded in 96-well plates, inhibitors were then added in each well at 16th hours after cell seeding. After 72 hours of incubation with the inhibitors, the cell viability of both groups was determined using CellTiter Glo assays. The synergistic effect of different drug combinations were assessed by SynergyFinder web application (<https://synergyfinder.fimm.fi>) based on results of CellTiter Glo assay. In general, the combination drug treatments displayed a strong synergistic effect on the growth of *Pdk1*^{WT} PDAC cells, while the *Pdk1*^Δ resistant PDAC cells were less sensitive to both Pdk1i/PI3Ki and RAFi combination treatments (Figure 14A). Notably and as expected due to Pdk1 deficiency, the combination of Pdk1i and RAFi treatments produced no synergistic effect on viability of *Pdk1*^Δ resistant cells, while most combinations of PI3Ki and RAFi treatments inhibited the viability of *Pdk1*^{WT} and *Pdk1*^Δ resistant PDAC cells significantly (Figure 14B-D). Of note, the synergistic interaction of the PI3Ki and AZ628, Ro5126766, Dabrafenib combinations in *Pdk1*^Δ cells was similar to, or stronger than their effect in *Pdk1*^{WT} PDAC cells (Figure 14B-D). This indicates that dual pathway inhibition by deletion of Pdk1 as well as blockade of upstream PI3K signaling is synergistic with RAF blockade.

In summary, the results of combination drug treatments demonstrated that normal PDAC cell lines were sensitive to PI3Ki/Pdk1i and RAFi combination treatments. In contrast, PI3Ki and RAFi combinations showed similar synergistic inhibitory effects on wild-type and resistant cells, particularly the combinations of PI3Ki with AZ628, Ro5126766 and Dabrafenib. Furthermore, the synergy map of various combinations showed that most compounds produced the strongest interactions at relatively low concentrations (Figure 14B-D). This makes the combination treatment of Pdk1i/PI3Ki and RAFi a safer and more efficient therapy,

as they are able to kill tumor cells at lower concentrations, thus reducing the possibility of treatment side effects.

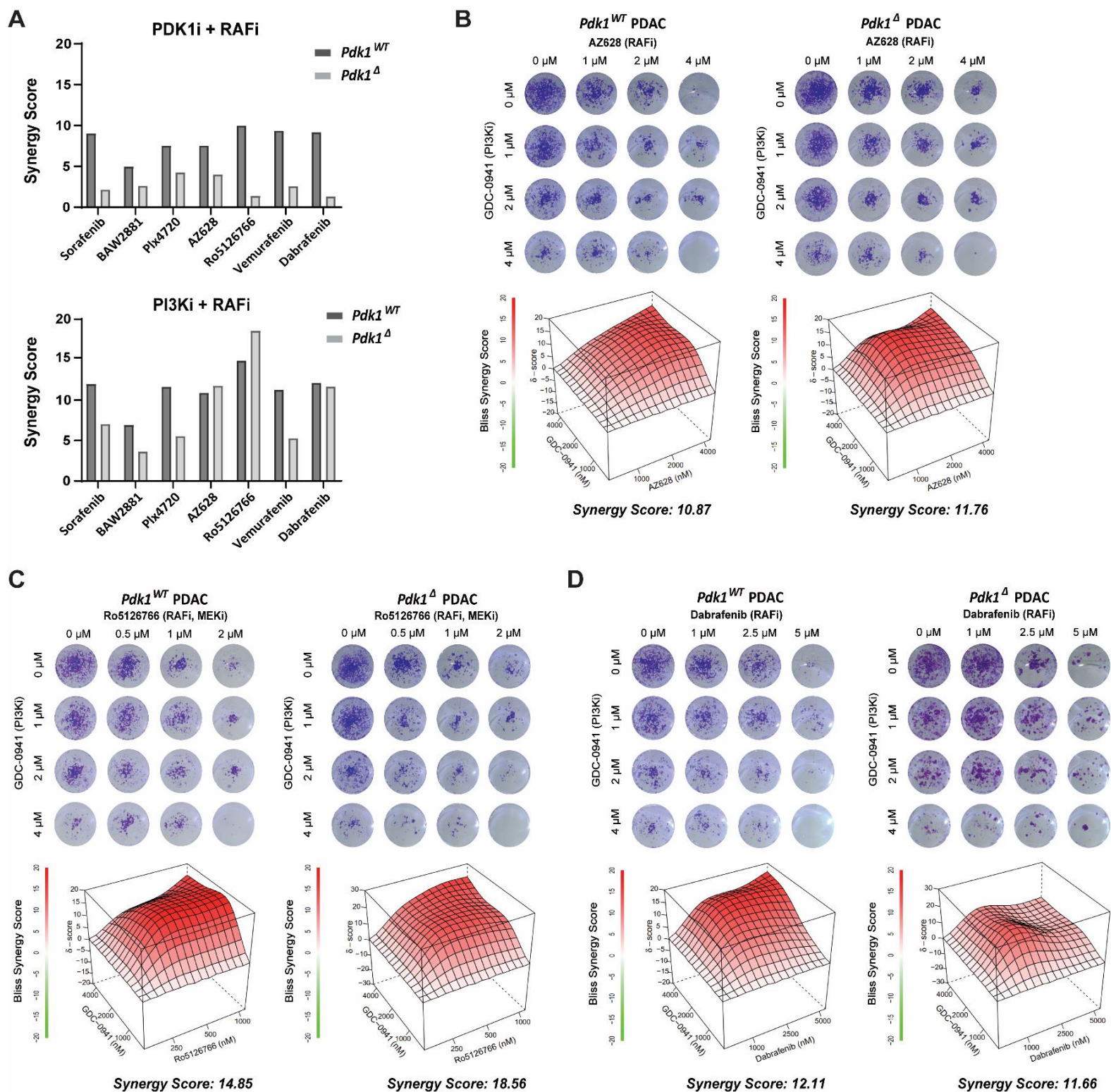


Figure 14. PI3K/*Pdk1* and RAF inhibitors show the strong synergistic interactions for PDAC cells

(A) Bliss synergy scores of *Pdk1*^{WT} and *Pdk1*^Δ resistant PDAC cells lines with PDK1i + RAFi (Top) and PI3Ki + RAFi (Bottom) combinatorial treatments respectively. *Pdk1*^{WT} cell line is depicted in dark grey and *Pdk1*^Δ resistant cells are in light grey color.

(B-D) The representative images of clonogenic assay and synergy maps of *Pdk1*^{WT} and *Pdk1*^Δ resistant PDAC cell lines with different combinatorial drug treatments. The synergy score and map were assessed by SynergyFinder web application.

4.2.9 Triple knock-out of *Pdk1*, *Braf* and *c-Raf* results in tumor regression of *Kras*^{G12D}-driven PDAC *in vivo*

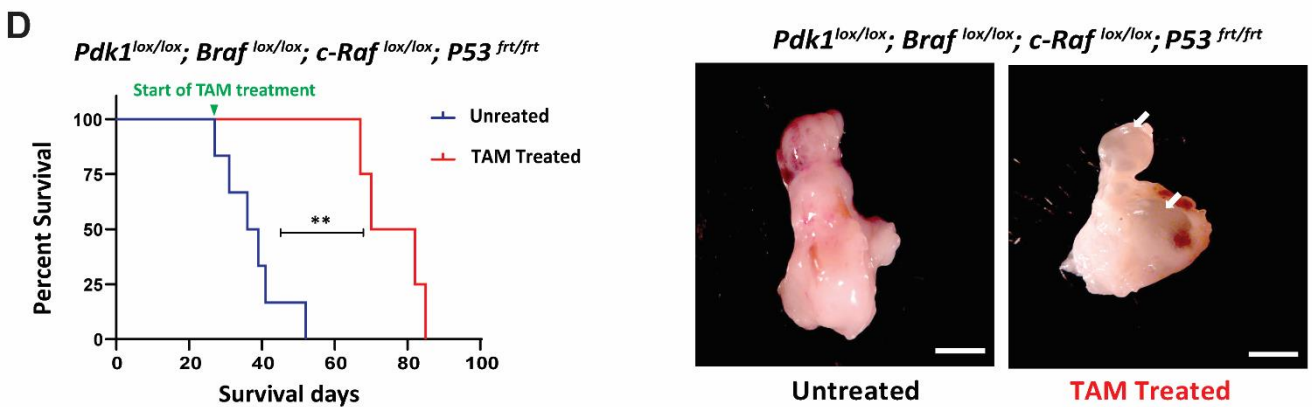
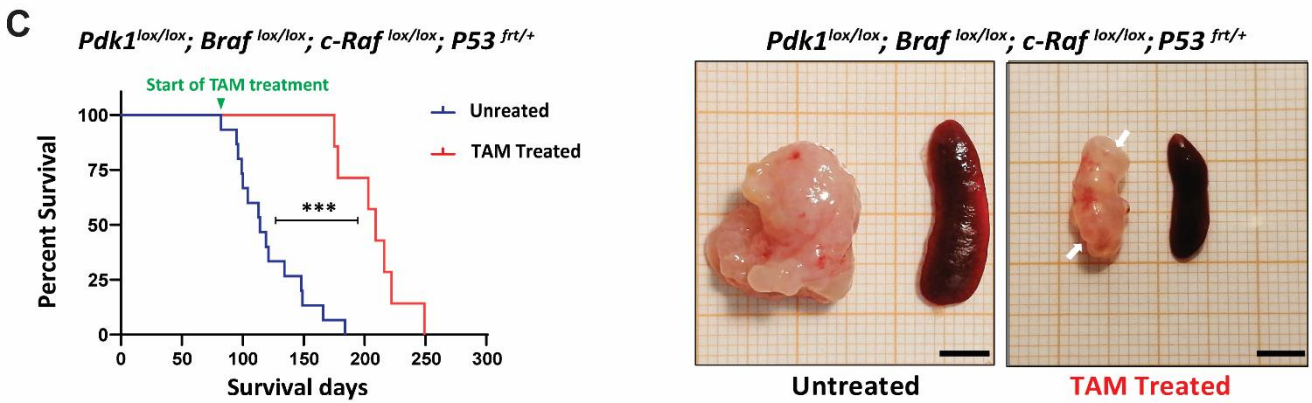
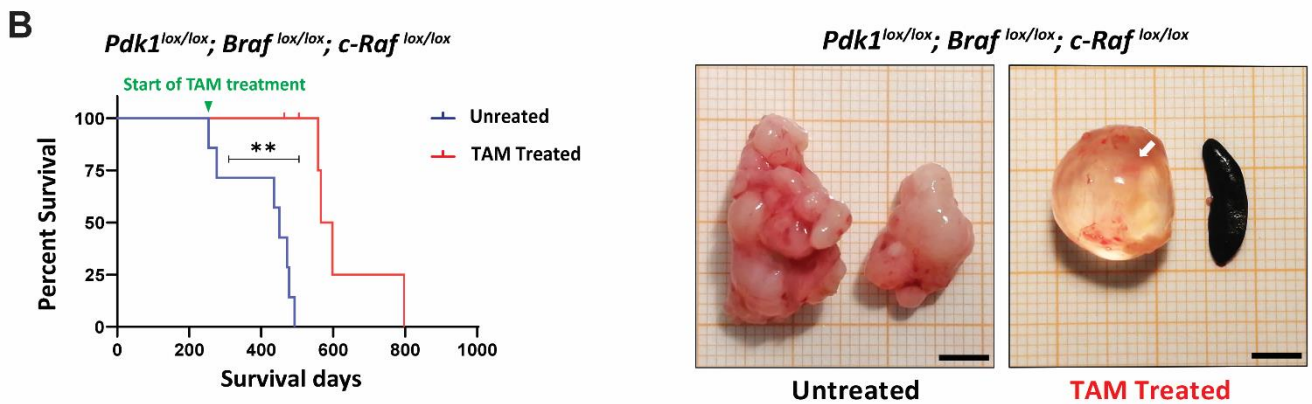
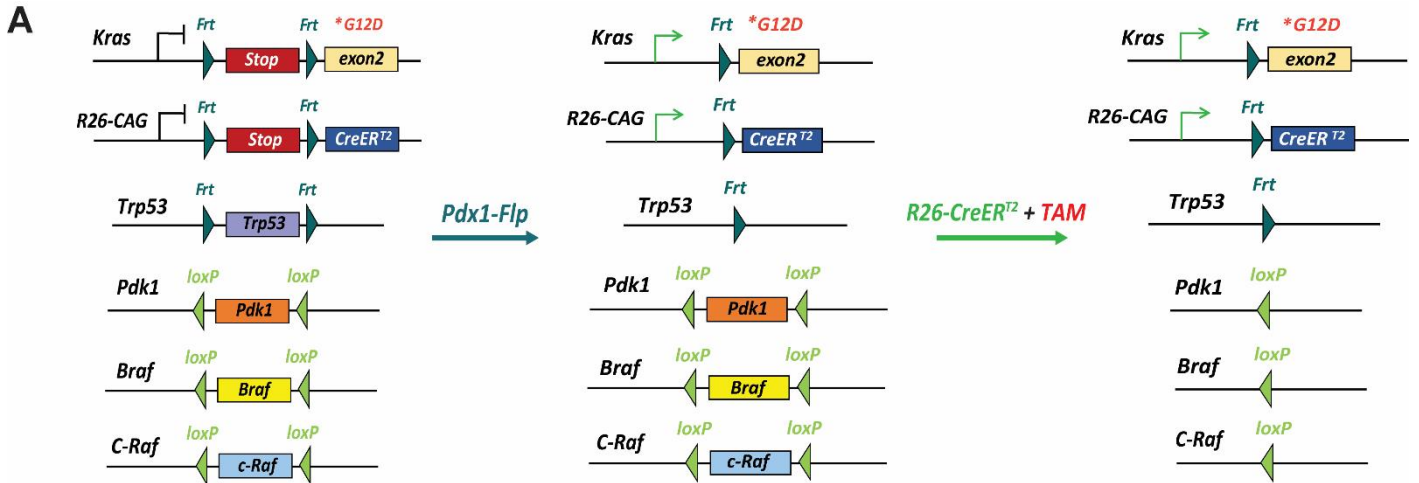
To further investigate the therapeutic efficacy of targeting *Pdk1*, *Braf*, and *c-Raf* in *Kras*^{G12D}-driven pancreatic tumor maintenance *in vivo*, mice with floxed *Pdk1*, *Braf*, and *c-Raf* alleles were treated with tamoxifen-containing from the earliest moment a pancreatic tumor could be palpated (around 12th–14th week for *Pdx1*^{Flp/+}; *FSF-R26CAG-CreERT2/+; *FSF-KrasG12D/+; *Pdk1lox/lox*; *Braflox/lox*; *C-Raflox/lox*; *Trp53frt/+*). In these PDAC mouse models, the expression of codon-optimized *Flp* recombinase (*FlpO*) was under the control of the pancreas-duodenum homeobox 1 (*Pdx1*) promoter. As *Pdx1* is only expressed in pancreatic acinar cells, ductal cells, islet cells and the epithelium of the duodenum, *Flp* is also expressed specifically in these *Pdx1* positive tissues. The FRT- flanked STOP cassette at the upstream of mutant *Kras*^{G12D} was excised using *Flp* recombinase, resulting in the expression of the mutant *Kras*^{G12D} protein in *Pdx1-Flp* positive cells, and ultimately inducing PanIN precursor lesions. Additionally, the FRT-flanked *Trp53* allele was deleted by *Flp* to recreate one of the common molecular features of PDAC, which is found in nearly 70% of *Kras*^{G12D}-driven PDAC patients and can significantly accelerate tumor progression significantly [220]. *Flp* also activated the tamoxifen-inducible *CAG-CreERT2* at the *Rosa26* locus, which had been silenced by the *FRT-stop-FRT* (*FSF*) cassette. This resulted in ubiquitous expression of *CreERT2* in *Pdx1*-positive cells. However, the *CreERT2* can only translocate into the cell nucleus and become activated when bound with tamoxifen. The mice were therefore treated with tamoxifen to induce the translocation of *CreERT2* to the cell nucleus, and to delete *Pdk1*, *Braf*, and *c-Raf* genes *in vivo* (Figure 15A).**

The lifespans of mice given the tamoxifen diet treatment were prolonged significantly, particularly for those with *Trp53* genetic mutations (Figure 15B). Furthermore, simultaneous

genetic deletion of *Pdk1*, *Braf* and *c-Raf* not only delayed pancreatic tumor progression, but also led to regression of the endogenous tumors in mice (Figure 15B-D). This was confirmed by the sizes of the pancreatic tumors assessed by *in vivo* imaging using MRI, which were much smaller in mice that received tamoxifen treatment compared to those that did not. Of note, most of these tumors were observed to have pancreatic cysts at the endpoint of the experiment, which rarely occurs in mice not treated with tamoxifen (Figure 15C).

Unpublished work of our group proved that *Pdk1* is a key effector of the maintenance of the *Kras*^{G12D}-driven PDAC, and that inactivation of *Pdk1* could effectively slow the rate of pancreatic cancer progression. However, *Pdk1* deletion was insufficient to block reduce tumor size in the endogenous mouse. As the data from this thesis showed that TKO of *Pdk1*, *Braf* and *c-Raf* could induce tumor cell apoptosis *in vitro*, we hypothesized that simultaneous deletion of *Pdk1*, *Braf* and *c-Raf* may lead to apoptosis of PDAC cells and tumor regression in mice. To investigate this, mice were either given or not given tamoxifen treatment, and were scanned regularly using magnetic resonance imaging (MRI) to monitor any dynamic changes in endogenous tumor volume.

To observe for the clear tumor regression, mice were palpated weekly until the solid pancreatic tumor was sufficient in size to be easily detected by MRI scanning. At that point, these mice were fed with tamoxifen-containing chow, and the tumor were scanned using MRI every two weeks. As depicted in **Figure 15E**, the volume of tumors treated with tamoxifen was found to decrease gradually, while tumors in untreated mice progressed rapidly. This result confirmed our prediction that concomitant inactivation of *Pdk1*, *Braf* and *c-Raf* not only slows PDAC progression, but also leads to tumor regression *in vivo*, which indicates that *Pdk1*, *Braf* and *c-Raf* could be useful as potential molecular targets for inducing synthetic lethality in pancreatic cancer cells.



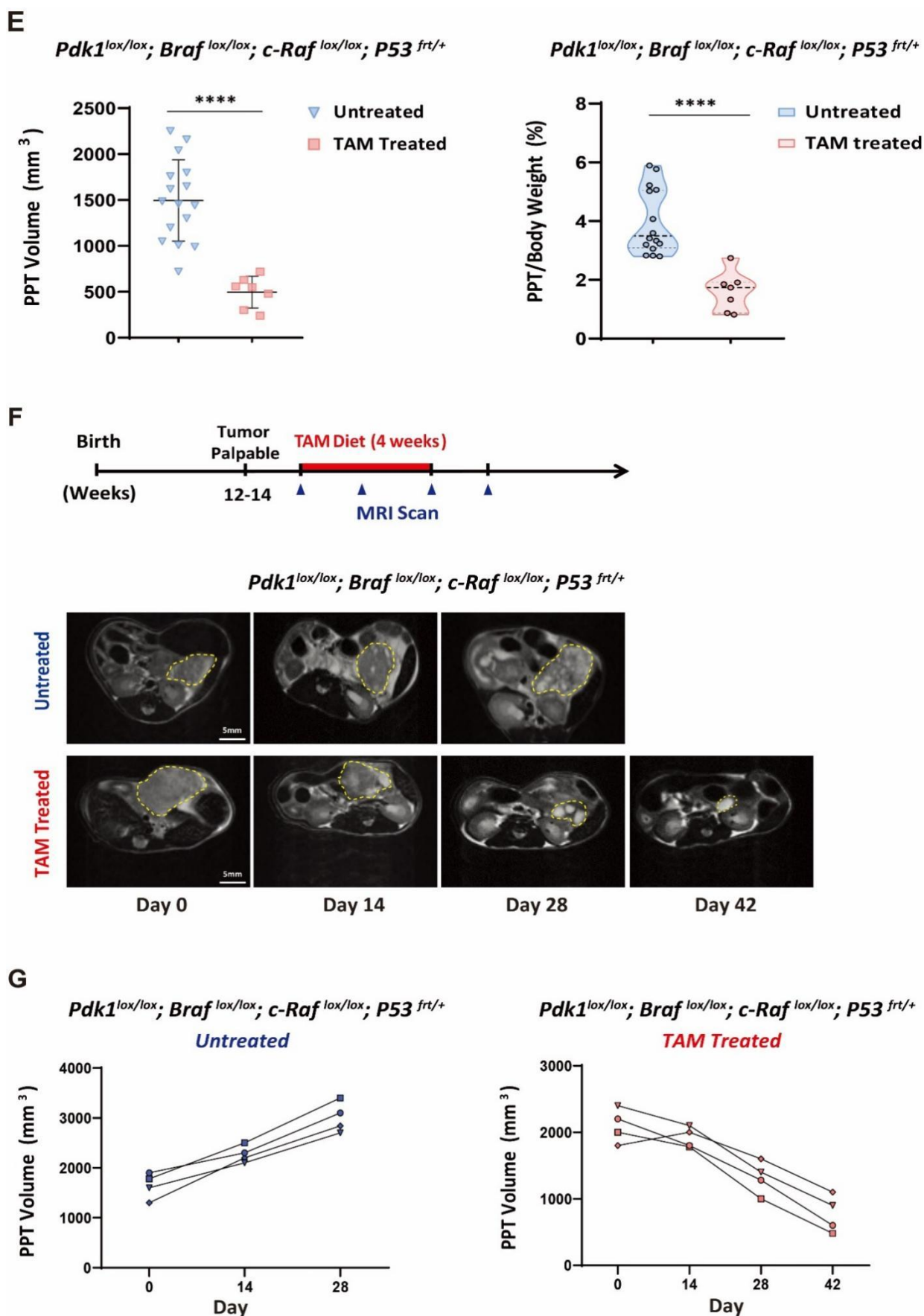


Figure 15. Inactivation of *Pdk1*, *Braf* and *c-Raf* blocks endogenous *Kras^{G12D}*-driven PDAC progression

(A) Schematic diagram shows the strategy to induce PDAC via the Flp/FRT system and inactivate *Pdk1*, *Braf* and *c-Raf* in established full blown PDAC *in vivo* in endogenous autochthonous GEMMs. TAM: tamoxifen.

(B-D) Kaplan-Meier survival analysis of indicated mouse models with/without tamoxifen treatment (left) and their representative macroscopic images (right). **PKPBC mice**, tamoxifen treatment started at Day 240-270, untreated group: n=6, median survival 450 days; tamoxifen treated group: n=8, median survival 582 days; **PKPBC, *Trp53*^{fr/+} mice**, tamoxifen treatment started at Day 84-98, untreated group: n=15, median survival 114 days; tamoxifen treated group: n=7, median survival 209 days; **PKPBC, *Trp53*^{fr/fr} mice**, tamoxifen treatment started at Day 21-28, untreated group: n=6, median survival 37.5 days; tamoxifen treated group: n=4, median survival 76 days. PKPBC: *Pdx1-Flp*; *FSF-Kras*^{G12D/+}; *FSF-Rosa26*^{CAG-CreERT2}; *Pdk1*^{lox/lox}; *Braf*^{lox/lox}; *c-Raf*^{lox/lox}. Scale bars indicate 5mm in Figure B and C. Scale bars indicate 200 Pixels in Figure D. ** $p < 0.01$, *** $p < 0.001$, log-rank (mantel-cox) test.

(E) The volume of primary pancreatic tumor (PPT) (left) and the ratio of PPT and mouse body weight (right) from tamoxifen-treated and untreated *Pdk1*^{lox/lox}; *Braf*^{lox/lox}; *c-Raf*^{lox/lox} mice. Primary pancreatic tumors were collected from experimental mice at the human endpoints. **** $p < 0.0001$, two tailed student's t test.

(F) Top: schematic of tamoxifen treatment and MRI scan experiments for *Pdk1*^{lox/lox}; *Braf*^{lox/lox}; *c-Raf*^{lox/lox} mice. Bottom: the representative MRI images of tamoxifen-treated and untreated mice respectively. Start of tamoxifen treatment is depicted as day 0. Scale bar, 5mm.

(G) The line graph shows the dynamic changes of the pancreatic tumor size from tamoxifen-treated (n=4) and tamoxifen-untreated mice (n=4), the tumor volume is assessed by MRI scanning.

4.2.10 Concomitant inactivation of *Pdk1*, *Braf* and *c-Raf* inhibits proliferation and promotes apoptosis of endogenous PDAC cells *in vivo*

As the expression of the Ki67 protein is strongly associated with the proliferation of tumor cells in multiple types of malignancies, it has been widely used for pathological diagnosis as a marker of tumor progression [221, 222]. Immunohistochemistry (IHC) analysis of Ki67 protein expression revealed that proliferation activity was significantly reduced in pancreatic tumors treated with tamoxifen, while untreated pancreatic tumors maintained strong Ki67 protein expression, suggesting that these untreated tumor cells retained strong capacity for proliferation and growth (Figure 16B).

Additionally, proteins were extracted from the pancreatic tumor tissues to identify cell apoptosis in tumor cells. Thereby, I could detect slightly increased level of cleaved-caspase 3 protein in tamoxifen-treated pancreatic tumors by immunoblotting. Whereas no evident cleaved-caspase 3 was detected in tumors from control mice (Figure 16C). These data

indicate that *Pdk1*, *Braf* and *c-Raf* TKO not only suppresses tumor proliferation, but also induces tumor regression by promoting apoptosis.

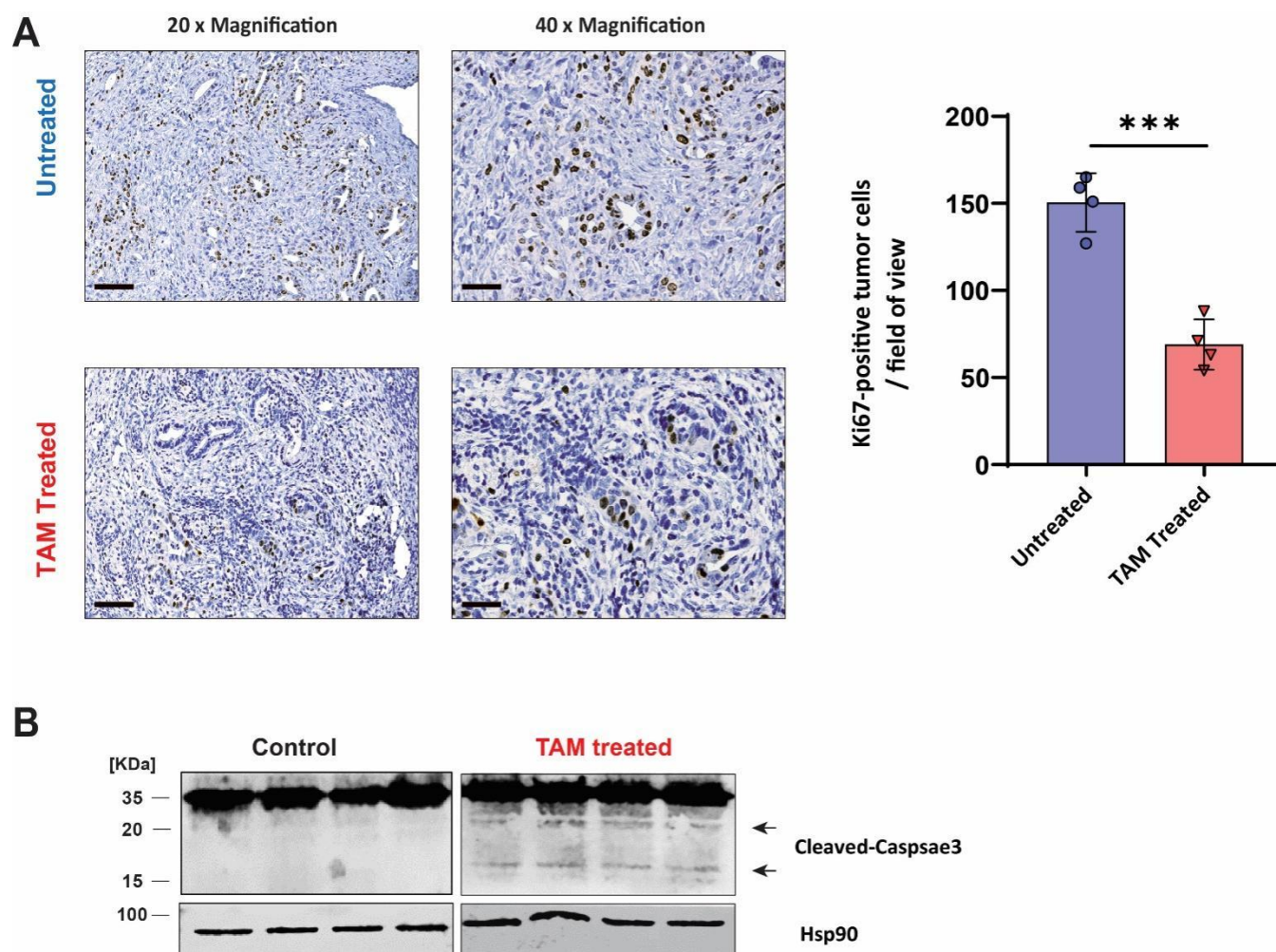


Figure 16 . Concomitant inactivation of *Pdk1*, *Braf* and *c-Raf* inhibits proliferation and promotes apoptosis

(A) Left: The representative images of Ki67 Immunohistochemistry (IHC) staining for tumor tissues from control and tamoxifen -treated mice respectively. Scale bar, 100 μ m. Right: Quantification of ki67-positive tumor cells in tumor tissue from control and tamoxifen-treated mice. Different field of views were randomly chosen from four sections for quantification of ki67-positive. Scale bar, 100 μ m (20x Magnification); 50 μ m (40x Magnification). *** p < 0.001, two- tailed student's t test.

(B) The western blotting results show the slightly increased level of cleaved-caspase3 protein in tumor tissues with tamoxifen treatment. The size of full length Caspase-3 protein is 35 KDa, the size of cleaved-Caspase3 proteins are 19 KDa and 17 KDa.

4.2.11 Depletion of *Pdk1*, *Braf* and *c-Raf* increases infiltration of lymphocytes in PDAC

PDAC is usually considered to be a non-immunogenic tumor, as it can develop an immunosuppressive tumor microenvironment (TME), which can restrict the anti-tumor functions of tumor-infiltrating lymphocytes (TILs), and eventually lead to evasion of the immune system and tumor progression [223, 224].

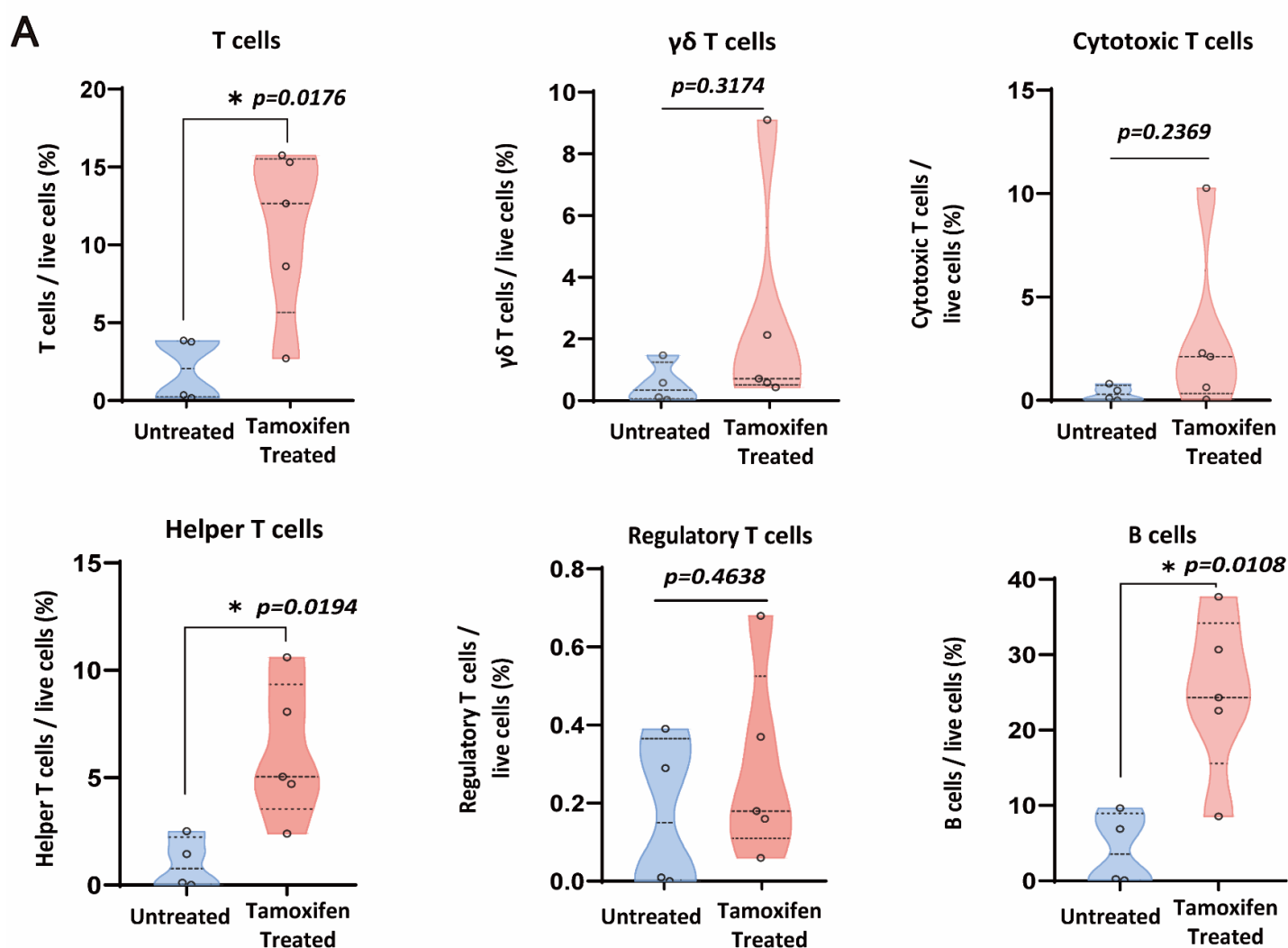
To study the effects of TKO of *Pdk1*, *Braf* and *c-Raf* on immune cell infiltration in the TME of PDAC, the solid tumors from endogenous tumor mice were collected and the immune cells in the TME were analyzed using FACS.

Regarding adaptive immune cells, T lymphocytes in pancreatic tumors were found to increase significantly following the deletion of *Pdk1*, *Braf* and *c-Raf* genes (Figure 17A). In contrast, the percentage of gamma-delta T cells (γ/δ T cells) and cytotoxic T cells relative to total single live cells showed no obvious change following tamoxifen treatment. CD4⁺ T cells (helper T cells), however, showed a clear increase following deletion of *Pdk1*, *Braf* and *c-Raf* genes *in vivo* (Figure 17A). Helper T cells have direct anti-tumor activity, as they produce cytokines such as interferon-gamma (IFN γ) and tumor necrosis factor-alpha (TNF α), which function to arrest tumor cell growth and cause necrosis or apoptosis of tumor cells, respectively [225, 226]. This suggests that helper T cells may also contribute to the regression of pancreatic tumors, in addition to tumor cell autonomous effects of the triple KO shown above. It has been reported that helper T cells are able to interact with B cells via the CD40 receptor, and thus drive B cell differentiation and maturation, allowing B cells to produce tumor-reactive antibodies to recognize and kill tumor cells [190]. Most tumors in this study displayed a high percentage of tumor-infiltrating B cells following deletion of *Pdk1*, *Braf* and *c-Raf*, and this could be due to the increase in helper T cells in the tumors.

On the other hand, the flow cytometry analysis for innate immune cells in pancreatic tumors showed that tumor-associated macrophages (TAMs) were remarkably reduced (p value = 0.0023) following tamoxifen treatment (Figure 17B). Indeed, TAMs can promote tumor development and create an immunosuppressive TME by secreting chemokines and cytokines [227]. Reducing the number of TAMs could restrict their pro-tumoral functions and allow for reactivation of anti-tumor immune cells in the TME. The presence of myeloid-derived

suppressor cells (MDSCs) in the TME also decreased following *Pdk1*, *Braf* and *c-Raf* deletion. MDSCs are immature myeloid cells with heterogeneous populations in tumors, and can promote tumor growth by blocking the anti-tumor functions of T and NK cells. In addition, MDSCs also contribute to angiogenesis and tumor progression by secreting cytokines such as IL-10 and TGF- β [228]. The levels of other key subsets of innate immune cells showed no significant changes (Figure 17B).

Together, these results suggested that inhibition of *Pdk1*, *Braf*, and *c-Raf* could promote specific immune responses in the TME of PDAC by stimulating both T and B lymphocytes, as well as decreasing the proportion of MDSCs and TAMs in pancreatic tumors, to prevent the progression of PDAC.



B

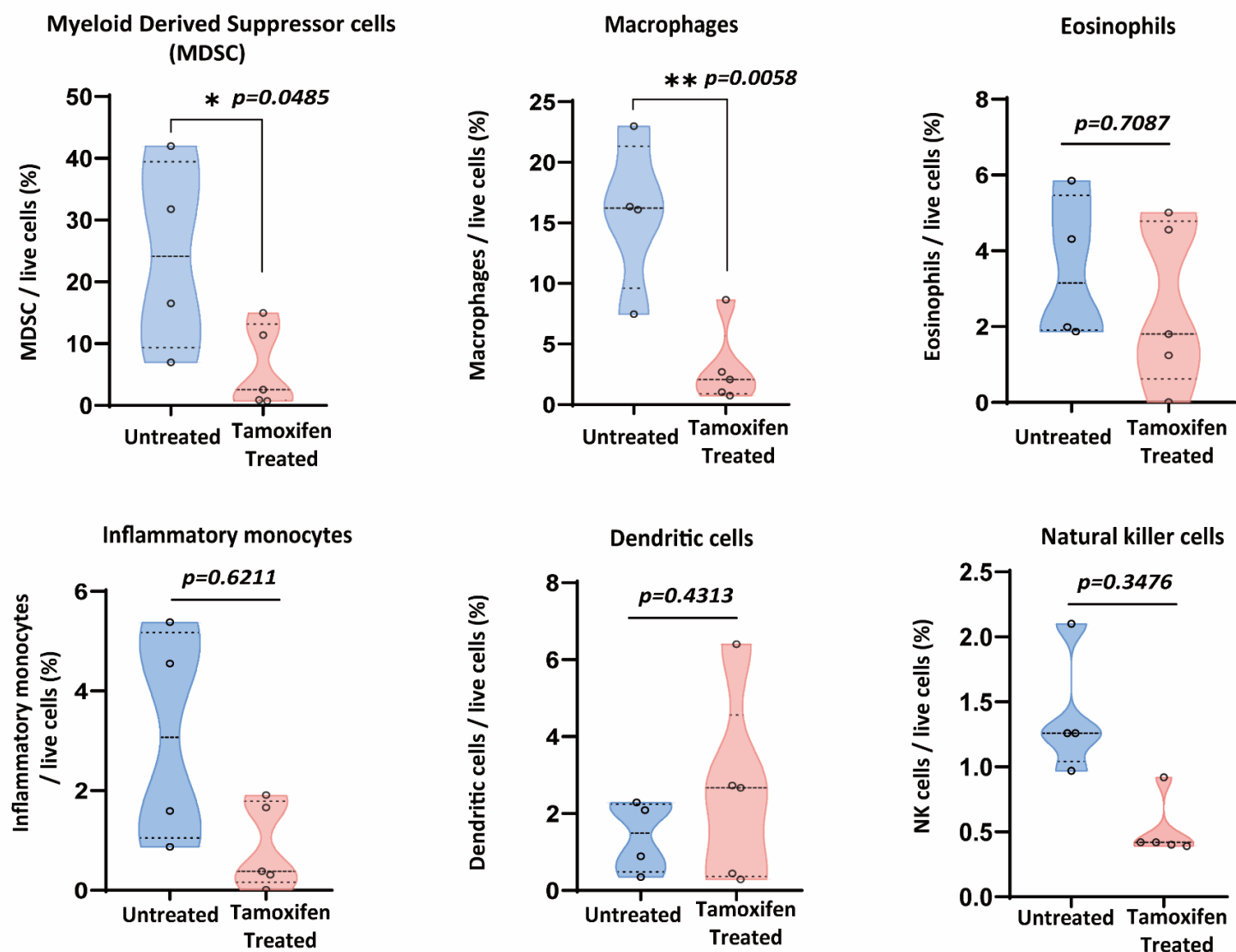


Figure 17. Depletion of *Pdk1*, *Braf* and *c-Raf* increases infiltration of lymphocytes in *Kras*^{G12D}-driven PDAC

(A) The percentages of T and B lymphocyte subpopulations in single live cells isolated from PDAC tumors of endpoint mice. Primary pancreatic tumors are obtained from PKPBC, *Trp53*^{fl/+} tamoxifen-untreated (n=4) and tamoxifen-treated (n=5) mice. Mice were treated with tamoxifen-containing diet (400 mg tamoxifen citrate / kg diet) for 4 weeks once the solid tumor could be palpated. Tumor tissues are digested into single cells with GentleMACS™ Tumor Tissue Dissociation Kit and stained with antibodies from BT panel and innate panel (Table 29, 30). The lymphocyte subsets are analyzed by FACS.

(B) The proportions of indicated cell subsets from innate immunity in single live cells. Two-tailed Student's t-test.

4.2.12 Genetic depletion of *Pdk1* in combination with *Braf* and *c-Raf* induces complete regression of orthotopically growing PDAC

Although the results from GEMMs described above are exciting and promising, there was significant variation in the pathological latency and progression of PDAC in these models. To further investigate the effect of TKO in PDAC, primary tumor cell lines CV7250 (*Pdk1*^{lox/lox}) and WM1047 (*Pdk1*^{lox/lox}; *Braf*^{lox/lox}; *c-Raf*^{lox/lox}) were orthotopically implanted into the pancreata of mice as described in **Methods, Section 3.2.3**.

For each cell line, mice were divided into two groups – experimental animals treated with tamoxifen to activate CreER^{T2} and delete *Pdk1* alone or in combination with *Braf* and *c-Raf*, and untreated control animals. One week following implantation, experimental mice were treated twice with tamoxifen intraperitoneally (i.p.) for one week, and were subsequently fed the tamoxifen-containing diet for another four weeks. Mice in the control group did not receive any treatments. All mice were kept until the human endpoint when their health deteriorated due to tumor progression.

All mice not given the tamoxifen treatment reached the human endpoint within one month following implantation, with a median survival time of 28 days and 31 days for CV7250 and WM1047 untreated mice, respectively. Although mice that were implanted with CV7250 cells and treated with tamoxifen had a prolonged life span, most did not survive more than 50 days following implantation (Figure 18A). Notably, mice in the tamoxifen treatment group with the WM1047 cell line implantation had significantly increased survival time, with most mice (five of six) surviving for more than 6 months, and a median survival time of 388 days (Figure 18A). Pancreatic tumors were resected from the mice immediately following euthanasia, and the weight, volume, and appearance of tumors documented. Overall, the pancreata from tamoxifen-treated mice in *Pdk1*^{lox/lox} cohort were similar with tumors of control mice, they all had invasive tumors with irregular and rough surface topography (Figure 18B). Whereas the tamoxifen-treated mice in *Pdk1*^{lox/lox}; *Braf*^{lox/lox}; *c-Raf*^{lox/lox} cohort exhibited significantly smaller pancreata with only PanINs around the implantation site (Figure 18B). The ratio of pancreatic tumor weight to mouse body weight was not found to be significantly different between untreated mice and mice treated with tamoxifen in the *Pdk1*^{lox/lox} implantation cohort (Figure 18C). In contrast, tamoxifen-treated mice in the *Pdk1*^{lox/lox}; *Braf*^{lox/lox}; *c-Raf*^{lox/lox} cohort were

found to have a reduced pancreas weight to mouse body weight ratio, in comparison to untreated mice (Figure 18C). In addition, metastases to the liver, peritoneum, and thoracic diaphragm were generally observed in mice in all untreated groups, as well as in *Pdk1*^{lox/lox} implanted mice in the tamoxifen treatment group. In contrast, none of the tamoxifen-treated mice in *Pdk1*^{lox/lox}; *Braf*^{lox/lox}; *c-Raf*^{lox/lox} cohort showed evident distant metastases to other organs.

To conclude, deletion of *Pdk1* could slow pancreatic tumor progression in orthotopic allograft models. However, the inhibitory effect of *Pdk1* ablation did not halt progression of PDAC completely. In contrast, inactivation of *Pdk1*, *Braf* and *c-Raf* was more efficient in inhibiting both the progression of PDAC and tumor metastasis, and was able to lead to complete tumor regression in most of the animals.

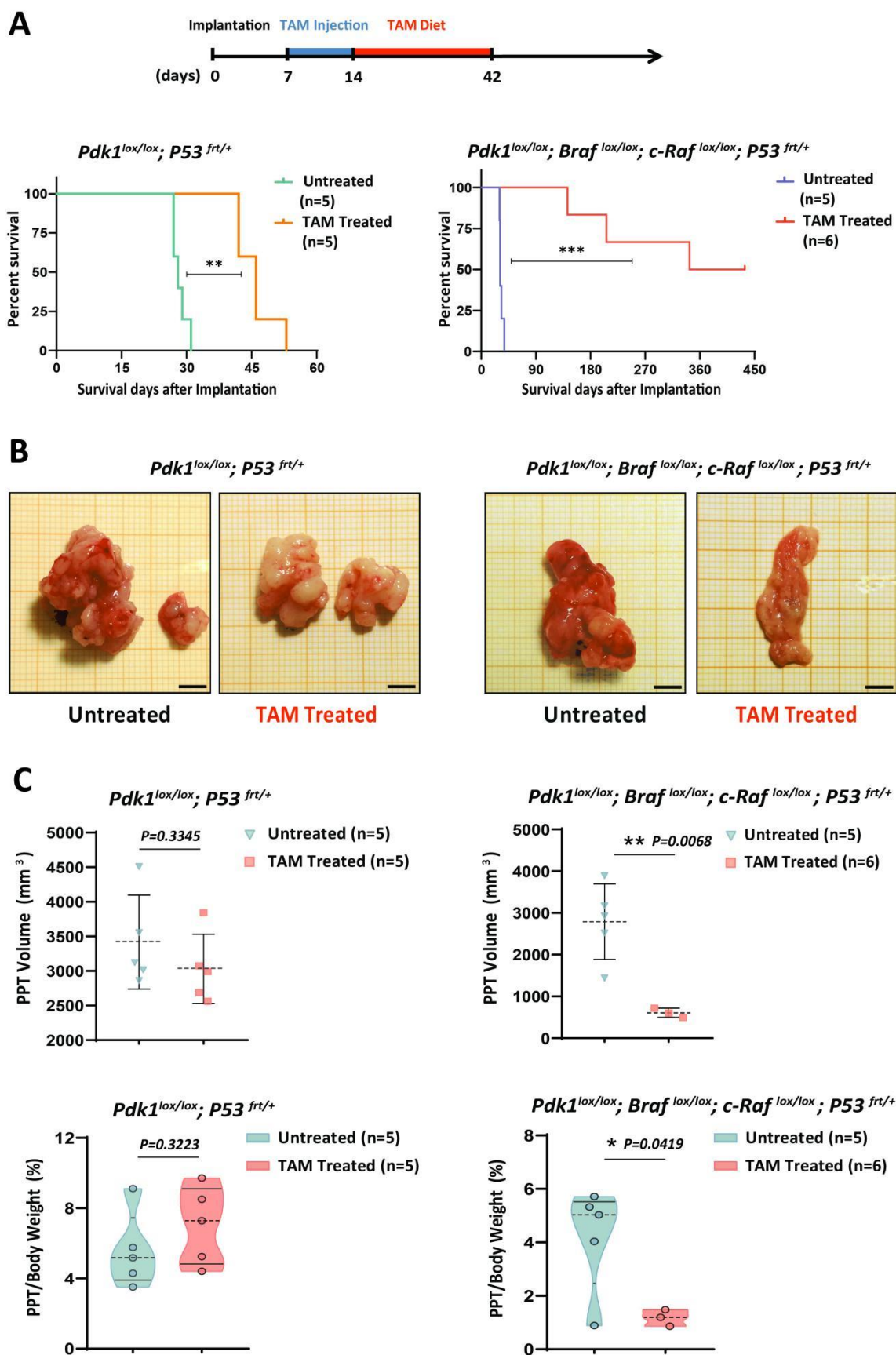


Figure 18. Orthotopic implantation of mPDAC cell lines in mice

(A) Top: schematic of tamoxifen treatment for orthotopic mouse models. TAM: Tamoxifen. TAM intraperitoneal injection: 4 mg tamoxifen / 30g body weight, twice per week, treatment last for one week. TAM diet: 400 mg tamoxifen citrate/ kg diet, treatment last for 4 weeks. Bottom: Kaplan-Meier survival analysis for orthotopic mice implanted with indicated PDAC cell lines. *Pdk1^{lox/lox}; p53^{frt/+}*, untreated (n=5, median survival 29 days); *Pdk1^{lox/lox}; p53^{frt/+}*, Tamoxifen-treated (n=5, median survival 46 days); *Pdk1^{lox/lox}; Bra^{flox/lox}; c-Raf^{lox/lox}; p53^{frt/+}*, untreated (n=5, median survival 31 days); *Pdk1^{lox/lox}; Bra^{flox/lox}; c-Raf^{lox/lox}; p53^{frt/+}*, Tamoxifen-Treated (n=6, median survival 388 days). ** $p < 0.01$, *** $p < 0.001$, log-rank (mantel-cox) test.

(B) Representative macroscopic images of pancreatic tumor from indicated orthotopic PDAC mice treated with and without tamoxifen. Scale bars, 5mm.

(C) The volume of primary pancreatic tumor (PPT) (Top) and the ratio of PPT and mouse body weight (Bottom) from indicated cohorts with or without tamoxifen treatment. * $p < 0.05$; ** $p < 0.01$; ns, not significant. two-tailed student's t test.

5. Discussion and outlook

PDAC is one of the most intractable malignancies, and is the 7th leading cause of cancer deaths worldwide [229]. The mutation of the *KRAS* gene is a major event in pancreatic cancer, and is the main driver of PDAC initiation in approximately 90% of all cases. *KRAS* mutations also play a key role in the progression of PDAC to advanced stages. However, *KRAS* mutations have long been considered undruggable due to the small size and relatively smooth surface of the protein product [230]. Although the novel drug Sotorasib, which can target the *KRAS*^{G12C} mutation specifically, has recently been approved for treatment of non-small cell lung cancer (NSCLC), it is only a treatment option for a small cohort of PDAC patients, because *KRAS*^{G12C} mutations are rare in PDAC (approx.1% of all patients). Development of safer and more effective therapeutic methods is therefore urgently required for PDAC clinical treatment. This study identified the *Kras* downstream effectors *Pdk1* and *Braf*, *c-Raf* as potential therapeutic targets using GEMMs, orthotopic allograft models and drug screening. *c-Raf* was also identified as a synergistic and synthetic lethal interaction partner with *Pdk1* inactivation in PDAC cells using CRISPR-Cas9-mediated LOF screening. Concomitant inhibition of *Pdk1* and *Braf*, *c-Raf* produced significant repression of proliferation and growth of PDAC cells both *in vitro* and *in vivo*.

PDAC is a cancer with significant metastatic potential, and this one of the primary reasons for its high mortality rate. The EMT process is widely thought to be associated with metastasis in different cancers. It is triggered by EMT-TFs, which display pleiotropic functions at various stages of cancer progression, such as initiation of tumor formation, tumor invasion, and metastasis, as well as chemo-resistance of cancer cells. However, the role of EMT-TFs in the development and metastasis of cancer remains controversial. In this study, the novel mouse models that can track the expression of EMT-TFs and EMT-related markers (*Col6a1*, *Fsp1*) using fluorescent proteins in tumor cells were established. In these mouse models, the normal functions of EMT-TFs would not be affected, which could enable a more objective evaluation of EMT-TFs functions. In addition, the dual-recombinase system (DRS) of these models would also allow further labelling of EMT-TFs positive cells with other distinguishable fluorescence, or even specific removal of EMT-TFs positive tumor cells *in vivo*. This could

provide a good opportunity to determine the relationship between the EMT process and metastasis of PDAC, as well as the specific functions of EMT-TFs during PDAC tumorigenesis.

***Pdk1*, *Braf* and *c-Raf* TKO significantly impedes viability and growth of PDAC cells, and induces apoptosis**

As a key effector of the *PI3K/AKT* signaling pathway in pancreatic cancer with *KRAS* mutations, *Pdk1* inactivation produced a strong effect on the proliferation and colony formation of PDAC cells. Inhibition of *Pdk1* in orthotopic allograft animal models could delay the progression of PDAC significantly. Nevertheless, it was insufficient to block the growth of PDAC completely, as some PDAC cells remained that could grow through *Pdk1*-independent pathways. In *Kras*^{G12D}-driven PDAC, the highly active *RAF/MEK/ERK* pathway was crucial for the proliferation, survival and motility of cancer cells. In addition, as the major downstream effectors of *KRAS* signaling, the *PI3K/AKT/mTOR* and *RAF/MEK/ERK* pathways also showed extensive interconnections with each other [231]. This could explain why inhibition of *PDK1* or *RAFTs* alone could not inhibit the growth and development of PDAC efficiently in our previous studies.

A putative therapeutic strategy for the treatment of *KRAS*^{G12D}-driven PDAC would therefore be concomitant inhibition of *PDK1* and *RAF*. Indeed, the growth of PDAC cells was almost completely blocked *in vitro*. Furthermore, concomitant inactivation of *Pdk1* and *Braf*, *c-Raf* led to increased apoptosis in tumor cells, while KO of *Pdk1* alone or double-KO of *Braf*, *C-Raf* failed to promote apoptosis significantly. One possible reason for this is that both the *PI3K/AKT/mTOR* and *RAF/MEK/ERK* pathways are able to regulate apoptosis through the Bcl-2 protein family. Bcl-2 is a pro-survival protein that prevents the oligomerization of BAX/BAK, which can induce the mitochondrial outer membrane permeabilization (*MOMP*) that eventually leads to apoptosis [232]. Inhibition of solely *Pdk1* or *Braf* and *c-Raf* in PDAC cells may result in activation of the compensatory mechanisms of *RAF* or *Pdk1*, which can still repress the BAX/BAK oligomerization via Bcl-2 and prevent apoptosis (Figure 19). In contrast, concomitant interruption of *Pdk1*, *Braf* and *c-Raf* might promote BAX/BAK to induce

the release of cytochrome C from the damaged mitochondria and the activation of caspase 9 by apoptotic protease activating factor 1 (*APAF1*), which eventually lead to apoptosis in PDAC cells. Future work should focus on establishing the specific mechanisms by which apoptosis is induced by *Pdk1* and *Braf/c-Raf* inactivation, which may, at least in part, elucidate the complicated cross-talk between the *PI3K/AKT/mTOR* and *RAF/MEK/ERK* pathways.

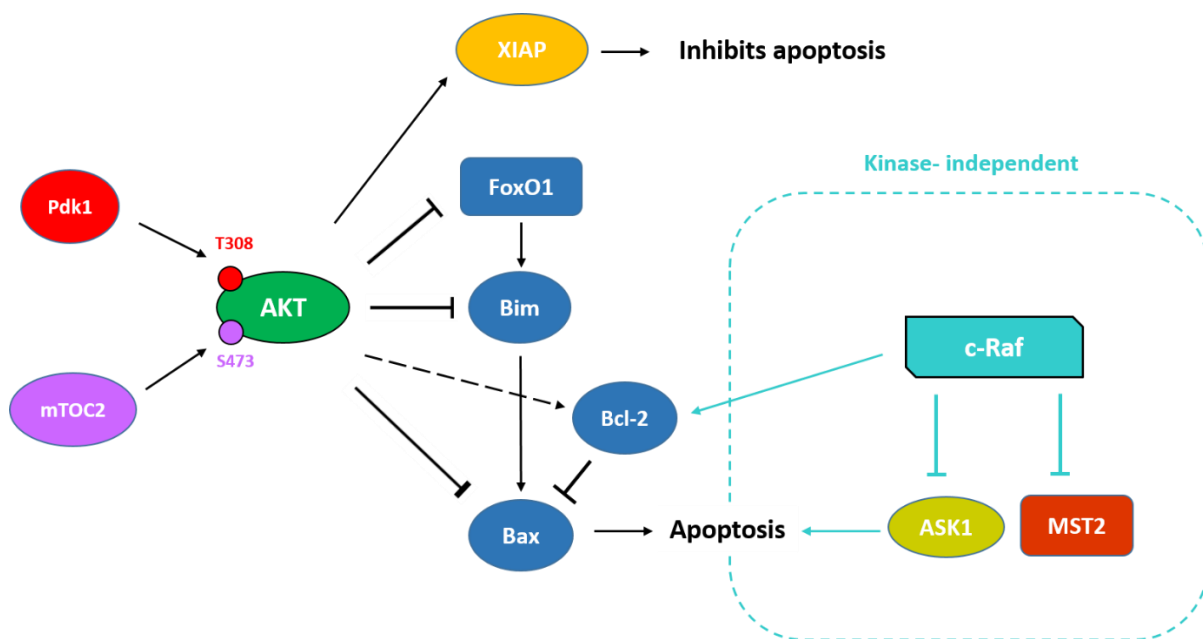


Figure 19. The potential compensatory mechanisms of *Pdk1* and *c-Raf* to prevent apoptosis

The hyperactive PDK1–Akt axis in *Kras*^{G12D}-driven pancreatic tumors can directly improve (black arrow) the activity of XIAP to maintain tumor cell viability, and can prevent apoptotic cell death by suppressing (blunt arrow) pro-apoptotic proteins (FoxO1, Bim and Bax). *c-Raf* can block apoptosis by positively regulating activity of anti-apoptotic protein- Bcl-2, and negatively regulating apoptosis activators - ASK1, MST2 through its kinase-independent mechanisms in PDAC cells.

Identifying synergistic and synthetic lethal gene interactions with *Pdk1* inactivation using CRISPR/Cas9-mediated LOF screens

The goal of genetic screening is to discover the relationship between genotype and phenotype by introducing large-scale genetic mutations. By reducing or eliminating the original genes, messenger RNA (mRNA), or proteins, gene LOF analysis clarifies the role and function of target genes. The functions of the original genes can then be deduced by

analyzing the changes in phenotype caused by perturbation of target genes [233]. Before the CRISPR/Cas9 system became widely used in molecular biology, the RNA interference (RNAi) technique was one of the most efficient and convenient platforms for genome-wide LOF screening. The RNAi library can produce thousands of double-stranded RNAs that target individual genes by binding to the mRNA of these genes and eventually suppressing the protein translation process. However, because the RNAi targets RNA rather than DNA, the RNAi-based genetic screens only produce partial and short-term gene suppression, rather than a complete LOF mutation. Additionally, the high off-target effects of RNAi can also cause false-positive results [234, 235].

CRISPR are short DNA sequences found in the genomes of prokaryotic organisms (such as bacteria and archaea), and are derived from phage DNA fragments that infected the prokaryote previously. Together with the CRISPR-associated (Cas) protein, the phage DNA becomes part of the adaptive immune system of the prokaryote, enabling it to recognize and destroy similar DNA in subsequent phage infections [196, 236, 237]. Since its development, researchers have widely applied the CRISPR/Cas9 system for genome engineering due to its high cleavage efficiency, specificity, flexibility and stability. CRISPR screens of our lab found that *c-Raf*, *EGFR* and *Grab2* were the top hits of negative selection screens in combination with *Pdk1*-inactivation in murine PDAC cells. A significant decrease in the sgRNAs of these genes was observed in 3 different PDAC cell lines using NGS. This suggests that *c-Raf*, *EGFR* and *Grab2* are potential synergistic and synthetic lethal genes in combination with *Pdk1* deletion, and that the combined inhibition of *Pdk1* and *c-Raf/EGFR/Grab2* may be useful clinically as a novel therapeutic approach.

Validating the functions of *c-Raf* in *Pdk1*-independent cells

The RAF proto-oncogene serine/threonine-protein kinase, also known as *c-Raf* or *Raf1*, is a kinase that links the *RAS* and *MEK/ERK* signaling pathways. Together with other RAF genes, *c-Raf* regulates crucial processes such as cell proliferation, differentiation and survival. In addition, *c-Raf* also plays important roles in tumorigenesis and cell migration, which are

mediated by the interaction of c-Raf with ROK- α kinase, a GTPase Rho effector and cytoskeletal reorganization regulator [238]. Moreover, c-Raf can directly or indirectly suppress apoptosis by regulating the activity of *Bcl-2*, *ASK-1* and the *MST-2* kinase, independently of the kinase activity of the *MEK-ERK* signaling pathway [239-241].

The results described in this thesis demonstrate that *c-Raf* is one of the top hits in the CRISPR/Cas9-mediated LOF screen, and that deletion of *c-Raf* in *Pdk1 Δ* resistant cells blocked cell colony formation and induced cell death. These results indicate that *c-Raf* has the potential to be an effective therapeutic target with *Pdk1*, and provides a theoretical basis and experimental evidence for the treatment of pancreatic cancer.

Drug treatment in *Pdk1^{WT}* and *Pdk1 Δ* resistant PDAC cells

Drug testing or screening is a common method for identifying antitumor activity of compounds *in vitro* using cultured tumor cells. *In vitro* drug testing allows researchers to directly evaluate the anticancer activity of drugs in specific cell line. Moreover, more detailed biological effects of drugs on cancer cells can be examined using high throughput drug screening in various cultured cell lines, which is important for assessment of drug effectiveness. In this study, eight *RAF* inhibitors were tested in *Kras^{G12D}*-driven murine PDAC cells. From single-drug treatment, the resistant PDAC cells were more sensitive to *RAF* inhibitors. In *Pdk1* deficient resistant cells, combinations of GDC-0941 and *RAFi* demonstrated stronger inhibitory effects than GSK2334470 and *RAFi* combination treatments. Of note, drug treatments of GDC-0941 with AZ628, Ro5126766, and Dabrafenib produced a high synergistic effect in both *Pdk1^{WT}* and *Pdk1 Δ* PDAC cells. Taken together, the results of drug testing prove that combined inhibition of *PI3K* or *PDK1* and *RAFs* (*Braf* and *c-Raf*) can block the growth and survival of PDAC cells effectively, which may provide a potential strategy for the clinical treatment of PDAC. Future studies should test the apoptosis, as well as inactivation of downstream signaling pathways following inhibition of *Pdk1*, *Braf* and *c-Raf* in PDAC cells to elucidate the mechanisms of PDAC cell growth arrest induced by *Pdk1*, *Braf* and *c-Raf* inhibition.

***Pdk1*, *Braf* and *c-Raf* TKO blocks tumor development significantly in PDAC endogenous mouse models**

GEMMs are mice with altered genes that have been introduced into their genome using genetic engineering techniques. Currently, GEMMs are commonly used for preclinical research of human genetic diseases, tumor biology, and responses to clinical therapy [242]. In the field of pancreatic cancer research, GEMMs of PDAC can faithfully mimic many of the key pathological features of human PDAC, including PDAC progression, high frequency of metastases, and inflammatory reactions during the stages of PanIN [243-245]. Our group established a novel DRS PDAC mouse model that integrated the DNA site-specific recombination techniques of *Cre-loxP* and *Flp-FRT*, which have also been shown to reproduce the pathological features of clinical PDAC [246].

The results of this thesis demonstrate that ablation of *Pdk1*, *Braf*, and *c-Raf* in the DRS endogenous tumor models significantly impedes the progression of PDAC, and remarkably extends the lifespan of these mice. Furthermore, significant tumor regression was observed in PDAC mouse models using MRI. The inhibitory effects of *Pdk1*, *Braf*, and *c-Raf* TKO on PDAC development indicates that these genes have potential as molecular targets for PDAC treatment. However, *Pdk1*, *Braf* and *c-Raf* were not deleted completely in tumors, which could be one reason that solid tumors continued to be observed in mice at the endpoint of the *in vivo* experiments. To further explore the clinical feasibility of *Pdk1*, *Braf*, and *c-Raf* deletion in PDAC treatment, drugs can be used to block the respective pathways. In addition, pathway inhibition needs to be validated in TKO tumors and the recombination efficacy tested.

Immune landscape changes in *Pdk1*^Δ, *Braf*^Δ and *c-Raf*^Δ tumors

The highly immunosuppressive TME of PDAC is one of the clinical features of this malignancy that may contribute to tumor evasion, as well as promote tumor cell resistance to anti-tumor therapeutic modalities, including chemotherapy, therapeutic cancer vaccines, and immune checkpoint inhibitors [223, 247]. The TME of PDAC is essentially composed of T regulatory

cells (Tregs), TAMs, and MDSCs, which inhibit CD8⁺ T cell recognition and destruction of tumor cells in solid tumors [247].

MDSCs in the tumor can stimulate the expression of programmed death-ligand 1 (PD-L1) through direct interaction with lymphocytes. The PD-L1 and PD1-specific interactions subsequently inhibit the activation and proliferation of T cells, ultimately leading to tumor immune evasion [248]. MDSCs have also been shown to suppress the antitumor functions of T cells by enhancing Treg proliferation and immunosuppression [249, 250].

TAMs are commonly abundant in the TME of pancreatic cancer, and can be distinguished as two distinct subpopulations with different functions, a process termed “polarization” of macrophages [251]. M1-like macrophages can secrete cytokines that promote inflammation, and have a predominantly inhibitory effect on PDAC development. Many studies have also shown that M2-like macrophages are involved in facilitating PDAC progression, immunosuppression, and angiogenesis by releasing a variety of cytokines, including epidermal growth factor (EGF), EGFR, transforming growth factor- β 1 (TGF- β 1) and vascular endothelial growth factor (VEGF) [252-255]. Although TAMs display different statuses and functions in PDAC, they tend to differentiate into the M2-like subset and demonstrate tumor-promoting effects, such as immunosuppressive TME formation, promotion of metastasis, and chemotherapy resistance [256]. Targeting M2-like macrophages in TME is therefore considered to be an effective way of hindering PDAC development and improving therapeutic efficiency for clinical PDAC treatment.

This study found that levels of MDSCs and TAMs in PDAC tumors significantly decreased following *Pdk1*, *Braf* and *c-Raf* deletion, indicating that simultaneous inhibition of these genes could weaken the immunosuppression of the TME by altering its composition. Furthermore, the increased percentage of CD4-positive cells (helper T cells) found in the tumors of PDAC endogenous mouse models also suggests that T cells were at least partially activated in the TME following the deletion of *Pdk1* and *RAFs*, promoting the antitumor immune activity in the mice. Together, these phenomena indicate that *Pdk1*, *Braf* and *c-Raf* may mediate the interaction and crosstalk between tumor cells and TME component cells in pancreatic tumors. Inactivation of *Pdk1*, *Braf* and *c-Raf* can give rise to a change in immune cell distribution in

the TME, and can eventually attenuate its immunosuppressive effect. In the future, the combination treatments of *Pdk1*, *Braf*, *c-Raf* and immune checkpoint inhibitors (e.g. PD-1 or PD-L1 inhibitors) can be further tested to develop more effective therapeutic method for PDAC.

Deletion of *Pdk1*, *Braf* and *c-Raf* leads to complete regression of orthotopic PDAC

GEMMs are traditional and common mouse models used in the field of cancer research, and are able to mimic the pathological features of different types of human cancers. They are therefore a powerful tool for understanding the molecular mechanisms of tumor development [257]. Nonetheless, GEMMs have some limitations in their use in preclinical studies. These include the significant length of time required for spontaneous tumor models to develop tumors, the high costs of mouse model generation and maintenance, the variable phenotypes resulting from individual differences, and the limitations for large-scale *in vivo* pharmacology studies [258-260]. In orthotopic mouse models, tumor cells are implanted into the corresponding organ in the mouse, allowing them to develop into a solid tumor in the appropriate TME. Furthermore, the tumor progression and response to therapeutics in orthotopic allograft models can be monitored and evaluated more accurately and faithfully than in GEMMs. Finally, the effect of genetic pathway disruption can be assessed in the same tumor cells side.

In this study, two different mouse primary PDAC cell lines (*Pdk1*^{lox/lox} and *Pdk1*^{lox/lox}; *Braf*^{lox/lox}; *c-Raf*^{lox/lox}) were implanted into the pancreata of mice. The mice were subsequently treated with IP injection of tamoxifen and food containing tamoxifen to inactivate *Pdk1* alone or in combination with *Braf* and *c-Raf* in PDAC cells. The results showed that *Pdk1* deletion prolonged the survival time of mice to some extent. In contrast, deletion of *Pdk1*, *Braf*, and *c-Raf* significantly blocked tumor development in orthotopic models, and all mice were able to survive for more than 6 months following orthotopic implantation. Compared to the spontaneous tumor models, the inhibitory effect of *Pdk1*, *Braf* and *c-Raf* deletion on tumor

growth was stronger in implantation mice. This could be due to the homogeneity of implanted tumor cells, which allowed them to respond more uniformly and effectively to *Pdk1*, *Braf* and *c-Raf* inactivation. To confirm the therapeutic effect of *Pdk1* and *RAFs* deletion for PDAC treatment, future studies should generate more orthotopic allograft models with cell lines representing different molecular PDAC subtypes. In addition, orthotopic implantation of primary mouse PDAC cell lines into immunodeficient mice (e.g. T cell deficient CD3 epsilon knock-out mice) should be performed, as it may allow us to further investigate the effects of deletion of *Pdk1* and *RAFs* on immune cells in the TME of pancreatic cancer.

Generation of EMT-TFs tracing mouse models

The EMT is a complex process that induces epithelial cells to lose the cell adhesion between adjacent cells, allowing them to migrate, invade, and eventually transform into mesenchymal cells [160]. This process plays a vital role at many stages of embryonic development, including gastrulation and neural crest formation [261]. It has also been reported that EMT is related to metastasis in a variety of human cancers [262].

The EMT process is induced by several EMT-TFs that are mainly from the *TWIST*, *SNAI* and *ZEB* families. These transcription factors can directly repress the expression of E-cadherin (*CDH1*) by binding to its promoter to block the transcription of *CDH1*. EMT-TFs can also induce the expression of mesenchymal markers, such as N-cadherin and vimentin, to promote the EMT process [263-265]. In addition to regulating the expression of *CDH1*, N-cadherin and vimentin, EMT-TFs have been found to control the EMT process by cooperating with microRNAs (miRs) such as miR-200, miR-205, miR-30a [266-268].

However, the role of EMT-TFs in tumorigenesis remains controversial due to their many pleiotropic functions, and particularly their tissue-specific functions in different types of cancer. The results of this thesis showed a novel EMT-TFs tracing model, which can be applied to further characterize the functions of EMT-TFs in pancreatic cancer, and to determine their involvement in tumor initiation, invasion metastasis and resistance to therapy. Although the functional validation of EMT-TF gene-modified ESCs demonstrated that the tracing system

works sufficiently well, more *in vivo* testing needs to be performed in the future, particularly to evaluate the practicability of the EMT-TFs tracing system in spontaneous tumor models.

Conclusion

The *PI3K/PDK1/AKT* signaling axis is a key downstream effector of oncogenic *KRAS*, which is involved in the regulation of tumor cell survival, growth, proliferation, and metabolism in pancreatic cancer. The previous study in our group demonstrated that genetic ablation of *Pdk1* could efficiently block tumor cell proliferation and PanIN lesion formation. However, inhibition of *Pdk1* alone was insufficient to block tumor progression entirely.

The results of this thesis prove that *c-Raf* is one of the synergistic and synthetic lethal genes in combination with *Pdk1* deletion for PDAC treatment, using CRISPR/Cas9-mediated LOF screening and a novel DRS mouse model. Furthermore, combination inhibition of *Pdk1* and *RAFs* produced a significant inhibitory effect on tumor cell growth and survival, giving us new insights into the interaction and relationship between the *PI3K/PDK1* and *RAF/MERK/ERK* signaling pathways in pancreatic cancer progression. Additionally, our data revealed that inactivation of *Pdk1*, *Braf*, and *c-Raf* could promote T and B lymphocytes infiltration, and attenuate the immunosuppressive effect of tumor microenvironment (TME) by decreasing the proportion of MDSCs and TAMs in pancreatic tumors.

The novel EMT-TFs tracing system has been established and validated *in vitro*. It can be applied to trace EMT-TF-positive cells spatially and temporally in pancreatic tumors, and allows us to further characterize the functions of EMT-TFs in PDAC.

6. Summary

The KRAS^{G12D}-driven pancreatic ductal adenocarcinoma (PDAC) is one of the most lethal malignancies worldwide. This devastating situation is mainly caused by the facts that lack of effective detection methods at the early stage of PDAC, the high metastatic potential of this aggressive malignancy and low efficiency of antitumor drugs to target the key driver of PDAC.

Recently, we proved that phosphoinositide 3-kinase (*PI3K*) and phosphoinositide-dependent kinase 1 (*Pdk1*) are key effectors of oncogenic *Kras* in PDAC, genetic ablation of *Pdk1* efficiently blocked the PanINs formation and PDAC cell growth in both genetically engineered mouse models (GEMMs) and primary pancreatic tumor (PPT) cells. However, a subpopulation of PDAC cells could survive and grow in the *Pdk1*-independent ways, this may contribute to therapy resistance and recurrence of *Kras*-driven PDAC. To further investigate the potential of *PI3K/Pdk1* as specific and efficient targets in targeted therapy for PDAC, our lab performed a CRISPR/Cas9-based large-scale gene loss-of-function (LOF) screen and identified *c-Raf* is one of the synergistic and synthetic lethal genes with *Pdk1* for PDAC treatment.

The results of *Pdk1*, *Braf*, *c-Raf* floxed GEMMs and orthotopic implantation mouse models prove that combination inhibition of *Pdk1* and *RAFs* produced a significant inhibitory effect on tumor cell growth and survival *in vivo*, which were caused by blocking the tumor cell proliferation, inducing apoptosis of tumor cells, increasing the infiltration of immune cells, reducing the suppressive capacity of myeloid-derived suppressor cells (MDSCs) and tumor-associated macrophages (TAMs). Taken together, these results giving us new insights into the interaction and relationship between the *PI3K/PDK1* and *RAF/MERK/ERK* signaling pathways in PDAC progression. These data also suggest that *PI3K/PDK1* and *RAFs* could be the potential therapeutic targets for PDAC treatment.

To further explore the EMT process and tissue-specific functions of EMT-TFs during pancreatic cancer tumorigenesis, a novel multicolor tracing system for EMT statuses and EMT-TFs was established and validated, which allows us to monitor, distinguish or even remove EMT-TF-positive cells spatially and temporally in pancreatic tumor without affecting the normal functions of EMT-TFs. This may facilitate the examination of EMT-TFs and EMT involved in pancreatic tumor progression as well as metastasis in the future studies.

7. Zusammenfassung

Das KRAS^{G12D}-gesteuerte duktale Adenokarzinom der Bauchspeicheldrüse (PDAC) ist eine der tödlichsten malignen Erkrankungen weltweit. Diese folgenschwere Situation ist vor allem darauf zurückzuführen, dass es an wirksamen Detektionsmethoden im Frühstadium des PDAC mangelt, dass diese aggressive bösartige Erkrankung ein hohes Metastasierungspotenzial hat und dass die Wirksamkeit von Antitumormedikamenten gegen den Hauptauslöser des PDAC gering ist.

Kürzlich haben wir nachgewiesen, dass die Phosphoinositid-3-Kinase (PI3K) und die Phosphoinositid-abhängige Kinase 1 (Pdk1) wichtige Effektoren der onkogenen Kras-Signaltransduktion in PDAC sind. Die genetische Ablation von Pdk1 blockierte effizient die Bildung von PanINs und das Wachstum von PDAC-Zellen sowohl in genetisch veränderten Mausmodellen (GEMMs) als auch in primären Pankreastumorzellen (PPT). Eine Subpopulation von PDAC-Zellen konnte jedoch überleben und mittels Pdk1-unabhängigem Signalweg wachsen. Dieser Mechanismus könnte zur Therapieresistenz und zum Wiederauftreten von Kras-gesteuerten PDAC führen. Um das Potenzial von PI3K/Pdk1 als spezifische und effiziente Ziele für die gezielte Therapie von PDAC zu untersuchen, hat unser Labor einen CRISPR/Cas9-basierten groß angelegten Gen-Loss-of-Function (LOF)-Screen durchgeführt und identifizierte *c-Raf* als eines der synergistischen und synthetischen letalen Gene mit Pdk1 in der PDAC-Behandlung.

Die Ergebnisse von *Pdk1*, *Braf* und *c-Raf* floxierten GEMMs und orthotopen Implantationsmausmodellen belegen, dass die kombinierte Hemmung von Pdk1 und RAFs eine signifikante Hemmwirkung auf das Wachstum und Überleben von Tumorzellen in vivo hat. Dies wurde hervorgerufen durch die Blockade der Tumorzellproliferation, die Induktion der Apoptose von Tumorzellen, die Erhöhung der Infiltration von Immunzellen und die Verringerung der suppressiven Kapazität von myeloiden Suppressorzellen (MDSCs) und tumorassoziierten Makrophagen (TAMs). Zusammengefasst geben uns diese Ergebnisse neue Einblicke in die Interaktion und Beziehung zwischen den PI3K/PDK1- und RAF/MERK/ERK-Signalwegen bei der PDAC-Progression. Diese Daten deuten auch darauf hin, dass PI3K/PDK1 und RAFs potenzielle therapeutische Ziele in der PDAC-Behandlung sein könnten.

Um den EMT-Hergang und die gewebespezifischen Funktionen von EMT-TFs während der Tumorentstehung des Bauchspeicheldrüsenkarzinoms weiter zu erforschen, wurde ein neuartiges mehrfarbiges System zur Verfolgung des EMT-Status und der EMT-TFs entwickelt und validiert, welches es uns ermöglicht, EMT-TF-positive Zellen in Bauchspeicheldrüsentumoren räumlich und zeitlich zu überwachen, zu unterscheiden oder sogar zu entfernen, ohne die normalen Funktionen der EMT-TFs zu beeinträchtigen. Dies

könnte die Untersuchung von EMT-TFs und EMT, die am Fortschreiten von Bauchspeicheldrüsentumoren und an der Metastasierung beteiligt sind, in zukünftigen Studien erleichtern.

Acknowledgements

The completion of this PhD dissertation is attributed to many people's support and assistance.

First, I would like to thank my supervisor Professor Dieter Saur to give me the opportunity to work on these interesting and exciting projects in his group. Prof. Dieter Saur's expertise was invaluable in formulating the research questions and methodology. His patient guidance, insightful feedbacks and valuable suggestions make me complete this dissertation.

Also, I would like to express my sincere gratitude to Prof. Marc Schmidt-Supprian and Prof. Angelika Schnieke for their fruitful discussions and enlightening suggestions as the members of my doctoral thesis committee.

I am very grateful to Barbara Seidler for her scientific contribution and kind help in generation of gene-targeting vectors. Further, I would like to thank Dr. Christian Veltkamp who established the floxed *Pdk1*, *Braf*, *c-Raf* mouse model for this thesis. I sincerely thank my colleagues - Katia Sleiman for the discussion about my PhD project and her kind help with the orthotopic implantation experiments; Tania Santos and Tatiana Martins for teaching me how to use confocal imaging and The Aperio VERSA scanning systems; Antonio Zaurito for his assistance with the performance of FACS analysis; Fabio Boniolo for his help for bioinformatics analysis; Magdalena Zukowska, Markus Raspe and Saskia Ettl for their excellent technical supports over these years.

I owe my gratitude to Dr. Tim Ammon and Katarzyna Jopek from group of Prof. Marc Schmidt-Supprian for helping me to perform *in vitro* cleavage efficiency of sgRNAs; Dr. Rupert Öllinger for his kind help with the ESC culture experiment; Prof. Susanne Kossatz and Markus Mittelhäuser for their assistance with MRI scans; all the animal caretakers for taking care of the mice; and all the members in the Saur, Schneider and Rad labs for creating the warm and nice work atmosphere.

In addition, I am particularly grateful to the China Scholarship Council for awarding me the four-year doctoral scholarships, and Prof. Dieter Saur for providing me with the 10-month PhD stipend in the last year, they were really the great financial support for my doctoral studying.

Last but not least, I would like to express my special thanks to my parents, younger sister and my friends for their constant care and support. Above all, I would like to thank my wife, it would be impossible for me to complete this dissertation without her tremendous support, encouragement and understanding in the past four and half years.

References

1. Sarantis, P., et al., *Pancreatic ductal adenocarcinoma: Treatment hurdles, tumor microenvironment and immunotherapy*. World J Gastrointest Oncol, 2020. **12**(2): p. 173-181.
2. Bray, F., et al., *Global cancer statistics 2018: GLOBOCAN estimates of incidence and mortality worldwide for 36 cancers in 185 countries*. CA Cancer J Clin, 2018. **68**(6): p. 394-424.
3. Siegel, R.L. and K.D. Miller, *Cancer statistics, 2020*. 2020. **70**(1): p. 7-30.
4. Ferlay, J., C. Partensky, and F. Bray, *More deaths from pancreatic cancer than breast cancer in the EU by 2017*. Acta Oncol, 2016. **55**(9-10): p. 1158-1160.
5. Kleeff, J., et al., *Pancreatic cancer*. Nat Rev Dis Primers, 2016. **2**: p. 16022.
6. Poruk, K.E., et al., *Screening for pancreatic cancer: why, how, and who?* Ann Surg, 2013. **257**(1): p. 17-26.
7. Morrison, A.H., K.T. Byrne, and R.H. Vonderheide, *Immunotherapy and Prevention of Pancreatic Cancer*. Trends Cancer, 2018. **4**(6): p. 418-428.
8. Huguet, F., S. Mukherjee, and M. Javle, *Locally advanced pancreatic cancer: the role of definitive chemoradiotherapy*. Clin Oncol (R Coll Radiol), 2014. **26**(9): p. 560-8.
9. Grasso, C., G. Jansen, and E. Giovannetti, *Drug resistance in pancreatic cancer: Impact of altered energy metabolism*. Crit Rev Oncol Hematol, 2017. **114**: p. 139-152.
10. Hessmann, E., et al., *Fibroblast drug scavenging increases intratumoural gemcitabine accumulation in murine pancreas cancer*. Gut, 2018. **67**(3): p. 497-507.
11. Caparello, C., et al., *FOLFIRINOX and translational studies: Towards personalized therapy in pancreatic cancer*. World J Gastroenterol, 2016. **22**(31): p. 6987-7005.
12. Yao, W., Maitra, Anirban, Ying, Haoqiang, *Recent insights into the biology of pancreatic cancer*. EBioMedicine, 2020. **53**: p. 102655.
13. Mizrahi, J.D., et al., *Pancreatic cancer*. The Lancet, 2020. **395**(10242): p. 2008-2020.
14. Sung, H., et al., *Emerging cancer trends among young adults in the USA: analysis of a population-based cancer registry*. Lancet Public Health, 2019. **4**(3): p. e137-e147.
15. Blackford, A., et al., *Genetic mutations associated with cigarette smoking in pancreatic cancer*. Cancer Res, 2009. **69**(8): p. 3681-8.
16. Yuan, C., et al., *Cigarette Smoking and Pancreatic Cancer Survival*. J Clin Oncol, 2017. **35**(16): p. 1822-1828.
17. Naudin, S., et al., *Healthy lifestyle and the risk of pancreatic cancer in the EPIC study*. Eur J Epidemiol, 2020. **35**(10): p. 975-986.
18. Jiao, L., et al., *A combined healthy lifestyle score and risk of pancreatic cancer in a large cohort study*. Arch Intern Med, 2009. **169**(8): p. 764-70.
19. Alsamarrai, A., et al., *Factors that affect risk for pancreatic disease in the general population: a systematic review and meta-analysis of prospective cohort studies*. Clin Gastroenterol Hepatol, 2014. **12**(10): p. 1635-44.e5; quiz e103.
20. Pericleous, M., et al., *Nutrition and pancreatic cancer*. Anticancer Res, 2014. **34**(1): p. 9-21.
21. De Rubeis, V., et al., *Trajectories of body mass index, from adolescence to older adulthood, and pancreatic cancer risk; a population-based case-control study in Ontario, Canada*. Cancer Causes Control, 2019. **30**(9): p. 955-966.
22. Zhang, C., et al., *Abdominal obesity and the risk of all-cause, cardiovascular, and cancer mortality: sixteen years of follow-up in US women*. Circulation, 2008. **117**(13): p. 1658-67.
23. Andersen, D.K., et al., *Diabetes, Pancreatogenic Diabetes, and Pancreatic Cancer*. Diabetes, 2017. **66**(5): p. 1103-1110.
24. Eibl, G., et al., *Diabetes Mellitus and Obesity as Risk Factors for Pancreatic Cancer*. J Acad Nutr Diet, 2018. **118**(4): p. 555-567.
25. Klein, A.P., *Genetic susceptibility to pancreatic cancer*. Mol Carcinog, 2012. **51**(1): p. 14-24.
26. Von Hoff, D.D., et al., *Increased survival in pancreatic cancer with nab-paclitaxel plus gemcitabine*. N Engl J Med, 2013. **369**(18): p. 1691-703.
27. Wolfgang, C.L., et al., *Recent progress in pancreatic cancer*. CA Cancer J Clin, 2013. **63**(5): p. 318-48.

28. De La Cruz, M.S., A.P. Young, and M.T. Ruffin, *Diagnosis and management of pancreatic cancer*. Am Fam Physician, 2014. **89**(8): p. 626-32.
29. Bond-Smith, G., et al., *Pancreatic adenocarcinoma*. Bmj, 2012. **344**: p. e2476.
30. Unger, K., et al., *Metabolomics based predictive classifier for early detection of pancreatic ductal adenocarcinoma*. Oncotarget, 2018. **9**(33): p. 23078-23090.
31. Yu, J., et al., *Digital next-generation sequencing identifies low-abundance mutations in pancreatic juice samples collected from the duodenum of patients with pancreatic cancer and intraductal papillary mucinous neoplasms*. Gut, 2017. **66**(9): p. 1677-1687.
32. Niederau, C. and J.H. Grendell, *Diagnosis of pancreatic carcinoma. Imaging techniques and tumor markers*. Pancreas, 1992. **7**(1): p. 66-86.
33. Seufferlein, T., et al., *Pancreatic adenocarcinoma: ESMO-ESDO Clinical Practice Guidelines for diagnosis, treatment and follow-up*. Ann Oncol, 2012. **23 Suppl 7**: p. vii33-40.
34. Jalanko, H., et al., *Comparison of a new tumour marker, CA 19-9, with alpha-fetoprotein and carcinoembryonic antigen in patients with upper gastrointestinal diseases*. J Clin Pathol, 1984. **37**(2): p. 218-22.
35. Azizian, A., et al., *CA19-9 for detecting recurrence of pancreatic cancer*. Sci Rep, 2020. **10**(1): p. 1332.
36. Perkins, G.L., et al., *Serum tumor markers*. Am Fam Physician, 2003. **68**(6): p. 1075-82.
37. Robert, M., et al., *Retrospective Analysis of CA19-9 Decrease in Patients with Metastatic Pancreatic Carcinoma Treated with FOLFIRINOX or Gemcitabine in a Randomized Phase III Study (ACCORD11/PRODIGE4)*. Oncology, 2017. **93**(6): p. 367-376.
38. Tsai, S., et al., *Importance of Normalization of CA19-9 Levels Following Neoadjuvant Therapy in Patients With Localized Pancreatic Cancer*. Ann Surg, 2020. **271**(4): p. 740-747.
39. Locker, G.Y., et al., *ASCO 2006 update of recommendations for the use of tumor markers in gastrointestinal cancer*. J Clin Oncol, 2006. **24**(33): p. 5313-27.
40. Oberstein, P.E. and K.P. Olive, *Pancreatic cancer: why is it so hard to treat?* Therap Adv Gastroenterol, 2013. **6**(4): p. 321-37.
41. Zhu, H., et al., *Pancreatic cancer: challenges and opportunities*. BMC Med, 2018. **16**(1): p. 214.
42. Siegel, R.L., K.D. Miller, and A. Jemal, *Cancer statistics, 2018*. CA Cancer J Clin, 2018. **68**(1): p. 7-30.
43. Evans, D.B., et al., *Preoperative gemcitabine-based chemoradiation for patients with resectable adenocarcinoma of the pancreatic head*. J Clin Oncol, 2008. **26**(21): p. 3496-502.
44. Ryan, D.P., T.S. Hong, and N. Bardeesy, *Pancreatic adenocarcinoma*. N Engl J Med, 2014. **371**(11): p. 1039-49.
45. Parekh, H.D., J. Starr, and T.J. George, Jr., *The Multidisciplinary Approach to Localized Pancreatic Adenocarcinoma*. Curr Treat Options Oncol, 2017. **18**(12): p. 73.
46. Tsitskari, M., et al., *The role of interventional oncology in the treatment of colorectal cancer liver metastases*. Ann Gastroenterol, 2019. **32**(2): p. 147-155.
47. Grandhi, M.S., K.J. Lafaro, and T.M. Pawlik, *Role of Locoregional and Systemic Approaches for the Treatment of Patients with Metastatic Neuroendocrine Tumors*. J Gastrointest Surg, 2015. **19**(12): p. 2273-82.
48. Vogl, T.J., et al., *Microwave ablation of pancreatic tumors*. Minim Invasive Ther Allied Technol, 2018. **27**(1): p. 33-40.
49. Ringel-Scaia, V.M., et al., *High-frequency irreversible electroporation is an effective tumor ablation strategy that induces immunologic cell death and promotes systemic anti-tumor immunity*. EBioMedicine, 2019. **44**: p. 112-125.
50. Zhang, Y., et al., *Molecular and histological study on the effects of non-thermal irreversible electroporation on the liver*. Biochem Biophys Res Commun, 2018. **500**(3): p. 665-670.
51. Gage, A.A. and J.G. Baust, *Cryosurgery - a review of recent advances and current issues*. Cryo Letters, 2002. **23**(2): p. 69-78.
52. Luo, X.M., et al., *Advances in cryoablation for pancreatic cancer*. World J Gastroenterol, 2016. **22**(2): p. 790-800.
53. Sacks, D., et al., *Multisociety Consensus Quality Improvement Revised Consensus Statement for*

- Endovascular Therapy of Acute Ischemic Stroke*. Int J Stroke, 2018. **13**(6): p. 612-632.
54. Gillen, S., et al., *Preoperative/neoadjuvant therapy in pancreatic cancer: a systematic review and meta-analysis of response and resection percentages*. PLoS Med, 2010. **7**(4): p. e1000267.
55. Heinemann, V., et al., *Meta-analysis of randomized trials: evaluation of benefit from gemcitabine-based combination chemotherapy applied in advanced pancreatic cancer*. BMC Cancer, 2008. **8**: p. 82.
56. Cunningham, D., et al., *Phase III randomized comparison of gemcitabine versus gemcitabine plus capecitabine in patients with advanced pancreatic cancer*. J Clin Oncol, 2009. **27**(33): p. 5513-8.
57. Moran, R.G. and K. Keyomarsi, *Biochemical rationale for the synergism of 5-fluorouracil and folinic acid*. NCI Monogr, 1987(5): p. 159-63.
58. Conroy, T., et al., *FOLFIRINOX or Gemcitabine as Adjuvant Therapy for Pancreatic Cancer*. N Engl J Med, 2018. **379**(25): p. 2395-2406.
59. Blomstrand, H., et al., *Real world evidence on gemcitabine and nab-paclitaxel combination chemotherapy in advanced pancreatic cancer*. BMC Cancer, 2019. **19**(1): p. 40.
60. Kalsner, M.H. and S.S. Ellenberg, *Pancreatic cancer. Adjuvant combined radiation and chemotherapy following curative resection*. Arch Surg, 1985. **120**(8): p. 899-903.
61. Neoptolemos, J.P., et al., *A randomized trial of chemoradiotherapy and chemotherapy after resection of pancreatic cancer*. N Engl J Med, 2004. **350**(12): p. 1200-10.
62. Lee, V.H., et al., *Dosimetric predictors of radiation-induced acute nausea and vomiting in IMRT for nasopharyngeal cancer*. Int J Radiat Oncol Biol Phys, 2012. **84**(1): p. 176-82.
63. Henson, C.C., et al., *Nutritional interventions for reducing gastrointestinal toxicity in adults undergoing radical pelvic radiotherapy*. Cochrane Database Syst Rev, 2013(11): p. Cd009896.
64. Taylor, C.W., et al., *Cardiac exposures in breast cancer radiotherapy: 1950s-1990s*. Int J Radiat Oncol Biol Phys, 2007. **69**(5): p. 1484-95.
65. Weintraub, N.L., W.K. Jones, and D. Manka, *Understanding radiation-induced vascular disease*. J Am Coll Cardiol, 2010. **55**(12): p. 1237-1239.
66. Rudra, S., et al., *Using adaptive magnetic resonance image-guided radiation therapy for treatment of inoperable pancreatic cancer*. Cancer Med, 2019. **8**(5): p. 2123-2132.
67. Cordo', V., et al., *T-cell Acute Lymphoblastic Leukemia: A Roadmap to Targeted Therapies*. Blood Cancer Discovery, 2021. **2**(1): p. 19-31.
68. Moore, M.J., *Brief communication: a new combination in the treatment of advanced pancreatic cancer*. Semin Oncol, 2005. **32**(6 Suppl 8): p. 5-6.
69. Waddell, N., et al., *Whole genomes redefine the mutational landscape of pancreatic cancer*. Nature, 2015. **518**(7540): p. 495-501.
70. Dantzer, F., et al., *Base excision repair is impaired in mammalian cells lacking Poly(ADP-ribose) polymerase-1*. Biochemistry, 2000. **39**(25): p. 7559-69.
71. Mirza, M.R., S. Pignata, and J.A. Ledermann, *Latest clinical evidence and further development of PARP inhibitors in ovarian cancer*. Ann Oncol, 2018. **29**(6): p. 1366-1376.
72. Syn, N.L., et al., *De-novo and acquired resistance to immune checkpoint targeting*. Lancet Oncol, 2017. **18**(12): p. e731-e741.
73. Brouwer, T.P., A.L. Vahrmeijer, and N. de Miranda, *Immunotherapy for pancreatic cancer: chasing the light at the end of the tunnel*. Cell Oncol (Dordr), 2021. **44**(2): p. 261-278.
74. Seidel, J.A., A. Otsuka, and K. Kabashima, *Anti-PD-1 and Anti-CTLA-4 Therapies in Cancer: Mechanisms of Action, Efficacy, and Limitations*. Front Oncol, 2018. **8**: p. 86.
75. Snyder, A., et al., *Genetic basis for clinical response to CTLA-4 blockade in melanoma*. N Engl J Med, 2014. **371**(23): p. 2189-2199.
76. Rizvi, N.A., et al., *Cancer immunology. Mutational landscape determines sensitivity to PD-1 blockade in non-small cell lung cancer*. Science, 2015. **348**(6230): p. 124-8.
77. Brahmer, J.R., et al., *Safety and activity of anti-PD-L1 antibody in patients with advanced cancer*. N Engl J Med, 2012. **366**(26): p. 2455-65.
78. Royal, R.E., et al., *Phase 2 trial of single agent Ipilimumab (anti-CTLA-4) for locally advanced or metastatic pancreatic adenocarcinoma*. J Immunother, 2010. **33**(8): p. 828-33.

79. Moncada, R., et al., *Integrating microarray-based spatial transcriptomics and single-cell RNA-seq reveals tissue architecture in pancreatic ductal adenocarcinomas*. Nat Biotechnol, 2020. **38**(3): p. 333-342.
80. Feig, C., et al., *The pancreas cancer microenvironment*. Clin Cancer Res, 2012. **18**(16): p. 4266-76.
81. Kwok, M., E.F. Fritsch, and C.J. Wu, *Cancer and COVID-19: On the Quest for Effective Vaccines*. Blood Cancer Discovery, 2021. **2**(1): p. 13-18.
82. Banerjee, K., et al., *Emerging trends in the immunotherapy of pancreatic cancer*. Cancer Lett, 2018. **417**: p. 35-46.
83. Kusmartsev, S., et al., *Antigen-specific inhibition of CD8+ T cell response by immature myeloid cells in cancer is mediated by reactive oxygen species*. J Immunol, 2004. **172**(2): p. 989-99.
84. Melief, C.J.M., et al., *Strong vaccine responses during chemotherapy are associated with prolonged cancer survival*. Sci Transl Med, 2020. **12**(535).
85. Kenter, G.G., et al., *Vaccination against HPV-16 oncoproteins for vulvar intraepithelial neoplasia*. N Engl J Med, 2009. **361**(19): p. 1838-47.
86. Kantoff, P.W., et al., *Sipuleucel-T immunotherapy for castration-resistant prostate cancer*. N Engl J Med, 2010. **363**(5): p. 411-22.
87. Salas-Benito, D., I. Melero, and M. Ponz-Sarvisé, *Vaccination for Pancreatic Ductal Adenocarcinoma: A Hard Nut to Crack*. Clin Cancer Res, 2019. **25**(18): p. 5435-5437.
88. Rosenberg, S.A. and N.P. Restifo, *Adoptive cell transfer as personalized immunotherapy for human cancer*. Science, 2015. **348**(6230): p. 62-8.
89. Patel, K., et al., *Pancreatic Cancer: An Emphasis on Current Perspectives in Immunotherapy*. Crit Rev Oncog, 2019. **24**(2): p. 105-118.
90. Svane, I.M. and E.M. Verdegaal, *Achievements and challenges of adoptive T cell therapy with tumor-infiltrating or blood-derived lymphocytes for metastatic melanoma: what is needed to achieve standard of care?* Cancer Immunol Immunother, 2014. **63**(10): p. 1081-91.
91. Eshhar, Z., et al., *Specific activation and targeting of cytotoxic lymphocytes through chimeric single chains consisting of antibody-binding domains and the gamma or zeta subunits of the immunoglobulin and T-cell receptors*. Proc Natl Acad Sci U S A, 1993. **90**(2): p. 720-4.
92. Kochenderfer, J.N., et al., *Eradication of B-lineage cells and regression of lymphoma in a patient treated with autologous T cells genetically engineered to recognize CD19*. Blood, 2010. **116**(20): p. 4099-102.
93. Kochenderfer, J.N., et al., *Chemotherapy-refractory diffuse large B-cell lymphoma and indolent B-cell malignancies can be effectively treated with autologous T cells expressing an anti-CD19 chimeric antigen receptor*. J Clin Oncol, 2015. **33**(6): p. 540-9.
94. Park, J.H., et al., *Long-Term Follow-up of CD19 CAR Therapy in Acute Lymphoblastic Leukemia*. N Engl J Med, 2018. **378**(5): p. 449-459.
95. Newick, K., E. Moon, and S.M. Albelda, *Chimeric antigen receptor T-cell therapy for solid tumors*. Mol Ther Oncolytics, 2016. **3**: p. 16006.
96. Li, D., et al., *Persistent Polyfunctional Chimeric Antigen Receptor T Cells That Target Glypican 3 Eliminate Orthotopic Hepatocellular Carcinomas in Mice*. Gastroenterology, 2020. **158**(8): p. 2250-2265.e20.
97. Schultz, L. and C. Mackall, *Driving CAR T cell translation forward*. Sci Transl Med, 2019. **11**(481).
98. Kranenburg, O., *The KRAS oncogene: past, present, and future*. Biochim Biophys Acta, 2005. **1756**(2): p. 81-2.
99. Buscail, L., B. Bournet, and P. Cordelier, *Role of oncogenic KRAS in the diagnosis, prognosis and treatment of pancreatic cancer*. Nat Rev Gastroenterol Hepatol, 2020. **17**(3): p. 153-168.
100. Ryan, D.P., T.S. Hong, and N. Bardeesy, *Pancreatic adenocarcinoma*. N Engl J Med, 2014. **371**(22): p. 2140-1.
101. Delpu, Y., et al., *Genetic and epigenetic alterations in pancreatic carcinogenesis*. Curr Genomics, 2011. **12**(1): p. 15-24.
102. Haigis, K.M., *KRAS Alleles: The Devil Is in the Detail*. Trends Cancer, 2017. **3**(10): p. 686-697.
103. Qian, Z.R., et al., *Association of Alterations in Main Driver Genes With Outcomes of Patients*

- With Resected Pancreatic Ductal Adenocarcinoma*. JAMA Oncol, 2018. **4**(3): p. e173420.
104. Cheng, H., et al., *Analysis of ctDNA to predict prognosis and monitor treatment responses in metastatic pancreatic cancer patients*. Int J Cancer, 2017. **140**(10): p. 2344-2350.
 105. Hamidi, H., et al., *KRAS mutational subtype and copy number predict in vitro response of human pancreatic cancer cell lines to MEK inhibition*. Br J Cancer, 2014. **111**(9): p. 1788-801.
 106. Jonckheere, N., R. Vasseur, and I. Van Seuningen, *The cornerstone K-RAS mutation in pancreatic adenocarcinoma: From cell signaling network, target genes, biological processes to therapeutic targeting*. Crit Rev Oncol Hematol, 2017. **111**: p. 7-19.
 107. Collins, M.A., et al., *Oncogenic Kras is required for both the initiation and maintenance of pancreatic cancer in mice*. J Clin Invest, 2012. **122**(2): p. 639-53.
 108. Ying, H., et al., *Oncogenic Kras maintains pancreatic tumors through regulation of anabolic glucose metabolism*. Cell, 2012. **149**(3): p. 656-70.
 109. Ancey, P.B., C. Contat, and E. Meylan, *Glucose transporters in cancer - from tumor cells to the tumor microenvironment*. Febs j, 2018. **285**(16): p. 2926-2943.
 110. di Magliano, M.P. and C.D. Logsdon, *Roles for KRAS in pancreatic tumor development and progression*. Gastroenterology, 2013. **144**(6): p. 1220-9.
 111. Tape, C.J., et al., *Oncogenic KRAS Regulates Tumor Cell Signaling via Stromal Reciprocation*. Cell, 2016. **165**(4): p. 910-20.
 112. Lesina, M., et al., *Stat3/Socs3 activation by IL-6 transsignaling promotes progression of pancreatic intraepithelial neoplasia and development of pancreatic cancer*. Cancer Cell, 2011. **19**(4): p. 456-69.
 113. Pylayeva-Gupta, Y., et al., *Oncogenic Kras-induced GM-CSF production promotes the development of pancreatic neoplasia*. Cancer Cell, 2012. **21**(6): p. 836-47.
 114. Cantley, L.C., *The phosphoinositide 3-kinase pathway*. Science, 2002. **296**(5573): p. 1655-7.
 115. Vanhaesebroeck, B., et al., *The emerging mechanisms of isoform-specific PI3K signalling*. Nat Rev Mol Cell Biol, 2010. **11**(5): p. 329-41.
 116. Mao, Y., et al., *Regulation of cell apoptosis and proliferation in pancreatic cancer through PI3K/Akt pathway via Polo-like kinase 1*. Oncol Rep, 2016. **36**(1): p. 49-56.
 117. Yuan, T.L. and L.C. Cantley, *PI3K pathway alterations in cancer: variations on a theme*. Oncogene, 2008. **27**(41): p. 5497-510.
 118. Schild, C., et al., *PI3K signaling maintains c-myc expression to regulate transcription of E2F1 in pancreatic cancer cells*. Mol Carcinog, 2009. **48**(12): p. 1149-58.
 119. Edling, C.E., et al., *Key role of phosphoinositide 3-kinase class IB in pancreatic cancer*. Clin Cancer Res, 2010. **16**(20): p. 4928-37.
 120. Leever, S.J., B. Vanhaesebroeck, and M.D. Waterfield, *Signalling through phosphoinositide 3-kinases: the lipids take centre stage*. Curr Opin Cell Biol, 1999. **11**(2): p. 219-25.
 121. Fruman, D.A., R.E. Meyers, and L.C. Cantley, *Phosphoinositide kinases*. Annu Rev Biochem, 1998. **67**: p. 481-507.
 122. Castellano, E. and J. Downward, *RAS Interaction with PI3K: More Than Just Another Effector Pathway*. Genes Cancer, 2011. **2**(3): p. 261-74.
 123. Ying, H., et al., *Genetics and biology of pancreatic ductal adenocarcinoma*. Genes Dev, 2016. **30**(4): p. 355-85.
 124. Hay, N. and N. Sonenberg, *Upstream and downstream of mTOR*. Genes Dev, 2004. **18**(16): p. 1926-45.
 125. Memmott, R.M. and P.A. Dennis, *Akt-dependent and -independent mechanisms of mTOR regulation in cancer*. Cell Signal, 2009. **21**(5): p. 656-64.
 126. Driscoll, D.R., et al., *mTORC2 Signaling Drives the Development and Progression of Pancreatic Cancer*. Cancer Res, 2016. **76**(23): p. 6911-6923.
 127. Morrison Joly, M., et al., *Rictor/mTORC2 Drives Progression and Therapeutic Resistance of HER2-Amplified Breast Cancers*. Cancer Res, 2016. **76**(16): p. 4752-64.
 128. Ruicci, K.M., et al., *Disruption of the RICTOR/mTORC2 complex enhances the response of head and neck squamous cell carcinoma cells to PI3K inhibition*. Mol Oncol, 2019. **13**(10): p. 2160-2177.

129. Roberts, P.J. and C.J. Der, *Targeting the Raf-MEK-ERK mitogen-activated protein kinase cascade for the treatment of cancer*. *Oncogene*, 2007. **26**(22): p. 3291-310.
130. Freeman, A.K., D.A. Ritt, and D.K. Morrison, *The importance of Raf dimerization in cell signaling*. *Small GTPases*, 2013. **4**(3): p. 180-5.
131. Morrison, D.K., *MAP kinase pathways*. *Cold Spring Harb Perspect Biol*, 2012. **4**(11).
132. Marais, R., J. Wynne, and R. Treisman, *The SRF accessory protein Elk-1 contains a growth factor-regulated transcriptional activation domain*. *Cell*, 1993. **73**(2): p. 381-93.
133. Morton, S., et al., *A reinvestigation of the multisite phosphorylation of the transcription factor c-Jun*. *Embo j*, 2003. **22**(15): p. 3876-86.
134. Chen, R.H., C. Abate, and J. Blenis, *Phosphorylation of the c-Fos transrepression domain by mitogen-activated protein kinase and 90-kDa ribosomal S6 kinase*. *Proc Natl Acad Sci U S A*, 1993. **90**(23): p. 10952-6.
135. Farrell, A.S. and R.C. Sears, *MYC degradation*. *Cold Spring Harb Perspect Med*, 2014. **4**(3).
136. Henderson, W.R., Jr., et al., *Blockade of human group X secreted phospholipase A2 (GX-sPLA2)-induced airway inflammation and hyperresponsiveness in a mouse asthma model by a selective GX-sPLA2 inhibitor*. *J Biol Chem*, 2011. **286**(32): p. 28049-55.
137. Reszka, A.A., et al., *Association of mitogen-activated protein kinase with the microtubule cytoskeleton*. *Proc Natl Acad Sci U S A*, 1995. **92**(19): p. 8881-5.
138. Northwood, I.C., et al., *Isolation and characterization of two growth factor-stimulated protein kinases that phosphorylate the epidermal growth factor receptor at threonine 669*. *J Biol Chem*, 1991. **266**(23): p. 15266-76.
139. Sebolt-Leopold, J.S., *Advances in the development of cancer therapeutics directed against the RAS-mitogen-activated protein kinase pathway*. *Clin Cancer Res*, 2008. **14**(12): p. 3651-6.
140. Wong, K.K., *Recent developments in anti-cancer agents targeting the Ras/Raf/ MEK/ERK pathway*. *Recent Pat Anticancer Drug Discov*, 2009. **4**(1): p. 28-35.
141. Corcoran, R.B., et al., *EGFR-mediated re-activation of MAPK signaling contributes to insensitivity of BRAF mutant colorectal cancers to RAF inhibition with vemurafenib*. *Cancer Discov*, 2012. **2**(3): p. 227-35.
142. Turski, M.L., et al., *Genomically Driven Tumors and Actionability across Histologies: BRAF-Mutant Cancers as a Paradigm*. *Mol Cancer Ther*, 2016. **15**(4): p. 533-47.
143. Witkiewicz, A.K., et al., *Whole-exome sequencing of pancreatic cancer defines genetic diversity and therapeutic targets*. *Nat Commun*, 2015. **6**: p. 6744.
144. Peng, S.B., et al., *Inhibition of RAF Isoforms and Active Dimers by LY3009120 Leads to Anti-tumor Activities in RAS or BRAF Mutant Cancers*. *Cancer Cell*, 2015. **28**(3): p. 384-98.
145. Haarberg, H.E. and K.S. Smalley, *Resistance to Raf inhibition in cancer*. *Drug Discov Today Technol*, 2014. **11**: p. 27-32.
146. Lito, P., N. Rosen, and D.B. Solit, *Tumor adaptation and resistance to RAF inhibitors*. *Nat Med*, 2013. **19**(11): p. 1401-9.
147. Holderfield, M., T.E. Nagel, and D.D. Stuart, *Mechanism and consequences of RAF kinase activation by small-molecule inhibitors*. *Br J Cancer*, 2014. **111**(4): p. 640-5.
148. Hatzivassiliou, G., et al., *RAF inhibitors prime wild-type RAF to activate the MAPK pathway and enhance growth*. *Nature*, 2010. **464**(7287): p. 431-5.
149. Poulikakos, P.I., et al., *RAF inhibitors transactivate RAF dimers and ERK signalling in cells with wild-type BRAF*. *Nature*, 2010. **464**(7287): p. 427-30.
150. Henry, J.R., et al., *Discovery of 1-(3,3-dimethylbutyl)-3-(2-fluoro-4-methyl-5-(7-methyl-2-(methylamino)pyrido[2,3-d]pyrimidin-6-yl)phenyl)urea (LY3009120) as a pan-RAF inhibitor with minimal paradoxical activation and activity against BRAF or RAS mutant tumor cells*. *J Med Chem*, 2015. **58**(10): p. 4165-79.
151. Yao, Z., et al., *RAF inhibitor PLX8394 selectively disrupts BRAF dimers and RAS-independent BRAF-mutant-driven signaling*. *Nat Med*, 2019. **25**(2): p. 284-291.
152. Lito, P., et al., *Disruption of CRAF-mediated MEK activation is required for effective MEK inhibition in KRAS mutant tumors*. *Cancer Cell*, 2014. **25**(5): p. 697-710.
153. Ryan, M.B., et al., *Targeting RAS-mutant cancers: is ERK the key?* *Trends Cancer*, 2015. **1**(3): p.

- 183-198.
154. Little, A.S., et al., *Amplification of the driving oncogene, KRAS or BRAF, underpins acquired resistance to MEK1/2 inhibitors in colorectal cancer cells*. *Sci Signal*, 2011. **4**(166): p. ra17.
155. Morris, E.J., et al., *Discovery of a novel ERK inhibitor with activity in models of acquired resistance to BRAF and MEK inhibitors*. *Cancer Discov*, 2013. **3**(7): p. 742-50.
156. Hayes, T.K., et al., *Long-Term ERK Inhibition in KRAS-Mutant Pancreatic Cancer Is Associated with MYC Degradation and Senescence-like Growth Suppression*. *Cancer Cell*, 2016. **29**(1): p. 75-89.
157. Micalizzi, D.S., S.M. Farabaugh, and H.L. Ford, *Epithelial-mesenchymal transition in cancer: parallels between normal development and tumor progression*. *J Mammary Gland Biol Neoplasia*, 2010. **15**(2): p. 117-34.
158. Nieto, M.A., et al., *Emt: 2016*. *Cell*, 2016. **166**(1): p. 21-45.
159. Yang, J., et al., *Twist, a master regulator of morphogenesis, plays an essential role in tumor metastasis*. *Cell*, 2004. **117**(7): p. 927-39.
160. Acloque, H., et al., *Epithelial-mesenchymal transitions: the importance of changing cell state in development and disease*. *J Clin Invest*, 2009. **119**(6): p. 1438-49.
161. Thiery, J.P., *Epithelial-mesenchymal transitions in tumour progression*. *Nat Rev Cancer*, 2002. **2**(6): p. 442-54.
162. Yingling, J.M., K.L. Blanchard, and J.S. Sawyer, *Development of TGF-beta signalling inhibitors for cancer therapy*. *Nat Rev Drug Discov*, 2004. **3**(12): p. 1011-22.
163. Zheng, X., et al., *Epithelial-to-mesenchymal transition is dispensable for metastasis but induces chemoresistance in pancreatic cancer*. *Nature*, 2015. **527**(7579): p. 525-530.
164. Fischer, K.R., et al., *Epithelial-to-mesenchymal transition is not required for lung metastasis but contributes to chemoresistance*. *Nature*, 2015. **527**(7579): p. 472-6.
165. Lamouille, S., J. Xu, and R. Derynck, *Molecular mechanisms of epithelial-mesenchymal transition*. *Nat Rev Mol Cell Biol*, 2014. **15**(3): p. 178-96.
166. Brabletz, T., et al., *EMT in cancer*. *Nat Rev Cancer*, 2018. **18**(2): p. 128-134.
167. Kalluri, R. and R.A. Weinberg, *The basics of epithelial-mesenchymal transition*. *J Clin Invest*, 2009. **119**(6): p. 1420-8.
168. Yang, J. and R.A. Weinberg, *Epithelial-mesenchymal transition: at the crossroads of development and tumor metastasis*. *Dev Cell*, 2008. **14**(6): p. 818-29.
169. Son, H. and A. Moon, *Epithelial-mesenchymal Transition and Cell Invasion*. *Toxicol Res*, 2010. **26**(4): p. 245-52.
170. Elaskalani, O., et al., *Epithelial-mesenchymal transition as a therapeutic target for overcoming chemoresistance in pancreatic cancer*. *World J Gastrointest Oncol*, 2017. **9**(1): p. 37-41.
171. Wang, J., et al., *Transition to resistance: An unexpected role of the EMT in cancer chemoresistance*. *Genes Dis*, 2016. **3**(1): p. 3-6.
172. Xu, Y., et al., *Breast tumor cell-specific knockout of Twist1 inhibits cancer cell plasticity, dissemination, and lung metastasis in mice*. *Proc Natl Acad Sci U S A*, 2017. **114**(43): p. 11494-11499.
173. Joyce, J.A. and D.T. Fearon, *T cell exclusion, immune privilege, and the tumor microenvironment*. *Science*, 2015. **348**(6230): p. 74-80.
174. Baghban, R., et al., *Tumor microenvironment complexity and therapeutic implications at a glance*. *Cell Commun Signal*, 2020. **18**(1): p. 59.
175. Jahanban-Esfahlan, R., et al., *Tumor Cell Dormancy: Threat or Opportunity in the Fight against Cancer*. *Cancers (Basel)*, 2019. **11**(8).
176. Seidi, K., et al., *Tumor target amplification: Implications for nano drug delivery systems*. *J Control Release*, 2018. **275**: p. 142-161.
177. Clara, J.A., et al., *Targeting signalling pathways and the immune microenvironment of cancer stem cells - a clinical update*. *Nat Rev Clin Oncol*, 2020. **17**(4): p. 204-232.
178. Li, W., et al., *Molecular alterations of cancer cell and tumour microenvironment in metastatic gastric cancer*. *Oncogene*, 2018. **37**(36): p. 4903-4920.
179. Tsao, A.S., et al., *Scientific Advances in Lung Cancer 2015*. *J Thorac Oncol*, 2016. **11**(5): p. 613-

- 638.
180. Cova, T., D.J. Bento, and S.C.C. Nunes, *Computational Approaches in Theranostics: Mining and Predicting Cancer Data*. Pharmaceutics, 2019. **11**(3).
181. Lu, C., et al., *Current perspectives on the immunosuppressive tumor microenvironment in hepatocellular carcinoma: challenges and opportunities*. Mol Cancer, 2019. **18**(1): p. 130.
182. Hiraoka, N., et al., *Prevalence of FOXP3+ regulatory T cells increases during the progression of pancreatic ductal adenocarcinoma and its premalignant lesions*. Clin Cancer Res, 2006. **12**(18): p. 5423-34.
183. Liou, G.Y., et al., *Macrophage-secreted cytokines drive pancreatic acinar-to-ductal metaplasia through NF- κ B and MMPs*. J Cell Biol, 2013. **202**(3): p. 563-77.
184. Labani-Motlagh, A., M. Ashja-Mahdavi, and A. Loskog, *The Tumor Microenvironment: A Milieu Hindering and Obstructing Antitumor Immune Responses*. Front Immunol, 2020. **11**: p. 940.
185. Riabov, V., et al., *Role of tumor associated macrophages in tumor angiogenesis and lymphangiogenesis*. Front Physiol, 2014. **5**: p. 75.
186. Hivroz, C., et al., *Crosstalk between T lymphocytes and dendritic cells*. Crit Rev Immunol, 2012. **32**(2): p. 139-55.
187. Hoyer, S., et al., *Concurrent interaction of DCs with CD4(+) and CD8(+) T cells improves secondary CTL expansion: It takes three to tango*. Eur J Immunol, 2014. **44**(12): p. 3543-59.
188. Zaretsky, J.M., et al., *Mutations Associated with Acquired Resistance to PD-1 Blockade in Melanoma*. N Engl J Med, 2016. **375**(9): p. 819-29.
189. De Sousa Linhares, A., et al., *Not All Immune Checkpoints Are Created Equal*. Front Immunol, 2018. **9**: p. 1909.
190. Tay, R.E., E.K. Richardson, and H.C. Toh, *Revisiting the role of CD4(+) T cells in cancer immunotherapy-new insights into old paradigms*. Cancer Gene Ther, 2021. **28**(1-2): p. 5-17.
191. Fukunaga, A., et al., *CD8+ tumor-infiltrating lymphocytes together with CD4+ tumor-infiltrating lymphocytes and dendritic cells improve the prognosis of patients with pancreatic adenocarcinoma*. Pancreas, 2004. **28**(1): p. e26-31.
192. Ene-Obong, A., et al., *Activated pancreatic stellate cells sequester CD8+ T cells to reduce their infiltration of the juxtatumoral compartment of pancreatic ductal adenocarcinoma*. Gastroenterology, 2013. **145**(5): p. 1121-32.
193. Ino, Y., et al., *Immune cell infiltration as an indicator of the immune microenvironment of pancreatic cancer*. Br J Cancer, 2013. **108**(4): p. 914-23.
194. Zhang, Y., et al., *CD4+ T lymphocyte ablation prevents pancreatic carcinogenesis in mice*. Cancer Immunol Res, 2014. **2**(5): p. 423-35.
195. Liu, Z., et al., *Systematic comparison of 2A peptides for cloning multi-genes in a polycistronic vector*. Sci Rep, 2017. **7**(1): p. 2193.
196. Barrangou, R., *The roles of CRISPR-Cas systems in adaptive immunity and beyond*. Curr Opin Immunol, 2015. **32**: p. 36-41.
197. Bak, R.O., N. Gomez-Ospina, and M.H. Porteus, *Gene Editing on Center Stage*. Trends Genet, 2018. **34**(8): p. 600-611.
198. Charpentier, E., et al., *Biogenesis pathways of RNA guides in archaeal and bacterial CRISPR-Cas adaptive immunity*. FEMS Microbiol Rev, 2015. **39**(3): p. 428-41.
199. Sanjana, N.E., O. Shalem, and F. Zhang, *Improved vectors and genome-wide libraries for CRISPR screening*. Nat Methods, 2014. **11**(8): p. 783-784.
200. Shalem, O., et al., *Genome-scale CRISPR-Cas9 knockout screening in human cells*. Science, 2014. **343**(6166): p. 84-87.
201. Di Franco, S., et al., *Role of Type I and II Interferons in Colorectal Cancer and Melanoma*. Front Immunol, 2017. **8**: p. 878.
202. Ferrantini, M., I. Capone, and F. Belardelli, *Interferon-alpha and cancer: mechanisms of action and new perspectives of clinical use*. Biochimie, 2007. **89**(6-7): p. 884-93.
203. Toker, A. and A.C. Newton, *Cellular signaling: pivoting around PDK-1*. Cell, 2000. **103**(2): p. 185-8.
204. Kim, J.W., et al., *HIF-1-mediated expression of pyruvate dehydrogenase kinase: a metabolic*

- switch required for cellular adaptation to hypoxia*. Cell Metab, 2006. **3**(3): p. 177-85.
205. Tan, J., et al., *PDK1 signaling toward PLK1-MYC activation confers oncogenic transformation, tumor-initiating cell activation, and resistance to mTOR-targeted therapy*. Cancer Discov, 2013. **3**(10): p. 1156-71.
206. Ischenko, I., et al., *Direct reprogramming by oncogenic Ras and Myc*. Proc Natl Acad Sci U S A, 2013. **110**(10): p. 3937-42.
207. Song, Y., et al., *Loss of ATOH8 Increases Stem Cell Features of Hepatocellular Carcinoma Cells*. Gastroenterology, 2015. **149**(4): p. 1068-81.e5.
208. Pi, W.C., et al., *E2A-PBX1 functions as a coactivator for RUNX1 in acute lymphoblastic leukemia*. Blood, 2020. **136**(1): p. 11-23.
209. Yang, Y., et al., *TRIM56 suppresses the malignant development of hepatocellular carcinoma via targeting RBM24 and inactivating the Wnt signaling*. Eur Rev Med Pharmacol Sci, 2021. **25**(2): p. 722-730.
210. Chen, Y., et al., *TRIM56 Suppresses Multiple Myeloma Progression by Activating TLR3/TRIF Signaling*. Yonsei Med J, 2018. **59**(1): p. 43-50.
211. Vrijzen, S., et al., *ATP13A2-mediated endo-lysosomal polyamine export counters mitochondrial oxidative stress*. Proc Natl Acad Sci U S A, 2020. **117**(49): p. 31198-31207.
212. Bourdenx, M., et al., *Chaperone-mediated autophagy prevents collapse of the neuronal metastable proteome*. Cell, 2021. **184**(10): p. 2696-2714.e25.
213. Wang, W.J., et al., *Overview of serpin B9 and its roles in cancer (Review)*. Oncol Rep, 2021. **46**(3).
214. Li, B., et al., *TMEM140 is associated with the prognosis of glioma by promoting cell viability and invasion*. J Hematol Oncol, 2015. **8**: p. 89.
215. Yen, T.J., et al., *CENP-E is a putative kinetochore motor that accumulates just before mitosis*. Nature, 1992. **359**(6395): p. 536-9.
216. Qiu, J., et al., *BUB1B promotes hepatocellular carcinoma progression via activation of the mTORC1 signaling pathway*. Cancer Med, 2020. **9**(21): p. 8159-8172.
217. Zhou, H., et al., *Elevated expression of minichromosome maintenance 3 indicates poor outcomes and promotes G1/S cell cycle progression, proliferation, migration and invasion in colorectal cancer*. Biosci Rep, 2020. **40**(7).
218. Mills, C.A., et al., *Nucleolar and spindle-associated protein 1 (NUSAP1) interacts with a SUMO E3 ligase complex during chromosome segregation*. J Biol Chem, 2017. **292**(42): p. 17178-17189.
219. Cros, J., et al., *Tumor Heterogeneity in Pancreatic Adenocarcinoma*. Pathobiology, 2018. **85**(1-2): p. 64-71.
220. Kim, M.P., et al., *Oncogenic KRAS Recruits an Expansive Transcriptional Network through Mutant p53 to Drive Pancreatic Cancer Metastasis*. Cancer Discov, 2021. **11**(8): p. 2094-2111.
221. Klöppel, G., A. Perren, and P.U. Heitz, *The gastroenteropancreatic neuroendocrine cell system and its tumors: the WHO classification*. Ann N Y Acad Sci, 2004. **1014**: p. 13-27.
222. Li, L.T., et al., *Ki67 is a promising molecular target in the diagnosis of cancer (review)*. Mol Med Rep, 2015. **11**(3): p. 1566-72.
223. Knudsen, E.S., et al., *Stratification of Pancreatic Ductal Adenocarcinoma: Combinatorial Genetic, Stromal, and Immunologic Markers*. Clin Cancer Res, 2017. **23**(15): p. 4429-4440.
224. Carstens, J.L., et al., *Spatial computation of intratumoral T cells correlates with survival of patients with pancreatic cancer*. Nat Commun, 2017. **8**: p. 15095.
225. Jorgovanovic, D., et al., *Roles of IFN- γ in tumor progression and regression: a review*. Biomark Res, 2020. **8**: p. 49.
226. Idriss, H.T. and J.H. Naismith, *TNF alpha and the TNF receptor superfamily: structure-function relationship(s)*. Microsc Res Tech, 2000. **50**(3): p. 184-95.
227. Lin, Y., J. Xu, and H. Lan, *Tumor-associated macrophages in tumor metastasis: biological roles and clinical therapeutic applications*. J Hematol Oncol, 2019. **12**(1): p. 76.
228. Law, A.M.K., F. Valdes-Mora, and D. Gallego-Ortega, *Myeloid-Derived Suppressor Cells as a Therapeutic Target for Cancer*. Cells, 2020. **9**(3).
229. Rawla, P., T. Sunkara, and V. Gaduputi, *Epidemiology of Pancreatic Cancer: Global Trends*,

- Etiology and Risk Factors*. World J Oncol, 2019. **10**(1): p. 10-27.
230. Liu, P., Y. Wang, and X. Li, *Targeting the untargetable KRAS in cancer therapy*. Acta Pharm Sin B, 2019. **9**(5): p. 871-879.
231. Mollinedo, F. and C. Gajate, *Novel therapeutic approaches for pancreatic cancer by combined targeting of RAF→MEK→ERK signaling and autophagy survival response*. Ann Transl Med, 2019. **7**(Suppl 3): p. S153.
232. Czabotar, P.E., et al., *Control of apoptosis by the BCL-2 protein family: implications for physiology and therapy*. Nat Rev Mol Cell Biol, 2014. **15**(1): p. 49-63.
233. Liu, J.-q. and T. Li, *CRISPR-Cas9-mediated loss-of-function screens*. Frontiers in Life Science, 2019. **12**(1): p. 1-13.
234. Sigoillot, F.D., et al., *A bioinformatics method identifies prominent off-targeted transcripts in RNAi screens*. Nat Methods, 2012. **9**(4): p. 363-6.
235. Khorashad, J.S., et al., *shRNA library screening identifies nucleocytoplasmic transport as a mediator of BCR-ABL1 kinase-independent resistance*. Blood, 2015. **125**(11): p. 1772-81.
236. Barrangou, R., et al., *CRISPR provides acquired resistance against viruses in prokaryotes*. Science, 2007. **315**(5819): p. 1709-12.
237. Marraffini, L.A. and E.J. Sonthheimer, *CRISPR interference limits horizontal gene transfer in staphylococci by targeting DNA*. Science, 2008. **322**(5909): p. 1843-5.
238. Varga, A., et al., *RAF1/BRAF dimerization integrates the signal from RAS to ERK and ROKα*. Sci Signal, 2017. **10**(469).
239. Matallanas, D., et al., *Raf family kinases: old dogs have learned new tricks*. Genes Cancer, 2011. **2**(3): p. 232-60.
240. Chen, J., et al., *Raf-1 promotes cell survival by antagonizing apoptosis signal-regulating kinase 1 through a MEK-ERK independent mechanism*. Proc Natl Acad Sci U S A, 2001. **98**(14): p. 7783-8.
241. O'Neill, E., et al., *Role of the kinase MST2 in suppression of apoptosis by the proto-oncogene product Raf-1*. Science, 2004. **306**(5705): p. 2267-70.
242. Singh, M., C.L. Murriel, and L. Johnson, *Genetically engineered mouse models: closing the gap between preclinical data and trial outcomes*. Cancer Res, 2012. **72**(11): p. 2695-700.
243. Guerra, C., et al., *Chronic pancreatitis is essential for induction of pancreatic ductal adenocarcinoma by K-Ras oncogenes in adult mice*. Cancer Cell, 2007. **11**(3): p. 291-302.
244. Hingorani, S.R., et al., *Preinvasive and invasive ductal pancreatic cancer and its early detection in the mouse*. Cancer Cell, 2003. **4**(6): p. 437-50.
245. Seidler, B., et al., *A Cre-loxP-based mouse model for conditional somatic gene expression and knockdown in vivo by using avian retroviral vectors*. Proc Natl Acad Sci U S A, 2008. **105**(29): p. 10137-42.
246. Schonhuber, N., et al., *A next-generation dual-recombinase system for time- and host-specific targeting of pancreatic cancer*. Nat Med, 2014. **20**(11): p. 1340-1347.
247. Beatty, G.L. and W.L. Gladney, *Immune escape mechanisms as a guide for cancer immunotherapy*. Clin Cancer Res, 2015. **21**(4): p. 687-92.
248. Huber, M., et al., *The Immune Microenvironment in Pancreatic Cancer*. Int J Mol Sci, 2020. **21**(19).
249. Huang, B., et al., *Gr-1+CD115+ immature myeloid suppressor cells mediate the development of tumor-induced T regulatory cells and T-cell anergy in tumor-bearing host*. Cancer Res, 2006. **66**(2): p. 1123-31.
250. Siret, C., et al., *Deciphering the Crosstalk Between Myeloid-Derived Suppressor Cells and Regulatory T Cells in Pancreatic Ductal Adenocarcinoma*. Front Immunol, 2019. **10**: p. 3070.
251. Lankadasari, M.B., et al., *TAMing pancreatic cancer: combat with a double edged sword*. Mol Cancer, 2019. **18**(1): p. 48.
252. Yin, M., et al., *Tumor-associated macrophages drive spheroid formation during early transcoelomic metastasis of ovarian cancer*. J Clin Invest, 2016. **126**(11): p. 4157-4173.
253. Griesmann, H., et al., *Pharmacological macrophage inhibition decreases metastasis formation in a genetic model of pancreatic cancer*. Gut, 2017. **66**(7): p. 1278-1285.

254. Nywening, T.M., et al., *Targeting both tumour-associated CXCR2(+) neutrophils and CCR2(+) macrophages disrupts myeloid recruitment and improves chemotherapeutic responses in pancreatic ductal adenocarcinoma*. *Gut*, 2018. **67**(6): p. 1112-1123.
255. Liou, G.Y., et al., *Mutant KRAS-induced expression of ICAM-1 in pancreatic acinar cells causes attraction of macrophages to expedite the formation of precancerous lesions*. *Cancer Discov*, 2015. **5**(1): p. 52-63.
256. Yang, S., Q. Liu, and Q. Liao, *Tumor-Associated Macrophages in Pancreatic Ductal Adenocarcinoma: Origin, Polarization, Function, and Reprogramming*. *Front Cell Dev Biol*, 2020. **8**: p. 607209.
257. Abate-Shen, C. and P.P. Pandolfi, *Effective utilization and appropriate selection of genetically engineered mouse models for translational integration of mouse and human trials*. *Cold Spring Harb Protoc*, 2013. **2013**(11).
258. Lin, J.H., *Applications and limitations of genetically modified mouse models in drug discovery and development*. *Curr Drug Metab*, 2008. **9**(5): p. 419-38.
259. Qiu, W. and G.H. Su, *Development of orthotopic pancreatic tumor mouse models*. *Methods Mol Biol*, 2013. **980**: p. 215-23.
260. Van Dyke, T. and T. Jacks, *Cancer modeling in the modern era: progress and challenges*. *Cell*, 2002. **108**(2): p. 135-44.
261. Kim, D.H., et al., *Epithelial Mesenchymal Transition in Embryonic Development, Tissue Repair and Cancer: A Comprehensive Overview*. *J Clin Med*, 2017. **7**(1).
262. Scimeca, M., et al., *Emerging prognostic markers related to mesenchymal characteristics of poorly differentiated breast cancers*. *Tumour Biol*, 2016. **37**(4): p. 5427-35.
263. Sánchez-Tilló, E., et al., *ZEB1 represses E-cadherin and induces an EMT by recruiting the SWI/SNF chromatin-remodeling protein BRG1*. *Oncogene*, 2010. **29**(24): p. 3490-500.
264. Vesuna, F., et al., *Twist is a transcriptional repressor of E-cadherin gene expression in breast cancer*. *Biochem Biophys Res Commun*, 2008. **367**(2): p. 235-41.
265. Casas, E., et al., *Snail2 is an essential mediator of Twist1-induced epithelial mesenchymal transition and metastasis*. *Cancer Res*, 2011. **71**(1): p. 245-54.
266. Gregory, P.A., et al., *The miR-200 family and miR-205 regulate epithelial to mesenchymal transition by targeting ZEB1 and SIP1*. *Nat Cell Biol*, 2008. **10**(5): p. 593-601.
267. Korpál, M., et al., *The miR-200 family inhibits epithelial-mesenchymal transition and cancer cell migration by direct targeting of E-cadherin transcriptional repressors ZEB1 and ZEB2*. *J Biol Chem*, 2008. **283**(22): p. 14910-4.
268. Kumarswamy, R., et al., *MicroRNA-30a inhibits epithelial-to-mesenchymal transition by targeting Snai1 and is downregulated in non-small cell lung cancer*. *Int J Cancer*, 2012. **130**(9): p. 2044-53.